diversity

MDPI

Article

New Skeletons of the Ancient Dolphin *Xenorophus sloanii* and *Xenorophus simplicidens* sp. nov. (Mammalia, Cetacea) from the Oligocene of South Carolina and the Ontogeny, Functional Anatomy, Asymmetry, Pathology, and Evolution of the Earliest Odontoceti

Robert W. Boessenecker [1,*] and Jonathan H. Geisler [2,3]

[1] University of California Museum of Paleontology, University of California, Berkeley, CA 94720, USA
[2] Department of Anatomy, New York Institute of Technology, Old Westbury, NY 11568, USA; jgeisler@nyit.edu
[3] Department of Paleobiology, National Museum of Natural History, Washington, DC 20560, USA
* Correspondence: boessenecker@gmail.com

Abstract: The early diverging, dolphin-sized, cetacean clade Xenorophidae are a short-lived radiation of toothed whales (Odontoceti) that independently evolved two features long thought to be odontocete synapomorphies: the craniofacial and cochlear morphology underlying echolocation and retrograde cranial telescoping (i.e., posterior migration of the viscerocranium). This family was based on *Xenorophus sloanii*, which, for the past century, has been known only by a partial skull lacking a braincase and tympanoperiotics, collected around 1900 from the Ashley Formation (28–29 Ma, Rupelian) near Ladson, South Carolina. A large collection of new skulls and skeletons (ChM PV 5022, 7677; CCNHM 104, 168, 1077, 5995) from the Ashley Formation considerably expands the hypodigm for this species, now the best known of any stem odontocete and permitting evaluation of intraspecific variation and ontogenetic changes. This collection reveals that the holotype (USNM 11049) is a juvenile. *Xenorophus sloanii* is a relatively large odontocete (70–74 cm CBL; BZW = 29–31 cm; estimated body length 2.6–3 m) with a moderately long rostrum (RPI = 2.5), marked heterodonty, limited polydonty (13–14 teeth), prominent sagittal crest and intertemporal constriction, and drastically larger brain size than basilosaurid archaeocetes (EQ = 2.9). Dental morphology, thickened cementum, a dorsoventrally robust rostrum, and thick rugose enamel suggest raptorial feeding; oral pathology indicates traumatic tooth loss associated with mechanically risky predation attempts. Ontogenetic changes include increased palatal vomer exposure; fusion of the nasofrontal, occipito-parietal, and median frontal sutures; anterior lengthening of the nasals; elaboration of the nuchal crests; and blunting and thickening of the antorbital process. The consistent deviation of the rostrum 2–5° to the left and asymmetry of the palate, dentition, neurocranium, mandibles, and vertebrae in multiple specimens of *Xenorophus sloanii* suggest novel adaptations for directional hearing driven by the asymmetrically oriented pan bones of the mandibles. A second collection consisting of a skeleton and several skulls from the overlying Chandler Bridge Formation (24–23 Ma, Chattian) represents a new species, *Xenorophus simplicidens* n. sp., differing from *Xenorophus sloanii* in possessing shorter nasals, anteroposteriorly shorter supraorbital processes of the frontal, and teeth with fewer accessory cusps and less rugose enamel. Phylogenetic analysis supports monophyly of *Xenorophus*, with specimens of *Xenorophus simplicidens* nested within paraphyletic *X. sloanii*; in concert with stratigraphic data, these results support the interpretation of these species as part of an anagenetic lineage. New clade names are provided for the sister taxon to Xenorophidae (Ambyloccipita), and the odontocete clade excluding Xenorophidae, *Ashleycetus*, *Mirocetus*, and Simocetidae (Stegoceti). Analyses of tooth size, body size, temporal fossa length, orbit morphology, and the rostral proportion index, prompted by well-preserved remains of *Xenorophus*, provide insight into the early evolution of Odontoceti.

Keywords: Xenorophidae; Odontoceti; Cetacea; Oligocene; asymmetry

check for updates

Citation: Boessenecker, R.W.; Geisler, J.H. New Skeletons of the Ancient Dolphin *Xenorophus sloanii* and *Xenorophus simplicidens* sp. nov. (Mammalia, Cetacea) from the Oligocene of South Carolina and the Ontogeny, Functional Anatomy, Asymmetry, Pathology, and Evolution of the Earliest Odontoceti. *Diversity* **2023**, *15*, 1154. https://doi.org/10.3390/d15111154

Academic Editors: Michelangelo Bisconti and Michael Wink

Received: 10 July 2023
Revised: 27 October 2023
Accepted: 27 October 2023
Published: 20 November 2023

Copyright: © 2023 by the authors. Licensee MDPI, Basel, Switzerland. This article is an open access article distributed under the terms and conditions of the Creative Commons Attribution (CC BY) license (https://creativecommons.org/licenses/by/4.0/).

1. Introduction

The Xenorophidae are a family-level clade of early diverging dolphins (stem Odontoceti) known from Oligocene strata of South Carolina. This clade represents one of the earliest diverging lineages amongst odontocetes and sheds considerable light upon the early evolution of echolocation, feeding adaptations, and encephalization within Odontoceti [1–5]. Fossils of Xenorophidae are restricted to South and North Carolina and Virginia [6] along the Atlantic Coastal Plain and do not occur in well-sampled Oligocene marine mammal assemblages in other ocean basins [1–5,7–9], suggesting that the Xenorophidae represent an early and localized diversification of stem odontocetes in the Western North Atlantic. Their skull morphology includes a number of plesiomorphic and unusual derived features. Plesiomorphic features include a limited degree of telescoping, an intertemporal constriction, and even a low sagittal crest in some specimens. Most of the unusual cranial morphology is expressed around the orbits and nares, relating to the nasal process of the premaxilla and the hypertrophied lacrimal. In a typical odontocete, stem or crown, the nasal process of the premaxilla consists of a dorsoventrally thin plate or strip overlying the maxilla and/or frontal; the lacrimal is typically relatively small, confined to the antorbital notch, and fused to the jugal. In Xenorophidae, however, the premaxilla is osteosclerotic (dense) and inflated ventrolaterally, so that the entire medial half of the maxilla overlaps the nasal process, leaving a thin strip of premaxilla dorsomedially that extends far posterior to contact the frontal (and nearly the parietal). Furthermore, the ventrolateral expansion of the nasal process is so extreme that a portion of the frontal no longer ossifies, revealing a 'frontal window' where the premaxilla and maxilla are exposed on the ventral surface of the supraorbital process posterior to the orbit [5,8,10]. Likewise, the unusual lacrimal of Xenorophidae is dense and greatly expanded posterodorsally so that it overlaps the frontal and forms the antorbital process and much of the dorsal surface of the supraorbital process, as well as retaining plesiomorphic separation from the jugal [5,8,10].

Members of the Xenorophidae have been key fossils for interpreting the early auditory evolution of Odontoceti. All extant Odontoceti use active echolocation or biosonar to detect prey underwater; sounds are produced at the phonic lips [11,12], a constriction in the nasal passages deep to the blowhole, are propagated anteriorly through the acoustic fats of the melon or are bounced off of the tissues of prey. Then, the delays between vocalization and hearing the resulting echoes are used to locate prey [13,14]. Odontocetes have a number of adaptations for directional hearing including acoustic fats and the mandibular fat pad (correlated with the pan bone), reduced bony connections between the tympanoperiotics and the cranium, and air-filled sinuses surrounding the tympanoperiotics which, along with reduced bony connections, reduce bone-conducted hearing that would prevent directional hearing [12,15,16]. Prior to contemporary study of Xenorophidae, anatomical features associated with echolocation, such as a concave facial plane (which accommodates the melon), asymmetry of the facial region of the skull, and the development of basicranial sinuses, suggested that many stem odontocetes were capable of echolocation [17,18].

Recently discovered Xenorophidae provided novel insights into the evolution of echolocation, locomotion, and feeding morphology of the earliest Odontoceti. *Cotylocara macei* was described by Geisler et al. [4], who reported craniofacial evidence of air sinuses supporting early development of ultrasonic sound production. Likewise, microCT study of the then-newly named *Echovenator sandersi* indicated that *Echovenator*, and likely other xenorophids, were capable of hearing ultrasonic sounds [3,19]. A dwarf, brevirostrine, and toothless xenorophid, *Inermorostrum xenops*, indicates that specialized suction feeding evolved rapidly during the Oligocene odontocete radiation [2]. Another small-bodied xenorophid, *Albertocetus meffordorum*, from the Oligocene Belgrade Formation of North Carolina [9], led to the formal naming of the Xenorophidae, and additional material from Charleston, South Carolina, revealed early expansion of brain size and EQ in Odontoceti as well as locomotor adaptations [1].

Despite recent and significant expansion in knowledge of the clade as a whole, the original species upon which the family was based, *Xenorophus sloanii*, has only one formally

described specimen—the holotype, USNM 11964, a partial skull consisting of an incomplete rostrum and interorbital region. For decades, a large collection of unstudied material informally recognized as *Xenorophus* has been amassed from the lower Oligocene Ashley Formation and upper Oligocene Chandler Bridge Formation of Charleston, South Carolina, though comparisons with the holotype were confused, owing to some of its unusual morphological features (e.g., small size, proportionally large teeth, short nasals). This new material includes numerous complete skulls with well-preserved mandibles, dentitions, and tympanoperiotics, and postcranial skeletons giving unprecedented insights into the feeding morphology, functional anatomy, postcranial anatomy, pathology, craniodental variation, and skeletal ontogeny of an early odontocete species. This study further recognizes two stratigraphically separated species, referring all specimens from the Ashley Formation to *Xenorophus sloanii* and naming a new species, *Xenorophus simplicidens* n. sp. from the overlying Chandler Bridge Formation. Unexpectedly, we report evidence of rostral, mandibular, dental, and even postcranial asymmetry in *Xenorophus* to accompany the cranial asymmetry described in the xenorophids *Cotylocara* and *Echovenator* [3,4]. Insights into taphonomy, body size, tooth size, tooth count, rostrum length, rostral deflection, and asymmetry are investigated in the context of early odontocete evolution. Lastly, key phylogenetic characters for early Neoceti are re-evaluated.

2. History of Study of the Xenorophidae

The earliest discovered xenorophid is a fragmentary maxilla from the Ashley River, collected by Francis Holmes and reported and figured by Joseph Leidy ([20]: 420, plate 29.1), which he named *Squalodon pelagius*. This specimen has a somewhat deep rostrum with long diastemata; double-rooted postcanine teeth with symmetrical crowns, smooth carinae, and faint labial cingula; and, most critically, embrasure pits on the maxilla nearly in line with the toothrow, unique to the Xenorophidae. Kellogg [8] offered no comment on the affinities of this taxon, aside from reiterating Leidy's [20] uncertainty over its status as a "squalodont". Fordyce [21] was the first to recognize xenorophid affinities, noting dental similarities with *Xenorophus*, and suggested that it represented a species of *Xenorophus*. He further identified the tooth as perhaps the P1 or P2. Subsequent finds indicate that the specimen belongs to *Albertocetus meffordorum* or perhaps a new species of *Albertocetus* represented by several skulls (ChM PV 4834, 8680, 8819, 9641), and that the two alveoli and tooth instead represent PC4–6. Dooley [22] noted that while Leidy [20] indicated that the holotype was at ANSP, he provided no number, and noted that "Gillette (1975) and Spamer et al. (1995) did not list it among the academy's collections" and further noted that he could not locate the specimen either. All of Fordyce's [21] observations only concern features visible in the single illustration, and it is unclear whether or not the specimen was at ANSP at the time of Fordyce's postdoctoral research. The type and only specimen of "*Squalodon*" *pelagius* is presumed lost. However, further study of small xenorophids with smooth carinae on anterior postcanines may be able to establish synonymy; the specimen is similar to *Albertocetus*, *Cotylocara*, and *Echovenator*.

Archaeodelphis patrius was named by Allen [23] based on a puzzling small skull. Allen [23] recognized its odontocete affinities, but later authors sometimes considered it to be an early mysticete [24]. More recently, it has been interpreted as a xenorophid [4,5,9,25]. The holotype skull was rediscovered in the early 20th century in the collections of MCZ without corresponding data [23], and its provenance is unknown and the source of much speculation. However, adhering matrix suggests derivation from the Tiger Leap Formation (=Edisto Formation, e.g., [26]: Figure 2) according to Weems (in [27]). The only other vertebrate fossils from the Tiger Leap Formation are the entelodont *Daeodon mento* and the equid *Anchippus texanus* [28]; however, in both cases, this inference is based on matrix adhering to the specimen and not collection records. Allen [23] speculated that *Archaeodelphis* was studied by Louis Agassiz in the 1850s while preparing a never-completed manuscript on "*Phocodon*". Uhen et al. [27] concluded that the Charleston area was the most likely origin of *Archaeodelphis*, since abundant Oligocene odontocetes have been collected and

reported from the area, whereas few to none are known anywhere else along the Gulf and Atlantic coastal plains. If the Agassiz connection mentioned by Allen [23] holds merit, it is worth noting that Agassiz also examined other specimens from Charleston, including the now-lost holotype of *Agorophius pygmaeus* and the *Simocetus*-like rostrum (ChM PV 1302) referred to *Agorophius* by early workers [21]. We agree with Uhen et al. [27] that *Archaeodelphis* likely originated from the Charleston area, but note that, of the many dozens of archaic odontocete skulls found in the Ashley Formation since the 1970s, none have been discovered that could be referable to *Archaeodelphis*. We also view its origin from the Tiger Leap Formation skeptically because exposures of this formation are exceedingly rare, and we are unaware of any vertebrate fossils being recovered from such exposures.

Xenorophus sloanii (frequently incorrectly spelled *sloani*; e.g., [4,5,9,17,18,27,29]) was named by Kellogg [8] based on of a small partial skull (USNM 11049) with the interorbital region, most of the rostrum, and several in situ teeth, collected on an unknown date prior to 1923 from man-made exposures of the Ashley Formation within a marl pit owned by the Ingleside Mining Company, about 100 m east of the Woodstock Rail Station in the vicinity of Ladson, South Carolina. Kellogg's [8] account is surprisingly brief, but, in our opinion, he clearly considered *Xenorophus* to be an archaic odontocete (*contra* [9]: 435), referring to it as a "dolphin" and making comparisons only with other archaic odontocetes like *Archaeodelphis*, *Agorophius*, and *Squalodon*. Kellogg [8] noted the double-rooted and "serrated" teeth, the unusually enlarged lacrimal, uniquely expanded nasal process of the premaxilla, which made up most of the supraorbital process, and the plesiomorphic retention of an intertemporal constriction. Kellogg's [8] study is otherwise restricted to a description. Kellogg [8] did not provide an etymology, but it is possible that Kellogg intended to mean "bearer of strangeness"—xenos + -phor, though, because the name *Xenophora* is preoccupied by the carrier shell snail, perhaps Kellogg deliberately altered the spelling [9]. That same year, Miller [30] assigned *Xenorophus* to the family Agorophiidae (now recognized as a taxonomic wastebasket), followed later by Kellogg [31]. Later authors including Whitmore and Sanders [24] and Fordyce [21] did not consider *Agorophius* and *Xenorophus* to be terribly similar despite both being Oligocene odontocetes and concluded these genera likely belong in separate families.

For nearly fifty years after the publication of *Xenorophus sloanii*, no new specimens of Xenorophidae were recovered. Many early cetacean discoveries in the Charleston area prior to the U.S. Civil War were made on plantations or in tidal exposures of the Ashley Formation, but, in the late 19th century, many finds were discovered during mining and dredging of the poorly defined "Ashley Phosphate Beds" [28,32–34]. These finds chiefly consisted of fragmentary specimens of uncertain stratigraphic origin. Extensive field studies undertaken by Albert Sanders of the Charleston Museum began uncovering a wealth of new fossil cetaceans in the Charleston area, beginning with a three-year long grid excavation from 1970 to 1972 near Chandler Bridge Creek in the vicinity of Summerville, South Carolina [24,35]. Sanders' excavation and a concurrent construction boom resulted in many new manmade exposures. This permitted the detailed stratigraphic study of cetacean-bearing Oligocene strata in the region for the first time (e.g., [35,36]), and the discovery of new fossils clarified the identification, morphology, and stratigraphic origins of many fossil cetaceans found during late 19th century phosphate mining [24,37,38]. The Chandler Bridge excavation led to the recognition of a new noncalcareous stratigraphic unit overlying the Ashley Formation [35], which was later named the Chandler Bridge Formation [36]. This excavation produced a skull initially identified as *Xenorophus sloanii* by Whitmore and Sanders ([24]: Figure 1a) in their review of Oligocene whales. However, this specimen is now considered to be a more derived xenorophid closer in morphology to *Cotylocara* [5,39]. Also discovered during the excavation were a skull and skeleton of the giant dolphin "Genus Y" (ChM PV 2764, *Ankylorhiza* sp.; also ChM PV 6083), several partial skulls of "Genus X" (possible waipatiid and/or agorophiid grade odontocetes ChM PV 2754, 2755, 2756, 2759, 6036), another agorophiid-grade taxon with highly cuspate teeth (ChM PV 2761), and several skulls of smaller xenorophids now identifiable as *Echovenator*

or *Echovenator sandersi* (ChM GPV 542, ChM PV 2776) and numerous additional partial skulls (ChM PV 487, 498, 499) of the aforementioned *Cotylocara*-like xenorophid previously identified by Whitmore and Sanders [24] as *Xenorophus sloanii*. While mostly unpublished, these early finds led Sanders to recognize the high diversity of Chandler Bridge Formation odontocetes in the 1970s [24,35]. Later finds would typically be made at other construction sites, and in the 1980s and 1990s, increasingly by private collectors. By the late 1990s, some specimens made their way into the commercial fossil trade. In a meeting abstract, Sanders [39] noted that there were at least three xenorophid species and that a new family was needed to contain them.

A cladistic study of cetacean relationships by Geisler and Sanders [10] was the first to include numerous Oligocene cetaceans assigned to stem Mysticeti and stem Odontoceti, and it included five undescribed xenorophid specimens in addition to *X. sloanii* and *Archaeodelphis*. These authors referred a number of skulls to *Xenorophus*, including ChM PV 4823 and ChM PV 5022. This was the first study to identify a clade uniting *X. sloanii* and several other stem odontocetes, critically positioned as the earliest diverging branch within the Odontoceti. Uhen [9] named a new genus and species, *Albertocetus meffordorum*, based on a well-preserved braincase with tympanoperiotics from the upper Oligocene Belgrade Formation of eastern North Carolina, collected as a loose concretion from Onslow Beach. While similar in size to the holotype of *X. sloanii*, the *Albertocetus* holotype is approximately 66–69% the size of the largest *X. sloanii* specimens reported herein (based on the postorbital width of CCNHM 1077), and larger than *Archaeodelphis*—and much more similar in overall form to *Xenorophus*, rather than *Archaeodelphis* [9]. The family Xenorophidae was finally named by Uhen [9], in which he included *Xenorophus*, *Archaeodelphis*, and the newly named *Albertocetus meffordorum*.

In a study of cetacean specimens from the Miocene Pungo River Formation and Pliocene Yorktown Formation of the Lee Creek Mine, further north in North Carolina, Whitmore and Kaltenbach ([40]: 188–189) reported an odontocete mandible fragment (USNM 182924) with widely spaced double rooted alveoli and embrasure pits in line with the toothrow, which they speculated might represent a xenorophid. Boessenecker [41] agreed, noting that such mandibular embrasure pits are otherwise unknown amongst stem odontocetes. Boessenecker [41] further identified an isolated xenorophid bulla (CCNHM 936) from the Pungo River Formation, and speculated that such specimens perhaps represent reworking of Oligocene fossils into the base of the Pungo River Formation or perhaps the survival of these archaic taxa into the earliest Miocene. More recent discoveries of xenorophid specimens apparently straddling the Oligocene–Miocene boundary [7] lend support to this latter hypothesis.

A new genus and species of xenorophid, *Cotylocara macei*, was reported by Geisler et al. [4] from the Chandler Bridge Formation, representing a highly derived xenorophid with small teeth and facial fossae. These fossae include antorbital fossae on either side of the bony nares and a deep postnarial fossa between the nasals and parietals that is excavated into the frontal bones. Geisler et al. [4] proposed that these fossae housed facial sinuses associated with ultrasonic sound production, with the antorbital fossa associated with a ventrolateral expansion of the premaxillary sinus fossa and the postnarial fossa associated with the inferior vestibule. They further suggested that the ability to produce ultrasonic sound emerged very early in odontocete evolution. Unfortunately, the inner ear of *Cotylocara* was not well preserved, and testing their hypothesis would require study of the cochlea of other xenorophids. An isolated periotic of an unidentified xenorophid dolphin was reported by Park et al. [19] from Onslow Beach, likely derived from the Belgrade Formation, and CT analysis indicated that this unidentified xenorophid was capable of high frequency hearing. Subsequently, a well-preserved skull with tympanoperiotics and a mandible was named *Echovenator sandersi* by Churchill et al. [3]. *Echovenator sandersi* is similar in size to *Albertocetus meffordorum*, but possesses more derived features such as a postnarial fossa, making it more similar to *Cotylocara*. CT analysis of the cochlea similarly found that it was capable of high frequency hearing (based on several features

including a long secondar bony lamina, narrow laminar gap, loosely coiled cochlea, and similar basal ratio to extant odontocetes) and thus likely could hear ultrasonic frequency sounds [3], confirming the hypothesis of Geisler et al. [4] that xenorophids were capable of echolocating. The periotic reported by Park et al. [19] was subsequently reidentified as *Echovenator* sp. by Boessenecker et al. [1]. More recently, the age of the Belgrade Formation was summarized as likely straddling the Oligo-Miocene boundary, and, in addition to *Albertocetus* and *Echovenator*, earbones of *Cotylocara* and *Xenorophus* (and many other Oligo-Miocene odontocetes) were also reported by Boessenecker [7], and their young age suggests xenorophids may have briefly persisted into the earliest Miocene.

In their study reporting the new *Simocetus*-like odontocete, *Ashleycetus planicapitis* from the Ashley Formation, Sanders and Geisler [5] provided a new diagnosis of the family Xenorophidae and provided an apomorphy-based definition of the clade, citing the unique morphology of the nasal process of the premaxilla. As defined by Uhen [9], the "Xenorophidae includes all other genera more closely related to *Xenorophus* than to any other Odontocete". According to Sanders and Geisler [5], this definition is imprecise and that *Archaeodelphis* critically lacks the unique premaxilla outlined earlier [39], and Sanders and Geisler [5] suggested that it may represent a separate family-level clade. The new definition of the clade based on this key synapomorphy excludes taxa such as *Archaeodelphis* (e.g., [9]) and *Olympicetus* (e.g., [25]), but includes *Xenorophus*, *Albertocetus*, *Cotylocara*, *Echovenator*, *Inermorostrum*, and several undescribed taxa coded into cladistic analyses (ChM PV 4746, 4834, 5711, 2758; [2–4,10]).

These authors also provided a revised diagnosis of *Xenorophus* (which is revised again in this study; see 5.1.3. Amended Diagnosis of Genus). These authors also considered most recently collected specimens of *Xenorophus* from the Ashley (ChM PV 5022) and Chandler Bridge formations (ChM PV 4823) to represent a different species from *X. sloanii* (e.g., [5]: 1), and highlighted that ChM PV 2758, previously referred to *Xenorophus* by Whitmore and Sanders [24], appears to represent an unnamed genus and species of xenorophid. By comparison with ChM PV 4823 (*Xenorophus* sp.), Sanders and Geisler [5] indicated that the anteriormost alveolus in the *Xenorophus sloanii* holotype represents the canine, indicating that the holotype had nine upper postcanine teeth. Phylogenetic analysis confirmed Xenorophidae as one of the earliest diverging odontocete clades, but found support for *Ashleycetus* as the earliest branch in some analyses. Subsequent analyses by Velez-Juarbe [25], after inclusion of the newly named *Simocetus*-like dolphin *Olympicetus avitus* from the Pysht Formation of Washington, resulted in *Ashleycetus* forming a clade with Xenorophidae (which [25], included within Xenorophidae, despite it lacking the apomorphy in the revised definition of the clade by [5]).

Additional specimens of *Albertocetus meffordorum*, including a well-preserved braincase and a partial skull with tympanoperiotics and scattered vertebrae from throughout the column, were reported by Boessenecker et al. [1] from the Ashley Formation of South Carolina. These specimens permitted preliminary observations of ontogenetic changes in xenorophid dolphins, and the vertebral morphology confirms that they were 'pattern 1' swimmers (e.g., [42]) using dorsoventral undulation throughout the lumbocaudal series and that it likely did not possess a narrow caudal peduncle (later confirmed in the later diverging odontocete *Ankylorhiza*; [37]), suggesting independent evolution of this feature in odontocetes and mysticetes. CT analysis of the endocast permitted EQ to be calculated, finding that xenorophids had relatively large brains (albeit smaller than delphinoids), therefore representing a profound leap in maximum cetacean EQ over a four million year period across the Eocene–Oligocene boundary (though the basilosaurid–Neoceti divergence was likely earlier; e.g., [43–45]).

The bizarre xenorophid *Inermorostrum xenops* was named from the Ashley Formation; *Inermorostrum* was a dwarf (estimated 1.2 m body length, the smallest cetacean ever), short-snouted, toothless dolphin [2]. This surprising feeding morphology and small body size is emblematic of the rapid diversification of Neoceti, paralleling dwarfism and unusual feeding morphology in Oligocene mysticetes [46–49]. More critically, *Inermorostrum* in-

dicates that Xenorophidae, and other early odontocete lineages, were capable of suction feeding. The highly variable tooth count, body size, and rostrum length within Xenorophidae contrasts quite strongly with the more conservative ancestral basilosaurid archaeocetes. Variation in rostrum length and loss of tooth occlusion seems to correspond closely with the initial evolution of polydonty [1].

In an analysis of cranial telescoping, Churchill et al. [50] proposed that, within the Xenorophidae, there is a parallel trend in posterior migration of rostral elements, following the trend from the base of the clade (*Archaeodelphis*: premaxilla terminates at the anterior margin of orbit), a more generalized member (*Xenorophus*: premaxilla terminates posterior to orbit), and a derived member (*Cotylocara*: premaxilla terminates far posterior to orbits). This study, which used comparative methods applied to 3D geometric morphometrics, was able to corroborate the qualitative observations of convergent xenorophid telescoping presented by Geisler et al. [4].

A fragmentary juvenile cranium of an *Olympicetus*-like odontocete from the Oligocene Pysht Formation of Washington was studied by Racicot et al. [51] and included in an expanded dataset of cetacean auditory anatomy, and found that this specimen plots in a region of morphospace close to protocetids, driven primarily by a more tightly coiled cochlea resembling archaeocete whales. Because this cf. *Olympicetus* specimen is on a more crownward branch of the odontocete stem than xenorophids, it implied that echolocation either evolved twice or was perhaps lost early on by some odontocetes. Parallel development of echolocation in Xenorophidae and the rest of stem Odontoceti is consistent with the finding of a parallel trend in cranial telescoping amongst xenorophids [50].

Other recent studies of cranial evolution in odontocetes have touched on Xenorophidae. Coombs et al. [52] indicated that a major shift in odontocete skull asymmetry occurs within the clade, likely corresponding to the initial evolution of echolocation [3,4,19]. In a study of orbit size evolution within odontocetes, Churchill and Baltz [53] found that xenorophids have a relatively similar orbit size to basilosaurid whales, indicating minimal evolution of vision across the basilosaurid–odontocete transition. Owing to their already derived cranial morphology, basal position within Odontoceti, and rapid divergence from Basilosauridae, Coombs et al. [54] found some of the highest evolutionary rates of skull evolution amongst cetaceans within the Xenorophidae, part of a rapid radiation of early Neoceti.

3. Geologic Background

The holotype specimen of *Xenorophus sloanii* (USNM 11049) was reported by Earl Sloan (in [8]) to have been collected from a marl pit owned and operated by the Ingleside Mining Company adjacent to Woodstock Station (Dorchester County, South Carolina), along with the holotype skull of the sea turtle *Carolinachelys wilsoni* and the paratype femur of the same species (subsequently reassigned to *Procolpochelys charlestonensis* by [55]. The *X. sloanii* type was collected about "15 feet below the top of the [Ashley Formation]" [8]. Since then, the Ashley Formation has been subdivided into three members of slightly different age [26]; in the vicinity, both the Givhan's Ferry Member (uppermost) and underlying Runnymede Marl Member have been mapped at depth. The nearest core sample ([26]: Figures 11 and 12) indicates that the Runnymede–Givhan's Ferry member contact is located about 22 feet below the ground surface.

Which member of the Ashley Formation did the *Xenorophus sloanii* holotype originate from? Cooke [56] examined the marl pit 20–30 years after collection of the specimen and statements like "marl pit at Woodstock, which was 76 feet deep in 1917" ([56]: 83) and "a pit said to be 76 feet deep" ([56]: 85) indicates that the pit was partially filled in by the time he examined it. Cooke [56] indicated that the Ashley Formation resembled "bed 2" of his measured section of a marl pit at Lambs 9 km to the south, which is a brownish "granular marl" (calcarenite) with a basal phosphate lag overlying a light gray finer-grained 'marl'. This matches field observations of the Ashley Formation at a construction site near Ladson SC, with the upper unit corresponding to the Givhan's Ferry Member and the lower unit corresponding to the Runnymede Marl, and broadly matches descriptions of

the intraformational contact by Weems et al. [26]. Cooke [56] further indicated that no analogous intraformational contact existed when he visited Woodstock Station, which would suggest that the *X. sloanii* type originated from the Givhan's Ferry Member of the Ashley Formation. However, it is unclear how filled in the marl pit was at the time. Sloan (in [8]: 2) states that an upper "drab green" marl is present and, while not explicitly stating that both the lower and upper units are exposed within the marl pit, nor explicitly stating which unit the type originated from, this strongly implies it was collected from the upper stratum by only describing the lithology of that unit at Woodstock Station. We therefore conclude that *Xenorophus sloanii* was collected from the upper olive green calcarenite and, thus, likely from the Givhan's Ferry Member of the Ashley. This seems to be corroborated by Weems et al. [57], who reported that, at a depth of 15 feet in an auger hole at the south end of the former Woodstock Station marl pit, the Ashley Formation consisted of fine-grained light-brown to olive-green calcarenite. While Weems et al. [57] only described the uppermost 10 feet of the Ashley and the holotype was collected from about 15 feet below, the description matches that of Sloan (in [8]) and Cooke [56], all pointing towards origination from the Givhan's Ferry Member of the Ashley Formation.

CCNHM 1077, ChM PV 5022, and CCNHM 7677 were all collected from the Ashley Formation in the vicinity of Crowfield Plantation subdivision, and CCNHM 104, 168, and 5995 were collected in the vicinity of Sawmill Branch Canal and the Ashley River southwest of Summerville, SC; in this general region, the contact between the Runnymede Marl Member and the Givhan's Ferry Member of the Ashley Formation is near ground level [26], and, thus, these specimens conceivably could have been collected from either member. Examination of associated matrix from these two general localities revealed olive to light brown quartzose phosphatic calcarenite from the Ashley Formation in Sawmill Branch canal, suggesting derivation from the Givhan's Ferry Member; we confirmed that CCNHM 303, a partial skeleton of *Albertocetus meffordorum* from the same locality, shares this matrix as well. Specimens CCNHM 1077 from Crowfield Plantation and ChM PV 5022 from Goose Creek revealed light yellowy tan massive calcisiltite, seemingly lacking quartz or phosphate grains; this lithology instead suggests derivation from the Runnymede Marl member of the Ashley Formation.

ChM PV 5020, on the other hand, was collected ex situ from spoil piles along the bank of the Wando River. In this area, the Givhan's Ferry Member is completely eroded away [26] and this specimen is clearly from the Runnymede Marl member, along with other cetaceans [1,2,48].

The Ashley Formation (Figure 1B,C) consists of 10–25 m of tan to olive, sparsely fossiliferous, massively bedded calcarenite and unconformably overlies the uppermost Eocene Harleyville Formation. The Ashley Formation contains several intraformational phosphatic bonebeds which mark boundaries between three different members by Weems et al. [26]: the Gettysville Member (only recognized in the Clubhouse Crossroads Core, Dorchester County, South Carolina), the completely calcareous Runnymede Marl Member, and the more quartzose Givhan's Ferry Member. The Ashley Formation preserves calcareous marine invertebrates including the gastropod *Epitonium* sp., the oyster *Cubitostrea* sp., and the barnacle *Concavus* sp., though little formal study of the marine invertebrate assemblage has been published [58]. Fossil vertebrates from the Ashley Formation include sharks [59], bony fish [60], sea turtles [55,61–63], sea birds (Boessenecker, pers. obs.), the most archaic known dolphin *Ashleycetus* [5], xenorophid dolphins like *Xenorophus*, *Albertocetus*, and *Inermorostrum* (Figure 1C; [1,2,8]), waipatiid-grade dolphins like *Ediscetus* [32], agorophiid-grade dolphins including *Agorophius* [21,38,64] and the gigantic macrophagous dolphin *Ankylorhiza* [37,65], the toothed baleen whale *Coronodon* [46,48], the eomysticetid whale *Micromysticetus* [66,67], and a number of sea cows, including *Crenatosiren olseni*, *Stegosiren macei*, *Priscosiren atlantica*, and possibly *Dioplotherium manigaulti* [68–71]. Pervasive bioturbation, phosphatic bonebeds, and fine- to very-fine-grained lithology suggest deposition in middle shelf settings. 87Sr/86Sr isotope ratios from the Runnymede Marl Member indicate an age of 29.0 Ma, and ratios from the overlying Givhan's Ferry Member indicate an age of

28.75–28.43 Ma [26]. The calcareous nannoplankton of zone NP24 [67] indicate an age of 28.73–26.57 Ma [72].

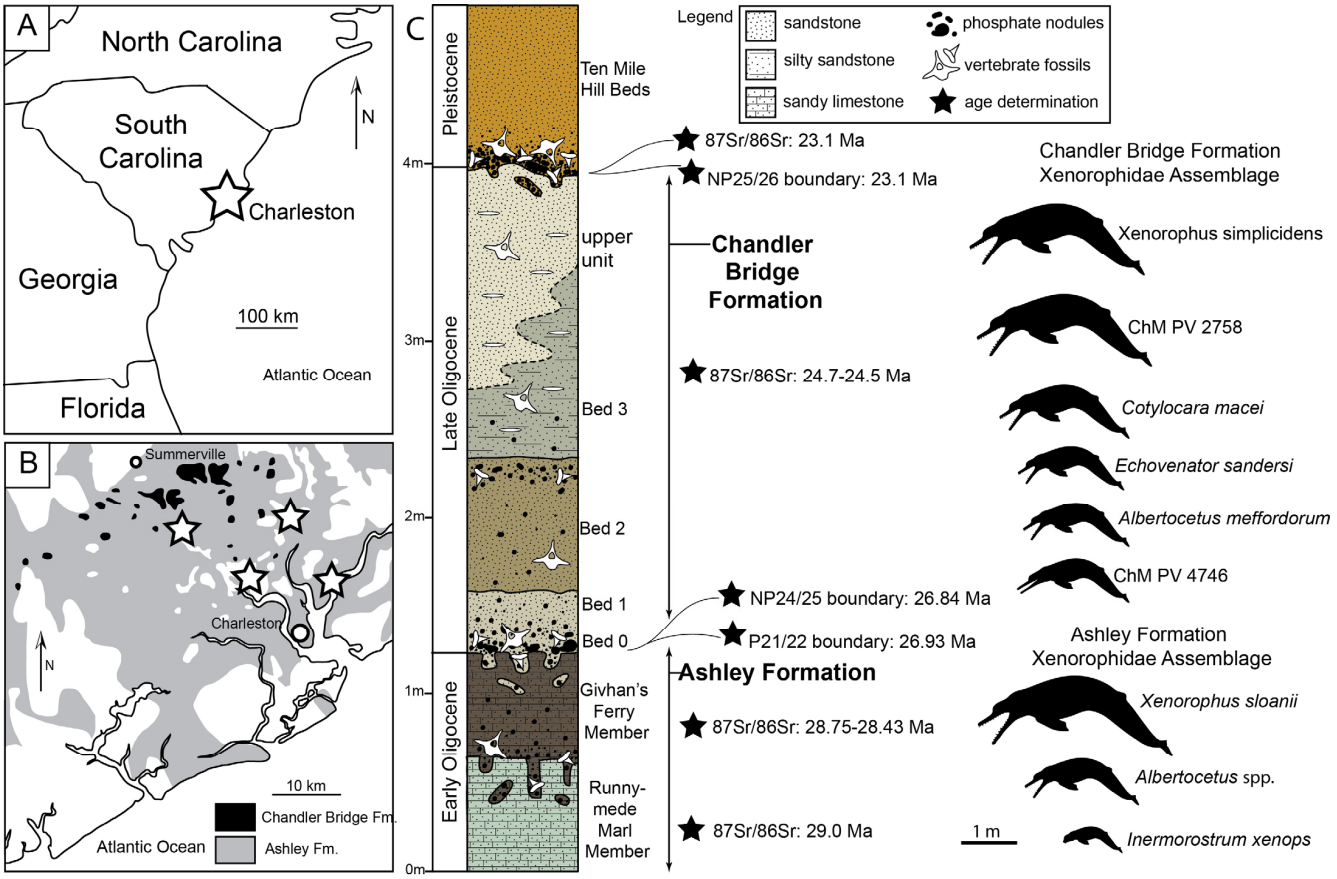


Figure 1. Geographic and geologic context of *Xenorophus* fossils from South Carolina. (**A**) Map of South Carolina. (**B**) Simplified geologic map of Oligocene rocks within the Charleston Embayment. (**C**) Stratigraphic column of the Ashley and Chandler Bridge formations of South Carolina, showing stratigraphic position of age determinations (stars) and silhouettes of the xenorophid assemblage known from each stratum. Modified from Boessenecker et al. ([73]: Figure 1).

The Chandler Bridge Formation (Figure 1B,C) unconformably overlies the Ashley Formation and consists of unconsolidated siltstone and sandstone. The Chandler Bridge Formation is patchy and, in many places, was either never deposited or eroded away (Figure 1B); where present, it is typically 20–70 cm in thickness, but can range up to 3–4 m thick in rare occurrences, such as in the vicinity of Ladson, South Carolina [74]. The Chandler Bridge Formation consists of four beds, numbered Bed 0 through Bed 3, interpreted as reflecting open marine conditions and shoaling into estuarine deposits based on lithology and pollen [75], though the shark, ray, and fish fauna is suggestive of open marine settings throughout deposition [76]. A rich marine vertebrate assemblage has been reported from the Chandler Bridge Formation, including a multitude of sharks [59,76], bony fish [60,74], sea turtles [55,61,63], sea birds [77], xenorophid dolphins including *Cotylocara*, *Echovenator*, and other unpublished forms (Figure 1C; [3,4,24]), agorophiid-grade dolphins including *Agorophius* [38] and the gigantic *Ankylorhiza* [37], toothed baleen whales *Coronodon* spp. [46], the eomysticetid whale *Eomysticetus* [78], and several sea cows including *Metaxytherium albifontanum*, and *Crenatosiren olseni* [69,79]. The Chandler Bridge Formation was formerly considered to only be slightly younger than the Ashley Formation, separated perhaps only by a million years in time [36], yet more recent dating using 87Sr/86Sr ratios from oysters indicate a much younger age of 24.7–24.5 Ma [26]. Owing to how tight these dates are, an 87Sr/86Sr ratio dating to 23.5 Ma from the overlying Edisto

Formation [26] has often been conservatively used as a minimum date for the Chandler Bridge Formation (e.g., [66]: 456–458).

All specimens of *Xenorophus simplicidens* were collected from the Chandler Bridge Formation. Only the holotype and paratype specimens, CCNHM 8720 and ChM PV 4823, have bed-level data. The holotype specimen is embedded in matrix consisting of silty massively bedded fine-grained light-brown to tan sandstone with abundant woody debris, phosphatic pebbles, terrigenous clasts, and shark teeth indicating derivation from Bed 2. Paratype specimen ChM PV 4823 was collected from an unusual deposit of the Chandler Bridge Formation, referred to as Bed 1A by Albright et al. [28], along the bank of the Edisto River, separated far from typical exposures of the unit. This unit warrants further field study.

4. Materials and Methods

4.1. Descriptive Methods and Anatomical Terminology

Anatomical terminology follows Mead and Fordyce [80] with some additions and modifications from Boessenecker and Fordyce [81] and Boessenecker et al. [1]. Photographs were taken with a Canon Rebel Eos T5 with an 18–55 mm zoom lens or 100 mm f/2.8 macro lens. Measurements were recorded using large calipers to the nearest millimeter and digital calipers for smaller (<30 cm) measurements to the nearest tenth of a millimeter; measurements exceeding 60 cm (i.e., CBL) were recorded using metric cloth tape measure.

4.2. Comparative Analyses of Orbit, Tooth, Temporal Fossa Size, and RPI

Measurements for these functionally informative metrics were taken using photographs from the published literature through ImageJ 1.50i as well as direct measurements of Oligocene specimens from Charleston, SC (CCNHM, ChM collections). Scatterplots were produced in PAST 4.13 [82].

4.3. Ontogeny

We assessed the relative ontogenetic status of *Xenorophus* specimens using the criteria of Perrin [83] and assigned each specimen to his age classes I through VI.

4.4. Phylogenetic Methods

We conducted a specimen-level-based phylogenetic analysis to test the monophyly of the genus *Xenorophus*, to determine if there is evidence for multiple species within this genus, and to determine where, within Xenorophidae, *Xenorophus* is placed. To this end, we started with a version of the matrix of Bianucci et al. [84] that includes some, but not all delphinids those authors sampled. These delphinids were excluded because they are not particularly relevant to basal odontocete relationships; matrix editing was carried out using Mesquite 3.81 [85]. To that matrix, we added 16 specimen-level OTUs, including specimens that can be referred to, or compare favorably with, *Xenorophus* (n = 9), *Albertocetus* (n = 8), and *Echovenator* (n = 2). We also retained other unnamed xenorophids that have been included in previous phylogenetic analyses at the specimen level (i.e., ChM PV4746, PV2758). In addition, we added 20 characters that showed particular promise for resolving relationships within Xenorophidae. All totaled, the final matrix has 141 OTUs (operational taxonomic units) coded for 394 morphological characters (Supplementary Files S1 and S2).

We assessed phylogenetic relationships using parsimony analyses, as implemented in the computer application TNT v1.5 [86,87]. The signal from molecular data, as reported by McGowen et al. [88], was included by enforcing a backbone constraint that specified the locations of all extant taxa; extinct taxa were identified as "floaters" and were positioned based on the morphological dataset. To find the most parsimonious tree (MPT), we used the default settings under a "New Technology search", except the settings were changed so that the search terminated after the shortest tree was found 1000, not 100, times. Often, analyses find multiple MPT's, but with the present dataset, only a single MPT was obtained (see *5.3*

Results of Phylogenetic Analysis). To assess nodal support, a bootstrap search was conducted with replacement. Additional changes to default settings included, reporting of absolute frequencies, traditional search conducted for each bootstrap replicate; each traditional search included 100 random taxon additional sequences, 20 trees were saved each time, and, then, as a cutoff, we used all groups that occurred in the single most parsimonious tree for the original, unaltered dataset. The last setting allowed us to acquire bootstrap values for all nodes in the MPT, including those below 50%. Ancestral Character State Reconstruction was conducted in Mesquite 3.81 [85] using parsimony.

5. Results

5.1. Systematic Paleontology

Mammalia Linneaus,1758 [89]
Cetacea Brisson, 1762 [90]
Odontoceti Flower, 1867 [91]
Xenorophidae Uhen, 2008 [9]

5.1.1. Definition

See Sanders and Geisler [5] for a definition of Xenorophidae.

5.1.2. Diagnosis

Xenorophidae is diagnosed nine synapomorphies, including ventral exposure of lacrimal and jugal being intermediate in size (80:1), posterior border of supraorbital process extending posteromedially from its lateral end (85:0), lateral side of postorbital process facing laterally instead of dorsolaterally (89:1), premaxillae dorsally separated by a gap that is between 32% and 56% the width of the external nares (94:1), premaxilla expanded laterally over the supraorbital process of the frontal and lying between that bone and the maxilla (106:1), premaxilla terminating over the posterior half of orbit (107:3), anterior edge of nasal terminating over anterior half of orbit (114:4), pachyostosis of premaxilla (125:1), and basioccipital crests forming a 45–68° angle (240:2). Character 106 is the basis of the definition of this family, and also shows no homoplasy on our most parsimonious trees. Similarly, character 85 state 0 and character 125 state 1 have only evolved once. The other character states evolved convergently in non-xenorophids as follows: character 80 state 1 occurs in ChM PV2761, PV4802, *Agorophius pygmaeus*, *Squalodon calvertensis*, and most crown odontocetes; character 89 state 1 also occurs in many crown odontocetes; character 94 state 1 occurs in *Phoberodon arctirostris* and most crown odontocetes; character 107 state 3 occurs in several Oligocene odontocetes including ChM PV5852, *Simocetus rayi*, and *Papahu taitapu*; character 114 state 4 also occurs in ChM PV5852, PV4178, and *Ankylorhiza*; and character 240 state 2 also occurs in *Simocetus rayi*, *Ankylorhiza tiedemani*, *Waipatia maerewhenua, Papahu taitapu*, and *Ediscetus osbornei*. All xenorophids, except for the unnamed taxon represented by ChM PV4746, are also characterized by the following derived characters, including lacrimal expanded dorsally and posteriorly over the supraorbital process of the frontal, lateral to the maxilla and premaxilla (76:2); presence of bilateral antorbital basins (92:1); ventral window in supraorbital process of frontal that exposes overlying maxilla and premaxilla (174:1); and posterior end of premaxilla widening abruptly (390:3). Xenorophids are also characterized by the following plesiomorphic characters, which are atypical of odontocetes, including a flat palate (but not ChM PV4746), absence of a dorsal infraorbital foramen on the supraorbital process, absence of an inflection of the premaxilla that separates a posteromedial splint from a posterolateral plate (but not in ChM PV4746), supraoccipital alone forming the vertex (but not in ChM PV4746), alisphenoid/squamosal suture is positioned anterior to foramen ovale, and lateral side of periotic having a sulcus for the capsuloparietal vein.

Xenorophus Kellogg, 1923 [8]

5.1.3. Amended Diagnosis of Genus

A large xenorophid dolphin with adult condylobasal length of 70–75 cm and bizygomatic width of 26–30 cm, and possessing the following synapomorphies of Xenorophidae, and the xenorophid clade excluding ChM PV 4746: nasal process of premaxilla hypertrophied, dense, expanded over the supraorbital process of the frontal, forming longitudinal paranaris crest adjacent to nares, and overlain by thin ascending process of maxilla; lacrimal expanded posterodorsally and covering most of anterolateral side of supraorbital process of the frontal; deeply excavated antorbital fossa on the posterior part of the maxilla; maxilla and premaxilla exposed ventrally in a 'frontal window' posterior to postorbital ridge; long bladelike lateral tuberosity of periotic; transversely narrow and bladelike anterior process of periotic; tympanic bulla with deep transverse sulcus giving involucrum a stepped dorsal margin; and primitively retaining a sagittal crest, parietals forming most of braincase, and upper and lower embrasure pits.

Xenorophus is characterized by the following features, to the exclusion of other xenorophids, unless where noted: palatal process of premaxilla extending posteriorly to level of PC3; rectangular/subrectangular nasals with flat dorsal surface (also shared with *Albertocetus*); relatively wide rostrum base (43–50% bizygomatic width); rostrum deviated 1.5–4.7° to the left; triangular apex of the supraoccipital shield (also shared with *Albertocetus*); present but low squamosal prominence; absence of a paranaris and postnarial fossae; nasals with a median furrow; rostrum at level of Pc1 wide (~20% of bizygomatic width; narrower in *Echovenator* and *Cotylocara*, ~15% BZW); asymmetrical and exceptionally large palatines, broadest anteriorly and tapering posteriorly, with right palatine extending further anteriorly than left (shared with *Albertocetus*); basioccipital crest bifurcated by a transverse cleft; periotic with thickened superior ridge bearing transverse striations and delimiting a small, deep, circular suprameatal fossa (shared with *Albertocetus*); proportionally large cheek teeth (5.5–7% of bizygomatic width); 9–10 maxillary teeth (probably 11, but possibly 12 in *Cotylocara*; 9 in *Echovenator*); distance between posterior edge of mandibular condyle and posteriormost tooth 1 cm shorter on left than right; and asymmetrical parapophyses and diapophyses on cervical vertebrae.

Xenorophus simplicidens sp. nov.

Xenorophus n. sp. Sanders, 1996 [39]
Xenorophus sp. Sanders and Geisler, 2015 [5]

Etymology: simplicidens—simplex + dens—meaning simple teeth in Latin, referring to the reduced cingula and smoother enamel of this species. This name was coined by Albert Sanders and conveyed to the second author prior to his passing.

Holotype: CCNHM 8720, a partial skeleton including a nearly complete but crushed skull, right mandible, nearly complete upper and lower dentition, five cervical vertebrae, eight or nine thoracic vertebrae, nine or ten lumbar vertebrae, and at least six ribs, collected in 2017 by Dean Rogers, Everett White, and Joshua Basak from Bed 2 of the Chandler Bridge Formation in the vicinity of North Charleston, Charleston County, South Carolina.

Paratype: ChM PV 4823, a complete cranium including partial left and right periotics and tympanic bullae and three teeth, collected prior to 1986 by Meg Goldchamp from submerged deposits of Bed 1A of the Chandler Bridge Formation in the Edisto River, Colleton or Dorchester County, South Carolina.

Referred Specimens: ChM PV 4822, a partial cranium, collected prior to 1982 by James Malcolm from the Chandler Bridge Formation in the vicinity of North Charleston, Charleston County, South Carolina; ChM PV 4266, a partial cranium with left and right periotics, left tympanic bulla, atlas, and two cervical and six thoracic vertebrae, collected 4/18/1984 by A. Sanders, P.S. Coleman, C. Newton, and A. Newton from the Chandler Bridge Formation in the vicinity of North Charleston, Charleston County, South Carolina.

Locality and Age: All specimens of *Xenorophus simplicidens* were collected from the upper Oligocene Chandler Bridge Formation in the Charleston Embayment, ranging in age from 24.7 to 23.5 Ma [26].

Diagnosis of Species: A large xenorophid dolphin, with approximate adult condylobasal length of 68–74 cm and bizygomatic width of 27–30.8 cm and differing from *Xenorophus sloanii* in possessing anteroposteriorly shorter nasals (16–19% of bizygomatic width vs. 22–29% in *X. sloanii*), nasal process of premaxilla lacking lateral overhanging crest adjacent to bony nares in adult specimens, right antorbital fossa longer than left (left longer than right in *X. sloanii*), rounded anterior margin of bony nares, anteroposteriorly shorter supraorbital process (distance from antorbital notch to posterior edge of supraorbital process 34% of bizygomatic width vs. 43% in *X. sloanii*), slightly narrower nasals with posterior end narrower than bony nares, left and right palatines separated by an anteroposteriorly long median triangular exposure of maxilla, paroccipital processes not extending posterior to occipital condyles, longer median furrow on the tympanic bulla (except ChM PV 4266), fewer teeth with accessory denticles (only on PC 7–9, as opposed to PC 5–9 in *X. sloanii*), fewer accessory denticles per tooth (three distal cusps vs. five in *X. sloanii*; one–three mesial cusps vs. three–four in *X. sloanii*), widespread striated enamel throughout dentition and nodular enamel only present on PC7–9 and less rugose than in *X. sloanii* (nodular enamel on PC5–9).

5.1.4. Description of *Xenorophus simplicidens* sp. nov.

The cranial description of *Xenorophus simplicidens* is restricted to features or regions that differ from *Xenorophus sloanii*; for a comprehensive description of the skull of *Xenorophus*, see the description of *Xenorophus sloanii* below. Much of the dorsal surface of the skull of the holotype (CCNHM 8720) is obscured by matrix and postcranial bones (Figure 2), and parts of the palate are highly fractured (Figure 3); the description is supplemented with observations from the paratype and referred specimens (Figures 4–7), including the braincase (ChM PV 4266, 4822, 4823), rostrum and palate (ChM PV 4823), and basicranium (ChM PV 4266, 4823).

Ontogenetic Status: Specimens were assigned to the growth classes of Perrin [83] based, chiefly, on tooth development, skull suture closure, and closure of vertebral epiphyseal sutures. Additional information, such as nasal length, was also considered.

Class I, II, and III: No specimens of *Xenorophus simplicidens* are assignable to either class I (fetus) or II (neonate).

Class IV: The holotype (CCNHM 8720) and referred specimen ChM PV 4822 represent Class IV, based on slightly smaller size than Class V specimens, no open sutures nor obliterated sutures, more than 75% of the vertebral column with fused epiphyses (CCNHM 8720), and relatively short nasal bones (ChM PV 4822), and light tooth wear (CCNHM 8720).

Class V and VI: Two specimens (ChM PV 4266, 4823) are assigned to class V based on their slightly larger size, all sutures being either strongly mortised (complex zigzag sutures with numerous parallel ridges and grooves, e.g., maxillofrontal, premaxilla–maxilla, nasofrontal, frontoparietal, occipital–parietal sutures) or obliterated, longer nasals than ChM PV 4822, and most vertebral epiphyses fused (though only thoracic and cervical vertebrae are represented in ChM PV 4266). ChM PV 4266 has the most well-developed nuchal crests of any specimen of *Xenorophus simplicidens*, and may represent either Class V or VI.

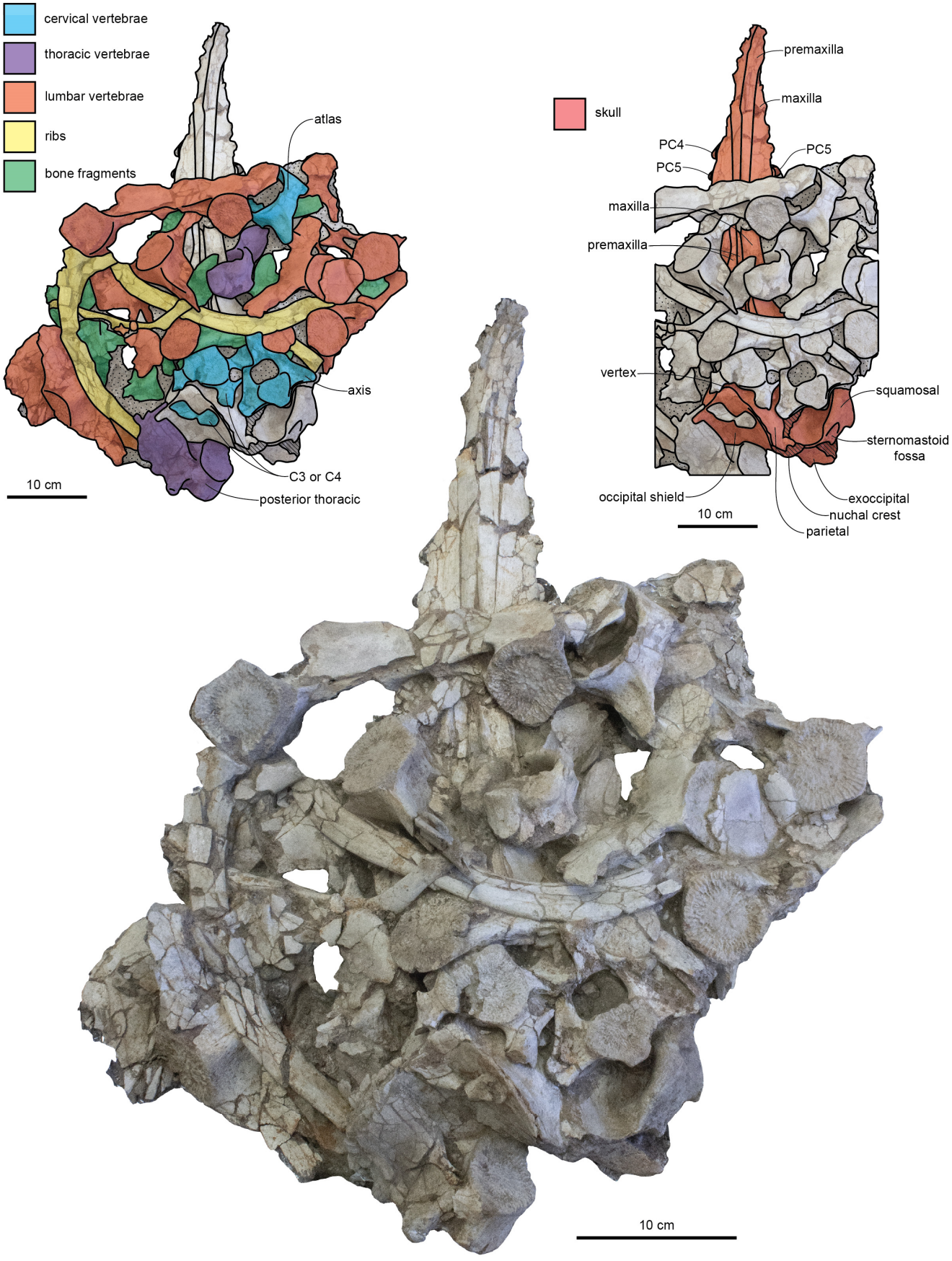


Figure 2. Holotype specimen of *Xenorophus simplicidens*, CCNHM 8720, shown with skull in dorsal view.

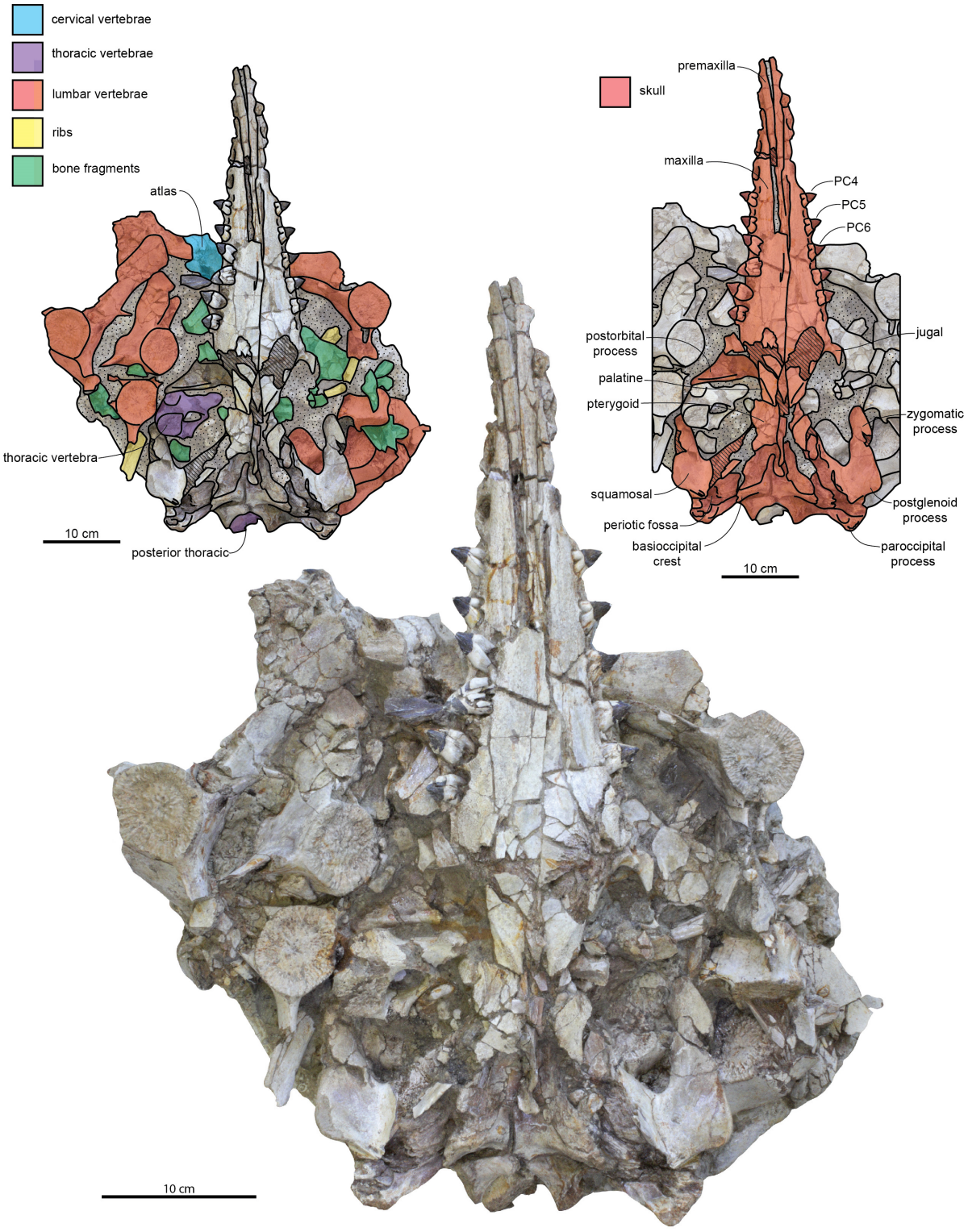


Figure 3. Holotype specimen of *Xenorophus simplicidens*, CCNHM 8720, shown with skull in ventral view.

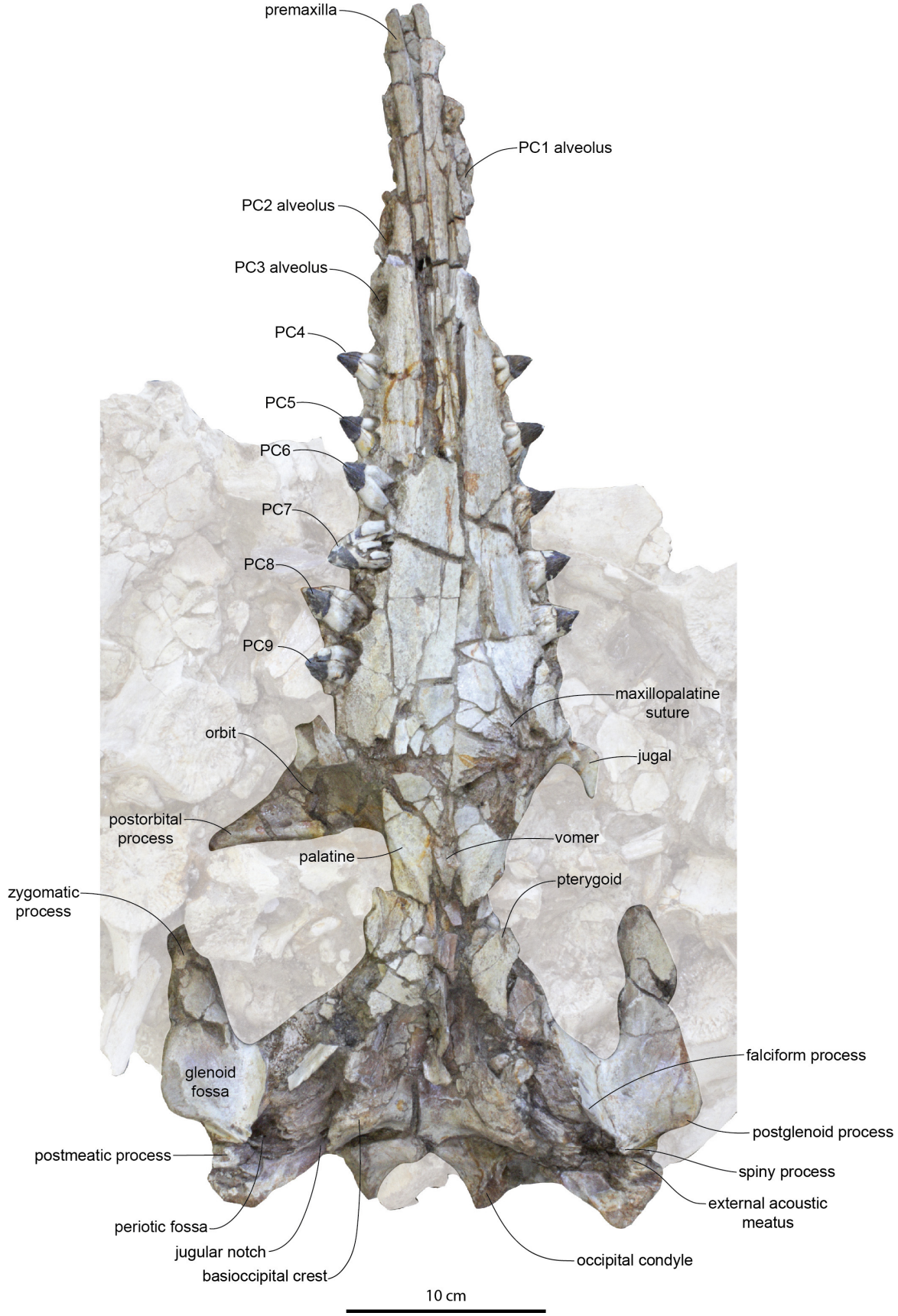


Figure 4. Holotype skull of *Xenorophus simplicidens*, CCNHM 8720, shown with non-cranial material slightly opaque.

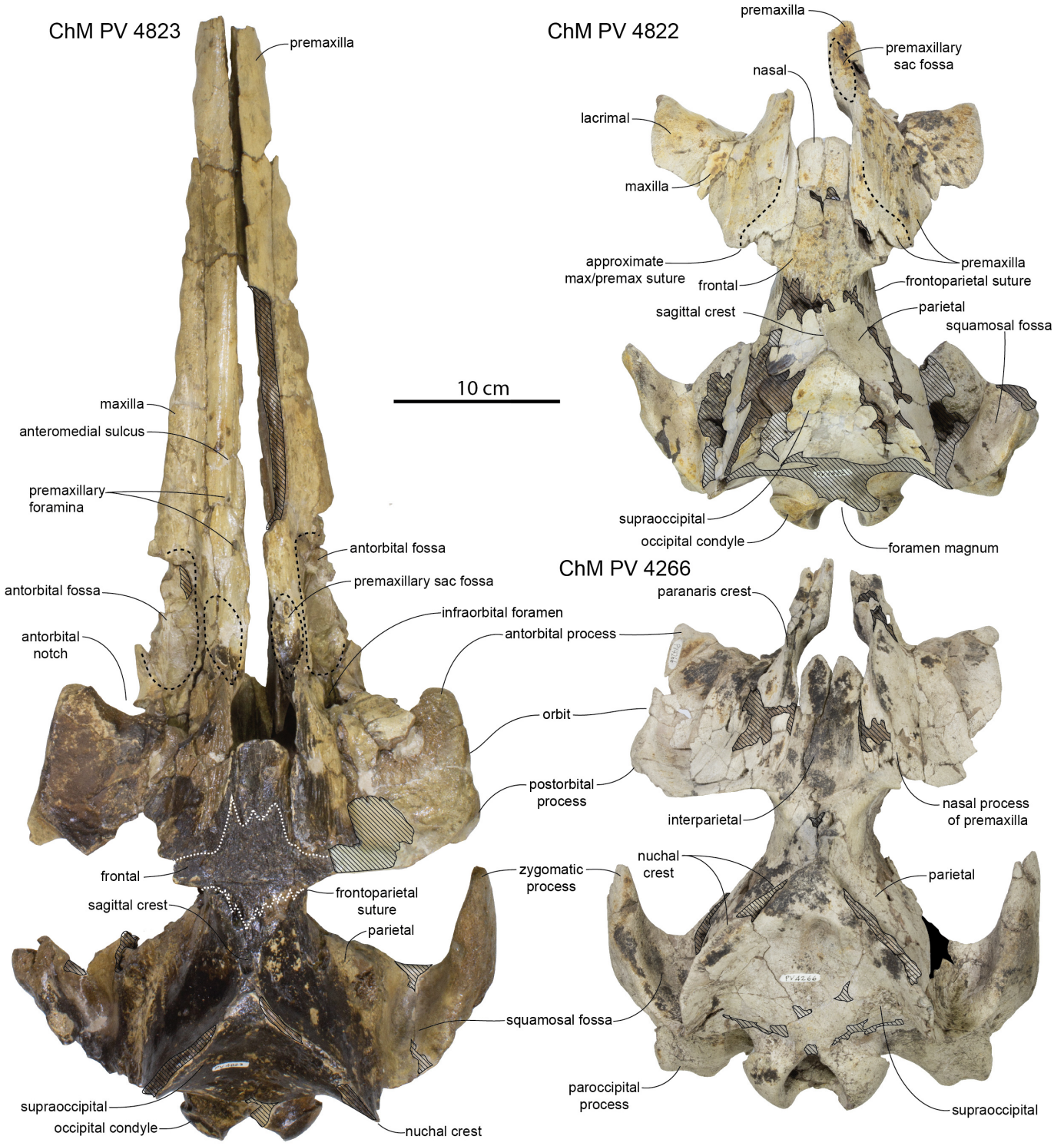


Figure 5. Paratype skull (ChM PV 4823) and referred skulls of *Xenorophus simplicidens* in dorsal view.

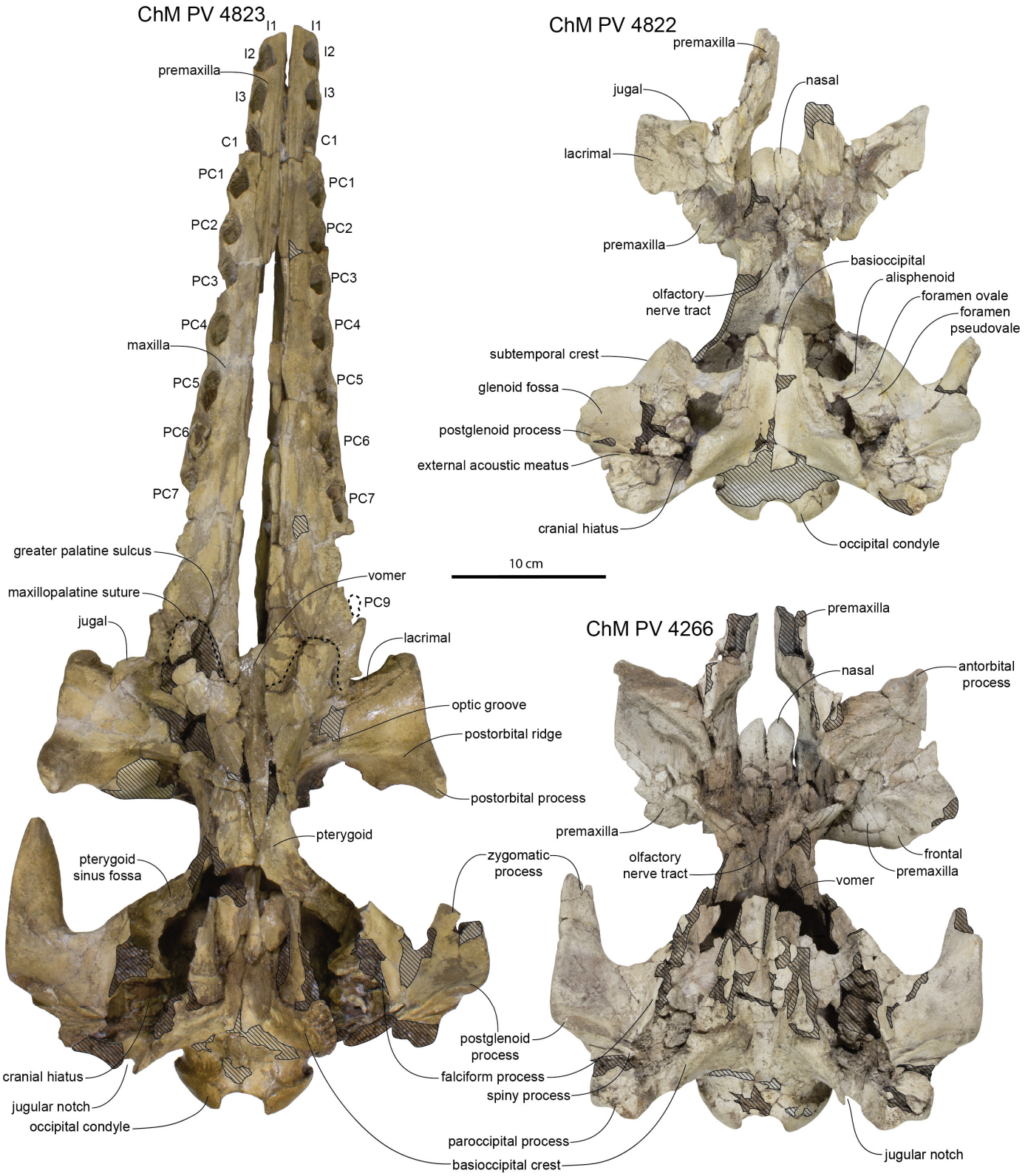


Figure 6. Paratype skull (ChM PV 4823) and referred skulls of *Xenorophus simplicidens* in ventral view.

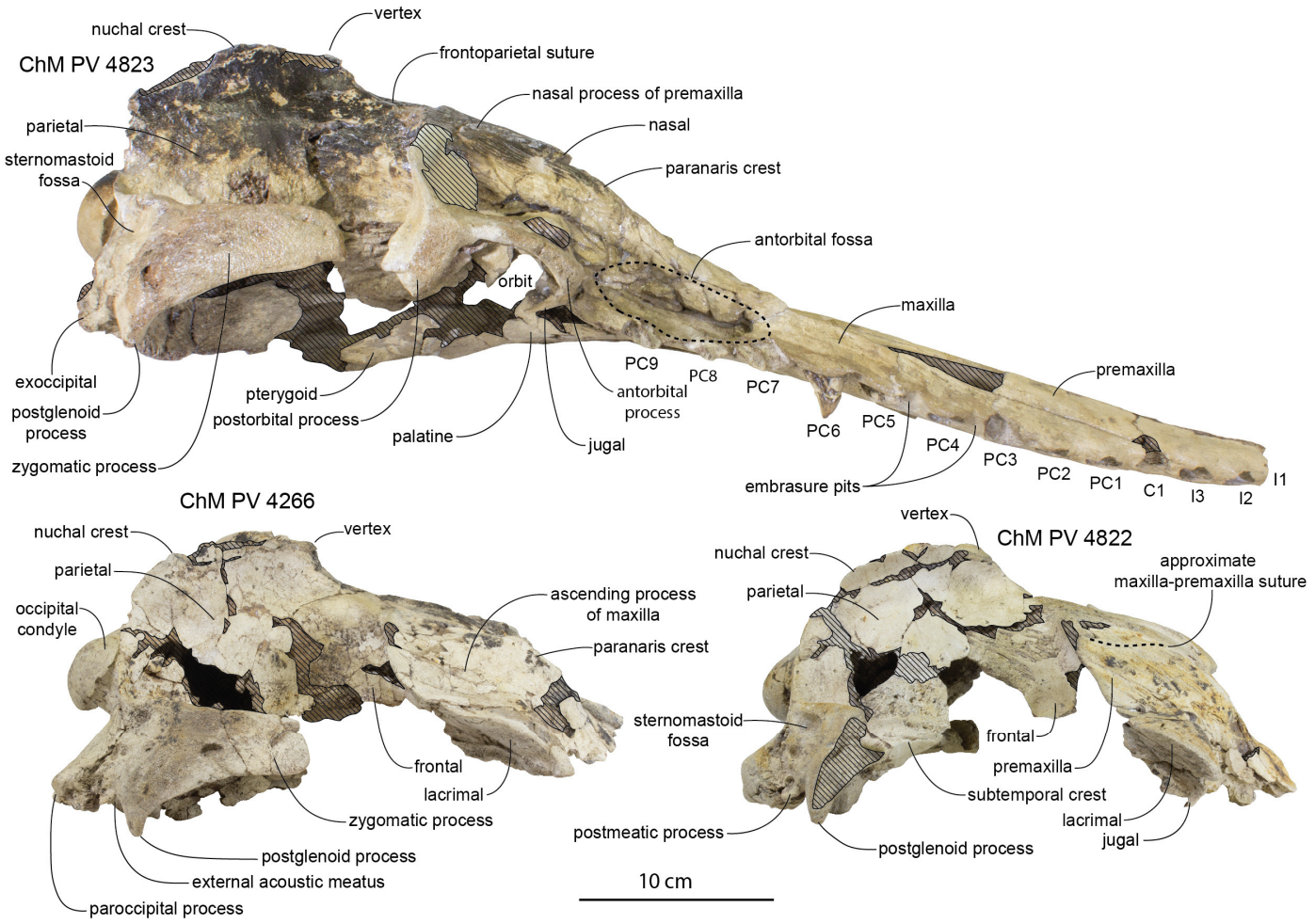


Figure 7. Paratype skull (ChM PV 4823) and referred skulls of *Xenorophus simplicidens* in lateral view.

Rostrum: The ventral surface of the holotype skull (CCNHM 8720) is well-exposed and slightly fractured (Figure 2; Table 1). In CCNHM 8720, the rostrum has a Rostral Proportion Index (RPI) of 2.78; in ChM PV 4823, the slightly shorter rostrum has an RPI of 2.41. This proportionally shorter and wider rostrum is perhaps a result of incorrect reassembly of ChM PV 4823 as it possesses an anomalously wide ventral gap between the maxillae (Figures 4 and 5); if this gap of 21–22 mm is subtracted, RPI is recalculated at 2.8. In CCNHM 8720, the premaxilla is incomplete but bears partial alveoli for I2 and I3. The maxilla of CCNHM 8720 is complete and preserves empty alveoli for C1 through PC3 and left PC9; all other maxillary teeth (left PC4–8, right PC4–9) are preserved in situ.

In CCNHM 8720, the premaxillae contact ventromedially along the anterior 140 mm of the rostrum, and the anterior 175 mm of the rostrum in the more completely preserved paratype (ChM PV 4823). A narrow, approximately 100 mm long vomerine window may have been present in CCNHM 8720, but is unclear owing to crushing; the vomer is incompletely preserved in ChM PV 4823, but the window appears to have been at least 175 mm long. The palatal process of the premaxilla is long, narrow, and bears a longitudinal groove; it extends approximately 130 mm posterior to the C1 in CCNHM 8720.

The posterior two thirds of the palate is ventrally flat, as in *Xenorophus sloanii*. A shallow furrow is present about 15 mm medial to PC5–3 and may be continuous posteriorly with the greater palatine foramen. On the left side, there is at least one greater palatine foramen opening at the position of PC7–8; on the right side, there is one large foramen with a long sulcus (positioned 12–13 mm anterior to the left greater palatine foramen) and one additional posterior foramen with a shorter sulcus, positioned slightly lateral to the primary foramen and at the level of PC9. These sulci open anteriorly.

Table 1. Skull measurements (in mm) of *Xenorophus simplicidens*. ? denotes missing measurements; e denotes an estimated measurement; + denotes a minimum measurement.

Measurement	CCNHM 8720	ChM PV 4266	ChM PV 4822	ChM PV 4823
Condylobasal length	?	?	?	655
CBL without premaxilla	644	?	?	578
Rostrum length	426+	?	?	399
Length of maxilla on rostrum	375	?	?	320
Maximum rostrum width	137	?	?	?
Rostrum width at antorbital notch	131	?	?	127.9
Postorbital width	?	230e	?	255
Bizygomatic width	304	252	220–230e	281.9
Exoccipital width	263	200	197	214.9
Depth of palate at maxillopalatine suture	9.5	?	?	12.9
Bony nares, transverse width	?	40	34.5	34.9
Maximum depth of rostrum	?	?	?	71
Width of gap between premaxilla anterior to nares	?	14.1	9–10e	17.6
Transverse width of premaxillae at antorbital notch	?	21.5	15.5	18.1
Nasal, depth 5 mm from anterior edge	?	5.4	4.6	5.9
Nasals, anterior/posterior combined width	?	33.5/26.5	27.8/26.4	26.9/26
Nasals, maximum width	?	33.5	27.8	26.9
Nasals, maximum length	?	42.9	37.4	46.9
Least interorbital width	?	210e	186	232
Separation of supraoccipital and posterior nasals	?	81.4	82	84.6
Transverse width of nasal process of premaxilla	?	34/33.5	35.6/35.1	?/38.3
Width across nasal processes of premaxillae	?	109.1	105	108.9
Anteroposterior length of frontal at midline	?	56.7	56.5	64.2
Anteroposterior length of parietal at midline	?	23.4	30.3	31.9
Maximum width of frontal between premaxillae/maxillae at vertex	?	53.3	58.1	49
Deviation of median parietal suture to left	?	7°	19°	8°
Length of occipital shield, foramen magnum to vertex	?	122.1	110.3	127.1
Occipital condyle breadth	101.7	83.7	78.5	83.6
Occipital condyle depth	48.7	54.5	49	53.4
Foramen magnum transverse width	63+	34.4	31.5	35.6
Foramen magnum depth	?	32.1	34.4	29.9
Transverse width across basioccipital crests	117.7	96.8	105.3	102.3
Maximum width of basioccipital crest	16.6	17.1	14.4	20.3
Height of nasals above rostrum base	?	?	?	87.3
Squamosal fossa depth	?	34.6	22.8	38.6/33.8
Distance from center of squamosal fossa to supramastoid crest	?	19.7	15.3	20/22.9
Transverse width of glenoid fossa	39	45	35	47
Angle between basioccipital rests	48°	36°	40°	43°
Width of squamosal lateral to exoccipital	237	17.5	24+	30.8

Table 1. *Cont.*

Measurement	CCNHM 8720	ChM PV 4266	ChM PV 4822	ChM PV 4823
Dorsoventral depth of zygomatic process at midpoint	?	36.1	?	?/36.9
Maximum anteroposterior length of temporal fossa	?	140.5	?	136/138
Maximum length of lacrimal, dorsal exposure	?	80.9	52.5	?
Maximum depth of antorbital process	?	25.5	21.6	?
Orbital diameter	?	63	?	59.6
Orbital angle	?	79°	?	76.5°
Maximum length of antorbital fossa L/R	?	?	?	99e/87e
Maximum width of antorbital fossa L/R	?	?	?	31+/29+
Minimum dorsoventral depth of the maxilla edge lateral to the antorbital fossa L/R	4.8/?	?	?	?
Separation of anterior nasals and supraoccipital apex	?	126	118.9	132.8
Least intertemporal width	?	57.3	53.9	56.2
Squamosal length, postglenoid process to zygomatic process	128	97+	70+	99
Maximum width of nasal, L/R	?	16.7/18.5	14.7/13.4	12.6/14.4
Maximum length of vomer in palate	110e	?	?	140+
Orbit height relative to rostrum edge	?	?	?	33
Antorbital notch to posterior lacrimal/jugal	?	?	15.7	7+
Antorbital notch to postorbital ridge	59	60+	?	57
Anteroposterior offset between left and right palatines, maxillopalatine suture	3	?	?	12.6
Deviation of posterior median palatine suture from midline	?	?	?	?
Deviation of anterior median palatine suture from midline	?	?	?	?
Greatest breadth palatines	98.1	?	?	103
Transverse diameter palatine L/R	54/44	?	?	49.1/41.8
Paroccipital process to posteriormost tooth	295/300	?	?	?
Postglenoid process to posteriormost tooth	246/253	?	?	219.5/232.4

In ChM PV 4823, the rostrum deviates 3.2° to the left (Figure 5), as in most specimens of *Xenorophus sloanii* (see below). In CCNHM 8720, the rostrum deviates 6.8° to the right, caused by diagenetic distortion. Indeed, deviation to the left was probably the case, given that the distance between the posteriormost tooth (PC9) and the postglenoid process is approximately 1 cm shorter on the left versus the right side in both ChM PV 4823 and CCNHM 8720, paralleling rostral and mandibular asymmetry in *Xenorophus sloanii* (e.g., CCNHM 168, 104, ChM PV 7677). In ChM PV 4823, the entire rostrum is twisted counterclockwise in anterior view by 6.3°.

Dorsally, the premaxilla has parallel lateral margins in the paratype (ChM PV 4823) and does not widen anteriorly (Figure 5). In lateral view, the rostrum is deepest at the level of PC1, and the rostrum bears a lightly sinuous ventral profile (Figure 6). Along the anterior third of the rostrum, the premaxilla faces dorsolaterally, but along the posterior 2/3, the premaxilla faces dorsally. The premaxillary sac fossa is positioned approximately 3 cm anterior to the antorbital notch, and there are two premaxillary foramina on the left side. The larger premaxillary foramen is positioned 118 mm anterior to the nasals, and the smaller is positioned 30 mm further anterior; both open posterodorsally. There is at least one right premaxillary foramen, the broken margin of which is positioned approximately

1 cm anterior to the primary left premaxillary foramen. The premaxillary sac fossae are narrow and face anteromedially and somewhat anterodorsally, and anteriorly transition into a subtle furrow that appears to be the posteromedial sulcus; this sulcus extends toward the posteriormost premaxillary foramen. Anteromedial to the premaxillary sac fossae, the medial edges of the premaxilla rise toward the midline and likely contacted each other as in other *Xenorophus* specimens; their separation in ChM PV 4823 is likely an artifact of reconstruction (see above). These dorsomedial ridges measured at least 110 mm in length and extended anterior to the anteriormost premaxillary foramen. These ridges are incomplete but clearly rotated to the left on both sides, resulting in a transversely deeper and trough-like premaxillary sac fossa on the left. On the left side, a poorly defined anteromedial sulcus flanks the dorsomedial ridge of the premaxilla. In addition to the paratype, both referred skulls ChM PV 4266 and 4822 possess a rounded, versus V-shaped (as in *X. sloanii*), anterior margin of the bony nares.

The antorbital fossae are clearly developed on both sides of the rostrum in the paratype (ChM PV 4823; Figure 4), but fracturing of the lateral edge of the maxilla precludes assessment of whether the degree of excavation of the fossae is asymmetrical in width and excavation (e.g., as in *Xenorophus sloanii*). However, the antorbital fossae are asymmetrical in length, measuring approximately 92 mm and 113 mm long on the left and right sides (respectively); this differs from *Xenorophus sloanii*, where the left antorbital fossa is longer than the right. Medial to the alveoli for PC8–9, the maxilla was excavated to a depth only a few mm in thickness by the fossae on both sides (2.2 mm on the left, 2.4 mm on the right). On the right side, there are at least three dorsal infraorbital foramina present dorsal to the infraorbital canal, the roof of which has broken away. The infraorbital canal is situated ventromedially within the fossa and the foramina dorsal to it are on the medial wall of the fossa; additionally, there is one laterally directed foramen emanating from the premaxilla–maxilla suture at the level of PC9. On the left side, the fossa appears to bear infraorbital foramina coalesced into a fenestra, though likely artificially expanded by fracturing. Each fossa is bilobate, with a low transverse ridge at the level of PC8 dividing it into a shallow oval-shaped trough posteriorly and a small circular fossa anteriorly. On the left side, a low and laterally dissipating transverse ridge is positioned posteromedially, partially dividing the posterior oval-shaped trough into two fossae. The primary dorsal infraorbital foramen is large, anteriorly facing, approximately circular, and interrupts a 'stepped' profile of the maxilla between the horizontal floor of the antorbital fossa and the subhorizontal ascending process of the maxilla overlying the frontal and premaxilla. On the right side, a secondary infraorbital foramen is positioned ventrolaterally to the primary foramen and along the posterolateral margin of the antorbital fossa; a longitudinal sulcus emanates from this foramen and extends anteriorly along the lateral edge of the fossa.

The antorbital notch appears nearly semicircular on the left side in ChM PV 4823 (Figure 5), but this is likely owing to loss of the maxilla and jugal within the notch; on the right side, the antorbital notch appears to have a straight and transverse posterior margin and a forms a right angle with the base of the rostrum, similar to *Xenorophus sloanii* specimens CCNHM 1077 and CCNHM 168, but differing from the nearly semicircular notch in CCNHM 104 and the *Xenorophus sloanii* holotype.

Facial/Interorbital Region: The nasals are well preserved in the paratype specimen and referred skulls (ChM PV 4266 and 4822); they are relatively short (Figure 5; 37–47 mm in length) compared to adult specimens of *Xenorophus sloanii* (66–79 mm; Table 1). ChM PV 4266 bears an anterior median cleft between the nasals, giving them an M-shaped anterior margin, but such a cleft is missing in ChM PV 4823 and 4822, where the nasals have a simple anteriorly convex margin. The nasals are widest anteriorly. The nasals are slightly separated posteromedially by an anterior median wedge of the frontal, which gives the posterior edge of the nasals a W-shape similar to some specimens of *Xenorophus sloanii* (e.g., CCNHM 168); the condition in ChM PV 4822 is unclear, and this specimen seems to have an irregular but approximately transverse frontonasal suture.

Lateral to the nares and anterior to the anterior margin of the nasals, the premaxilla is transversely narrow and dorsoventrally anteriorly positioned nares (e.g., *Simocetus*, *Ashleycetus*, *Olympicetus*, other Xenorophidae); this crest rises in height posteriorly toward the nasals (Figure 7). There is no laterally overhanging crest in ontogenetically mature specimens such as ChM PV 4823 and 4266, unlike *Xenorophus sloanii* (e.g., CCNHM 1077).

In ChM PV 4266 (Figure 5), there is a large anterior median interparietal (AMI; [92]) that is dorsally exposed, measuring approximately 41 mm long and 17 mm wide. The AMI contacts the posterior edge of the nasals and nearly completely separates the left and right frontals at the midline. The sutures of the AMI seem vertical and deep, suggesting that this element is dorsoventrally thick, as in other Xenorophidae [92].

Anterior Basicranium: The palatines are crushed but appear to be widest anteriorly and taper posteriorly into a sub-cylindrical shape; the ventrolateral surface of the palatines bear low posteromedially trending ridges (Figures 3 and 6). The pterygoid is poorly preserved, but the pterygoid–palatine suture is somewhat mortised and overall has a posteromedial orientation and meets the midline about halfway between the choanae and the posteriormost maxillopalatine suture. In addition to the vomerine window present on the rostral portion of the palate, a 63 mm long and 15 mm wide posterior exposure of the vomer is present between the posterior palatines and pterygoids as in *Xenorophus sloanii*. The exposure of the vomer in ChM PV 4823 appears to be anteroposteriorly continuous from the anterior rostrum to the choanae, though this is perhaps best interpreted as a result of incorrect assembly of the rostrum with an artificial gap between the left and right maxillae (see above). The medial margin of the pterygoid suggests a narrow gap was present at the anterior margin of the choanae between the pterygoid and the vomer (as in *Albertocetus meffordorum*). The posterior edge of the pterygoid is posterolaterally oriented. The posterior lamina of the pterygoid underlaps the basisphenoid and extends posteriorly to the level of the falciform process of the squamosal.

Vertex and Dorsal Braincase: The intertemporal constriction is narrow but anteroposteriorly short (Figure 5; Table 1). The median parietal suture is at the midline and not asymmetrical in any specimen, unlike some adult specimens of *Xenorophus sloanii* and *Albertocetus meffordorum* (see below; [1]). There is only a low sagittal crest in subadult specimen ChM PV 4822, but not in the adult specimens (ChM PV 4266, 4823), unlike the low sagittal crest in *Xenorophus sloanii*. Instead, there are low anterolaterally diverging temporal ridges defining a triangular, flat dorsal surface. Where the ridges converge posteriorly at the vertex, the intertemporal constriction is rounded in cross-section in the adult specimens; in old adult specimens of *Xenorophus sloanii*, the sagittal crest is only present immediately anterior to the vertex where the temporal lines converge. The frontoparietal suture forms a shallow V-shape and converges posteromedially in ChM PV 4823 and possibly ChM PV 4266; in this latter specimen, the suture is completely remodeled, but a low ridge seems to demarcate the position. This suture is more approximately transverse in ChM PV 4822.

The vertex (defined as the apex of the supraoccipital) is elevated far above the parietals in all specimens (Figure 7). The apex of the occipital shield is triangular and pointed. The occipital shield of the most mature specimen, ChM PV 4266, bears short anteroposteriorly aligned ridges for neck muscle attachments. The occipital shield (Figure 8) in all specimens is shallowly transversely concave; flattest in ChM PV 4822, slightly more concave in ChM PV 4823 and CCNHM 8720, and most concave in ChM PV 4266. In dorsal view, the nuchal crest is sinuous in ChM PV 4823 (slightly anterolaterally concave in its anterior half, and laterally convex posteriorly), and the nuchal crest is continuously convex in ChM PV 4266. In all specimens, the nuchal crest is dorsoventrally deep and in lateral view, forms a posterodorsally convex arc; the crest is lowest in ChM PV 4822 and highest in ChM PV 4266 (Figure 8). In lateral view, the frontoparietal suture ascends the anterior wall of the braincase posterodorsally along its ventral two-thirds, and in the dorsal third, trends anterodorsally.

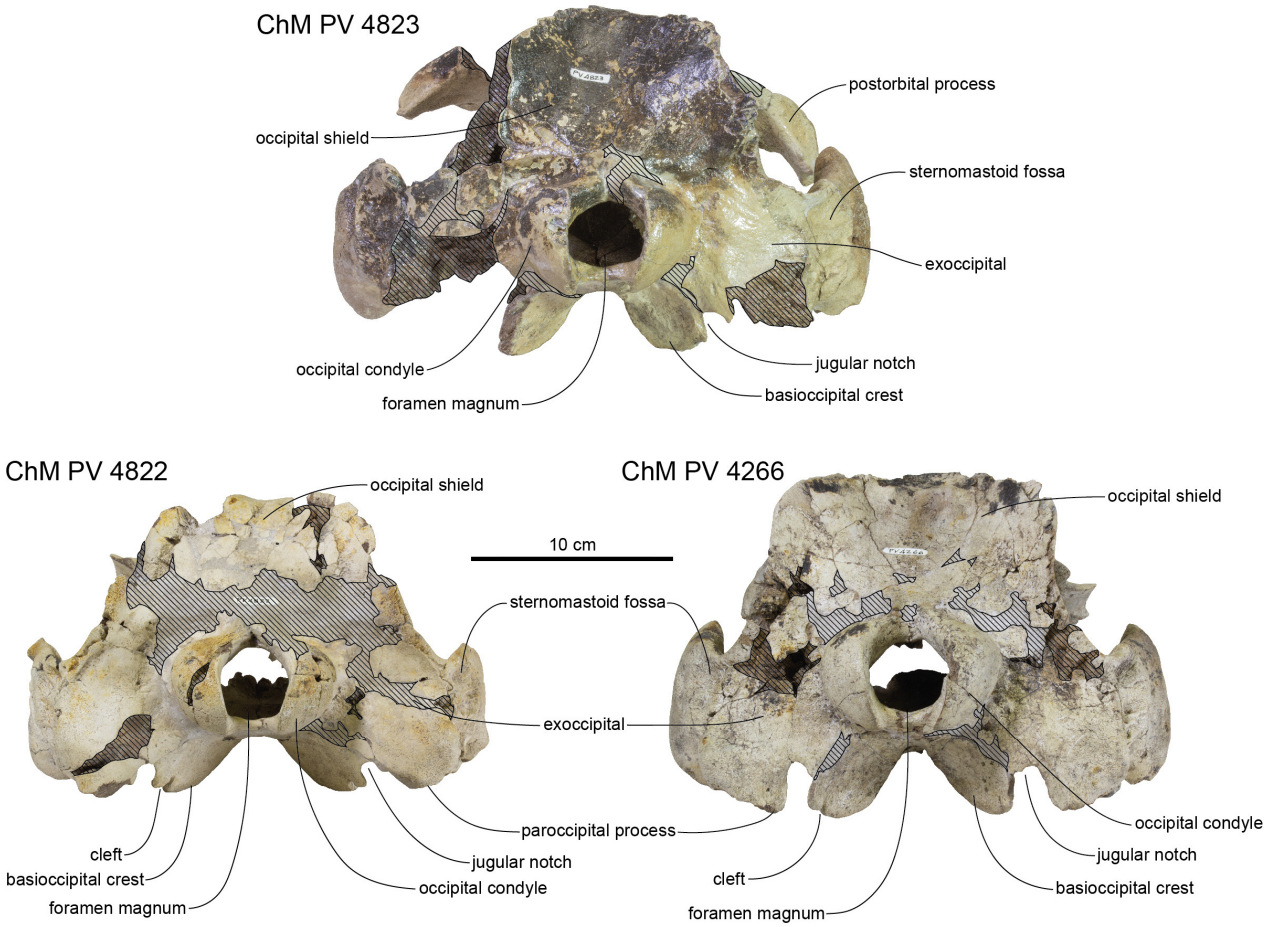


Figure 8. Paratype skull (ChM PV 4823) and referred skulls of *Xenorophus simplicidens* in posterior view.

Posterior Basicranium and Squamosal: The basioccipital of the holotype is flattened taphonomically but exhibits basioccipital crests diverging at a 44° angle and measuring about 19 mm in maximum thickness, about 6.2% of bizygomatic width (Figures 3 and 4). Other specimens (ChM PV 4266, 4822, 4823) similarly possess basioccipital crests diverging between a 43 and 47° angle (Figure 6).

Despite crushing of the holotype skull, the periotic fossa and cranial hiatus are well-preserved (Figures 3 and 4). The falciform process is straight and trends posterolaterally toward the deeply excavated periotic fossa. The fossa includes a deep bowl-shaped fossa named the suprameatal pit [10], positioned dorsolateral to the spiny process (broken); this bowl-shaped fossa bears minute spurs. It is separated posteriorly by a transverse ridge from a posterior shelf-like fossa for the posterior process of the periotic. Ventromedially, a rugose laminated sheet of the alisphenoid covers (underlaps) the squamosal medial to the suprameatal pit and forms the medial rim of the pit. This inflated region of the alisphenoid appears to have contacted the suprameatal fossa of the periotic, or at least the superior process, which loosely contacts the alisphenoid.

The lateral tuberosity of the periotic fits into a shallow fossa immediately anterior to the spiny process of the squamosal. The spiny process is broken but articulates with the hiatus epitympanicus of the periotic. When the periotic is placed into articulation, there is a slight gap between the base of the anterior process of the periotic and the falciform process, as in other Xenorophidae. A large gap is present dorsal to the superior process of the periotic and the roof of the bowl-shaped fossa within the periotic fossa, perhaps as great as 10 mm.

The zygomatic process is similar in length to *Xenorophus sloanii*, but its tip is abraded; as preserved, it tapers transversely and terminates at the level of the supraoccipital apex but likely met the postorbital process, as in *X. sloanii* (Figures 3–6). In lateral view, the zygomatic process is roughly rectangular. The squamosal prominence is low and less prominent than in *Xenorophus sloanii* (e.g., CCNHM 168, 1077). The sternomastoid fossae are similar to *Xenorophus sloanii*; each consists of a series of oval fossae separated by three to four low anteroposterior ridges in all specimens. These specimens also exhibit a deeply incised furrow along the anterior margin of the fossa (Figure 7); a shallow furrow is only developed in some specimens of *Xenorophus sloanii* (e.g., CCNHM 168).

In posterior view, the occiput is less trefoil-shaped, owing to exoccipitals that extend less laterally than in *Xenorophus sloanii* (Figure 8). In ChM PV 4266, the foramen magnum bears a deep median cleft dorsally, as in some *Xenorophus sloanii* (e.g., CCNHM 168). The jugular notch is transversely wide and semicircular in all specimens, as opposed to the narrower and more acute notch in *Xenorophus sloanii*.

Periotic: The left periotic of CCNHM 8720 is well-preserved but missing part of the anterior process; both periotics are preserved in ChM PV 4266 and ChM PV 4823, though the left periotic of the former is fractured and both periotics of the latter are missing the pars cochlearis (Figures 9–12; Table 2). The periotic is nearly identical to *Xenorophus sloanii* (see below) and *Albertocetus meffordorum* [1], though larger than the latter; it shares with these taxa relatively small size, and a proportionally large pars cochlearis (Figure 9). In addition, these periotics share the following combination of features unique to Xenorophidae (but not synapomorphies of the entire clade): transversely narrow and bladelike anterior process; dorsoventrally deep hatchet-shaped anterior process with flat anterior margin, prominent spine-like anterodorsal angle; long, bladelike lateral tuberosity (synapomorphy of Xenorophidae); transversely rounded and widened superior process; small suprameatal fossa formed as deeply excavated pit; long posterior cochlear crest; small, flat, quadrate posterior bullar facet (Figures 9–12).

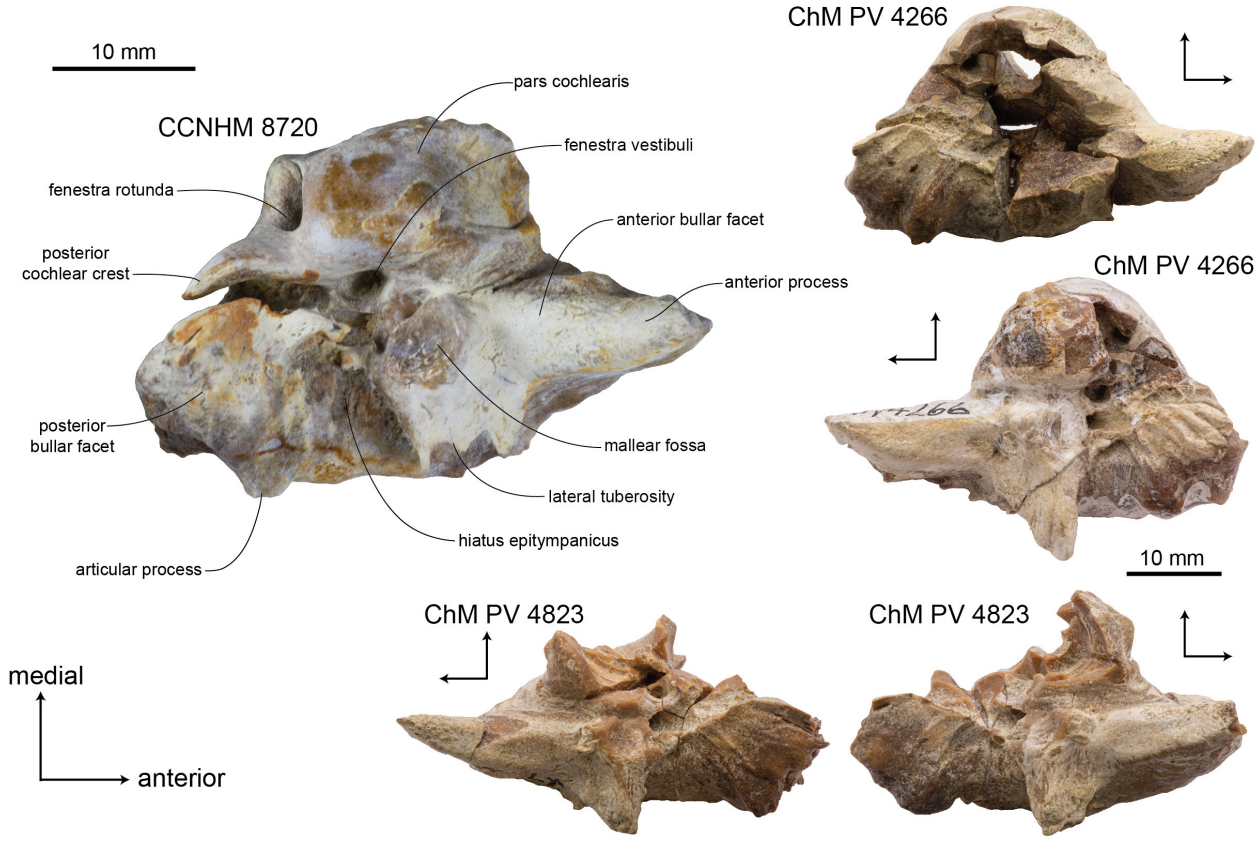


Figure 9. Periotics of *Xenorophus simplicidens* in ventral view.

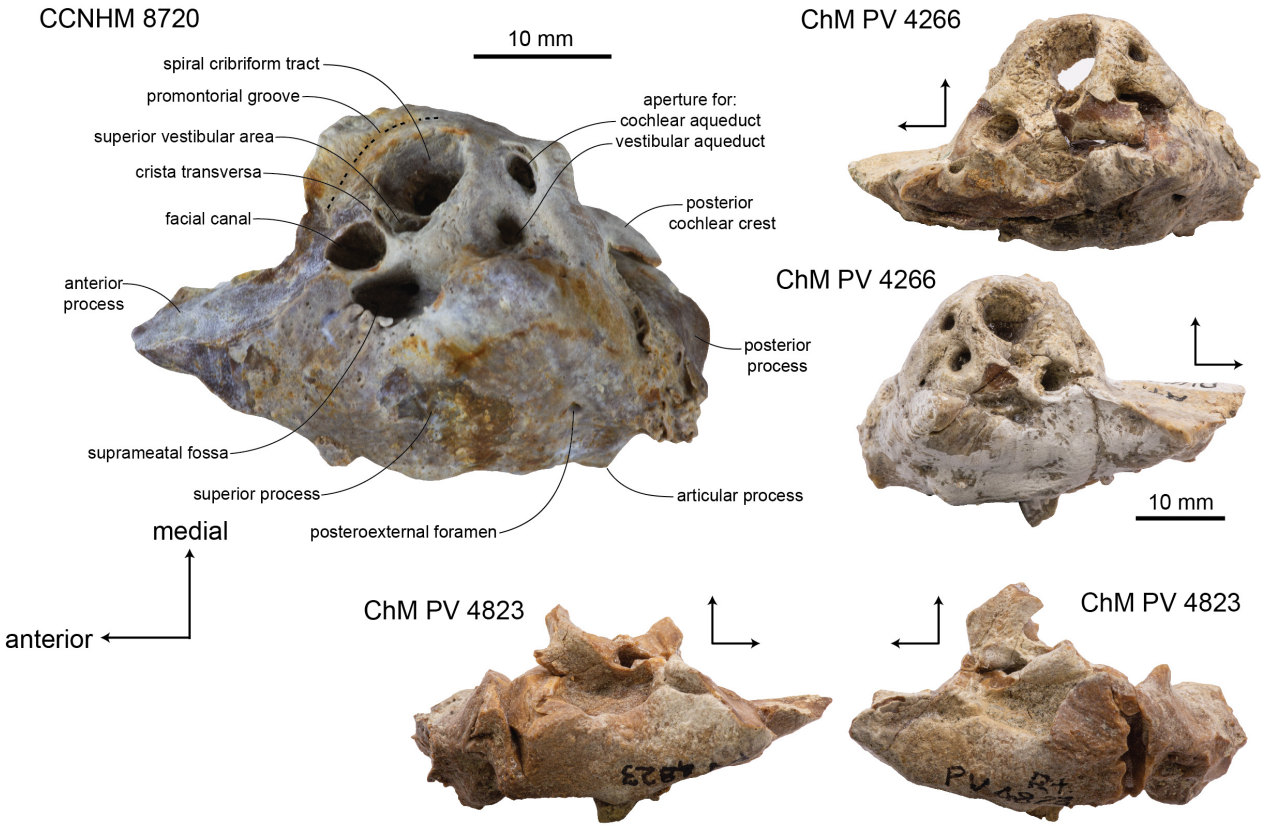


Figure 10. Periotics of *Xenorophus simplicidens* in dorsal view.

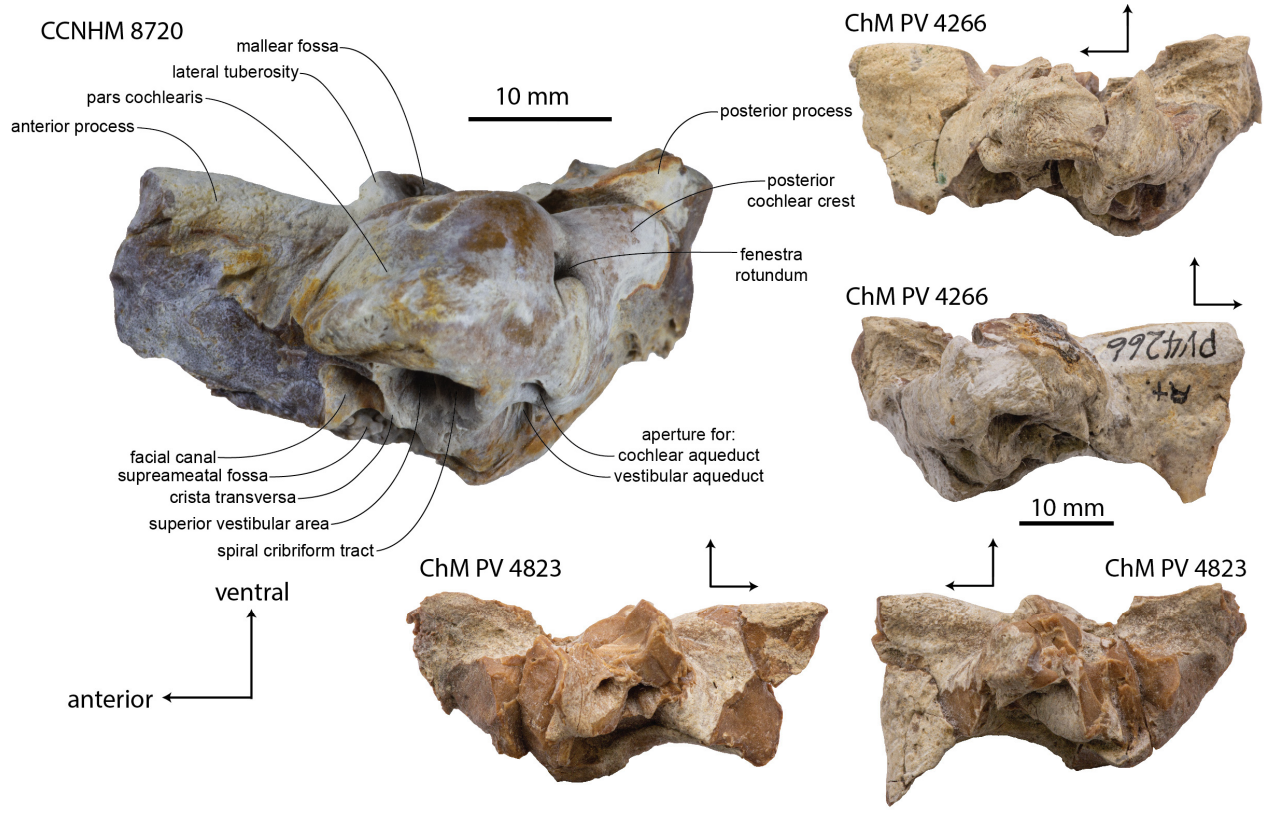


Figure 11. Periotics of *Xenorophus simplicidens* in medial view.

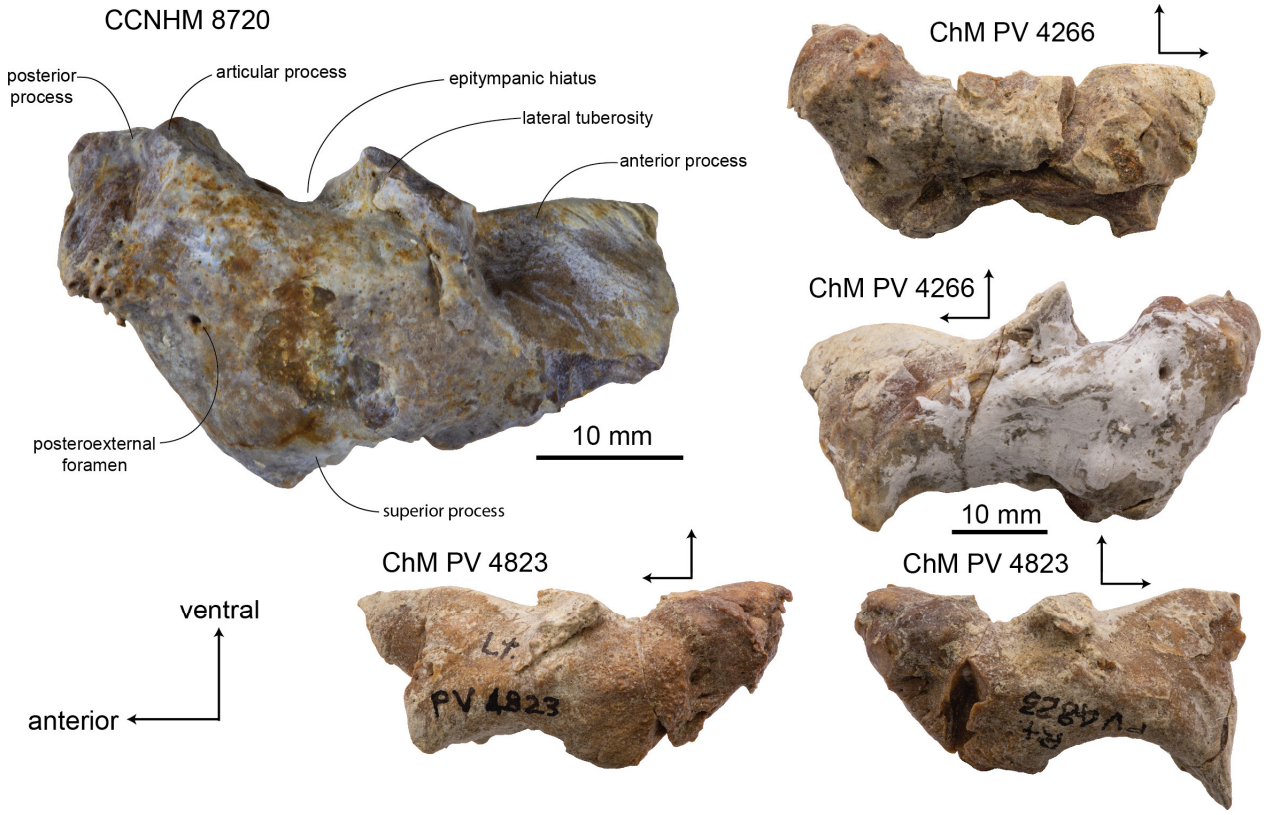


Figure 12. Periotics of *Xenorophus simplicidens* in lateral view.

Table 2. Periotic measurements (in mm) of *Xenorophus simplicidens*. ? denotes missing measurements; e denotes an estimated measurement; + denotes a minimum measurement.

Measurement	CCNHM 8720	ChM PV 4266	ChM PV 4823
Anteroposterior length L/R	41/?	44.5/45.1	41+/45.8
Transverse width pars cochlearis L/R	11/?	?/12.2	?
Pars cochlearis anteroposterior length L/R	21.8/?	21.1/23.1	?
Pars cochlearis dorsoventral depth L/R	13.8/?	?/14	?
Promontorium anteroposterior length L/R	17.6/?	16.7/18.5	?
anterior process anteroposterior length L/R	12+/?	12.3/15.1	?
Anterior process, transverse width at midpoint L/R	7.1/?	8/7.4	9.9/6+
Anterior process, dorsoventral width at midpoint L/R	14.8/?	17.6/17.1	19.3/16+
Separation of fenestra rotundum and cochlear aqueduct, L/R	7.2/?	?/8	?
Separation of fenestra rotundum and vestibular aqueduct, L/R	9/?	?/8.7	?
Separation of fenestra rotundum and fenestra ovalis, L/R	5.2/?	?	?
Internal acoustic meatus, maximum length, L/R	12.2/?	17.6/14.5	?
Internal acoustic meatus, maximum width, L/R	7.3/?	8.4/7+	?
Suprameatal fossa, anteroposterior length, L/R	6.9/?	13.8/7.2	15.4/11.7
Suprameatal fossa, transverse width, L/R	4.3/?	5.6/3.4	6.1/6.9
Posterior bullar facet, max length, L/R	14.1/?	7.6/6.4	8.5/8.7
Posterior bullar facet, max width, L/R	9.7/?	7.5/4+	7.3/7.8

The anterior process is best-preserved in ChM PV 4823 (Figures 12 and 13); the anterior and ventral margins meet at a right angle, and the anterior margin is straight and vertically oriented. The anterodorsal angle is a long triangular spur, giving the anterior process a hatchet shape like *Xenorophus sloanii* (ChM PV 7677, CCNHM 1077), *Albertocetus meffordorum*, and *Cotylocara macei*. The lateral tuberosity is longest in the most mature specimen, ChM PV 4266, and shorter in ChM PV 4823.

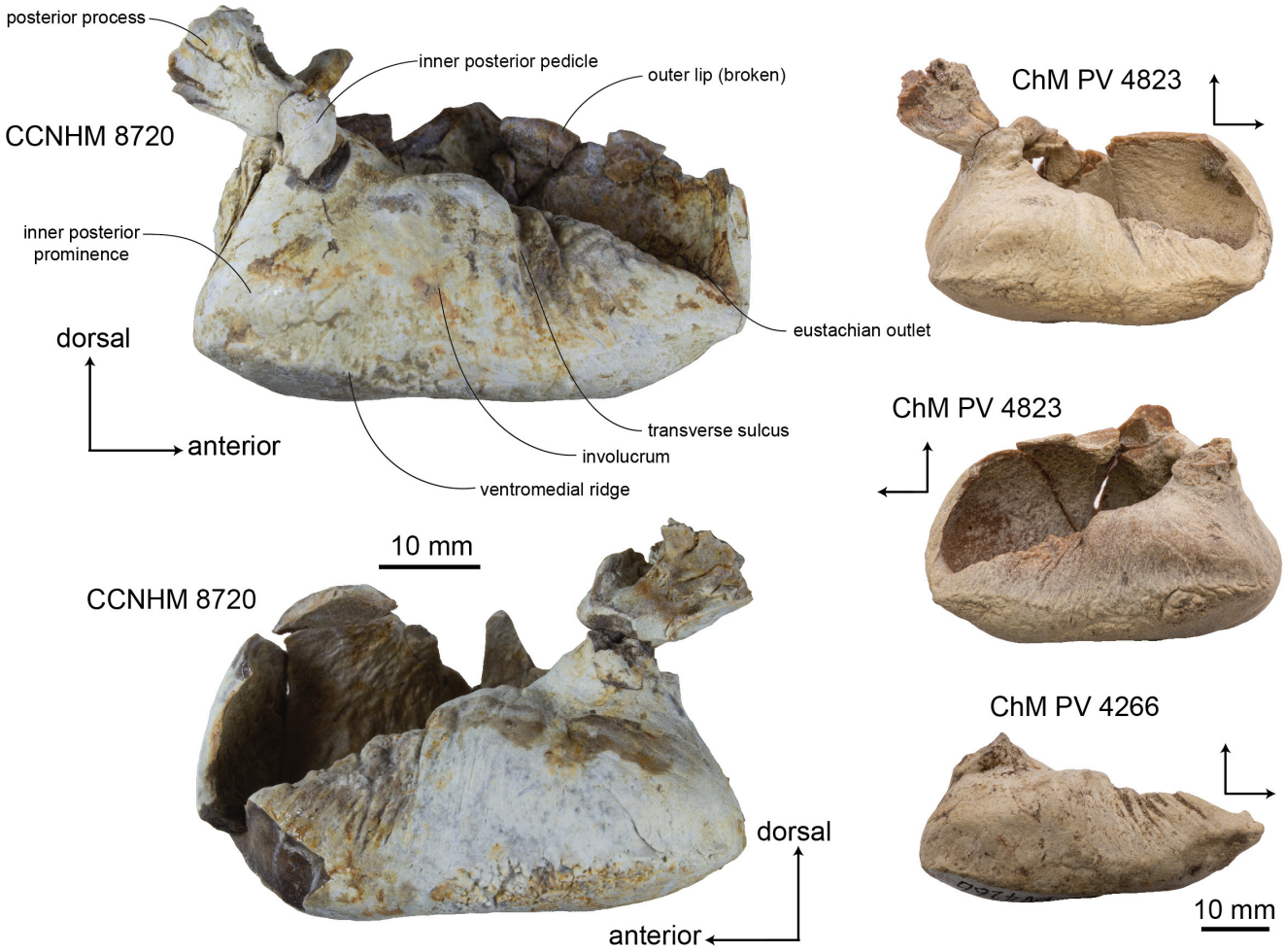


Figure 13. Tympanic bullae of *Xenorophus simplicidens* in medial view.

The pars cochlearis is subrectangular in CCNHM 8720 owing to a dorsoventrally shallow flange at its anteromedial corner (Figure 10). In ChM PV 4266 the pars cochlearis lacks such a flange and is more hemispherical in shape. Though broken, an intermediate condition seems to have been present in the left periotic of ChM PV 4823, which possesses a small flange along the broken anterior base of the pars cochlearis. The posterior cochlear crest is long and shelf-like in CCNHM 8720, paralleling the facial crest; it curves posterolaterally at its apex. CCNHM 8720 possesses a tubercle dorsal to the fenestra rotunda; owing to breakage, it is unclear if this was present in ChM PV 4266.

The suprameatal fossa is variable within *Xenorophus simplicidens* (Figure 10). It is developed as a deep pit in CCNHM 8720 and ChM PV 4266; this pit is nearly circular with steep walls in the former, and somewhat larger in the latter with a deep posterior fissure lateral to the aperture for the vestibular aqueduct. In ChM PV 4823, the suprameatal fossa is transversely wider and much longer, in addition to a deep posterior groove as in ChM PV 4266. In ChM PV 4266, the fossa is kidney-shaped and wraps around the circular opening of the facial canal, separated by a narrow ridge.

The superior process is greatly expanded and transversely rounded in all specimens, but most extremely so in CCNHM 8720; it is less expanded in ChM PV 4823 (Figures 10 and 12). The dorsal margin of the superior process is anteriorly concave in lateral view and broadly convex posteriorly; an obvious posterodorsal angle is not present in ChM PV 4823 or 4266, but there is a slight bluntly triangular posterodorsal angle in CCNHM 8720. A single posteroexternal foramen is present on the lateral surface, on the base of the posterior process (Figure 12). The posterior surface of the posterior process is rugose for an articular surface with the postmeatic process of the squamosal. The posterior bullar facet is quadrate in all specimens, is transversely flat and slightly longitudinally convex at the posterolateral end, and bears posterolaterally oriented ridges (Figure 9).

Tympanic bulla: The left and right bullae of the holotype (CCNHM 8720) and paratype (ChM PV 4823) are well-preserved; the left bulla of ChM PV 4266 is fragmentary (Figures 13–17; Table 3). The bulla is similar in size and overall proportions to *Xenorophus sloanii* (see below) but all bullae of *Xenorophus simplicidens* critically differ in possessing a deeply incised transverse sulcus positioned at about the midpoint of the involucrum (Figures 13 and 15). This sulcus is overlapped by a swollen ridge of the posterior involucrum on the dorsal and medial side. In CCNHM 8720, the involucrum immediately anterior to the transverse sulcus is rugose and bears many minute finger-like nodules. The ventral margin of the bulla in lateral view is nearly straight (Figure 12), similar to some specimens of *Xenorophus sloanii* (CCNHM 1077, ChM PV 5022). The cavum tympani is divided into anterior and posterior portions by a transverse ridge at mid-length (Figure 15). At the anterior end of the cavum tympani, the eustachian outlet is developed as a triangular anteroventrally directed trough.

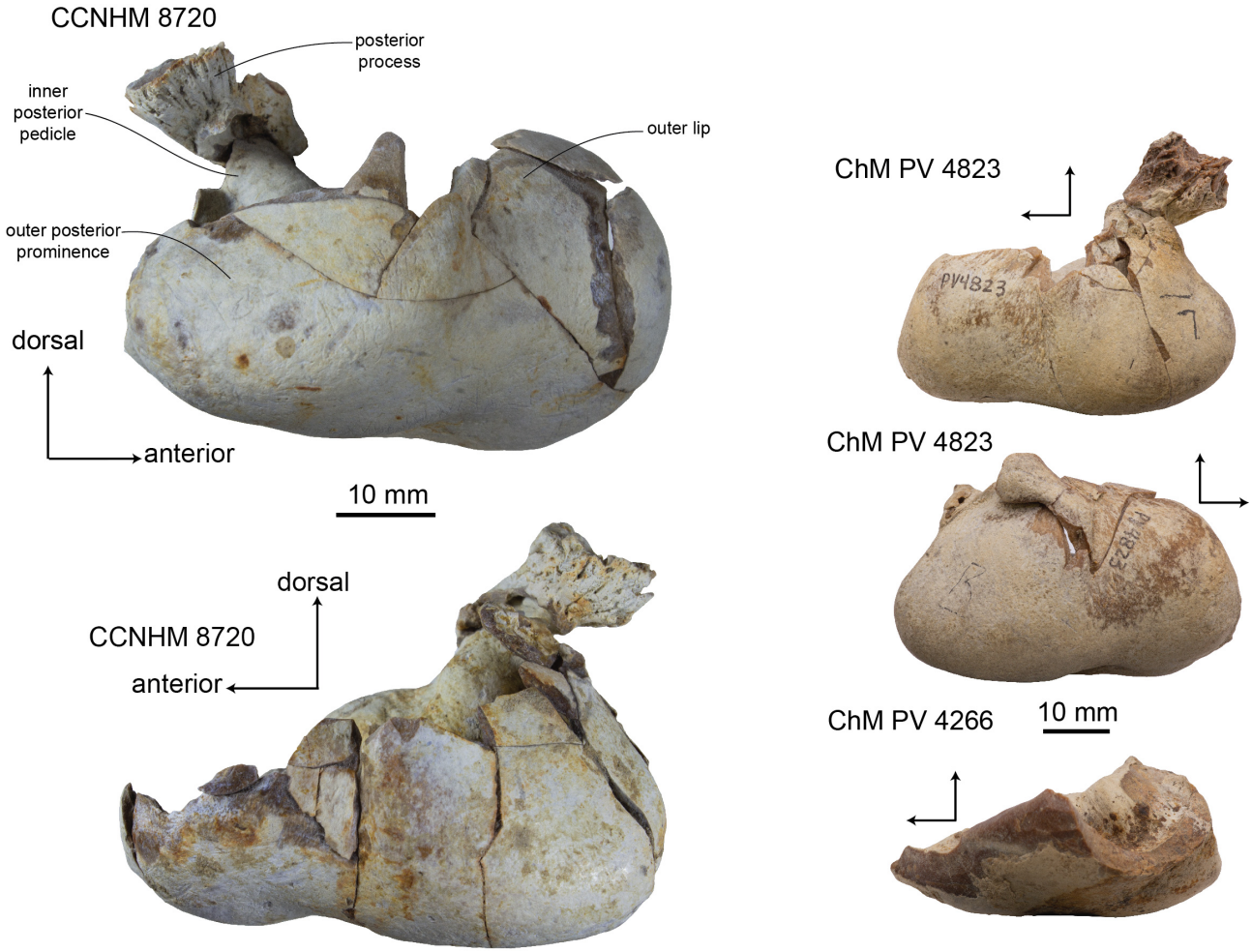


Figure 14. Tympanic bullae of *Xenorophus simplicidens* in lateral view.

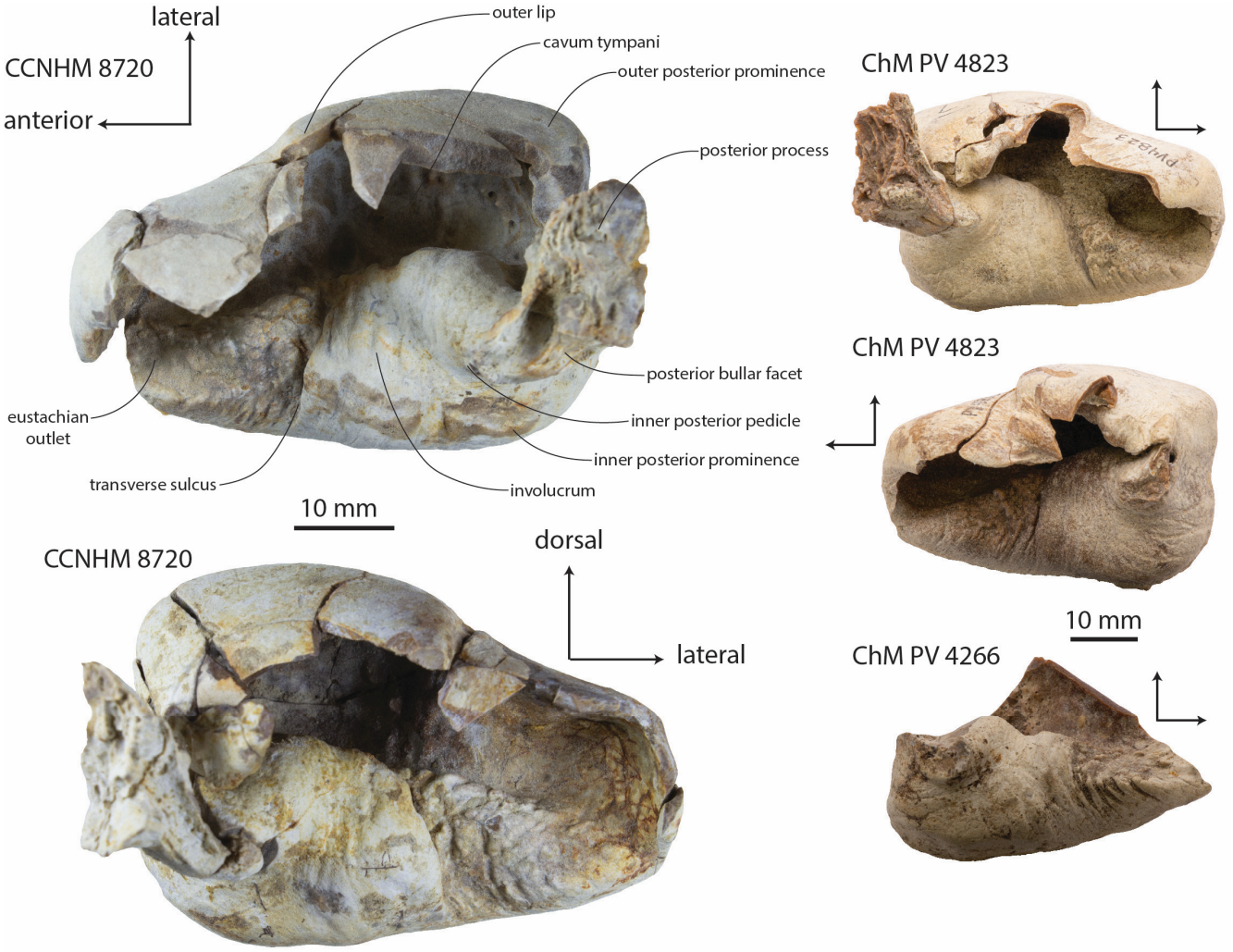


Figure 15. Tympanic bullae of *Xenorophus simplicidens* in dorsal view.

Table 3. Tympanic bulla measurements (in mm) of *Xenorophus simplicidens*. ? denotes missing measurements.

Measurement	CCNHM 8720	ChM PV 4266	ChM PV 4823
Maximum length, L/R	51.8/51.6	50.5/?	50.3/20.9
Bulla, transverse width at sigmoid process, L/R	35.6/35.2	?	34.4/33.6
Bulla, length posterior to lateral furrow, L/R	31.5/31.7	?	31.5/31.6
Bulla, width of medial lobe, L/R	20/19.5	19.7/?	17.6/17.1
Bulla, width of lateral lobe, L/R	19.3/17.5	?	16.8/16.5
Bulla, maximum width of posterior lobe, L/R	37.1/36.2	?	16.6/16.7
Maximum depth of involucrum, L/R	21.7/20.9	19.5/?	21.7/20.6
Minimum depth of involucrum, L/R	14.4/12.2	13.5/?	12.5/13.2

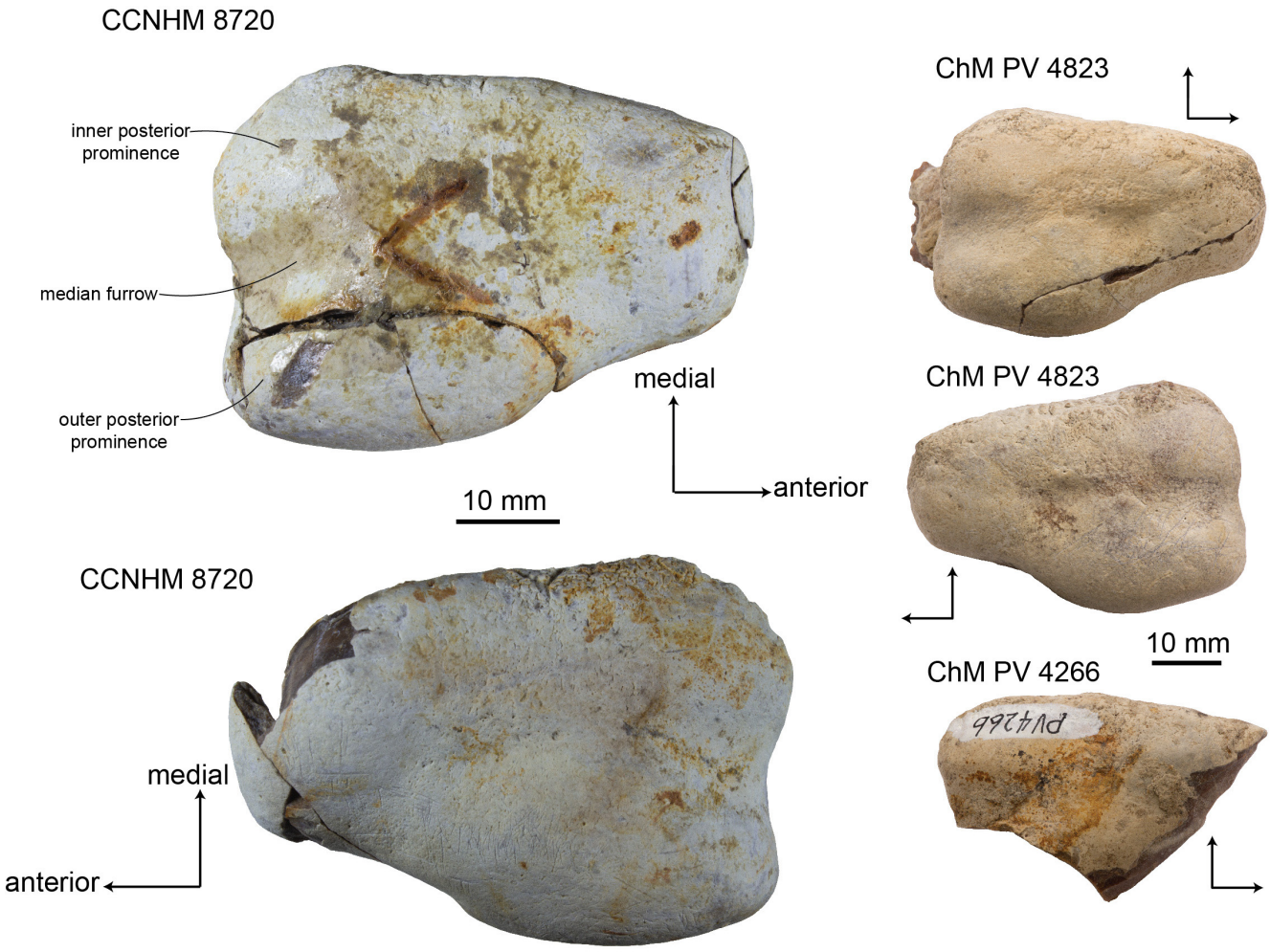


Figure 16. Tympanic bullae of *Xenorophus simplicidens* in ventral view.

In dorsal view, the bulla narrows anteriorly to the lateral furrow, while the posterior lobe is subrectangular and the anterior lobe is subtriangular (Figure 15). Ventrally, the median furrow is short and restricted to the posterior third of the ventral surface (Figure 16); it is interrupted by a low convex prominence, as in Basilosauridae. The elliptical foramen, posterior process, and pedicles (Figure 17) are better preserved in CCNHM 8720 and ChM PV 4823 than in any specimen of *Xenorophus sloanii* or other previously reported xenorophids. The elliptical foramen is small, 3 mm in diameter, and elevated dorsally on the posterior surface, placed at the level of the inner posterior pedicle (Figure 17). The elliptical foramen is planoconvex with a straight, lateral margin and a convex medial margin. The inner posterior pedicle is an inflated conical tubercle; the outer posterior pedicle is broken but developed as a narrow vertical flange.

The posterior process is posterolaterally oriented and bears a small trapezoidal posterior facet with longitudinal grooves (Figures 13 and 15); the facet deepens posteriorly and has a sinusoidal longitudinal profile (concave posteriorly and convex anteriorly, when viewed on edge in anterodorsal or posteroventral view). The posterior process bears a deep longitudinal trough dorsally. The posterior end of the posterior process has a deep transverse groove ventrally on the lower third of the process; the upper two-thirds bear a rugose articular surface for the postmeatic process of the squamosal. Anteriorly, there is a concave fossa on the posterior process just dorsal to the elliptical foramen.

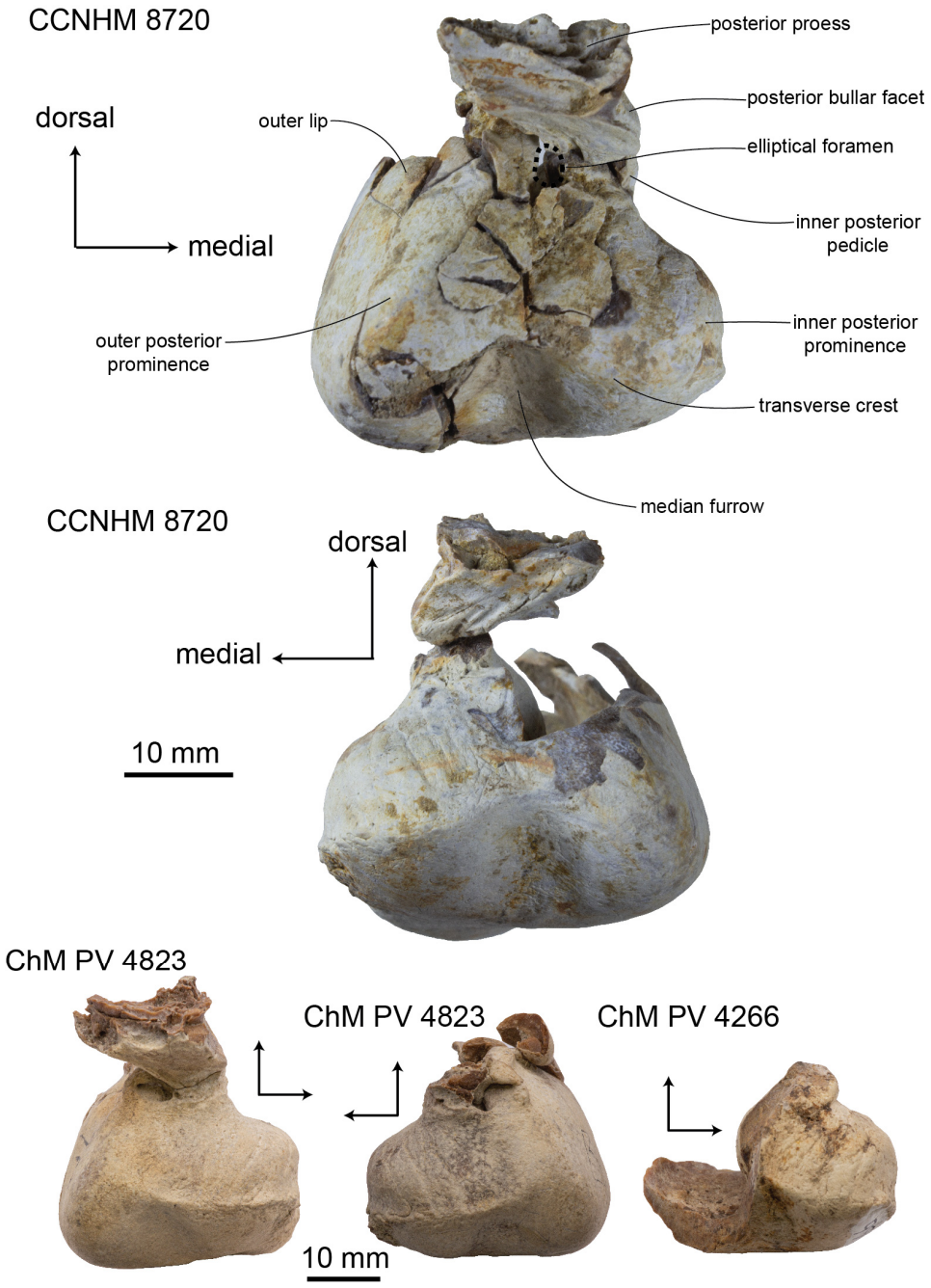


Figure 17. Tympanic bullae of *Xenorophus simplicidens* in posterior view.

Upper Dentition: The holotype rostrum preserves right PC4–9 and left PC4–8 within their alveoli; empty alveoli for I2–3, C1, PC1–3, and left PC9 are present (Figures 3, 4, 18 and 19; Table 4); alveoli for I1 are not preserved owing to incompleteness. Twelve isolated anterior teeth are present along with the isolated left PC9 (Figures 18 and 19). The isolated anterior teeth have roots that are oval to bilobate in cross-section and conical to triangular unicuspid crowns; their position is uncertain, owing to near-uniform root curvature in xenorophid upper and lower teeth. However, three teeth are possible lowers and differ from the remaining nine unicuspid teeth in having slightly more lingually curved crowns and somewhat more striated enamel basally on the lingual side of the crown.

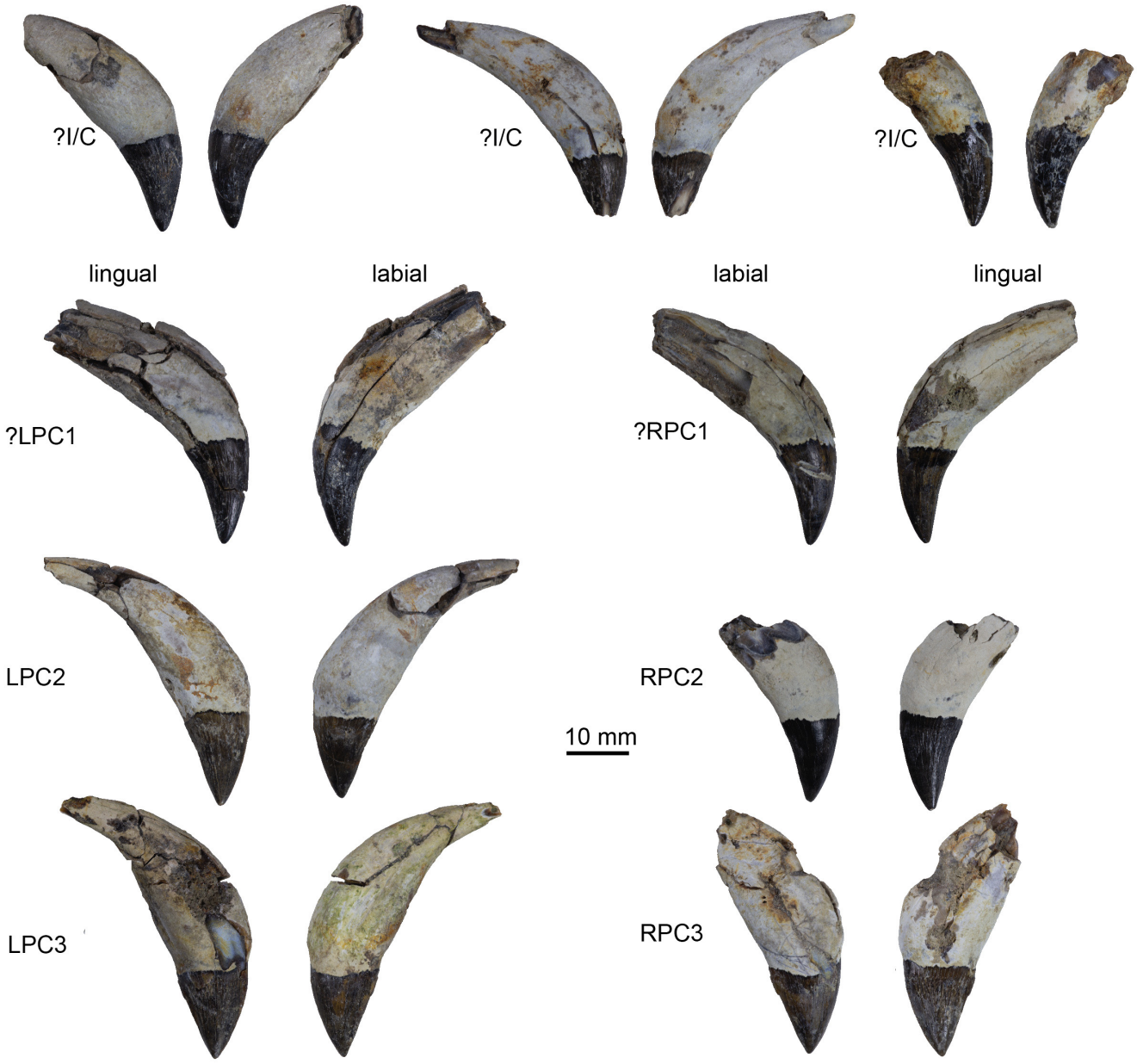


Figure 18. Isolated upper teeth of the *Xenorophus simplicidens* holotype (CCNHM 8720). ? denotes uncertainty of locus assignment.

I2 through PC2 alveoli are oval in shape (Figure 19). The presumed upper unicuspid teeth can be arranged into an anteroposterior series based upon crown diameter, and represent most positions between I1 and PC3, though most are not assignable to an exact position owing to their similarity (Figure 19). Left and right PC3 are clearly identifiable based on their anteroposteriorly elongate and somewhat bilobate roots, matching the identically shaped alveolus for PC3. The PC3 crown lacks cingula and has a triangular and slightly anteroposteriorly longer than wide crown, smooth and sharp mesial and distal carinae, a single distal cuspule at the crown base, and faint labial apicobasal striations and somewhat stronger lingual striations (Figure 18). The bilobate root bears a shallow labial sulcus and a faint lingual sulcus.

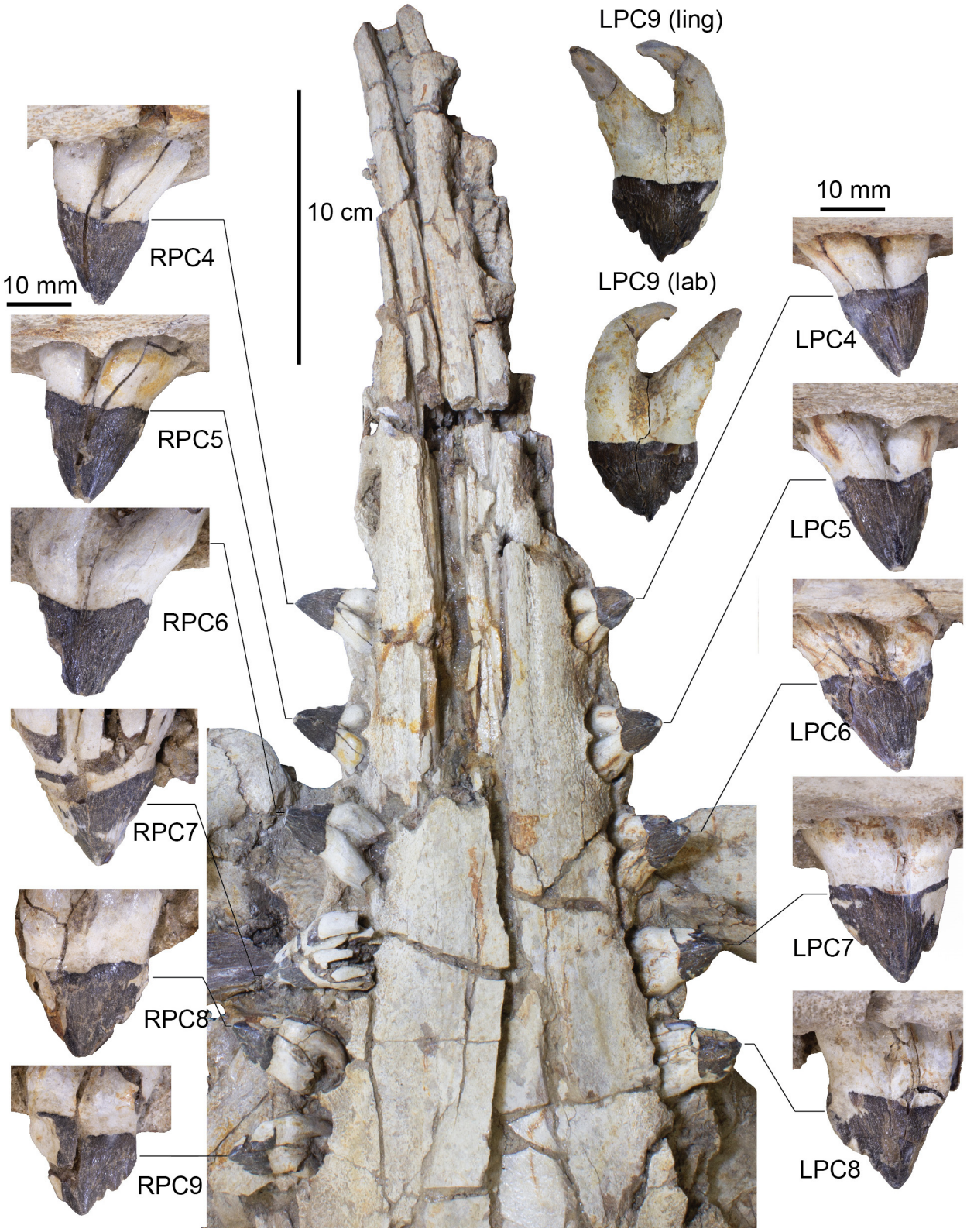


Figure 19. Upper dentition and palate of the *Xenorophus simplicidens* holotype (CCNHM 8720).

Table 4. Measurements (in mm) of upper dentition of *Xenorophus simplicidens* (CCNHM 8720) and *Xenorophus sloanii* (CCNHM 104, CCNHM 168, CCNHM 1077, 5995, ChM PV 7677, 5022). ? denotes missing measurements; e denotes an estimated measurement; + denotes a minimum measurement.

Measurement	CCNHM 8720	CCNHM 5995	CCNHM 104	CCNHM 168	CCNHM 1077	ChM PV 7677	ChM PV 5022
I1, crown height	?	?	?	?	?	?	?
I1, mesiodistal length	?	?	?	?	?	?	?
I1, crown width	?	?	?	?	?	?	?
I2, crown length	?	?	?	?	?	?	?
I2, mesiodistal length	?	?	?	?/8.9	?	?	?
I2, crown width	?	?	?	?/8	?	?	?
I3, crown length	?	?	?	?/14.9	?	?	?
I3, mesiodistal length	?	?	?	?/9.4	?	?	?
I3, crown width	?	?	?	?/8.6	?	?	?
C1, crown length	?	?	?	?/13.5	?	?	13/?
C1, mesiodistal length	?	?	?	?/9.8	?	?	7.7/?
C1, crown width	?	?	?	?/8.1	?	?	7/?
PC1, crown length	16.1/17.1	?	?	13+/14.2	?	?	?/13.9
PC1, mesiodistal length	10/10	?	?	9./9	?	?	?/8.9
PC1, crown width	8.8/9.2	?	?	8/8.6	?	?	?/7.7
PC2, crown length	15.6/15.2	?	?	?/14.2	?	?	?
PC2, mesiodistal length	10.1/10.2	?	?	9.9/10.1	?	?	?
PC2, crown width	7.8/8.1	?	?	8.3/8.3	?	?	?
PC3, crown length	14.7/14.0	?	?	11+/?	?	?	?
PC3, mesiodistal length	11.5/11.5	?	12.2/?	10.3/?	?	?	?
PC3, crown width	7.8/7.5	?	7.5/?	8/?	?	?	?
PC4, crown length	14.7/13.8	?	?	?/13.8	?	13.8/11+	12.7/?
PC4, mesiodistal length	13.7/14.5	?	14.1/13.4	?/12	?	13.2/12.9	10.9/?
PC4, crown width	7.7/7.7	?	7.3/7.3	?/7.4	?	7/7	7/?
PC5, crown length	14.4/14.3	16.3/?	?	15.9/13.8	?	?/14.8	12+/13.7
PC5, mesiodistal length	14.9/15.6	14.5/?	?/15.9	14.3/14.3	?	?/14.7	12.5/12.3
PC5, crown width	8.9/9.2	8.9/?	?/7.8	8.2/8.3	?	?/8.1	7.9/7.2
PC6, crown length	15/14.6	?	?	?/15.5	?/16e	?/15	14/?
PC6, mesiodistal length	17.2/16.4	?	15.5/17.4	?/15.7	?/15.7	?/16	14.9/?
PC6, crown width	9.8/9.5	?	?/8.5	?/8.2	?/8.9	?/8.2	8.5/?
PC7, crown length	15.5/15.8	?	?	16.1/13+	?/16.8	13.8/15.9	?/12.4
PC7, mesiodistal length	17.9/18.8	?	?	17.4/?	?/16.3	17/17.1	?/15+
PC7, crown width	9.2/9.5	?	8.9/9.2	9/8.3	?/8.7	8.4/8.1	?/8.5
PC8, crown length	14.9/15.1	?	?	14.8/?	?/14.6	12/?	16/?
PC8, mesiodistal length	18.4/19.2	?	?	18.1/?	?/17e	16.7+/?	16.6/?
PC8, crown width	9.4/?	?	8.9/?	8.9/?	?/9	8.6/?	8.7/?
PC9, crown length	13.3/14	?	?	?	?/10.1	10.1/10.6	?
PC9, mesiodistal length	16.7+/17.6	?	17e/?	?	?/15.5e	13.9/14	?
PC9, crown width	8.9/9.7	?	9/?	?	?/7.9	7.6/7.8	?

PC4–5 have similar crowns to PC3; these crowns are triangular in lingual/labial view, slightly anteroposteriorly longer than PC3, with a single basal cuspule on the distal carina (Figure 19). The crowns appear subtriangular in occlusal view. There are faint apicobasal striations labially, and slightly stronger lingual striations. The root is clearly double-rooted, with a larger and transversely thicker posterior root, especially in PC5. This larger posterior root corresponds to the posterolingual swelling of the crown.

PC6–7 have slightly anteroposteriorly longer crowns. Both possess a distal accessory cusp larger than those on PC4–5; PC6 lacks a mesial cusp, but a single mesial accessory cusp is present in PC7 (Figure 19). Lingual striations are slightly stronger on PC6–7 than in PC 4–5, and the labial face is less striated. Both teeth are double-rooted, with a greatly inflated posterior root. There is a faint labial cingulum on PC7.

PC8–9 are the most complex upper teeth; they possess one or more mesial cusps, with the apical-most cusp positioned high and near the principal cusp (Figure 19). Additional basal cusps may have been present but destroyed by tooth wear. These teeth are also the only teeth in the dentition to possess a third "demi root" on the lingual side, in between the anterior and posterior root lobes. This demi root is small and likely did not project beyond the isthmus between the two root lobes. The left PC9 is loose, and less worn than the right PC9 and PC8. It possesses two apically positioned mesial cusps and three distal cusps. It bears striated enamel anteriorly that transitions into slightly nodular enamel posteriorly on the lingual side. The labial side of PC9 bears some basal striations along with a very low but continuous labial cingulum. Apically, the labial surface is smoother. The root lobes of PC9 curve posteriorly and are equal in size and roughly conical.

The upper dentition of *Xenorophus simplicidens* is asymmetrical, with many teeth shifted further anterior to their counterparts on the opposite side (Figure 19). While some positions on the left side (PC4–6) are 2 mm further anterior than the right PC4–6, the manner in which the rostrum has been reconstructed—perhaps forcing the rostrum to be symmetrical—has resulted in the left premaxilla extending 6 mm further anterior to the right premaxilla. This would suggest that the right teeth would instead be positioned up to 4 mm further anterior to those on the left, unlike the condition in *Xenorophus sloanii* (e.g., USNM 11049, CCNHM 168; see below). More complete specimens of *Xenorophus simplicidens* with three dimensionally preserved and undistorted rostra are needed to further evaluate dental asymmetry.

Mandible: The nearly complete right mandible of CCNHM 8720 is the only one preserved for *Xenorophus simplicidens* (Figure 20; Table 5). This mandible is missing only the anterior tip, part of the "pan bone", part of the mandibular condyle, and the angular process. The horizontal ramus is nearly rectilinear but deepens in height posteriorly, with a shallowly and continuously concave dorsal margin between pc4 and the coronoid apex (Figure 20B,C); as a result, the posterior dentition (pc4–8) is elevated, with each tooth slightly higher than the preceding one. The horizontal ramus is roughly rectangular in cross-section and somewhat transversely flattened (Figure 20D); the anterior tip and the i1 alveolus are missing, but the i2 alveolus is partially preserved; i3, c1, and pc1 alveoli are present but poorly preserved owing to crushing. The symphyseal surface is poorly preserved but appears to have extended posteriorly to the level of pc2. At least four mental foramina are present, approximately 1–2 mm in diameter with anteroposteriorly short sulci; they are positioned 10 mm below the alveolar margin at pc4, 5, and 6. The ventral margin of the mandible is straight anteriorly and slightly concave in its posterior half where the ascending ramus deepens.

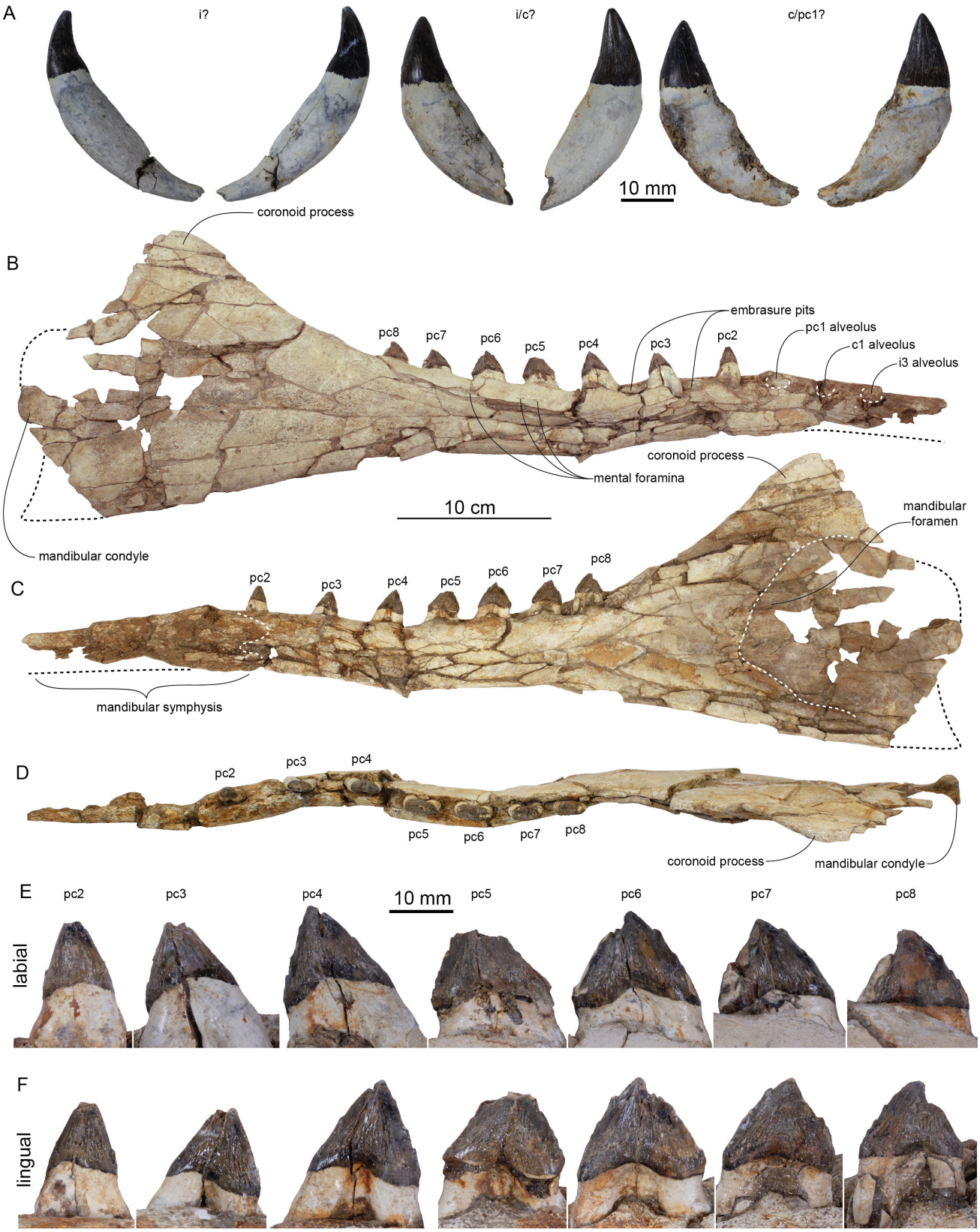


Figure 20. Lower dentition and mandible of the *Xenorophus simplicidens* holotype (CCNHM 8720). (**A**) Isolated lower teeth. (**B**) Right mandible in lateral view. (**C**) Right mandible in medial view. (**D**) Right mandible in dorsal view. (**E**) In situ postcanine teeth in labial view. (**F**) In situ postcanine teeth in lingual view.

Table 5. Mandibular measurements (in mm) of *Xenorophus simplicidens* (CCNHM 8720) and *Xenorophus sloanii* (CCNHM 104, 168, 1077). ? denotes missing measurements; e denotes an estimated measurement.

Measurement	CCNHM 8720	CCNHM 104	CCNHM 168	CCNHM 1077
Maximum length	?/696	?	684/680	?
Length of mandibular symphysis	?/155	?	206.5/212	?
Maximum height at coronoid process	?/183	?	178/180	?
Condyle, maximum width	?/192	?	37/35	?/44
Condyle, maximum depth	?	51.9/?	49/44.5	?/55.2
Mandibular foramen, maximum depth	?/123	?	?/124	?
Separation of condyle and last tooth	?/237	242/?	251/256	?/266
Mandibular width at last tooth		33.5/35	35/31	
Mandibular depth at last tooth	?/55	70e/?	76.5e/62	?/55e
Maximum length of toothrow	?/374	?	430e/426	?
Maximum length of postcanine toothrow	?/260	272	?/336	?

Embrasure pits are present in between teeth from pc2 through pc8. The pits between pc2, pc3, and pc4 are positioned slightly lateral to the toothrow and, from pc5 through pc8, the pits are positioned in the middle of the mandible. Lateral to the pc7–8, the lateral edge of the mandible is raised into a ridge and leads into the base of the coronoid process. This ridge is much higher than the alveolar margin on the medial side of the mandible and the last embrasure pit. This ridge obscures the root and base of the crown of pc8 in lateral view.

The coronoid process is subtriangular and symmetrical with a rounded apex (Figure 20B,C); the coronoid is nearly vertical but slightly medially deflected at the apex. The mandibular foramen is cavernous and has an evenly concave/arcuate margin; the anterior edge is slightly further anterior to the apex of the coronoid process. The pan bone is slightly thinner than in *Xenorophus sloanii*, being 2.3–2.5 mm in thickness anterior to the mandibular condyle. The mandibular condyle is incomplete, but the ventral portion suggests that it was quite transversely narrow, posteriorly convex, and medially excavated by the mandibular fossa. In lateral view, the posterior margin of the mandible ventral to the condyle is steeply anteroventrally oriented, suggesting a posteriorly concave margin above the angular process; it is unclear how far posteriorly the angular process extended.

Lower Dentition: Three aforementioned unicuspid teeth preserved ex situ represent uncertain loci, except for one nearly straight tooth with a relatively small (12.5 mm long) and slightly procumbent crown, likely representing the i1 (Figure 20A; Table 6) based on comparison with Basilosauridae and other stem odontocetes (*Ankylorhiza*, *Otekaikea*, *Waipatia*) that possess a procumbent first incisor. A slightly larger unicuspid tooth represents i2, i3, or c1. The c1 alveolus is approximately circular. A tooth with an anteroposteriorly broader root with oval cross-section and more triangular crown likely represents pc1; this tooth has a nearly smooth labial surface with faint striations and slightly stronger lingual striations. Carinae are poorly developed in the teeth representing i2, i3, or c1, and faint mesial and distal carinae are only present along the apical third of the crown; slightly stronger carinae are present in pc1.

The pc2 has a triangular crown with a smooth labial surface and faint apicobasal striations and sharp mesial and distal carinae (Figure 20E). Discontinuous apicobasal striations are more pronounced lingually; rougher striations form a poorly developed lingual cingulum with lightly nodular enamel. The root bears a vertical sulcus labially and lingually; CT data confirm that the root lobes are fused into an isthmus in their proximal half and diverge within the mandible. A single mesial basal cuspule is present. pc3 has a similar crown that is slightly broader anteroposteriorly, with similar ornamentation and a

poorly developed cingulum. This is the anteriormost tooth with clearly divided root lobes, though pc3 through pc8 have an isthmus visible at the alveolar margin, indicating that the root lobes diverge internally.

Table 6. Measurements (in mm) of lower dentition of *Xenorophus simplicidens* (CCNHM 8720) and *Xenorophus sloanii* (CCNHM 104, CCNHM 168, CCNHM 1077, 5022). ? denotes missing measurements; e denotes an estimated measurement; + denotes a minimum measurement.

Measurement	CCNHM 8720 Left	CCNHM 104 Left	CCNHM 104 Right	CCNHM 168 Left	CCNHM 168 Right	CCNHM 1077 Right	ChM PV 5022
i1, crown height	?	?	?	?	?	?	?
i1, mesiodistal length	?	?	?	?	?	?	?
i1, crown width	?	?	?	?	?	?	?
i2, crown length	?	?	?	?	16.6	?	?
i2, mesiodistal length	?	?	?	?	8.8	?	?
i2, crown width	?	?	?	?	8.5	?	?
i3, crown length	?	?	?	?	15.5	?	?
i3, mesiodistal length	?	?	?	?	9.5	?	?
i3, crown width	?	?	?	?	8.2	?	?
c1, crown length	?	?	?	?	?	?	?
c1, mesiodistal length	?	?	?	?	9e	?	?
c1, crown width	?	?	?	?	7.8	?	?
pc1, crown length	?	?	?	?	13e	?	?
pc1, mesiodistal length	?	?	?	?	9.9	?	?
pc1, crown width	?	?	?	?	7.4	?	?
pc2, crown length	11.7+	?	?	?	?	?	12.7/?
pc2, mesiodistal length	11.5	?	?	?	?	?	10.3/?
pc2, crown width	7.4	?	?	?	?	?	7.1/?
pc3, crown length	12.3	11+	14e	?	?	?	?
pc3, mesiodistal length	15.6	12.4	12.5	?	13	?	?
pc3, crown width	7	6.9	7.1	?	7.2	?	?
pc4, crown length	15.5	14e	?	?	15	?	?
pc4, mesiodistal length	17.9	15.2	15.7	?	16.1	?	?
pc4, crown width	7.9	7.3	?	?	7.8	?	?
pc5, crown length	13+	15	?	15.3	?	14.7	?
pc5, mesiodistal length	21.5	18.7	18.2	18.1	17.5	18.2	?
pc5, crown width	9	8.3	8	7.8	8.0	8.5	?
pc6, crown length	16.3	?	15.3	14.5	?	15.7	?
pc6, mesiodistal length	21.9	?	20.2	21	?	19.5	
pc6, crown width	9.1	?	8.9	8.3	?	8.9	
pc7, crown length	15.7	14+	12.3+	15.4	?	14.5	?/14.2
pc7, mesiodistal length	19.6	19.9+	20.5+	20.1	?	?	?/18.5
pc7, crown width	8.8	9.3	9.6	10.5	?	9.1	?/9.9
pc8, crown length	13.5	?	11.5+	15.2	?	12.9	?/12.6
pc8, mesiodistal length	18.2	?	19+	17.9	?	17.3	?/14.3
pc8, crown width	9.4	8.5	9.7	9.3	?	9.6	?/11.5
pc9, crown length	?	?	12.9	11.9	11.6	?	11.8/?
pc9, mesiodistal length	?	?	18+	13.2	13.4	?	14.2/?
pc9, crown width	?	?	9.8	9.6	9.8	?	8.4/?

Pc4 is anteroposteriorly broader and higher than pc3, with sharp mesial and distal carinae, slightly stronger labial apicobasal striations, and much stronger lingual striations on the basal two-thirds of the crown (Figure 20E). There is one mesial cusp at mid-crown height, and three distal cusps: one just below the principal cusp, and the other two in the basal half. There is a near-continuous but weakly developed lingual cingulum consisting of a narrow basal band of rugose enamel; a discontinuous labial cingulum is also poorly developed, but confined to the mesial and distal ends of the crown.

Posterior cheek teeth pc5–7 are similar to one another in morphology and are the largest mandibular teeth; all are double-rooted (Figure 20E). The triangular multicuspate crowns bear faint labial striations and strong lingual striations on the basal two-thirds of the crown, as well as sharp carinae interrupted only by accessory cusps. Mesial accessory cusps are uncertain in pc5, but there are four distal accessory cusps; pc6 has two mesial cusps along the apical half of the carina, and possibly three–four distal cusps (uncertainty owing to tooth wear); and pc7 has two large mesial cusps on the apical half of the carina and some basal mesial cuspules where the poorly developed cingulum meets the carina, as well as possibly up to four distal cusps which are mostly destroyed by a distal wear facet. pc5–7 all bear a weak lingual cingulum formed from a band of nodular enamel and a slight labial cingulum, again confined mesially and distally. The crown of pc8 is slightly anteroposteriorly narrower than pc7 and bears three prominent mesial cusps, a cuspule near the principal cusp, and at least one distal cusp; more were likely present but removed by tooth wear. The apicalmost distal cusp is separated from the principal cusp by a deep notch. pc8 has the strongest lingual cingulum in the dentition, forming a narrow shelf; otherwise it shares discontinuous apicobasal lingual striations and faint labial striations with more anteriorly positioned teeth (Figure 20E).

Starting with pc5, each tooth is successively slightly elevated relative to the preceding tooth; along with this, the diastemata become narrower (Figure 20B,C). The widest diastemata are between pc2 and pc3 (24.5 mm), whereas the narrowest diastema is between pc7–8 and measures only 7.4 mm.

Tooth Wear: Tooth wear is minimal on the upper anterior teeth (Figure 18), and wear is greatest on the posterior postcanines (Figure 19). The teeth on the right are generally worn more extremely than teeth on the left side. A few upper anterior teeth have minute apical wear facets with a small circle of dentine exposed (?PC2 and ?PC3). PC4 has a larger apical wear facet, but lacks wear on either carina. PC5 is the anteriormost tooth with mesial and distal wear facets (3 mm from crown base). It bears a 4–5 mm long mesial wear facet; on the left, the single mesial cuspule bears a facet. PC5 has a slightly larger apical wear facet. The distal facets are small and located along the carina, 2–3 mm long, and 2–2.5 mm from the crown base. PC6 has the largest apical wear facet, a somewhat larger mesial wear facet than PC5, and a similarly small distal wear facet.

The right PC7 has a slightly smaller mesial wear facet than PC6, and lacks apical wear (Figure 19). A large mesial wear facet is present that extends posterobasally onto the lingual surface of the crown to within 1 mm of the crown base, along the anterior third of the crown, and along the basal half of the crown and carina. The distal wear facet is large and placed along the distal edge of the accessory cusp. An irregular and horizontal 5.8 mm long wear facet just above the crown base and along the posterolingual margin of the tooth is present.

PC8 has a minute apical wear facet on the right side whereas the left is unworn (Figure 19). The mesial wear facet is large, shallowly concave, and has removed 80% of the apicobasal length of the mesial carina. The distal wear facet has removed accessory cusps and is continuous on the right PC8 with a cingular wear facet basally. On the left PC9, this cingular wear facet (as in PC7) is separate from the distal wear facet.

The left and right PC9 lack apical wear facets but possess large mesial wear facets (Figure 19). On the right side, this facet has removed approximately 50% of the apicobasal length of the carina. On the left side, there is a separate facet on the mesial accessory cusps. The distal carina and accessory cusps are unworn.

Tooth wear is less extreme in the lower dentition (Figure 20A,E), and none of the complete teeth possess an apical wear facet on the principal cusp. Mesial wear facets are sporadic and confined to individual accessory cusps throughout the dentition; distal wear facets on pc2–5 are similarly only on accessory cusps. Distal wear on pc6–8 consists of single continuous facets along the lingual side of the distal carina and cusps. In pc6, it extends from the apicalmost cusp to the base of the crown. In pc7–8, the facets are similar but extend onto the posterolabial side of the tooth crown.

Cervical Vertebrae: The atlas vertebra (total width: 134 mm) is complete but partially obscured in the holotype (CCNHM 8720; Figures 2 and 3). Even so, it has large, dorsally positioned transverse processes with a rectangular outline, like some *Albertocetus meffordorum* (CCNHM 303, Boessenecker et al., 2017B), but differing from specimens of *Xenorophus sloanii* that possess a bifurcated transverse process with two tubercles (CCNHM 1077) and *Echovenator sandersi*. The atlas bears a low neural spine, a prominent hypapophysis, and an oval outline of the occipital articular facets; the shape of the neural canal is unclear owing to obscuring matrix. The atlas of ChM PV 4266 is similar but has a proportionally larger neural canal, a slightly higher neural spine, and transversely narrower facets for the occipital condyles and axis relative to specimens of *Xenorophus sloanii.*

The axis is only preserved in the holotype (CCNHM 8720), and the posterior side is exposed in relief (Figure 2). The posterior face of the centrum is subtriangular and ventrally pointed but lacks a clear hypapophysis. In posterior view, the transverse process is rectangular and transversely longer than in *Xenorophus sloanii*. The neural spine is wide, subrectangular, and transversely widens dorsally; it further bears a bifurcated apex, as in *Xenorophus sloanii*. The neural canal is more circular than in *Xenorophus sloanii*.

A mid-cervical, C3 or C4, is preserved overlying the skull vertex of CCNHM 8720; it has a subtriangular centrum and does not differ from *Xenorophus sloanii*. A partial C3 or C4 is preserved in ChM PV 4266 and it differs from the holotype in having a round centrum. A partial C6 is preserved in CCNHM 8720, and a more complete C6 is preserved in ChM PV 4266 (Figure 21). It bears a long and ventrolaterally projecting parapophysis with a small dorsolateral tubercle partially defining the lateral margin of the vertebrarterial canal.

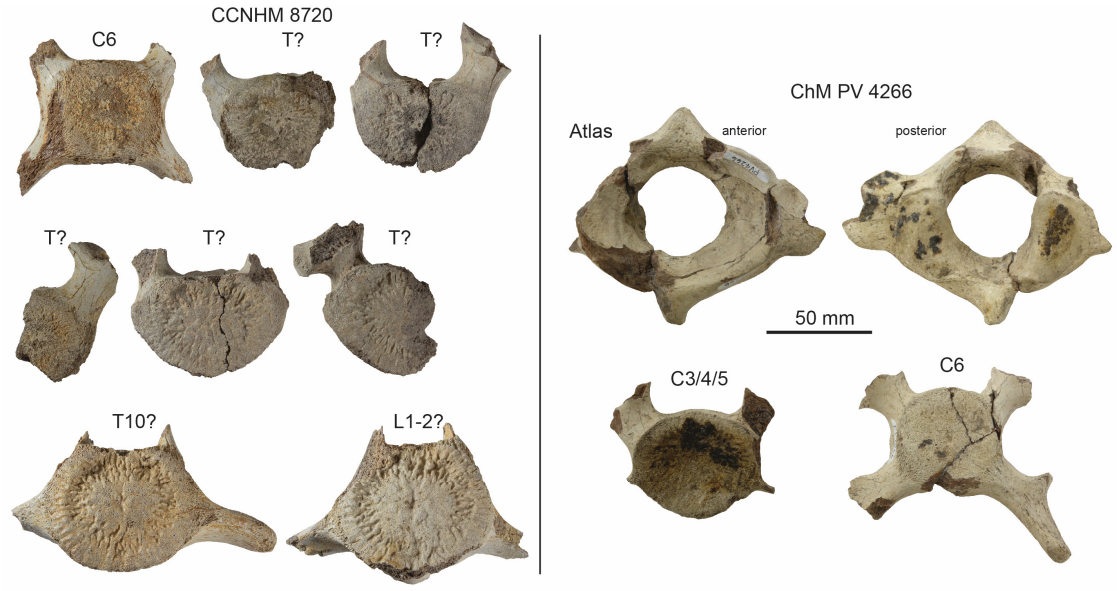


Figure 21. Vertebrae of *Xenorophus simplicidens* in anterior view, unless otherwise noted. ? denotes uncertain vertebral number assignment.

Thoracic Vertebrae: Eight or nine thoracic vertebrae are preserved in CCNHM 8720; they measure 58–65 mm in centrum width and approximately 43–49 mm in centrum depth (Figures 2, 3 and 21). Like the remaining vertebrae of CCNHM 8720, these vertebrae are

smaller than their counterparts in adults of *Xenorophus sloanii* (CCNHM 104, 168, 1077, ChM PV 5022). Two vertebrae with laterally protruding tuberosities, with costal facets and facets for the tubercles of the ribs, correspond to posterior-mid thoracics, perhaps T5–8. One vertebra, likely T10, has a short ventrolaterally extending transverse process with a blunt apex for the articulation of what is probably the last rib. T10 resembles lumbar vertebrae but lacks a ventral median keel.

Lumbar Vertebrae: Nine lumbar vertebrae are preserved (Figures 2, 3 and 21). Owing to their exposure in relief, they cannot be arranged into an anteroposterior series; they measure between 68 and 73 mm in centrum width, 48 and 61 mm in centrum length, and 67 and 69 mm in centrum depth. Neural spines and transverse processes are preserved in some and are quite long (spines up to 155 mm and transverse processes up to 100 mm). Neural spines anteroposteriorly widen dorsally in lateral view, and transverse processes are rectangular in dorsal outline. The neural canal diameter ranges from 29 mm wide in the anterior lumbars to 11 mm wide in posterior lumbars. No caudals or posteriormost lumbar with hemal facets are preserved. All exposed lumbars of CCNHM 8720 possess ventral median keels.

Ribs: Several ribs are preserved in relief and ex situ in CCNHM 8720 (Figures 2 and 3). They are poorly preserved but most are anteroposteriorly flattened and bear a subrectangular cross-section, transitioning to a rhomboid or lenticular cross-section distally. The ribs are narrow and do not thicken distally.

Xenorophus sloanii Kellogg, 1923 [8]

Xenorophus sloani [17]
Xenorophus sloani [18]
Xenorophus sloani [9]
Xenorophus sloani [27]
Xenorophus sloani [4]
Xenorophus sloani [5]
Xenorophus sloani [29]

Holotype: USNM 11049, partial juvenile cranium including maxillary part of the rostrum, orbital region, frontals, and some postcanine teeth (left and right PC6–8), collected sometime prior to 1908 by unknown collectors, presumably quarry workers, from Ashley Formation exposures in a marl pit near Woodstock Station (Charleston County, South Carolina) owned by the Ingleside Mining Company. The specimen resided in the collection of the pit's superintendent, who gave the specimen to Sloan, who later donated the specimen to USNM for study by Kellogg [8].

Referred Specimens: CCNHM 104, a partial skeleton including a nearly complete cranium, left and right mandibles, four cervical vertebrae, four thoracic vertebrae, two lumbar vertebrae, and one caudal vertebra, collected summer 2006 by P. Bailey from the vicinity of Summerville, Dorchester County, South Carolina; CCNHM 168, a partial skeleton including nearly complete cranium, left and right mandibles, thyrohyal, seven cervical vertebrae, four thoracic vertebrae, three lumbar vertebrae, and ten ribs, collected May or June 1997 by W. Hillenius and Dana Cope from the vicinity of Summerville, Dorchester County, South Carolina; CCNHM 1077, nearly complete skeleton including a partial cranium lacking much of the rostrum, partial mandibles, seven cervical vertebrae, ten thoracic vertebrae, ten lumbar vertebrae, and six caudal vertebrae, collected by Steven Miller and M. Havenstein in 2002 from the vicinity of Crowfield Plantation subdivision in Goose Creek, Berkeley County, South Carolina; CCNHM 5995, partial skull with associated caudal vertebra, collected by Craig Garrison in June 2015 in the vicinity of Summerville, Dorchester County, South Carolina; ChM PV 5022, partial skeleton including partial cranium lacking anterior rostrum, seven cervical vertebrae, seven thoracic vertebrae, ten lumbar vertebrae, three caudal vertebrae, and at least six ribs, collected 17–21 May 1991 by Albert Sanders, Jonathan Geisler, Bricky Way, Betsi Nemeth, and Aaron Stokes, collected just south of Crowfield Plantation subdivision, Goose Creek, Berkeley County, South Carolina; ChM PV 7677, a nearly complete skull with one cervical and three associated thoracic vertebrae, collected

August 1986 by S. Miller, S. Faust, and V. McCollum from the vicinity of Crowfield Plantation subdivision, Goose Creek, Berkeley County, South Carolina; ChM PV 5020, associated left and right partial mandibles, collected March 1987 by B. Albright from spoils at Wando Terminal, Charleston County, South Carolina; ChM PV 5709, left partial mandible and isolated rib, collected 26 March 1985 by S. Faust and students in the vicinity of Summerville, Dorchester County, South Carolina.

Locality and Age: All known specimens of *Xenorophus sloanii* were collected from the lower Oligocene Ashley Formation in the Charleston Embayment, ranging in age from 30.0 to 28.0 Ma [26].

Amended Diagnosis of Species: A large xenorophid dolphin with approximate adult condylobasal length of 74 cm and bizygomatic width of 29–30 cm and differing from *Xenorophus simplicidens* in possessing anteroposteriorly longer nasals (22–29% of bizygomatic width vs. 16–19% in *X. simplicidens*), nasal process of premaxilla possessing lateral overhanging crest adjacent to bony nares in adult specimens, left antorbital fossa longer than right (right antorbital anteroposteriorly longer than left in *Xenorophus simplicidens*), longer supraorbital process (distance from antorbital notch to posterior margin supraorbital process 43% of bizygomatic width vs. 34% in *X. simplicidens*), nasals that broaden posteriorly and approximate or exceed nares width, left and right palatines separated by anteroposteriorly short median triangular exposure of maxilla, paroccipital processes extending posterior to occipital condyles, shorter median furrow on the tympanic bulla, more teeth with accessory denticles (on PC5–9 as opposed to PC7–9 in *X. simplicidens*), more accessory denticles per tooth (five distal cusps vs. three in *X. simplicidens*; three–four mesial cusps vs. one–three in *X. simplicidens*), and more rugose enamel throughout the dentition, with nodular enamel present on PC5–9 (only present on PC7–9 in *X. simplicidens* and less rugose than in *X. sloanii*).

5.1.5. Description of *Xenorophus sloanii*

The description of the skull, mandibles, and dentition is based on the most completely preserved skull, CCNHM 168, but is supplemented by CCNHM 104, 1077, 5995, ChM PV 5020, 5022, and 7677, in addition to the holotype (USNM 11049). Where polymorphisms exist among specimens, they are noted; if a statement in the description does not refer to a particular specimen, it is a feature that is identical in all specimens that preserve that structure. Descriptions of the tympanic bullae are based chiefly on CCNHM 168, CCNHM 104, CCNHM 1077, and ChM PV 5022. Descriptions of the periotic are based chiefly on CCNHM 104, CCNHM 1077, ChM PV 5022, and CCNHM 7677. Descriptions of the postcrania are based (in descending order of importance) on CCNHM 1077, ChM PV 5022, CCNHM 168, and CCNHM 104.

Ontogenetic Status: In all specimens the following sutures remain open or unfused (i.e., a suture line that is not obliterated or completely fused/invisible): maxilla–premaxilla, squamosal–parietal, parietal–occipital, squamosal–occipital, maxilla–frontal, median nasal, median parietal, and frontonasal suture (the latter appears obliterated in CCNHM 104, similar to the *Echovenator* holotype; [3]). In CCNHM 1077, the median frontal suture is nearly completely fused and the frontonasal suture is barely visible. In CCNHM 1077, the median parietal suture is sinuous and fine. In contrast, the median parietal suture in CCNHM 104 is straight and open (a fissure several mm wide dorsally), although this may be an artifact of preservation and reassembly.

Tooth wear varies between specimens. The holotype bears no visible wear facets; the entire mesial and distal edges of all cheek teeth in CCNHM 104 are obliterated by large wear facets along with the complete loss of LC1 and LPC1 crowns and most of LI2. In CCNHM 168, there are small mesial and distal wear facets on PC7–8 and, in CCNHM 1077, there are wear facets on the mesial edge only of B1–2 (=PC8–10 or so, depending upon tooth count). Similar patterns of tooth wear exist on the lower dentition of each specimen. Tooth wear does not appear to correlate perfectly with body size as subadult specimen CCNHM 104 has rather extreme tooth wear and incomplete cranial suture closure, whereas the

largest specimens (CCNHM 1077, CCNHM 168, and ChM 5022) possess more completely closed sutures, more strongly developed crests, and less strongly developed tooth wear (yet, more than in the holotype specimen). If extreme tooth wear in CCNHM 104 is the cause of unusual behavior in this individual (see *6.5. Feeding Ecology of* Xenorophus), tooth wear otherwise seems to correspond to ontogenetic status with juveniles (class III) lacking tooth wear, subadults (class IV) possessing minor tooth wear, and adults (class V and VI) possessing more extreme wear including large shearing facets.

Specimens were assigned to the growth classes of Perrin [83] based chiefly on tooth development, skull suture closure, and closure of vertebral epiphyseal sutures. Additional information, such as nasal length, was also considered.

Class I and II: No specimens of *Xenorophus sloanii* are assignable to either class I (fetus) or II (neonate).

Class III: The holotype specimen (USNM 11049) and CCNHM 5995 (Figures 22–25) were assigned to Class III of Perrin [83] owing to the following combination of features (some preserved only in one specimen): small size, unworn teeth, relatively short nasals, cranial sutures either open or lightly sutured, but not strongly mortised, and, in the case of CCNHM 5995, completely unfused vertebral epiphyses.

Class IV: two specimens (ChM PV 7677, CCNHM 104; Figures 24–27) represent Class IV, based on slightly larger size than Class III, no open sutures (except the median parietal suture in CCNHM 104) nor obliterated sutures, more than 75% of the vertebral column with fused epiphyses (mostly open in ChM PV 7677), and relatively short nasal bones. While ChM PV 7677 exhibits unworn teeth, the teeth of CCNHM 104 record the heaviest wear of any specimen of *Xenorophus*—few teeth have any carinae preserved, and some anterior teeth (LI2, LC1, LPC1) are completely missing the crown. Vertebrae of these specimens have a mixture of fused and open epiphyseal sutures.

Class V: two specimens (CCNHM 168, CCNHM 1077; Figures 24–29) are assigned to class V based on large size, all sutures being either strongly mortised or obliterated, long nasals, and most—but not all—vertebral epiphyses fused. CCNHM 1077 is perhaps the most mature specimen based upon skull size, nuchal crest height, and cranial suture development—but still has a few vertebrae with unfused epiphyses. If preserved from a skull only, his specimen would have likely been assigned to class VI.

Class VI: Only one specimen (ChM PV 5022; Figures 24, 25, 28 and 29) is assigned to class VI—based on large size, long nasals, mostly obliterated (and some mortised) skull sutures, and completely fused epiphyses throughout the vertebral column.

Other features such as the development of the paranaris crest, nasal length, nuchal crests, length of the supraoccipital, development of the sternomastoid fossa, and surface texture of the occipital condyles are ontogenetically informative in Xenorophidae and other early Odontoceti, yet not part of Perrin's [83] framework. In Class III–V, the paranaris crest is vertical, yet in Class VI, the crest has a slight lateral overhang resembling the condition in *Cotylocara macei* and more mature (but unpublished) specimens of *Echovenator* (CCNHM 217, 219). The nasal bones are relatively short in Class III (31–34 mm, USNM 11049), are similar to somewhat longer in class IV (28–31 mm, ChM PV 7677; 48+ mm, CCNHM 104), and are longest in class V and VI (66–79 mm; Figures 30 and 31). The nuchal crests are vertically higher in successively more mature specimens (Figure 25), with relatively low crests in Class III, slightly higher crests in Class IV, and much higher crests in Class V and VI. Along with dorsal growth of the nuchal crests, the supraoccipital lengthens during ontogeny resulting in a longer distance from the foramen magnum to the supraoccipital apex (Figures 30 and 31). In Class III and IV, the length is 107–117 mm (CCNHM 104, ChM PV 7677), and longer in Class V and VI (123–128 mm, CCNHM 1077, ChM PV 5022). An exception to this is Class V specimen CCNHM 168 (113 mm), owing to a deep dorsal notch in the margin of the foramen magnum. Concomitant with anterodorsal growth of the supraoccipital, the anteroposterior length of the parietal decreases slightly during late postnatal ontogeny as it is overridden by the supraoccipital, with the longest length present in Class IV specimens like ChM PV 7677 (55.6 mm), and generally shorter lengths

in class V and VI specimens (34–42 mm; CCNHM 168, CCNHM 1077; note that these specimens are similar in bizygomatic skull width; Figure 31). A much shorter length in Class III individual CCNHM 5995 is due to the smaller size of the skull. In Class III specimen CCNHM 5995, the occipital condyles bear porous rather than smooth finished bone surfaces. The sternomastoid fossa is shallow, less rugose, and anteroposteriorly shorter in Class IV (CCNHM 104, ChM PV 7677) than Class V and VI (CCNHM 168, CCNHM 1077, ChM PV 5022).

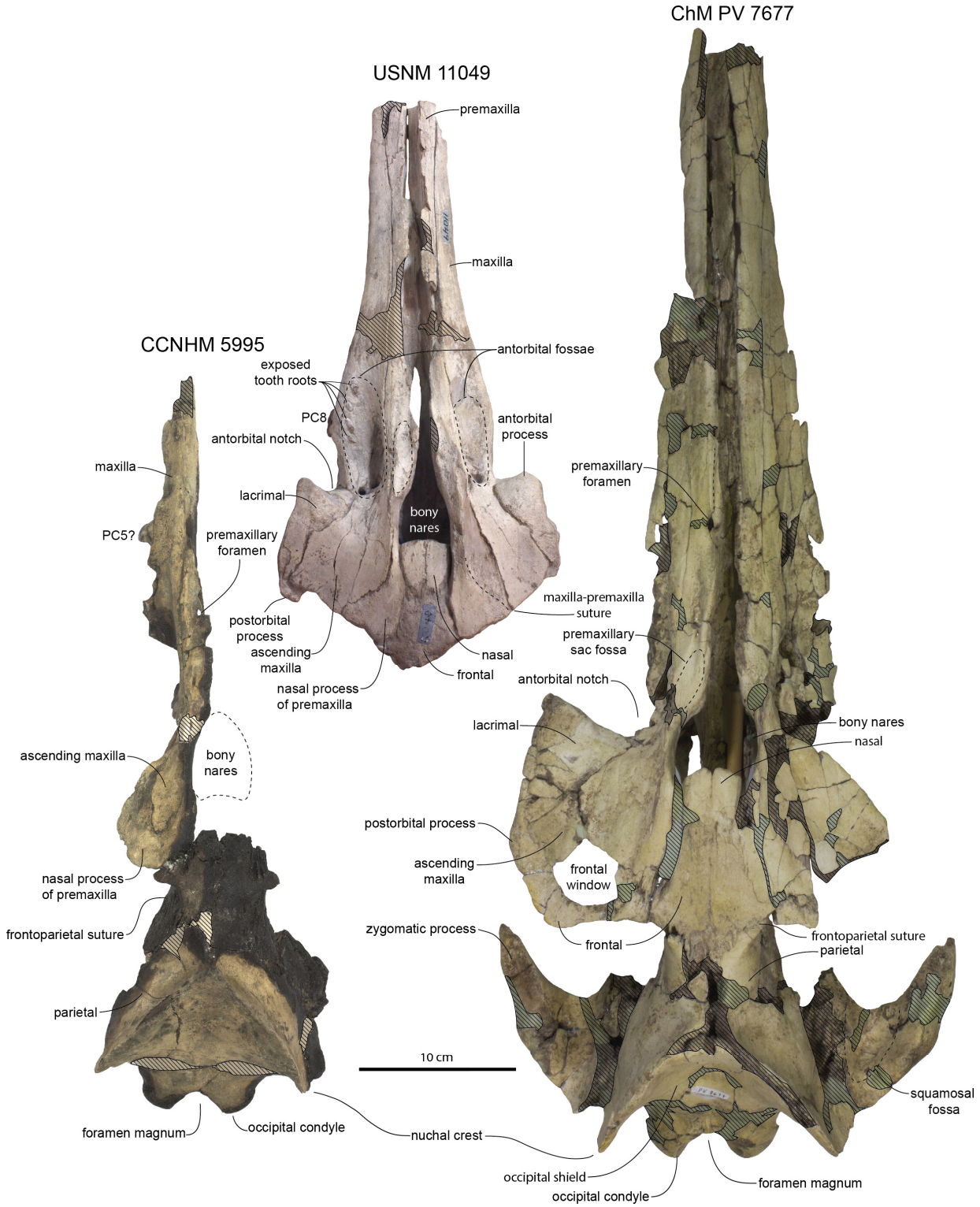


Figure 22. Holotype and referred skulls of juvenile and subadult *Xenorophus sloanii* in dorsal view.

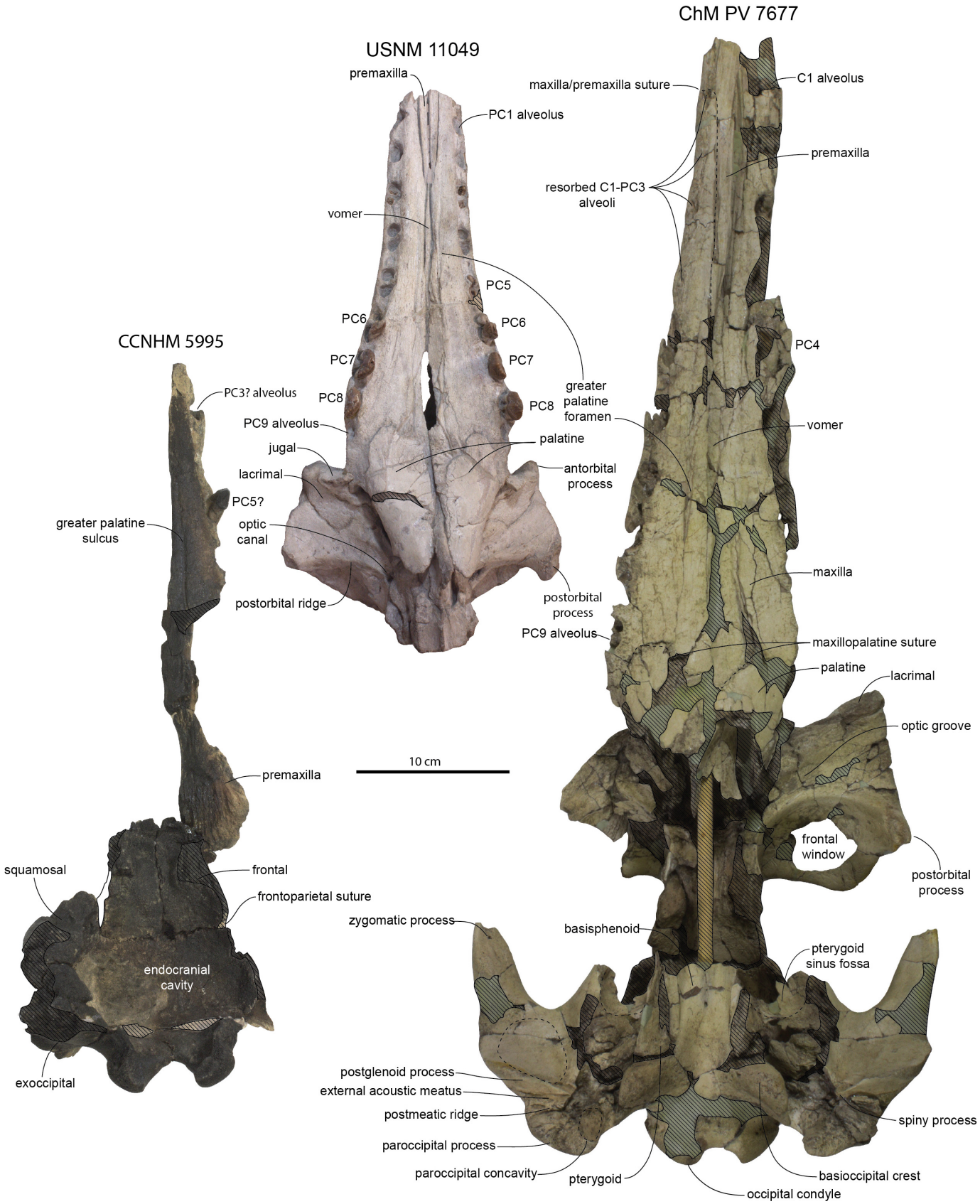


Figure 23. Holotype and referred skulls of juvenile and subadult *Xenorophus sloanii* in ventral view.

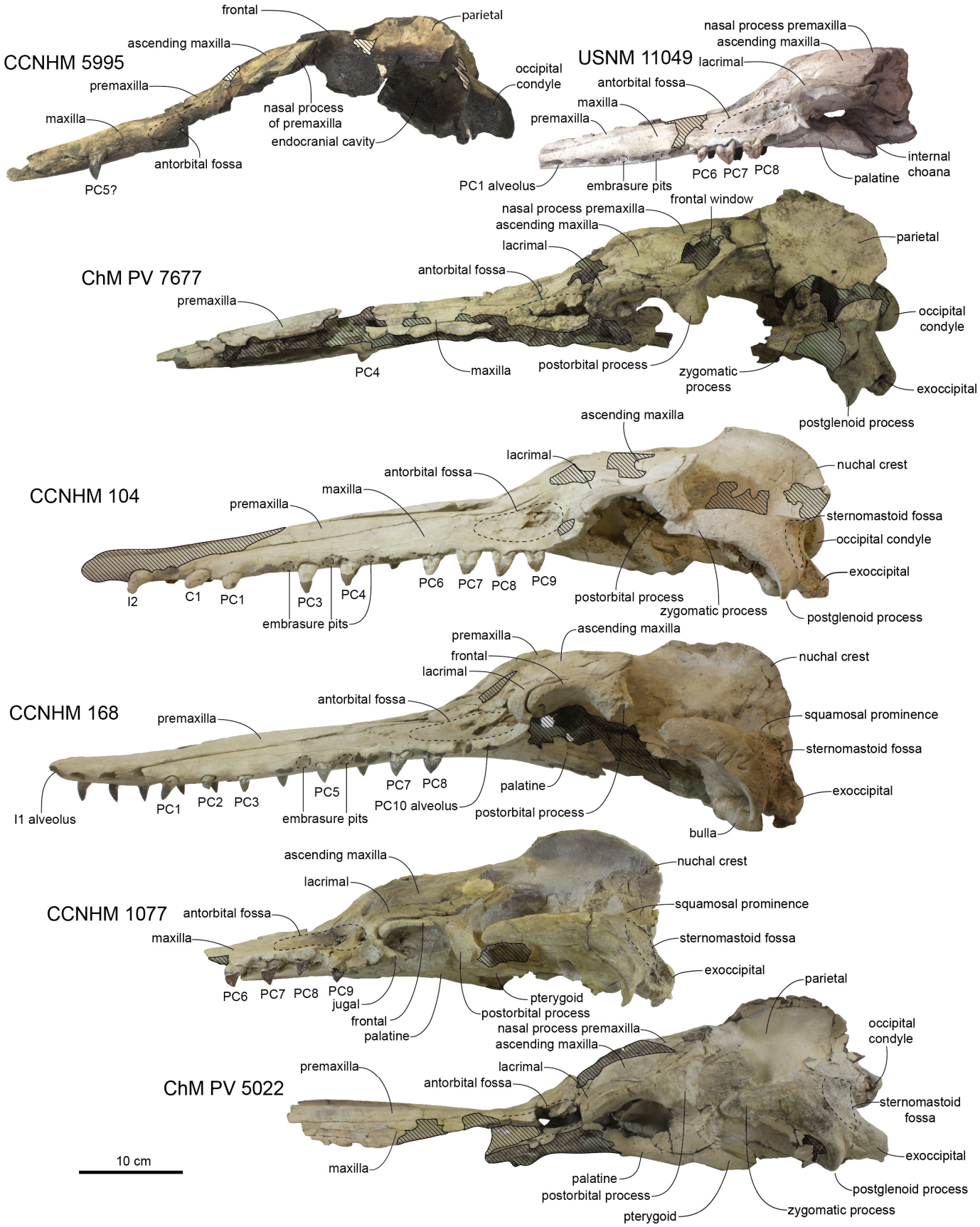


Figure 24. Holotype and referred skulls of *Xenorophus sloanii* in lateral view.

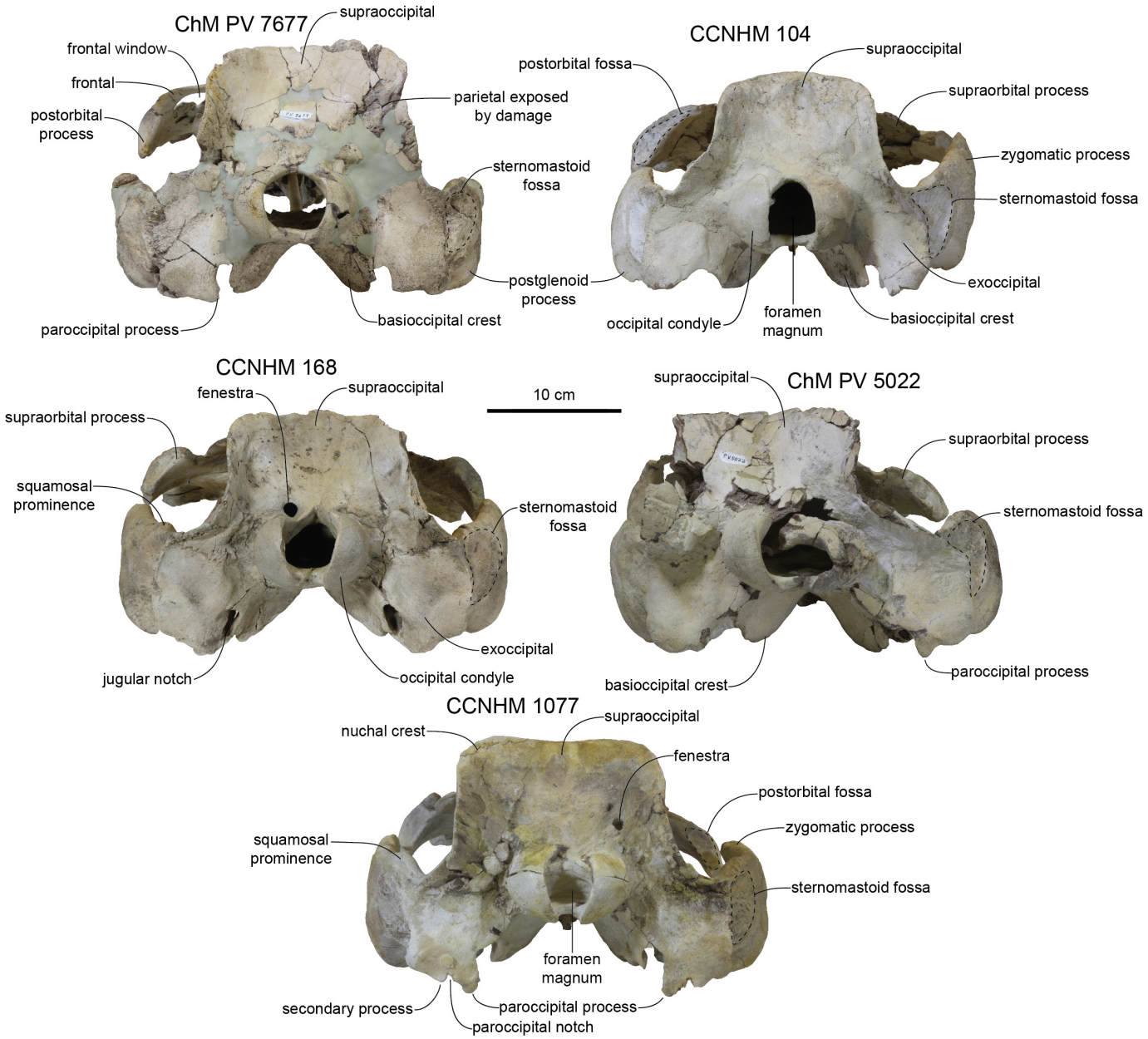


Figure 25. Referred skulls of *Xenorophus sloanii* in posterior view.

Rostrum and Palate: The rostrum is relatively elongate, with RPI values in the range of 2.44–2.62 (Max: CCNHM 104; min: ChM PV 7677; Figures 22, 23, 26, 27 and 30; Table 7). In CCNHM 168, the anterior 90 mm of the rostrum is formed by the premaxilla only. The premaxillae do not taper anteriorly in dorsal view but have a smoothly convex anterolateral margin rather than a triangular apex of the premaxilla. There is a slight bulging around tooth roots giving the premaxilla a subtle 'scalloped' edge, which continues along the anterior half of the maxilla. In dorsal view the rostrum is triangular but has a sinuous lateral margin; the rostrum widens greatly in its posterior third and then narrows precipitously at the antorbital notch, making the posterior 10 cm of the maxilla markedly laterally convex.

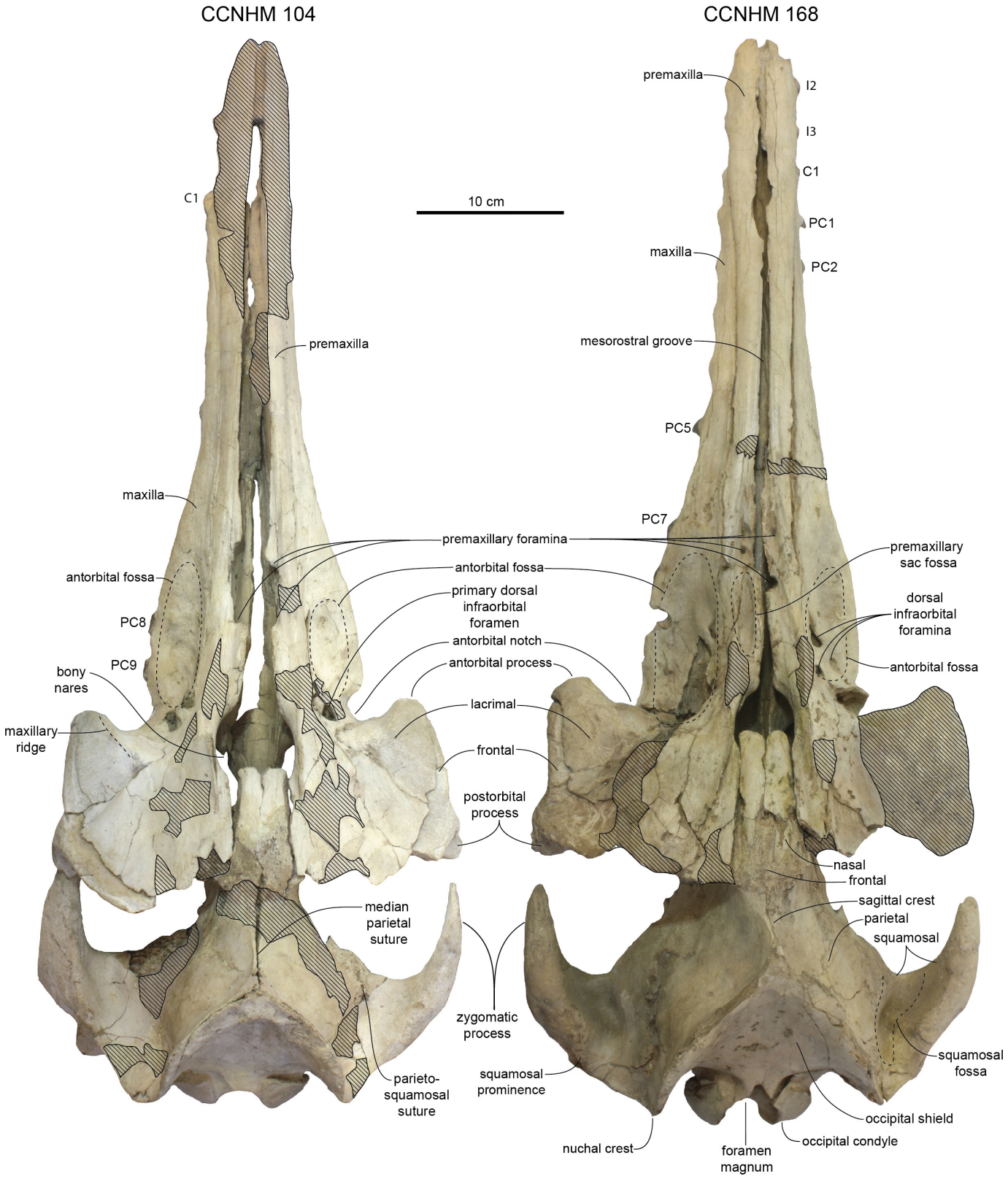


Figure 26. Referred skulls of subadult and adult *Xenorophus sloanii* in dorsal view.

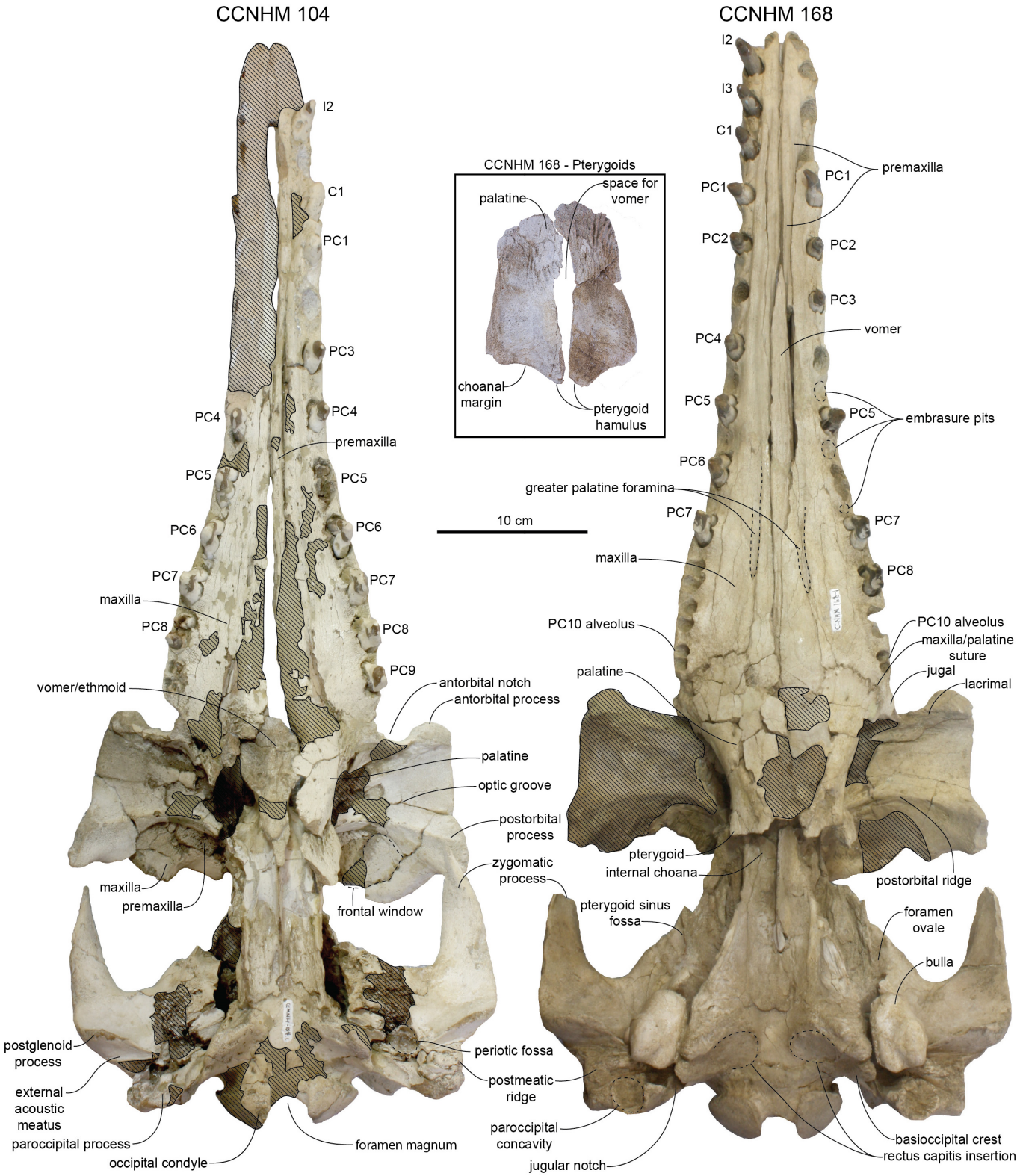


Figure 27. Referred skulls of subadult and adult *Xenorophus sloanii* in ventral view.

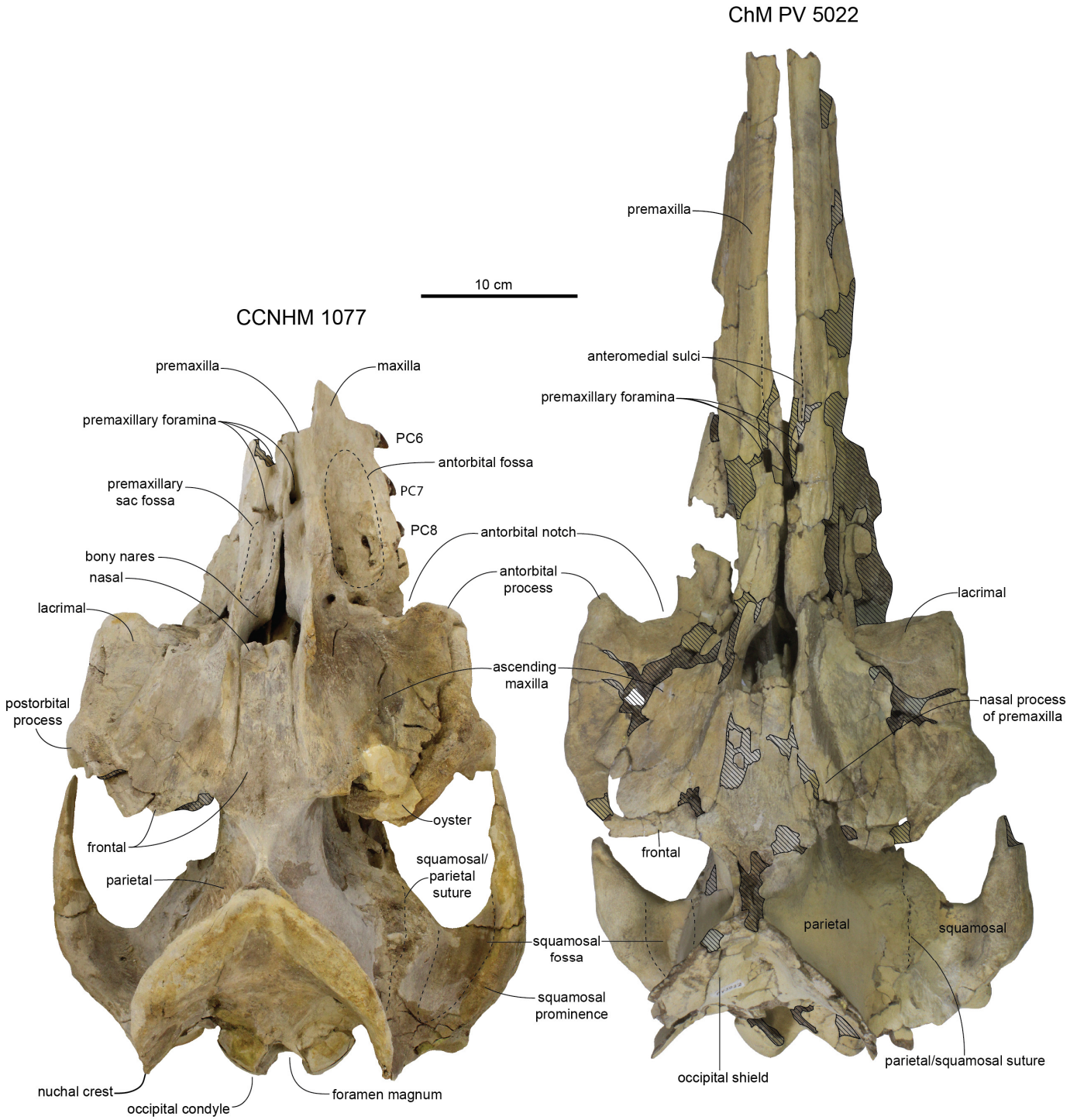


Figure 28. Referred skulls of adult *Xenorophus sloanii* in dorsal view.

The rostrum in all specimens of *Xenorophus sloanii* diverges from the sagittal plane within the braincase and interorbital region by approximately 1.5–4.7° to the left side (determined in dorsal and ventral view, measured in ImageJ based on the osteological midline of the rostrum and braincase, with an angle vertex placed at about least interorbital width; Figures 22, 23, 26, 27 and 30). It is least divergent in ChM PV 7677 (0.9°), somewhat more divergent in CCNHM 168 (2.3°) and most divergent in CCNHM 104 (4.7°) and the holotype (~4.0°). In lateral view the rostrum is nearly straight with a slightly sinuous ventral margin, the palatal margin becoming slightly ventrally convex anteriorly and concave posteriorly. The rostrum is slightly downturned relative to the basicranial stem; in

CCNHM 168 and CCNHM 104, it descends anteroventrally 22° from the horizontal plane, and only 14° in ChM PV 7677, though this may be due to diagenetic distortion near the vertex and it was likely closer to or exceeding 20°. Lastly, the rostrum is also twisted along its longitudinal axis (counterclockwise in anterior view) by 11° in CCNHM 168 (Figure 32).

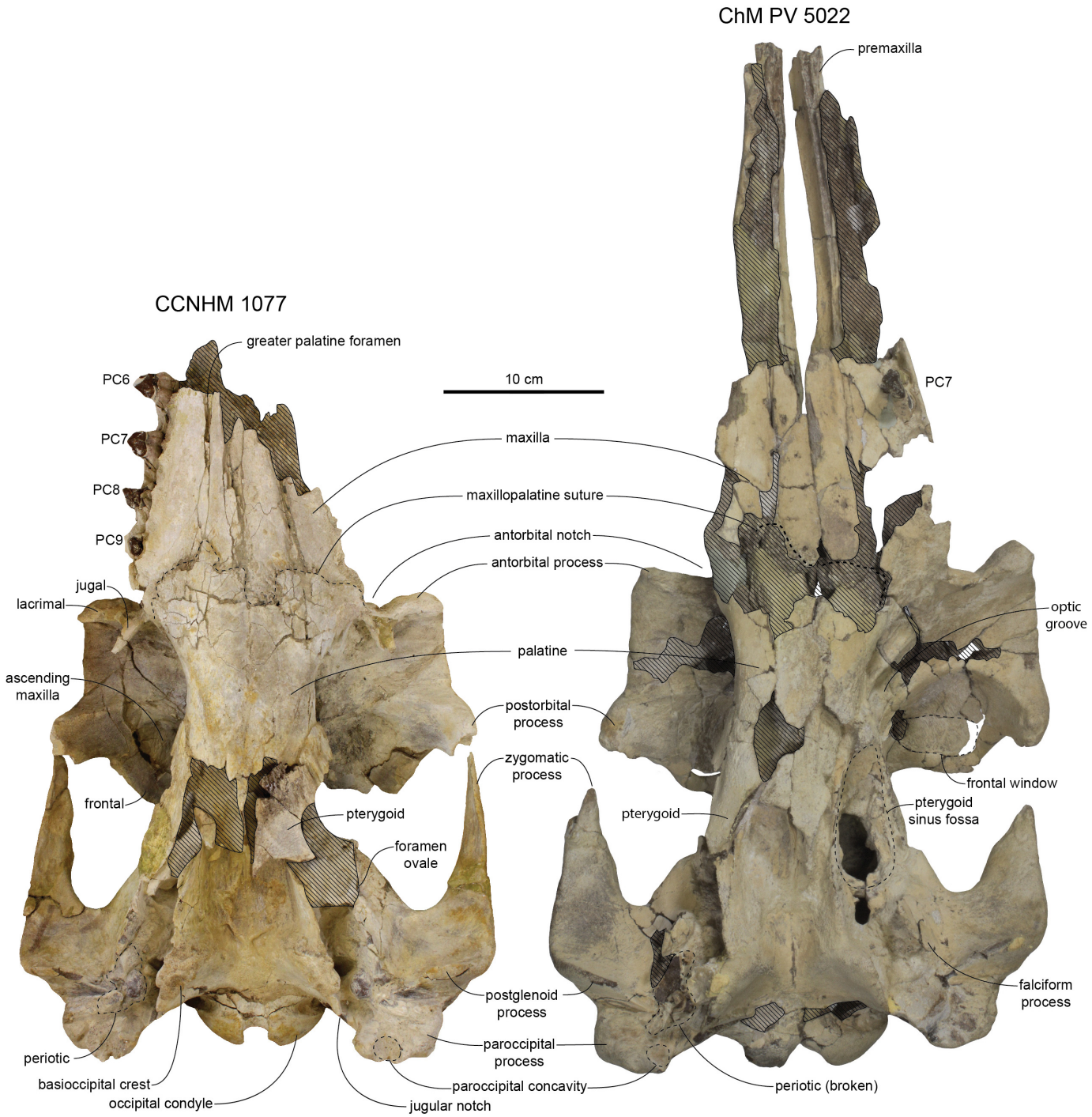


Figure 29. Referred skulls of adult *Xenorophus sloanii* in ventral view.

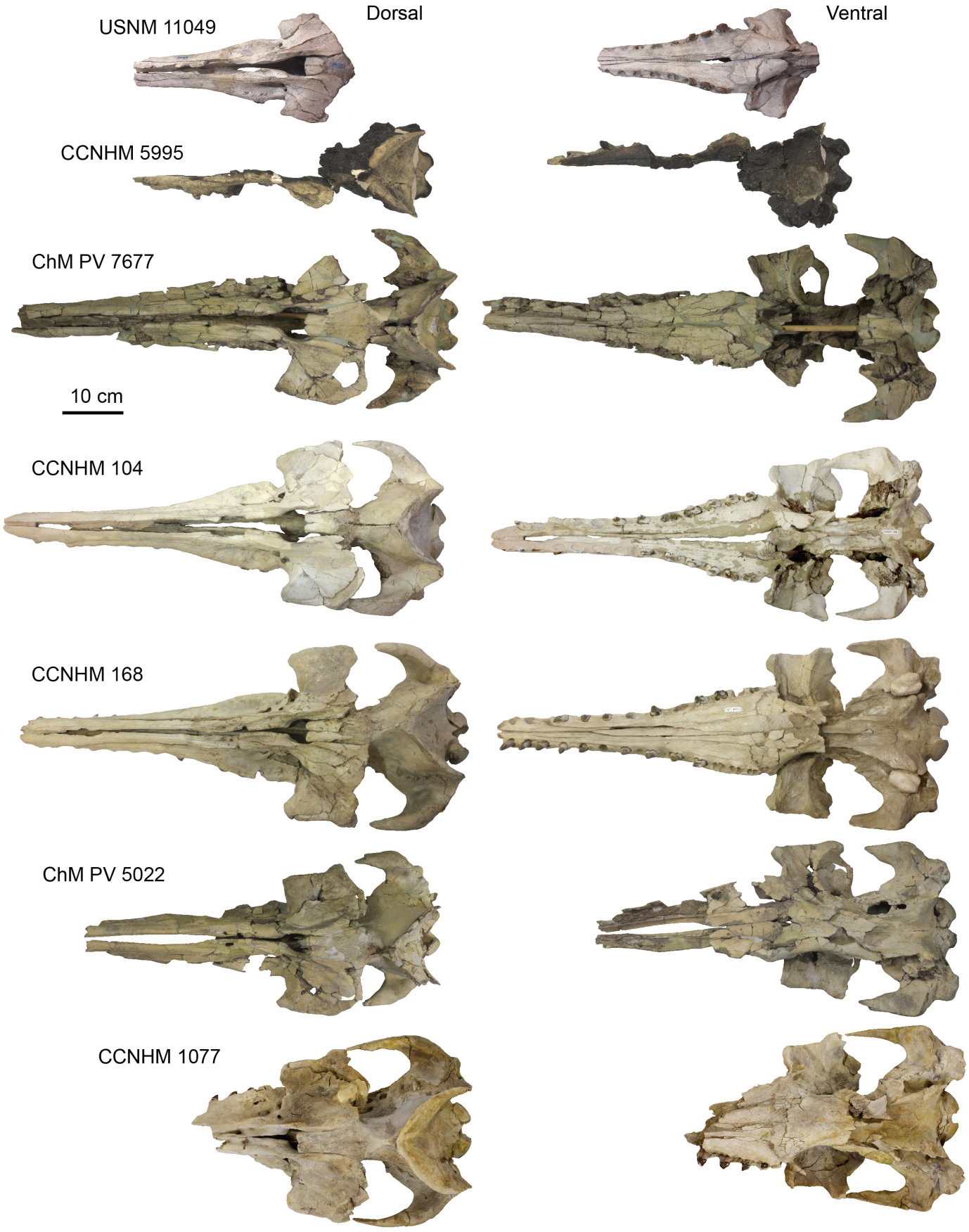


Figure 30. Skulls of *Xenorophus sloanii* in dorsal view, aligned by the antorbital notch.

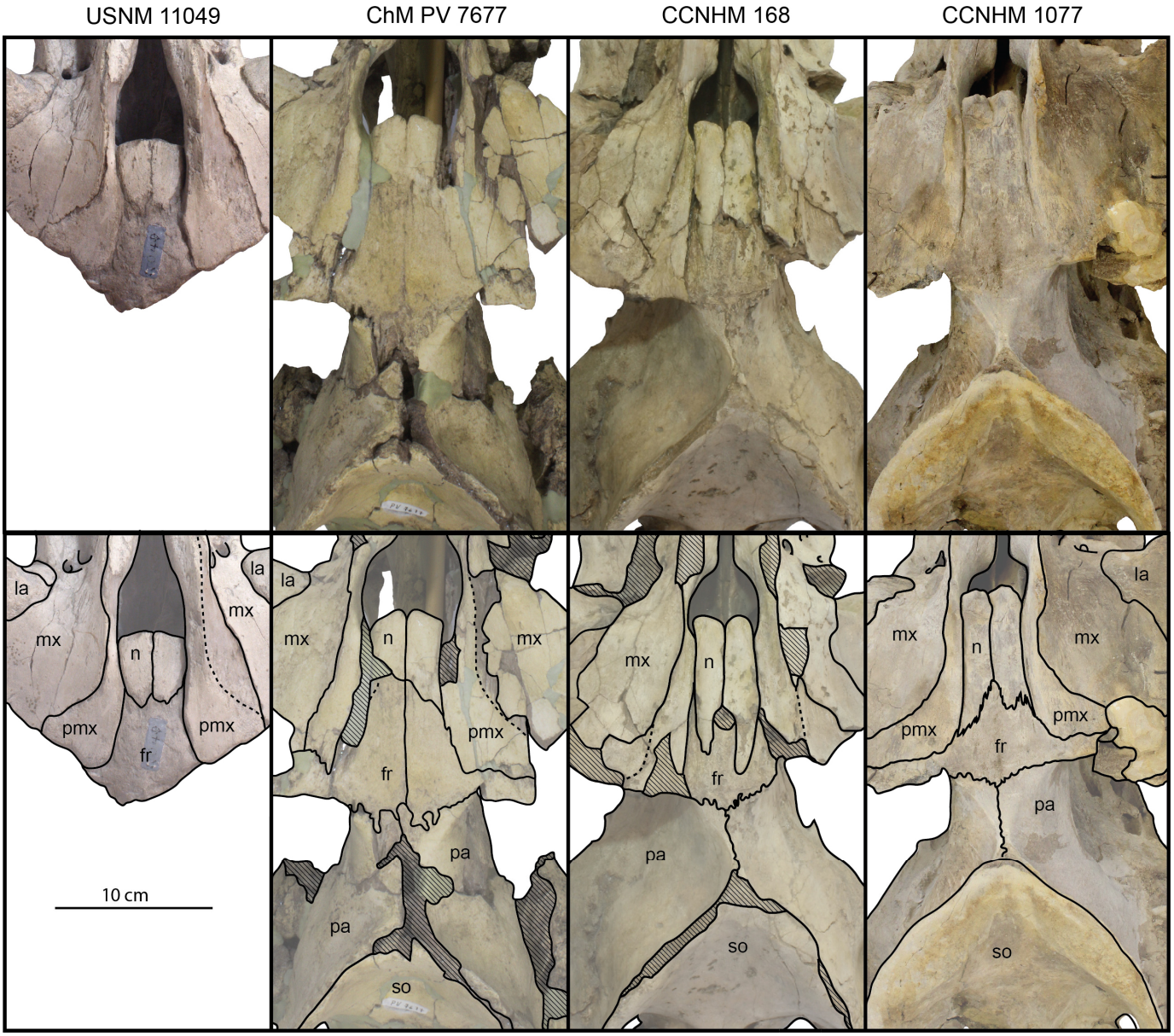


Figure 31. Ontogeny of the cranial vertex in *Xenorophus sloanii*. Abbreviations: fr, frontal; la, lacrimal; mx, maxilla; n, nasal; pa, parietal; pmx, premaxilla; so, supraoccipital.

In dorsal view the premaxilla has a nearly straight lateral edge (Figures 22, 26 and 30). The lateral edges of the premaxillae are nearly parallel along the posterior half of the rostrum, but widen gradually and diverge along the anterior half. The premaxillae are completely separated along their entire length by a continuous and parallel-sided mesorostral groove, measuring about 5–10 mm wide. The groove is artificially widened (by about 10–11 mm) in CCNHM 104 by a combination of diagenetic deformation and difficulty of reassembling the deformed rostrum. The premaxilla–maxilla suture is formed as a narrow fissure, though not positioned within a deep longitudinal furrow as in many other odontocetes. The lateral surface of the rostrum is nearly planar, giving it an approximately triangular cross section along the anterior two-thirds of the rostrum. The anteriormost part of the rostrum is slightly wider than deep, and nearly an equilateral triangle in cross section, and becomes relatively wider and shallower posteriorly.

Table 7. Skull measurements (in mm) of *Xenorophus sloanii*. ? denotes missing measurements; e denotes an estimated measurement; + denotes a minimum measurement.

Measurement	CCNHM 5995	ChM PV 7677	CCNHM 104	CCNHM 168	CCNHM 1077	ChM PV 5022
Condylobasal length	?	710+	680–690e	744	?	?
CBL without premaxilla	?	663	611	649	?	?
Rostrum length	?	440+	453	468	?	?
Length of maxilla on rostrum	?	396	357	376	?	?
Maximum rostrum width	?	120–130e	191	143	166	120e
Rostrum width at antorbital notch	?	120e	131	139	143.9	116
Postorbital width	?	240	263	281	280	254
Bizygomatic width	?	282	270	298	306	263
Exoccipital width	190e	200	209	239	233	222
Depth of palate at maxillopalatine suture	?	3.3	3	4.5	10.8+	?
Bony nares, transverse width	?	48	48	37	36	33
Maximum depth of rostrum	?	73.6	62	72	63	75
Width of gap between premaxilla anterior to nares	?	20.8	2.2	8.5	7.3	5.6
Transverse width of premaxillae at antorbital notch	?	55.8	?	58	51	50e
Nasal, depth 5 mm from anterior edge	?	9.5	6.8	5.9	8.2	3.6
Nasals, anterior/posterior combined width	?	29.6/27.4	29.9/31.7	30.3/30.1	31.2/32.4	31.3/33.2
Nasals, maximum width	?	29.6	31.7	32	32.4	33.2
Nasals, maximum length L/R	?	31.6/28	?	70.3/79.1	71.2/66.4	62e/54.1
Least interorbital width	?	21.6	242	26.5	247.3	22.9
Separation of supraoccipital and posterior nasals	74.4	112.4	83.8	57.9	83.7	80
Transverse width of nasal process of premaxilla	30.4	37.2/39+	26.6	27.5	27.9	38.9/42.6
Width across nasal processes of premaxillae	103e	115+	101e	104e	107	119
Anteroposterior length of frontal at midline	41e	69.7	43e	51.1	54	50.9
Anteroposterior length of parietal at midline	36	55.6	40e	34.1	42	37.9
Maximum width of frontal between premaxillae/maxillae at vertex	36.6	59.6	48.7	47.5+	51.5	44.9
Deviation of median parietal suture to left	0	0	4.9	14.3	6e	12e
Length of occipital shield, foramen magnum to vertex	117	112.6	107e	113.8	128.3	123e
Occipital condyle breadth	73.5	81.3	91.7	84.3	86.7	97
Occipital condyle depth	51e	50.3	57.6	57.5	55	55
Foramen magnum transverse width	30.3	40.4	33e	36	32.7	46
Foramen magnum depth	?	36.5	39e	35.4	23.5	?
Transverse width across basioccipital crests	?	94.7	103.9	117	112.7	94.9
Maximum width of basioccipital crest	?	18.1	13.5	17.5	23.2	15.6
Height of nasals above rostrum base	?	94.7	80e	95	90e	?
Squamosal fossa depth	?	25/25.3	31.1	26.1	33	17.7/26.1
Distance from center of squamosal fossa to supramastoid crest	?	25.7/20.9	20.5	21.5	24.5	25/24.7
Transverse width of glenoid fossa	?	47	55e	50	57	53.6
Angle between basioccipital rests	?	32°	42°	37°	28.5°	32°
Width of squamosal lateral to exoccipital	?	28	27	21	25	23.5
Dorsoventral depth of zygomatic process at midpoint	?	?	32.7	36	31.5	26+
Maximum anteroposterior length of temporal fossa	134e	155.1	148	175.5	200	147
Maximum length of lacrimal, dorsal exposure	61.6	75.5	68.3	77.7	77.5	93.3/86.9

Table 7. *Cont.*

Measurement	CCNHM 5995	ChM PV 7677	CCNHM 104	CCNHM 168	CCNHM 1077	ChM PV 5022
Maximum depth of antorbital process	?	27.8	34.9	35.9	38	35.6
Orbital diameter	?	66.7	73.8	58	78.5	64
Orbital angle	?	78.5°	79.7°	82.5°	73.6°	86.2°
Maximum length of antorbital fossa L/R	?	77+/65.7	90.1/79	105/75	?/85	103+/?
Maximum width of antorbital fossa L/R	?	14+/25e	27.7/24	40/31	?/33.6	28e/?
Minimum dorsoventral depth of the maxilla edge lateral to the antorbital fossa L/R	?	?/14e	8.8/14.7	10.1/14	?/10.4	8.2/?
Separation of anterior nasals and supraoccipital apex	?	144.9	136.4	137	156.4	131.3
Least intertemporal width	58.6	67.1	53.6	94	63	60
Squamosal length, postglenoid process to zygomatic process	?	77+	100	125+	128	85+
Maximum width of nasal, L/R	?	16.4/14.6	12.7/15.7	14.2/18.3	17.3/17.3	16.9/15.4
Maximum length of vomer in palate	?	146	190–200e	255	?	?
Orbit height relative to rostrum edge	19	41		53	19	31
Antorbital notch to posterior lacrimal/jugal	26.4	?	25e	20.4	26.4	22.8
Antorbital notch to postorbital ridge	68.3	53e	54.4	57.9	68.3	56.9
Anteroposterior offset between left and right palatines, maxillopalatine suture	26	19	19e	17.4	26	17e
Deviation of posterior median palatine suture from midline	?	?	?	5° (to left)	4° (to left)	?
Deviation of anterior median palatine suture from midline	?	?	?	3° (to left)	4° (to left)	?
Greatest breadth palatines	?	95+	107e	124.3	122.2	98.1
Transverse diameter palatine L/R	?	?/55.2	?	61.7/57.1	58.6/62.4	40.7/52.4
Paroccipital process to posteriormost tooth	?	290.2/294.5	257/263	290/290	304/317	272/289e
Postglenoid process to posteriormost tooth	?	250.5/253.6	215/219	235/241	247/262	222/244e

Embrasure pits are present on the maxilla but not the premaxilla (Figure 27). Shallow pits with clusters of minute foramina occur on the ventrolateral edge from between C1–PC1 to just anterior to PC4; deep embrasure pits are present posterior to PC4 (8.7 mm deep) and end anterior to PC7. Embrasure pits are largely laterally positioned on the maxilla anterior to PC4, but from just posterior to PC4 to just anterior to PC7, the embrasure pits shift medially so they are in line with the toothrow. No embrasure pits are present behind PC7, contrasting with the deep posterior embrasure pits on the mandible (see below). From medial to lateral, a longitudinal ridge and groove are present on the palatal surface of the maxilla, running from the anterior tip to the level of PC3, just medial to the teeth. We interpret this as a homolog of the alveolar groove in later diverging odontocetes. In the holotype, the diastemata are narrow and the embrasure pits small and shallow, positioned between PC2–6 (Figure 23). In ChM PV 7677, the right maxilla is complete but C1–P3 and their corresponding alveoli are not present (Figures 23 and 33). Instead, shallow vascularized pits are present; while the lateral edge of the left maxilla is damaged, these embrasure pits are less excavated than in other specimens of *Xenorophus sloanii* (e.g., CCNHM 104, 168). The C1–P3 alveoli are replaced with shallow vascularized pits with punctate bone texture, with a deeper pit with numerous small foramina present at the approximate position of the former PC2 alveolus. The left maxilla has all the alveoli preserved as in other specimens, indicating this is a pathology on the right side. Likewise, shallow embrasure pits are present on the right maxilla of ChM PV 7677 between PC1–4, as in other specimens.

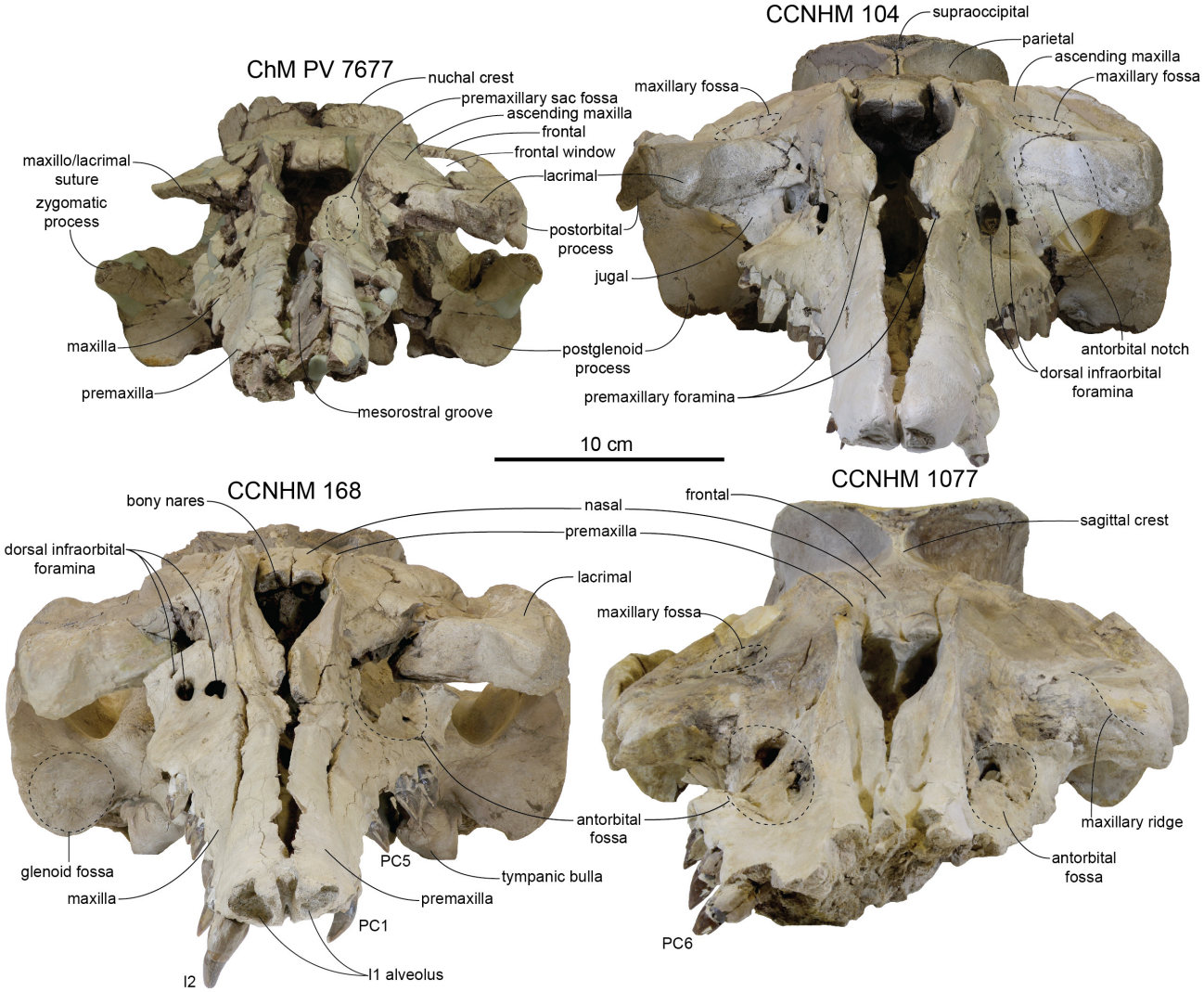


Figure 32. Referred skulls of adult *Xenorophus sloanii* in anterior view.

Ventrally, the maxilla bears a tongue-like sheet that extends anteromedial to C1 (Figures 23 and 27). Medial to this is a fissure-like premaxilla–maxilla suture on the palate, which continues posteriorly. The premaxilla has an anteroposteriorly long and transversely narrow splint-like palatal exposure that tapers posteriorly and terminates against the vomer; in CCNHM 168, it terminates 165 mm posterior to the anterior edge of C1. The premaxilla bears longitudinal grooves ventrally. A lanceolate exposure of vomer attains a length of 270 mm on the palate of CCNHM 168 and a maximum width of 10.5 mm; it is asymmetrical, with a trapezoidal outline, and its exposure is shifted approximately 5 mm to the left side so that the right maxilla–vomer suture is closer to the midline than the left maxilla–vomer suture. Accordingly, at the level of PC5, the vomer is 21 mm from right PC5 and 17 mm from left PC5. The vomer is more symmetrical and narrow in juveniles like the holotype (USNM 11049; Figures 23, 27 and 34). The anterior palatal exposure of the vomer is smallest in juveniles, measuring 61% of antorbital rostrum width in the holotype (USNM 11049), 100–110% in subadults ChM PV 7677 and CCNHM 104, and 191% in adult CCNHM 168 (Figure 34). A posterior palatal exposure of the vomer is present between the palatines and pterygoids, and is longest in juvenile specimens like the holotype (USNM 11049) where it separates the palatines along at least 75% of their length; in ontogenetically mature specimens like CCNHM 1077, the vomerine exposure is restricted far posteriorly and the palatines contact each other for at least 80% of their length (Figures 23, 27, 29, and 34).

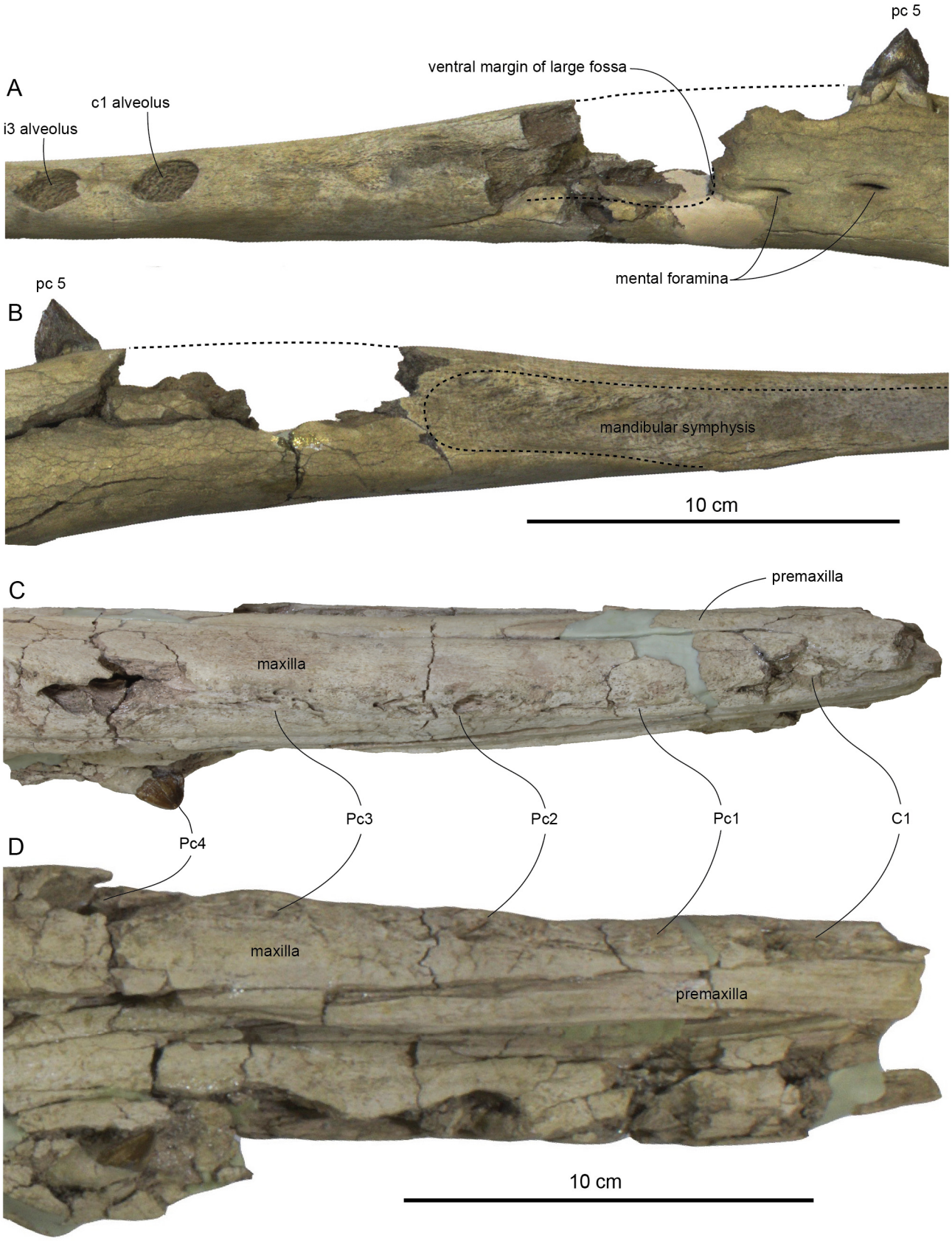


Figure 33. Oral pathologies in referred specimens of *Xenorophus sloanii*. Right mandible of CCNHM 168 in lateral (**A**) and medial (**B**) views. Right maxilla of ChM PV 7677 in lateral (**C**) and ventral (**D**) views.

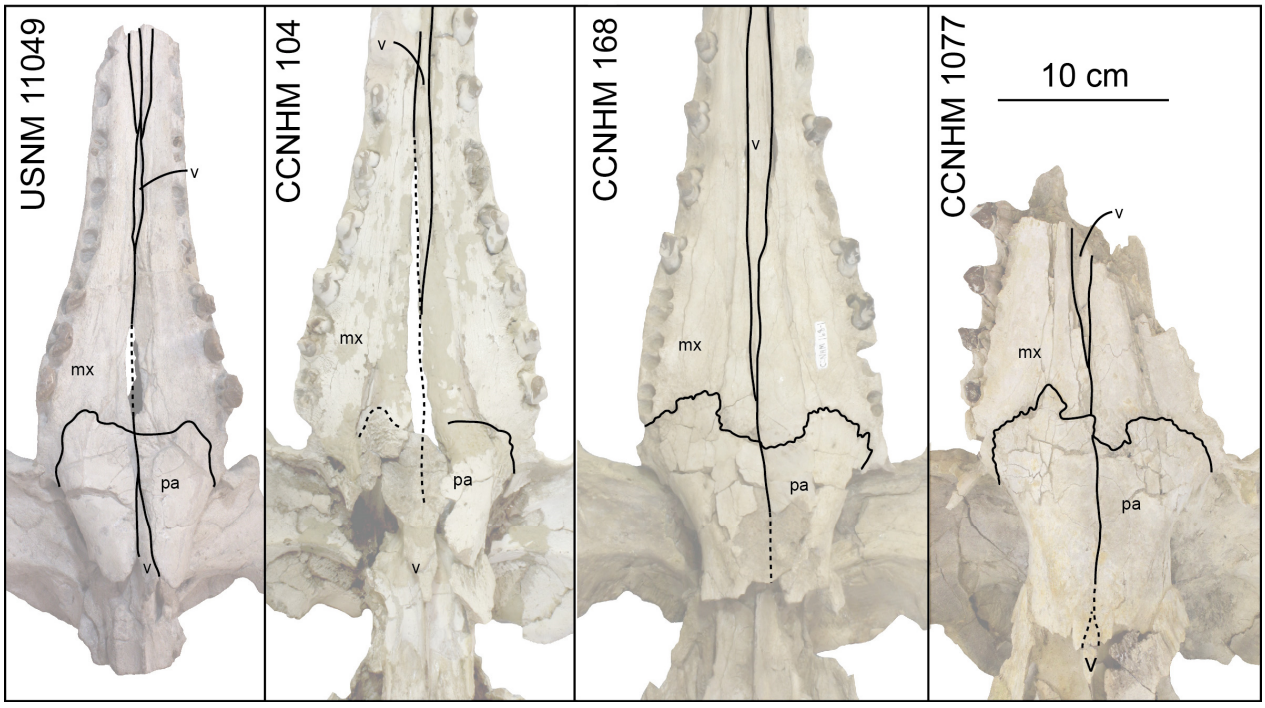


Figure 34. Ontogeny of the palate in *Xenorophus sloanii*. Abbreviations: mx, maxilla; pa, palatine; v, vomer.

The palate is nearly completely flattened transversely in cross-section in most specimens but slightly more convex in CCNHM 1077. The greater palatine foramina open at the level of PC8 on the maxilla and close to the midline (~18 mm from midline) and are confluent with anteriorly widening trough-like sulci with well-defined edges for ~55 mm (Figures 27 and 29). Anteriorly, the sulci become diffuse (but palpable) and continue anteriorly to the level of PC2. The foramina are asymmetrically positioned with the left positioned further posterior to the right by 11 mm in CCNHM 168 and 20 mm in ChM PV 7677.

The maxilla–palatine suture is 'M'-shaped with wide lobate posterior median wedge of maxilla penetrating between palatines, which extend anteriorly to the position of the posteriormost tooth (Figures 23, 27, 29 and 34). Like the greater palatine foramina, the right palatine extends further anterior to the left. This style of asymmetry with an anteriorly positioned right palatine is consistently developed in all skulls of *Xenorophus sloanii* as well as *Albertocetus*-group specimens. Amongst adult specimens, the right palatine is shifted anteriorly relative to the left as little as 8 mm (ChM PV 7677), 19 mm in subadult CCNHM 104, 17.4 mm in adult CCNHM 168, and as much as 26 mm in CCNHM 1077; in the holotype (USNM 11049), it is only 6 mm anterior. In addition to the asymmetrical anterior margin, the median palatine suture is asymmetrical and deviated to the left of the midline in all specimens where the palatines are complete (CCNHM 168, 1077).

The pterygoid is most completely preserved in CCNHM 1077 (Figure 29); it is plate-like and bears a small (15 mm long) triangular hamulus that terminates near the posterior margin of the temporal fossa. The lateral side of the pterygoid bears longitudinal striations. The pterygoid–palatine suture begins dorsally at the level of the postorbital process and descends ventromedially. The pterygoid articulates with the squamosal 10 mm anteroventral to the foramen ovale and this suture continues anterior at least 30 mm from the foramen.

In lateral view, the palate appears slightly ventrally concave because the palatines conform to the basicranial stem and the 22° deflected rostrum (Figure 24). The palatines are damaged in most specimens with broken lateral edges but where preserved, appear to become more transversely convex posteriorly (Figures 23, 27 and 29). In CCNHM 1077, the palatines are more completely preserved and form a transversely convex, sub-cylindrical

shape anterior to the ventral part of the bony nares. The palatines in this specimen bear a low crest emanating medial to the antorbital notch and converge posteromedially towards the medial pterygo-palatine suture (Figure 29).

The left and right premaxillae bear elongate, transversely narrow premaxillary sac fossae (Figures 22, 26 and 28), which, in CCNHM 168, measure approximately 100 mm long and 20 mm at the widest. The premaxillary sac fossae are asymmetrical, with the left fossa somewhat wider, placed further anteriorly, and more deeply concave than the right fossa. A poorly developed anteromedial sulcus is present in CCNHM 168 but more strongly entrenched in CCNHM 104. About 30–60 mm anterior to the nares, the premaxillae form median ridges which are closely appressed to one another, closing the mesorostral canal. In CCNHM 168, this ridge is high and twisted so that the mesorostral groove is tilted to the left of the sagittal plane; this is associated with the more deeply concave left premaxillary sac fossa.

The premaxillary foramina (Figures 22, 26 and 28) are present at the level of PC7 in CCNHM 168; in this specimen, three are present on left and two are present on the right. They measure 3–5 mm in diameter, except for the posterior right foramen which is 8.2 mm. Most open dorsally, but the anteriormost foramina open slightly anterodorsally. In CCNHM 1077, there is a large right premaxillary foramen with a narrow, oval foramen just posterior to it. Two premaxillary foramina are present on the left, and they are offset anteriorly relative to their counterparts on the right; the smaller anterior and larger posterior left premaxillary foramina are positioned about 15 mm anterior to and 10 mm posterior to the anteriormost right premaxillary foramen (respectively). In CCNHM 104, the premaxilla here is broken, but there are bilateral large posterior left and right foramina at the same level; there is an additional foramen on the right positioned 4 cm anterior. In ChM PV 5022, there is a large single premaxillary foramen on the left and two on the right; the left premaxillary foramen is shifted slightly further anterior to the large posterior foramen on the right. In ChM PV 7677, there is similarly only a single large premaxillary foramen, but on the right, there is only a single small foramen located somewhat further posterior. The premaxillae are too fractured in the holotype to evaluate. In CCNHM 168, a shallow posterolateral sulcus extends posterolaterally 50 mm from the anteriormost premaxillary foramina and sits adjacent to a longitudinal sharp ridge leading to the dorsolateral edge of the nares.

A shallowly excavated antorbital fossa is present on the base of the maxilla and also excavates the antorbital region, forming a steep, transverse, vertical, surface that separates the rostral part of the maxilla from its ascending process (Figure 22, 26, 28, 32, and 35). The antorbital fossa is shallower in ontogenetically immature specimens (ChM PV 7677). The antorbital fossae are consistently longer on the left than on the right, differing from the condition in *Xenorophus simplicidens* (see above). Furthermore, the left antorbital fossa is more deeply excavated on the left than on the right; the minimum depth of the maxilla lateral to the fossa on the left side is 59% of the depth on the right in CCNHM 104 and 72% the depth of the right side in CCNHM 168. The pattern and number of dorsal infraorbital foramina are variable and obscured by breakage in these specimens. At least two separate small foramina are present on the left side of CCNHM 168, along with a cavernous space for the infraorbital canal exposed by surficial bone breakage, with unclear margins. In CCNHM 168, a cluster of four dorsal infraorbital foramina are present on the right side, with two small foramina opening dorsally to dorsolaterally (8.5 and 5 mm wide, respectively) and two large (10–12 mm wide) anteriorly opening foramina anteroventral to these. In CCNHM 104, there is one small (3 mm wide) posterodorsal foramen opening dorsally and three larger (9–15 mm wide) foramina opening (from anterior to posterior) anteriorly, posterodorsally, and dorsolaterally. All dorsal infraorbital foramina are located in the posterior half of the antorbital fossa. In CCNHM 1077, the dorsal infraorbital foramina are asymmetrical and coalesced into a 20–30 mm fenestra on the left side with an additional foramen 15 mm further anteriorly; three separate foramina are present on the right side (Figure 35), one large dorsally opening foramen medial to the antorbital notch, a smaller

dorsally opening foramen positioned further dorsally, and a large anteriorly positioned and anteriorly opening foramen 20 mm further anterior. The foramina on the left are similarly coalesced into a large fenestra in the holotype and ChM PV 7677; a similar condition may be present in ChM PV 5022, though obscured by damage. The medial wall of the antorbital fossa (Figure 35) is vertical in some individuals (CCNHM 104) and subvertical in others (CCNHM 168). In summary, the dorsal infraorbital foramina are consistently coalesced on the left side and appear to be separated on the right.

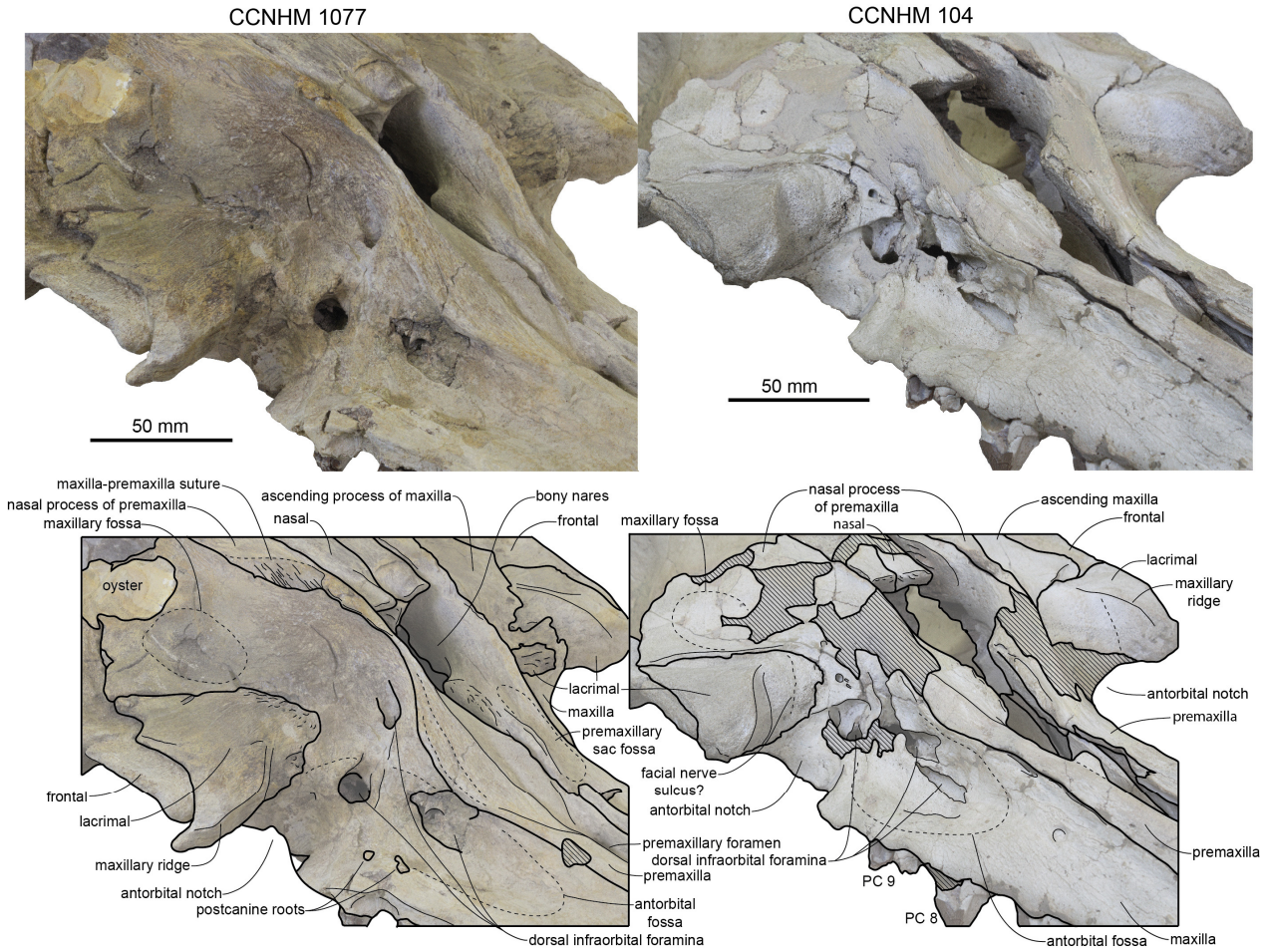


Figure 35. Morphology of the facial antorbital region in *Xenorophus sloanii*.

Facial Region: In dorsal view, the bony nares are oval-shaped with the posterior margin transversely oriented and straight, truncated by the nasals (Figures 22, 26 and 28; Table 7). The nasal passages are approximately vertical, and confluent anteriorly with the mesorostral groove. The "frontal shield" is approximately twice as wide as long (~240 × 110 mm in CCNHM 168) and includes portions of the maxilla, frontal, lacrimal, and premaxilla. Medially, it is horizontal, but slopes gradually ventrolaterally towards the orbital margin.

Medially, a flat subrectangular table is formed by the nasals, frontal, and nasal processes of the premaxillae just anterior to the vertex (here defined as the parietal–occipital contact at the midline; Figures 22, 26 and 28). The combined width of the nasals is about twice as long as their greatest length; there is a shallow median furrow anteriorly with a short median fissure that continues posteriorly as the internasal suture in adult specimens (CCNHM 1077, ChM PV 5022), whereas they are transversely flat in younger specimens (USNM 11049, ChM PV 7677, CCNHM 104). The nasals are anteroventrally excavated with concave oval fossae facing anteroventrally, roofing over the anterodorsal part of the narial passage. The nasals are slightly longitudinally arched in some specimens (CCNHM 168)

and flat in others (CCNHM 104). The lateral edges of the nasals are nearly parallel but slightly converge posteriorly in the holotype; in other specimens they are parallel (CCNHM 104, 168; ChM PV 5022, 7677) and widen slightly posteriorly in the largest individual (CCNHM 1077).

In larger specimens, there is a triangular (CCNHM 1077) or tongue-shaped (CCNHM 168) median wedge of the frontal which extends anteriorly between the nasals (Figures 26 and 28). No such wedge is present in the holotype, and, instead, the left and right nasals converge posteriorly to a point at the midline. In CCNHM 168, the nasals bear a posterior splint that is separated laterally from the nasal process of the premaxilla by a triangular prong of the frontal, whereas in CCNHM 1077, posterior splints are not evident, and the nasofrontal suture is partially obliterated; this suture is at least partially obliterated in CCNHM 104 as well, though breakage and putty obscure the suture. A shorter, more blunt splint appears on the right nasal of ChM PV 5022 with a lateral wedge of the frontal. ChM PV 7677 highlights a transitional morphology between CCNHM 168 and the holotype: a shallow median frontal triangle is present, short and blunt posterior splints of the nasals are present, and a shallow lateral wedge of the frontal is also present.

In some specimens, the nasals are asymmetrical (Figures 22, 26, 28, 30 and 31; Table 7), with the left slightly narrower than the right (CCNHM 168, 88% of right; CCNHM 1077, 92% of right); in all others they are approximately symmetrical (CCNHM 104, ChM PV 5022, 7677, USNM 11049). In ontogenetically immature specimens, the nasals are anteroposteriorly shorter (holotype USNM 11049, ChM PV 7677, CCNHM 104).

Immediately anterior to the nasals, the premaxilla nasal process is laterally abutted by the ascending maxilla. The two bones together form a vertical longitudinal paranaris crest lateral to the nares; dorsally, the crest curls over laterally, forming a slight overhang in larger individuals (CCNHM 1077, present but broken in ChM PV 5022; Figure 32), but not as extreme as in *Cotylocara macei*. This ridge continues posteriorly along the premaxilla–maxilla suture to the level of the posterior half of the nasals. A posteriorly widening wedge-shaped strip of premaxilla is exposed dorsally and laterally along the entire length of the nasal (Figures 22, 26, 28, and 31), as in other xenorophids. Where preserved well (e.g., the holotype, CCNHM 1077, ChM PV 5022), this exposure of the premaxilla widens gradually until the level of the posteriormost nasals, where they widen abruptly, doubling in width to over 35 mm. The posterior edge of the nasal process of the premaxilla dorsally meets the medial part of the frontal. This triangular dorsal exposure of the premaxilla separates the frontal and nasal from the ascending process of the maxilla.

The ascending process of the maxilla is fan-shaped with a convex posterior margin (although a posterolateral corner is formed in ChM PV 7677), and paralleled by a convex posterior edge of the supraorbital process of the frontal; this curved strip behind the maxilla extends about 15–17 mm more posteriorly (Figures 22, 26, 28, and 31). The posteromedial part of the maxilla and frontal are damaged in most specimens, but well-preserved in CCNHM 1077 and ChM PV 7677; a shallow transverse trough is developed on the dorsally exposed part of the frontal, parallel with the posterior margin. In some of the larger specimens (CCNHM 1077, ChM PV 5022), there is a low, laterally positioned maxillary ridge along the maxilla–lacrimal suture.

The lacrimal is greatly enlarged with a large, triangular, dorsal exposure where it has overlapped the preorbital process and the anterolateral part of the supraorbital process of the frontal (Figures 22, 26, 28 and 35). The lacrimal is shaped as a concavo-convex lensoidal element in lateral view, convex dorsally and thickened anteriorly to form the antorbital process and curling ventrally to underlap the preorbital process of the frontal. Posteriorly, the lacrimal thins dorsoventrally into a sheet. The transverse width of the exposure (on one side) measures about 22% of the interorbital width in CCNHM 168. Anteriorly, a steep face on the anterior side of the lacrimal contributes to the posterior margin of the antorbital fossa; this surface is ventral to a sharp ridge that continues posteromedially.

Only the proximal part of the jugal is preserved (e.g., CCNHM 1077; partial in ChM PV 5022 and CCNHM 168) where it is "hammer" or T-shaped in ventral view; it bears

a transversely expanded anterior end that articulates with the lacrimal and maxilla and quickly transitions into a transversely narrow, dorsoventrally thin and strap-like bone (Figures 24, 29, and 36). In specimens where the jugal is missing, a clear transverse rectangular articular facet is present on the lacrimal, indicating the two were not fused as in later diverging odontocetes even later into ontogeny (e.g., CCNHM 168). A clear suture is present in even adult specimens where the jugal is preserved, such as CCNHM 1077.

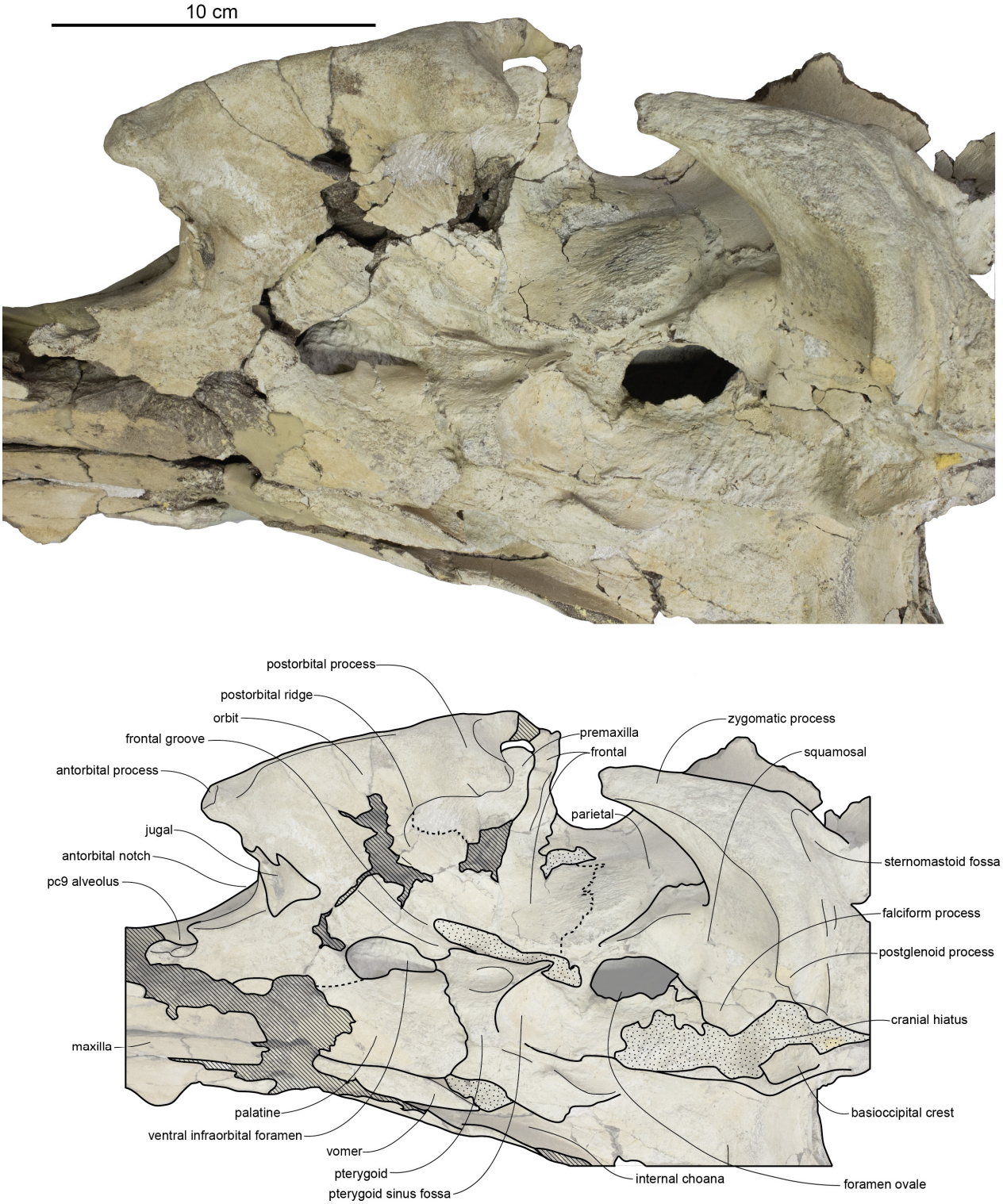


Figure 36. Basicranial morphology of *Xenorophus sloanii* (ChM PV 5022) in ventrolateral view.

The frontal is exposed laterally along the orbital margin as a thin strip lateral to the lacrimal (Figures 22, 26 and 28). The lacrimal never reaches the lateral edge of the orbital margin and is separated by an anteriorly narrowing wedge of exposed frontal. The orbit is ventrally concave in lateral view and posteriorly defined by a large, subrectangular, and posteroventrally oriented postorbital process (Figure 24). The orbit diameter measures approximately 23–26% of bizygomatic width, with subadult specimen ChM PV 7677 having the proportionally smallest (22.5%) and adult specimen ChM PV 5022 having the largest (28%). Orbital angles (*sensu* [93]) range from 73 to 86°, with extremely anteriorly tilted orbits present in the juvenile holotype (73.6°), slightly less anteriorly tilted orbits in subadults and adults (e.g., 78.5° in ChM PV 7677, 79.7° in CCNHM 104), and nearly laterally facing orbits in adults (82.5° in CCNHM 168, and an average of 81.3° on the distorted orbits of ChM PV 5022). One outlier is adult specimen CCNHM 1077, which has a low angle and anteromedially shifted orbits (75°); this is largely driven by the more laterally extending postorbital processes, perhaps caused by diagenetic crushing. A lunate fossa for the masseter origin emarginates the posterolateral edge of the postorbital process. The frontal groove is shallowly concave, approximately horizontal, and bordered posteriorly by a low postorbital ridge. No diploic foramina are present. Posterior to the postorbital ridge, the ventral surface of the composite supraorbital process is flat to shallowly concave. Posterior to the postorbital process, the frontal bears a ridge that parallels the edge of the supraorbital process and bears grooves for the ascending process of the maxilla; though incomplete in CCNHM 168, a complete ascending process is preserved in CCNHM 1077, ChM PV 5022, and nearly complete in CCNHM 104. A well-developed frontal window (Figure 37; [5]) exposes the premaxilla (medially) and maxilla (laterally). Judging from this exposure and fractured specimens, the nasal process of the premaxilla is osteosclerotic, inflated, and forms the core of the supraorbital process medially and thins laterally. The premaxilla posteriorly terminates within the frontal window and the maxilla occupies the remainder of the window. Within the window, the premaxilla–maxilla suture is anterolaterally directed and planar. The posterior margin of the supraorbital process is developed as a thin sheet of frontal encircling the posterior edge of the frontal window; this is damaged in most specimens (including the holotype) but is smoothly convex in CCNHM 1077 and formed as a posterolateral corner in ChM PV 7677 (Figures 22, 23, 28 and 29).

Vertex and Dorsal Braincase: An intertemporal constriction is formed by the parietals that contact at the midline, separating the frontals from the occipital (Figures 22, 23 and 26–30; Table 7). An anteroposteriorly short sagittal crest is present and deviates to the left in most adult specimens (CCNHM 168: 9°; ChM PV 5022: 6–12°; CCNHM 1077: 4°), although it is approximately anteroposteriorly aligned in juveniles CCNHM 5995 and subadults ChM PV 7677 and CCNHM 104. The intertemporal constriction is quite narrow and measures about 20% of bizygomatic width in all specimens.

In dorsal view, the braincase is roughly triangular and bears a dorsoventrally blunt subtemporal crest anteroventrally, formed by the squamosal and alisphenoid (Figures 22, 23, 26–30 and 36). Most of the lateral side of the braincase is formed by the parietal and is slightly convex (Figures 24 and 36). The frontal is exposed anteriorly on the lateral side of the braincase, but is hidden in dorsal view by the supraorbital process (Figure 36). It underlaps the nasal process of the premaxilla medially and thins towards the frontal window. The frontoparietal suture is nearly transverse and nearly closed in all specimens (CCNHM 168, CCNHM 1077, CCNHM 5995, ChM PV 5022, ChM PV 7677) with a well-developed and slightly anteroposteriorly mortised suture. The suture is closed but less mortised in CCNHM 5995; this suggests that the posterior end of the frontals in the holotype (USNM 11049) is fractured rather than representing a naturally open suture (Figure 22).

The occipital shield is triangular and bears a pointed apex, forming about a 95–100° angle in dorsal view (Figures 22, 25, 26, 28 and 30; Table 7). The shield is steep and plunges 50–60° from the roughly horizontal plane of the nasals and frontals. A distinct attachment scar for some of the neck muscles (rectus capitis, obliquus capitis superior, and/or semispinalis) is present as a pitted band parallel to the dorsolateral edge of the

nuchal crests. There is no external occipital crest; instead, the dorsal half of the shield is shallowly transversely concave. The nuchal crests are highly elevated and, in lateral view, they are posteriorly convex and overhang the exoccipital posteroventrally. In some specimens (CCNHM 104, 1077), the nuchal crests extend further posteriorly than the occipital condyles; in others, they approach but do not pass the condyles (ChM PV 5022, 7677; CCNHM 168). Although difficult to quantify, they are more strongly developed and elevated above the vertex in absolutely larger individuals such as CCNHM 168, 1077, and ChM PV 5022.

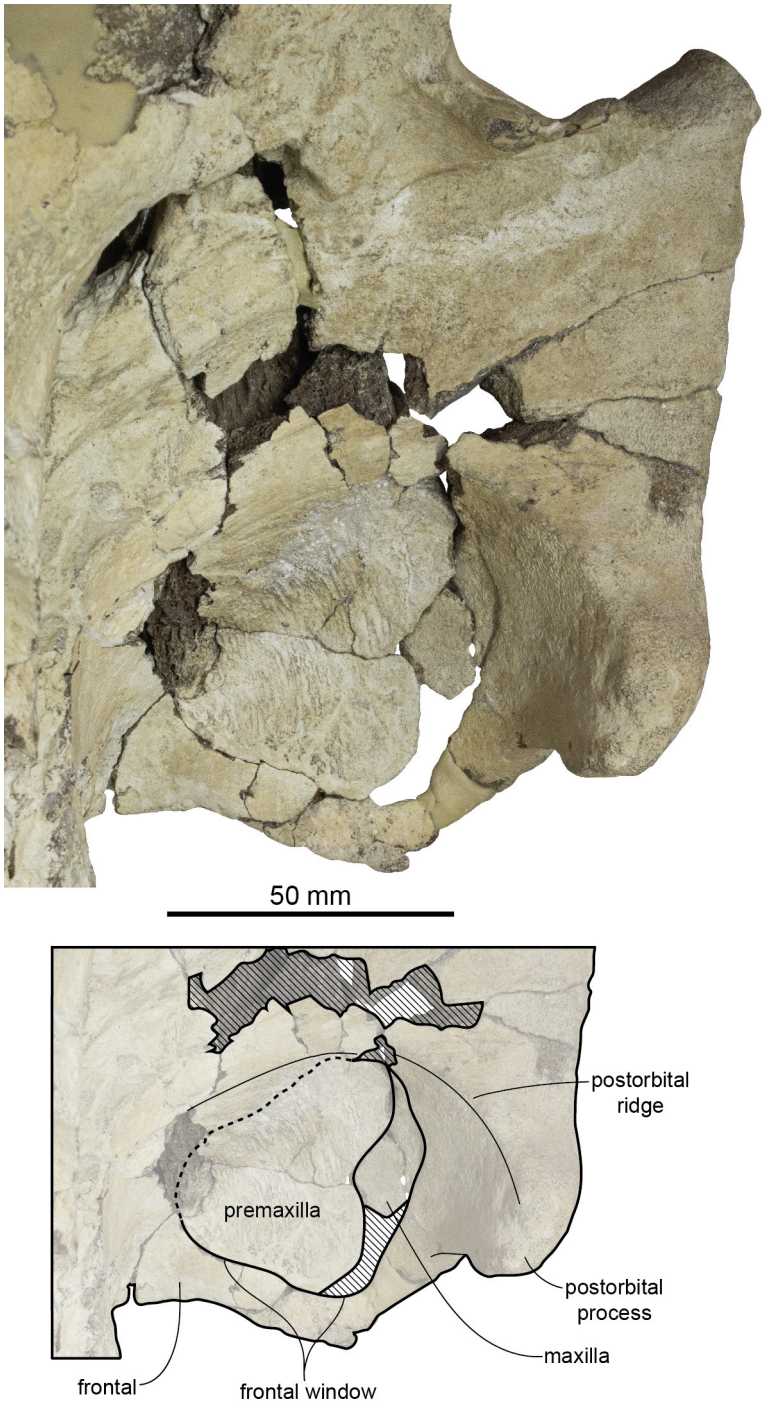


Figure 37. Orbital morphology and the frontal window of *Xenorophus sloanii* (ChM PV 5022) in posteroventral view.

Deep, subhorizontal, and reniform dorsal condyloid fossae are present in most specimens (Figure 25); they are shallower in CCNHM 104. In CCNHM 168, the left fossa bears an 11 mm wide, circular fenestra of probable pathologic or developmental origin in the occipital; a similar 7.6 mm wide fenestra is present in the occipital within the right fossa. The condyles are set out on a short but well-defined neck that is salient in dorsal and ventral view. The combined width of the condyles is slightly greater than their height; they encircle a circular foramen magnum (CCNHM 104, CCNHM 1077, ChM PV 7677), although in CCNHM 168 the foramen is teardrop-shaped with a triangular dorsal cleft.

The occipital shield is trefoil-shaped with a posterior and ventrolaterally flaring exoccipital (Figure 25). The exoccipital is quadrate and flat posteriorly, and bears a ventrally convex paroccipital process with a medial point in some specimens (CCNHM 168, ChM PV 7677) and a much longer sharply triangular prong in others (CCNHM 1077, ChM PV 5022).

Basicranium—Exoccipital and Basioccipital: In ventral view, the outline of the basioccipital is triangular, narrow anteriorly and widening posteriorly at the basioccipital crest (Figures 23, 27, 29, 38 and 39; Table 7). The basioccipital crests (Figure 23, Figure 27, Figure 29, and Figure 38) are oriented ventrolaterally and are transversely thickened (14–21 mm; 5–7% of bizygomatic width) to a similar degree as in basilosaurids (2.5–7% of bizygomatic width) and thicker than the plate-like crest in crown odontocetes (typically 0.9–3.5% of bizygomatic width, with some extinct outliers with thicknesses from 4 to 5%, including *Pomatodelphis* and *Kampholophos*). The apex of the crest is rugose in adults (CCNHM 168, 1077; ChM PV 5022) and smooth and punctate in subadults CCNHM 104 and ChM PV 7677. The crest transitions anteriorly into a plate-like pharyngeal crest. The basioccipital crest in some specimens (CCNHM 168, 1077) is bifid with a transverse cleft about 10 mm anterior to the jugular notch dividing the crest into a large primary crest and a small secondary posterior crest. This cleft is a possible autapomorphy of *Xenorophus*. A shallower cleft is present in *Echovenator* and *Cotylocara* but absent in all known specimens of *Albertocetus*. An approximately transverse, posteriorly concave crescent-shaped scar for the insertion of the rectus capitis ventralis is present medial to the basioccipital crest. This scar terminates laterally at the apex of the primary basioccipital crest. A deeply incised jugular notch is developed and, in CCNHM 168, is 20 mm deep (relative to the apex of the secondary basioccipital crest). The paroccipital process extends further ventrally than the basioccipital crest with a triangular medial spur (Figure 25) as in *Albertocetus* and *Echovenator*. The medial edge of the paroccipital process is concave. A deeply excavated subcircular paroccipital concavity is present on the anterior face of the process and is floored with rugose bone (Figures 38 and 39). No obvious ventral condyloid fossa are present. Lateral to the condyles the entire occipital forms a horizontal trough; in lateral view, the exoccipital and paroccipital processes are oriented posteroventrally and this trough is overhung by the posterior apex of the nuchal crest.

Squamosal and Auditory Region (Excluding Tympanoperiotics): The zygomatic process is elongate, transversely narrow, and crescent-shaped in lateral view with a concave anteroventral margin (Figure 24; Table 7). The zygomatic apex tapers anteriorly and is triangular in lateral view. The supramastoid crest is transversely sharp along the anterior 20 mm of the zygomatic, and the ventral edge is sharp. The zygomatic process is rotated longitudinally so that the lateral side faces slightly dorsolaterally (Figures 26 and 28), broadly analogous to the condition in eomysticetid baleen whales. The squamosal fossa is deep and developed as a short parasagittal trough; the posterior end of the supramastoid crest terminates in a small knob-like squamosal prominence (Figure 24), developed more strongly in larger specimens (CCNHM 168, 1077, and ChM PV 5022) and weaker in CCNHM 104. The squamosal prominence is present in Basilosauridae but positioned further anteriorly, and a similar squamosal prominence is widespread among toothed mysticetes like the Aetiocetidae; such a prominence is otherwise unknown in stem odontocetes.

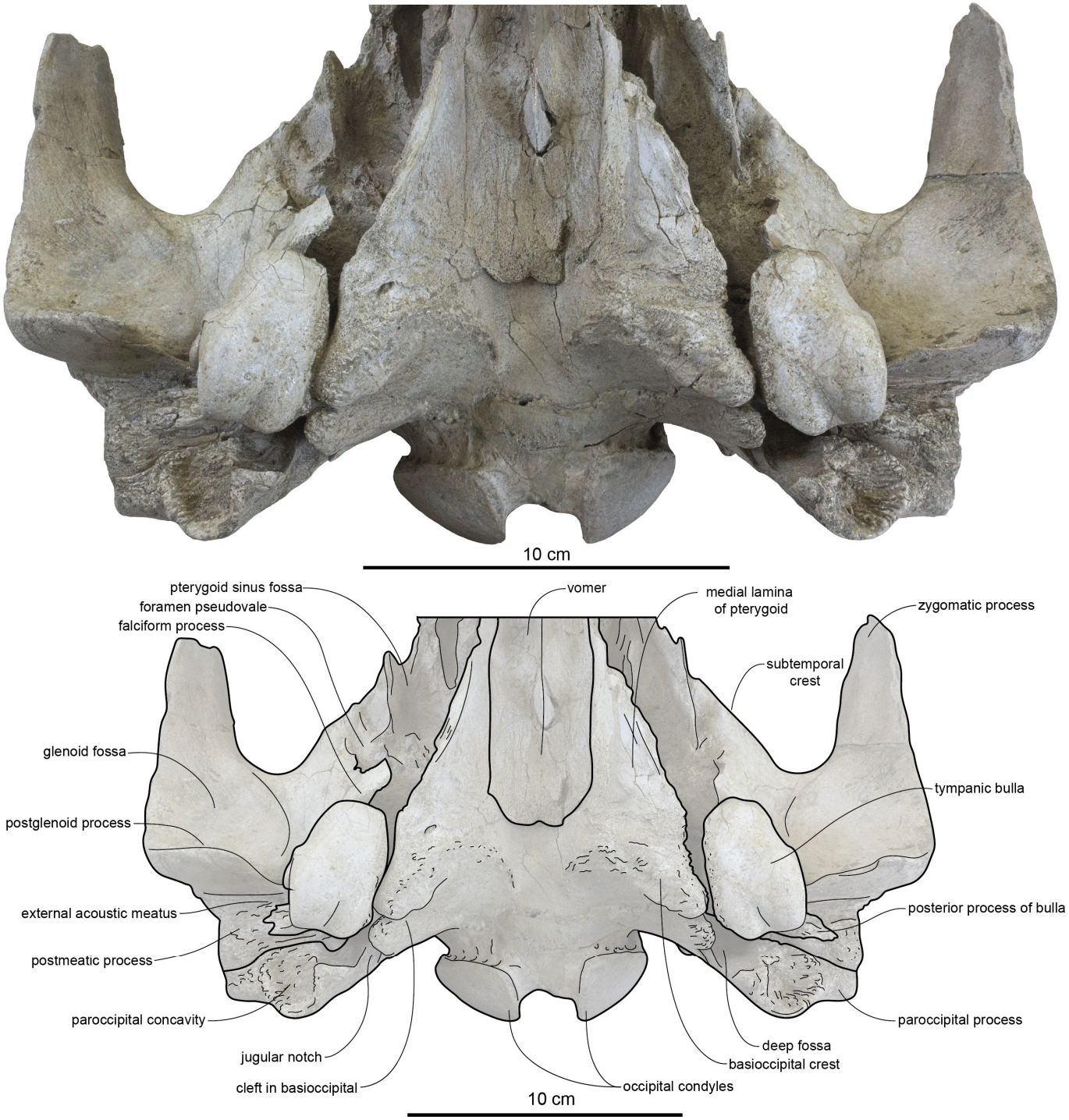


Figure 38. Basicranial morphology of *Xenorophus sloanii* (CCNHM 168) in ventral view.

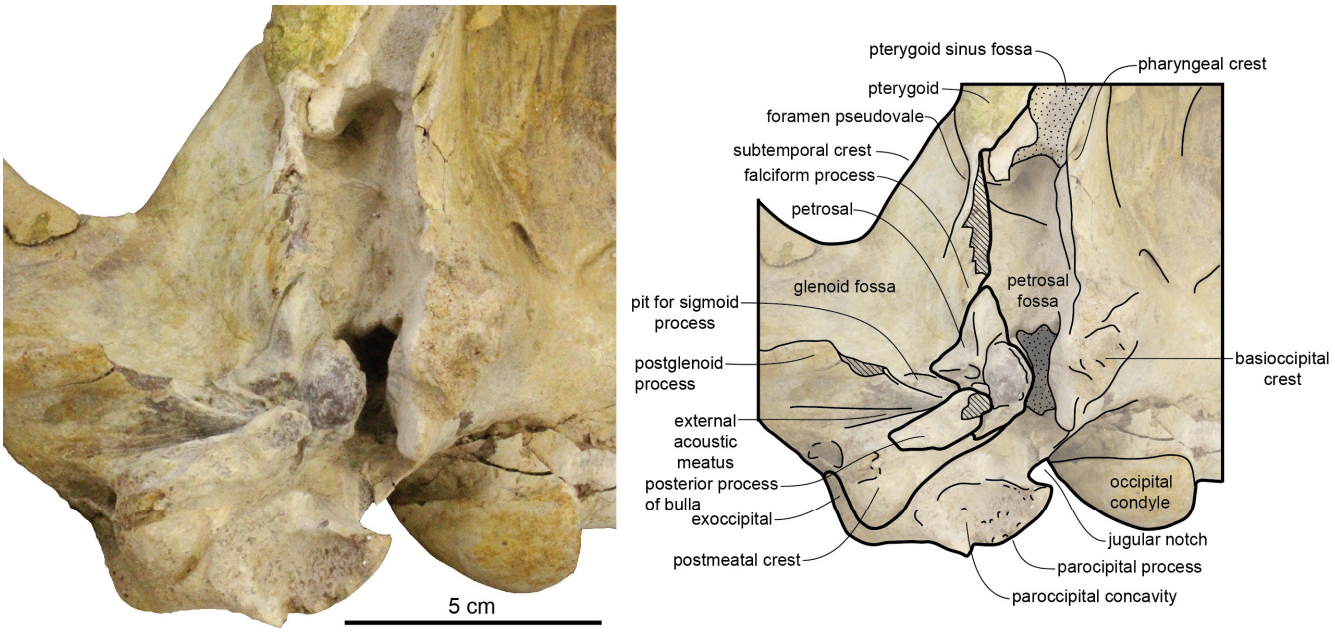


Figure 39. Auditory region of *Xenorophus sloanii* (CCNHM 1077) in ventral view.

The sternomastoid fossa is large, pitted, and lunate (Figures 24 and 25); like *Albertocetus*, the sternomastoid fossa does not extend onto the lateral part of the exoccipital as it does in *Echovenator* and *Cotylocara*. In CCNHM 1077, it is not developed as a fossa but rather a rugose but flat scar. The sternomastoid fossae of CCNHM 168 are asymmetrical (29.5 mm long, 66 mm deep on left vs. 35.1 mm long and 72 mm deep on right). The fossa is similarly shallow in ChM PV 7677. The medial surface of the zygomatic process is shallowly concave with a longitudinal trough. Posteriorly, the glenoid fossa is also shallowly concave and nearly flat anteriorly, equidimensional and quadrate in ventral view (Figure 38). A parasagittally oriented shallow trough delimits the medial edge of the glenoid fossa; this trough is not easily visible, but palpable. This trough may be the homolog of the tympanosquamosal recess in later diverging odontocetes. The postglenoid process projects ventrally and has a parabolic outline in posterior view (Figure 25); it extends ventrally to about the level of the ventral margin of the bulla.

The falciform process is broken in most specimens but appears to have been a triangular transversely narrow sheet that conformed to the outer lip of the bulla (Figures 23, 27, 29 and 38). Anteriorly, the falciform is perforated by the external foramen ovale, which is about 10 mm wide in most specimens (Figure 38). Anteromedially, the squamosal forms a delicate thin sheet overlapping the greatly enlarged and pachyostotic alisphenoid. The alisphenoid is typically completely covered by a thin lamina of the squamosal in well-preserved large specimens (CCNHM 168, 1077) but, in others, the squamosal is flaked off, exposing a highly rugose external surface of the alisphenoid (e.g., CCNHM 104, Figure 27).

The periotic fossa is exposed well in CCNHM 104, 1077, and ChM PV 7677 (Figures 23 and 27), but obscured by damage in ChM PV 5022 and by the bulla in CCNHM 168 (Figure 38). The fossa consists of a deep circular pit medial to the spiny process; the anterior partition of the fossa is damaged in CCNHM 104. Medial to and on the ventral side of the spiny process is a rectangular pit for the sigmoid process of the bulla. Posterior to the periotic fossa, a shallowly excavated "deep fossa" is present on the anterior side of the paroccipital process, immediately posterior to the stylomastoid fossa of the periotic and extending ventrally as a vertical trough.

The external acoustic meatus is developed as an anteroposteriorly narrow, acutely V-shaped trough (Figure 24). The post-tympanic process is a low transverse ridge that merges with the posterior process of the bulla evenly and without an obvious suture (Figures 38

and 39). A shallow transverse trough is present between the post-tympanic ridge and the paroccipital process.

The pterygoid sinus fossa is deeply excavated (Figures 27, 29 and 38). The lateral wall of this fossa is formed by the pterygoid but is missing in most specimens, except for CCNHM 1077 and ChM PV 5022. The fossa is medially walled off by the basisphenoid and pharyngeal crest. It extends anteriorly to the level of the postorbital process. Where exposed (CCNHM 104, 168, ChM PV 7677), the dorsal part of the fossa is smoothly concave.

Anterior Basicranium: The internal choanae are nearly horizontal and tube-like, rather than steeply inclined or vertical as in many extant odontocetes. A median nasal septum extends posteriorly to the level of the posterior edge of the temporal fossa. The posterior end of the vomer is at the level of the anterior edge of the bulla. The basisphenoid vomer suture is straight and parasagittal.

Part of the lateral lamina of the pterygoid is preserved in CCNHM 1077; despite crushing, it seems to have been evenly convex in cross section along its entire length. The alisphenoid and possibly pterygoid seem to have formed the ventral edge of the temporal fossa; the alisphenoid is exposed ventral to the parietal in CCNHM 1077 and ChM PV 5022 as a dorsoventrally shallow strip.

Periotic: The periotic is preserved in several specimens (Figures 39–44; Table 8); it is loose in CCNHM 104, ChM PV 7677, and 5022, and articulated (but visible) in CCNHM 1077, and articulated but obscured by the bulla in CCNHM 168. Overall, the periotic is quite similar to and slightly larger in absolute size (e.g., anteroposterior length) than *Albertocetus meffordorum*. They are best preserved in ChM PV 5022 and 7677.

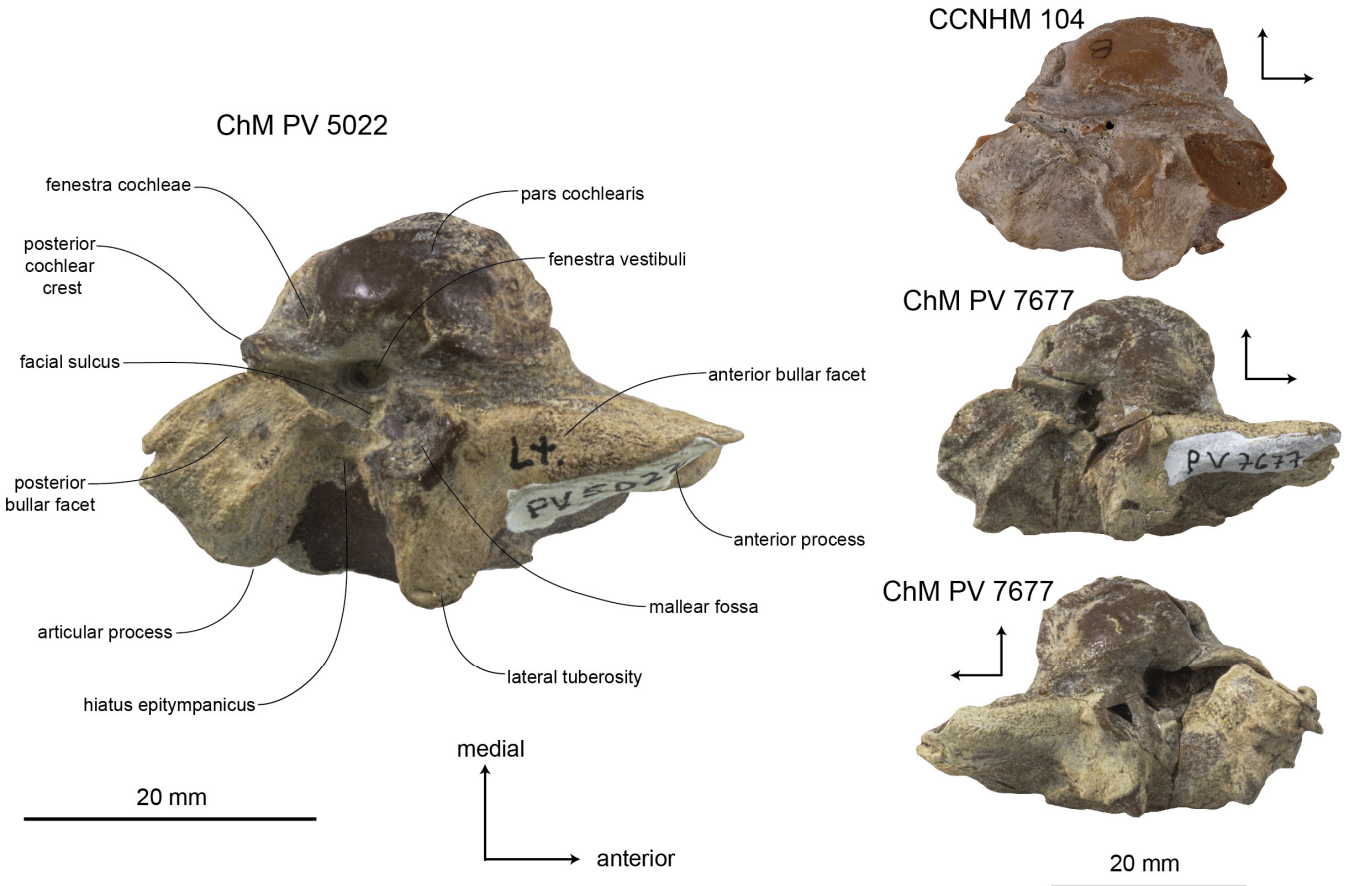


Figure 40. Periotics of referred specimens of *Xenorophus sloanii* in ventral view.

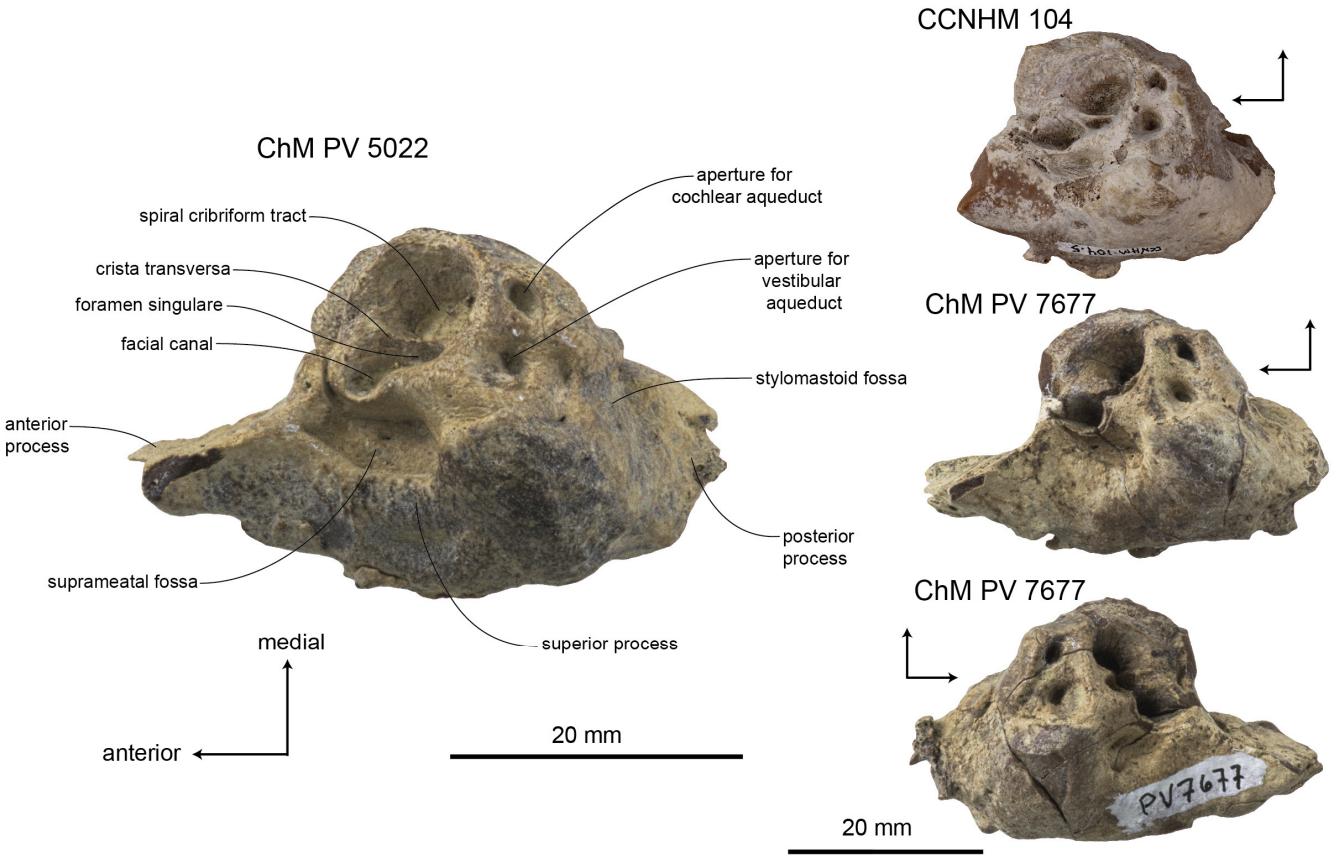


Figure 41. Periotics of referred specimens of *Xenorophus sloanii* in dorsal view.

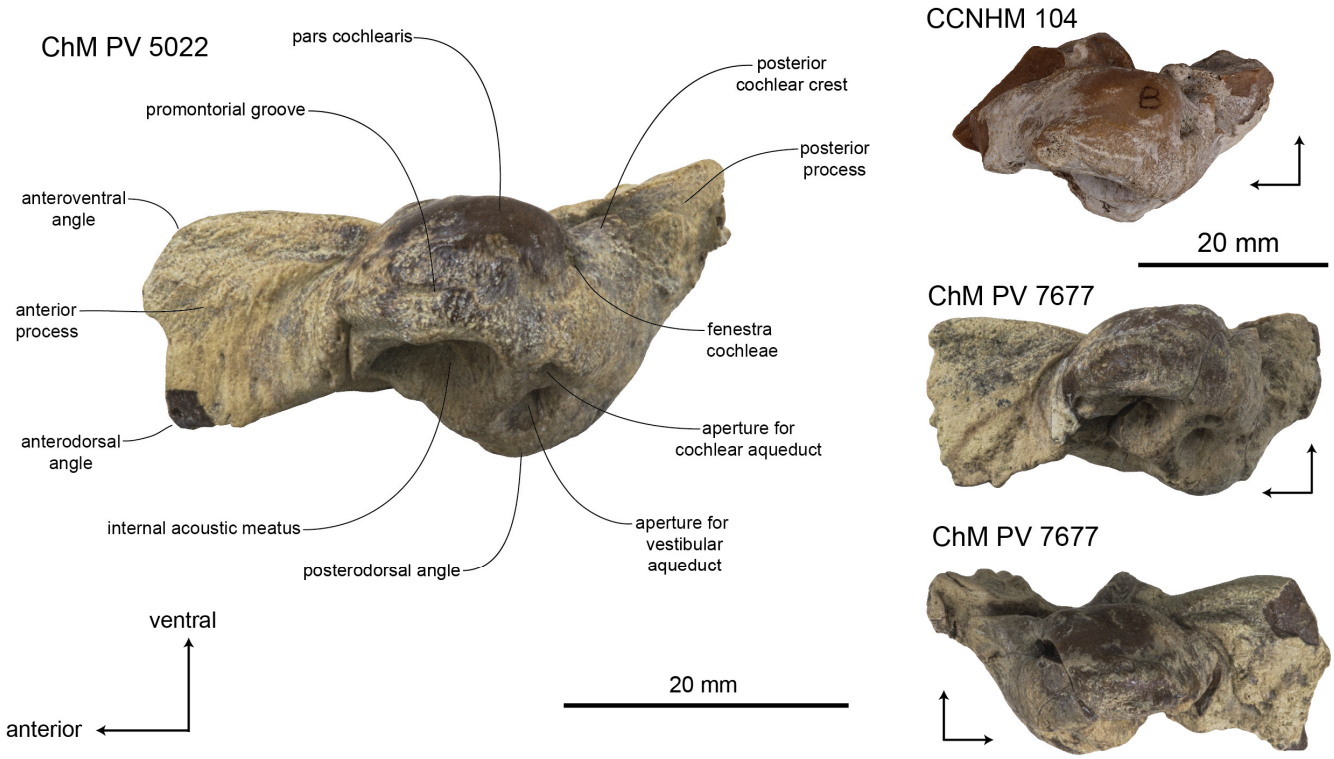


Figure 42. Periotics of referred specimens of *Xenorophus sloanii* in medial view.

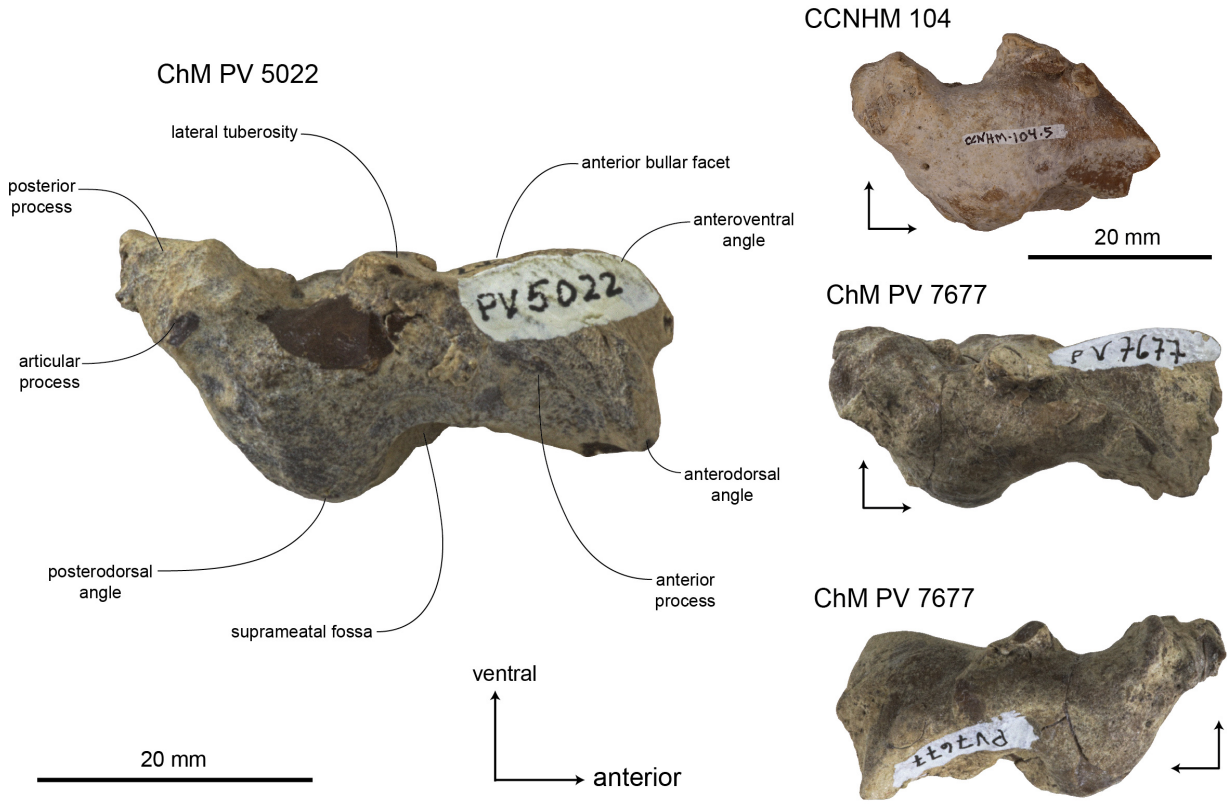


Figure 43. Periotics of referred specimens of *Xenorophus sloanii* in lateral view.

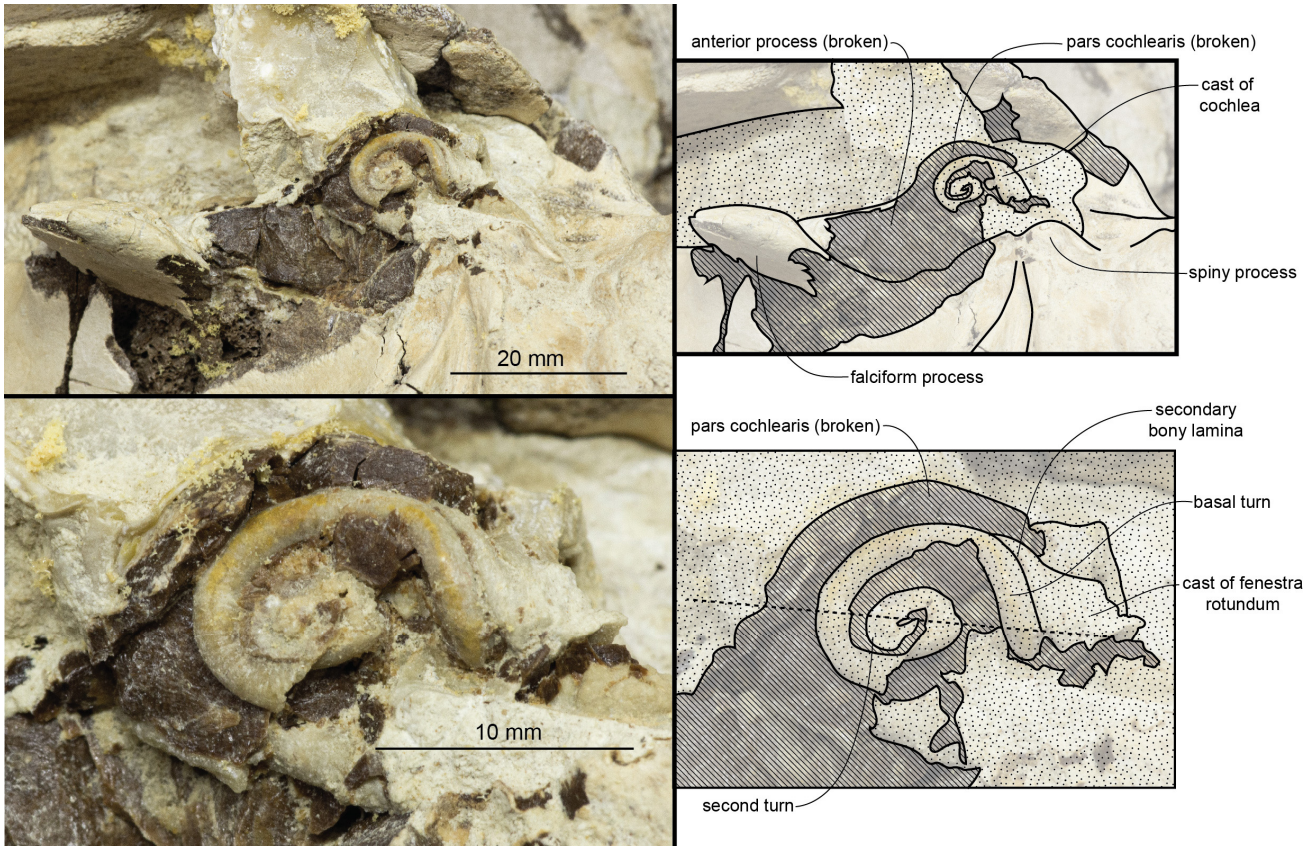


Figure 44. Cochlear endocast of *Xenorophus sloanii* (ChM PV 5022) in ventral view.

Table 8. Periotic measurements (in mm) of *Xenorophus sloanii*. ? denotes missing measurements, e denotes estimated measurement; + denotes a minimum measurement.

Measurement	ChM PV 7677	CCNHM 104	CCNHM 1077	ChM PV 5022
Anteroposterior length L/R	41.2/42.5	?	?	41.9/44.1
Transverse width pars cochlearis L/R	9.8/10.3	10.3/?	12.4/12.9	10.3/?
Pars cochlearis anteroposterior length L/R	20.8/20.2	21.1/?	19.8/19.9	21.7/?
Pars cochlearis dorsoventral depth L/R	11.7/12	11.6/?	?	12.7/?
Promontorium anteroposterior length L/R	16.8/16.2	16.3/?	17.2/17	16.5/?
anterior process anteroposterior length L/R	13.7/15	? /?	14.2/15.3	13.5/13.6
Anterior process, transverse width at midpoint L/R	5.7/6.7	8e/?	?T	6.8/6.4
Anterior process, dorsoventral depth at midpoint L/R	16.3/15.2	13.8/?	20e/20.5	14.9/?
Separation of fenestra rotundum and cochlear aqueduct, L/R	7.5/7.4	7.3/?	?	7.4/?
Separation of fenestra rotundum and vestibular aqueduct, L/R	7.8/7.7	8.1/?	?	8.1/?
Separation of fenestra rotundum and fenestra ovalis, L/R	4.6/4.3	4.3/?	?	4/?
Internal acoustic meatus, maximum length	12.3/12.8	14/?	?	12.2/?
Internal acoustic meatus, maximum width	7.5/7.1	8.3/?	?	8.8/?
Suprameatal fossa, anteroposterior length	7.9/6	10.8/?	?	9.6/?
Suprameatal fossa, transverse width	4.2/6.3	5.1/?	?	4.5/?
Posterior bullar facet, max length	12.6/10	12/?	?	12.2/11.2
Posterior bullar facet, max width	8.5/9.7	7.9/?	?	8.9/6.6+

The anterior process has a similar hatchet shape and a transversely narrow triangular profile in ventral view, and a lenticular cross section (Figures 40–43). The anterior process has a straight, vertical anterior margin with a spine-like anterodorsal angle (Figures 42 and 43). The lateral tuberosity is large, triangular, blade-like, and overlaps the squamosal just anterior to the pit for the sigmoid process (Figures 39 and 40). A deeply excavated mallear fossa is present on the posteromedial side of the lateral tuberosity; anterolateral to the lateral tuberosity is a small, table-like accessory process in all specimens (ChM PV 5022, 7677, and CCNHM 104). A much less prominent tubercle is present in *Albertocetus meffordorum* (CCNHM 303). A shallow transverse trough on the lateral tuberosity leads to a tubercle on the anterior rim of the mallear fossa, also present in simocetid-grade odontocetes (e.g., cf. *Olympicetus*, [51]). It is not clear if an accessory ossicle was present, and the anterior bullar facet is not clearly divided from the fovea epitubaria (articular surface for the accessory ossicle). No xenorophid specimen is preserved with an accessory ossicle; numerous acid-prepared simocetid-grade odontocetes in CCNHM collections from the Pysht Formation of Washington possess accessory ossicles (CCNHM 8714, 8715, 8751) and their presence is expected in Xenorophidae. Well-preserved periotic and bulla were found in articulation in a juvenile cf. *Albertocetus* (CCNHM 1838), and when in articulation, there is a gap between the outer lip of the bulla and the fovea epitubaria of the periotic, yet no ossicle was present in this space; perhaps the ossicle is unfused or only delicately connected to the outer lip of the bulla in Xenorophidae, as it is in simocetid-grade odontocetes.

In ChM PV 7677, a distinct groove for the tensor tympani insertion is present along the anterior margin of the pars cochlearis (Figure 42). A shallow anterolaterally directed sulcus trends toward the anterodorsal angle which bears two spurs: one just anterodorsal to the lateral tuberosity and another anterior to this and separated by an anterodorsally short sulcus branch; these spurs are larger on the left side.

The pars cochlearis is proportionally large (51–54% of periotic length) and has a subrectangular outline in ventral view in some specimens (CCNHM 104, ChM PV 7677) and a rounded profile in others (CCNHM 1077, ChM PV 5022; Figure 40; Table 8). The anteromedial margin is corner-like and forms a 100° angle in CCNHM 104 (Figure 40). A low longitudinal ridge is present on the ventral surface of the pars cochlearis, just medial to

the fenestra ovalis; this ridge is similar to but less extreme than the basilosaurid condition. The fenestra rotunda is small and subtriangular, but lacks a dorsal fissure; a low tubercle is present dorsal to the fenestra. In ChM PV 7677, the fenestra rotunda is circular and 2.3 mm in diameter. The caudal tympanic process is broken in CCNHM 104, but in ChM PV 7677 it is intact; it is long, posterolaterally deflected, and separated from the facial crest by a 1.5 mm gap.

No specimen of *Xenorophus* has yet been scanned using MicroCT and the complete morphology of the bony labyrinth has not yet been studied. However, breakage of the right pars cochlearis of ChM PV 5022 has revealed an endocast consisting of approximately two-thirds of the entire cochlea (Figure 44). The cochlear endocast preserves a large basal turn with a deep sulcus corresponding to the secondary bony lamina; the basal half of the first turn is separated from the second turn of the cochlea by a relatively wide gap, indicating a loosely coiled cochlea. The spiral-shaped bone in between the cochlear turns indicates that the cochlea had approximately two turns (similar to *Echovenator*); further, the second turn and apical half of the first turn are more tightly coiled (Figure 44).

In dorsal view, the internal acoustic meatus is large and oval, and dominated by a large, funnel-shaped spiral cribriform tract (Figure 41). A transversely narrow oval and small foramen singulare is positioned lateral to the spiral cribriform tract and separated from it by a low, sharp crest. This crest is slightly lower than the similarly sharp crista transversa in CCNHM 104 and ChM PV 5022, but higher than the crista transversa in ChM PV 7677. The facial canal opens anterodorsally with a teardrop-shaped outline, narrowing anteriorly towards the fissure-like hiatus fallopii. The internal acoustic meatus is separated from the deeply excavated, pit-like suprameatal fossa by a low transversely sharp crest. The suprameatal fossa is transversely narrow, oval, and very deep; it is anteroposteriorly short and less than half the anteroposterior length of the pars cochlearis (Figure 41), like *Albertocetus* and unlike the longer and larger but shallower fossa in *Echovenator* and *Cotylocara*. Faint radiating ridges emanate from the margins of the fossa in CCNHM 104 and ChM PV 7677, and are more strongly developed in ChM PV 5022. The superior ridge lies lateral to the fossa but bears a saddle-shaped concavity on the dorsal margin in lateral view at about the level of the pars cochlearis (Figures 41 and 42). The ridge rises dorsally anteriorly and posteriorly to the anterodorsal angle and broadly convex posterodorsal angle (=tegmen tympani of [10,94]).

The apertures for the cochlear and vestibular aqueducts are both small though the former is slightly smaller; they are equally sized in ChM PV 7677 (Figure 41). The entire posterior side of the pars cochlearis faces posterodorsally. The posterior process is short with a rectangular, flat posterior bullar facet. Longitudinal ridges of the posterior bullar facet are absent in CCNHM 104, but in ChM PV 7677, there are two strong ridges on the left and one on the right posterior process (Figure 40). An oval-shaped flat surface that articulates with the post-tympanic process is present posterolaterally on the periotic. In ChM PV 7677, this surface is somewhat rugose with dorsally oriented spurs. ChM PV 7677 also possesses an anterolaterally directed articular process, rising about 2.5 mm and 7–8 mm in length. A smaller tubercle is present instead in ChM PV 5022. An identical structure is present in *Albertocetus* (CCNHM 303), but not described by Boessenecker et al. [1]. During removal of the right periotic of CCNHM 303, the articular process remained embedded in the skull and could not be removed (Boessenecker, pers. obs.), similar to removing periotics in crania of extant *Platanista* (R.E. Fordyce, pers. comm.). A small pore-like posteroexternal foramen is present between the posterior process and posterodorsal angle (Figure 43).

When in articulation with the skull, there is a narrow gap with the exoccipital formed by the deep fossa (Figure 39) of Geisler et al. [4]. In specimens where the periotic is free, the posterolateral edge of the periotic articulates tightly with the medial side of the post-tympanic ridge. The periotic otherwise only articulates along its lateral edge with the squamosal and along most of the anterior process (Figure 45). The dorsal part of the superior process appears to not contact the squamosal (Figure 45), which is deeply excavated in CCNHM 104 and ChM PV 7677. However, the degree of contact in ontogenetically more

mature specimens (ChM PV 5022) is unclear owing to adhering matrix. In CCNHM 1077, the elongate spur-like anterodorsal angle articulates tightly with the alisphenoid. The anterior process is complete, unlike CCNHM 104, and is transversely narrow and bladelike in ventral view. The lateral surface of the periotic appears to have had extensive contact with the squamosal and alisphenoid. This suggests that the periotic is likely much more tightly articulated with the basicranium in adult xenorophids than in later odontocetes (Figure 45), and perhaps similar to the condition in basilosaurids. In medial view, the anterior process is rectangular and bears a deep tensor tympani groove at the junction with the pars cochlearis.

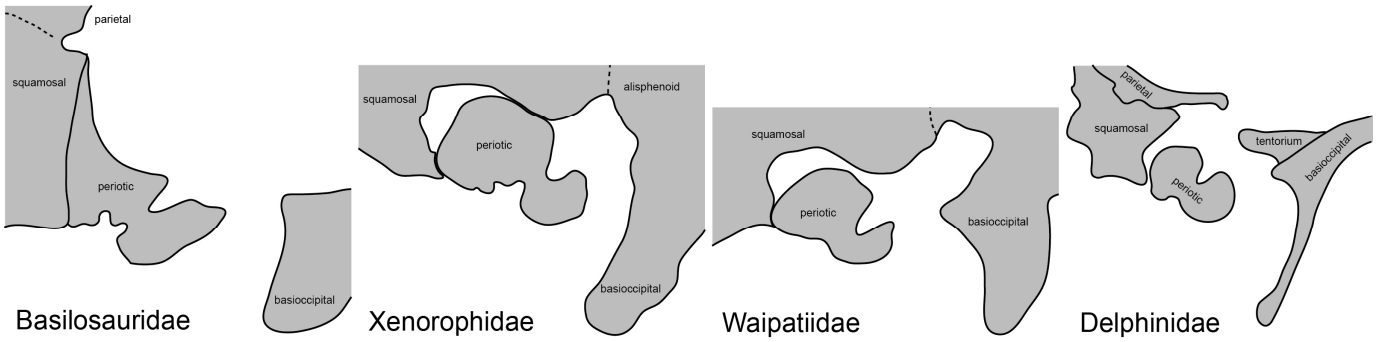


Figure 45. Articulation between the periotic and skull in Xenorophidae (based chiefly on *Xenorophus* and *Albertocetus*), Basilosauridae, Waipatiidae, and Delphinidae; modified from Fordyce ([17]: Figure 9).

Tympanic Bulla: The tympanic bullae of CCNHM 168 are complete but still in articulation (Figure 38); the bulla of CCNHM 104 is incomplete (missing the outer lip) but separate from the skull; the bullae of ChM PV 5022 (left) and CCNHM 1077 (both) are complete, and separated from the skull (Figures 46–48; Table 9). The bulla is missing in ChM PV 7677 and the holotype. The tympanic bulla is similar to other xenorophids; it is proportionally quite large for an odontocete of this size (16–17% of bizygomatic width, vs. 8% in *Tursiops truncatus*).

Table 9. Tympanic bulla measurements (in mm) of *Xenorophus sloanii*. ? denotes missing measurements, e denotes estimated measurements.

Measurement	CCNHM 104	CCNHM 168	CCNHM 1077	ChM PV 5022
Maximum length, L/R	48.7/?	50.7/51	50.4/50.7	51.8/?
Bulla, transverse width at sigmoid process, L/R	34.2/?	32/32	34.9/35	34/?
Bulla, length posterior to lateral furrow, L/R	?	30.9/30.4	30.2/30	31.3/?
Bulla, width of medial lobe, L/R	17/?	15/17	17/17.7	18.5/?
Bulla, width of lateral lobe, L/R	17.2/?	17/19	13e/12e	17.1/?
Bulla, maximum width of posterior lobe, L/R	19.3/?	34/?	18.5/17.9	35.1/?
Maximum depth of involucrum, L/R	22.3/?	?	21.1/21.3	21.1/?
Minimum depth of involucrum, L/R	14.3/?	?	13/13.5	13.2/?

The involucrum is large, transversely wide, and dorsoventrally thickest posteriorly (Figures 46 and 47). Several transverse creases are present on the anterior two-thirds of the involucrum. In CCNHM 104 and 1077, along the dorsal crest of the involucrum, the ridges separated by these ridges terminate into three–five small finger-like projections, chiefly along the anterior half of the involucrum (Figure 47). Some creases at the anteroposterior midpoint of the involucrum are deeply incised and divide the involucrum into a deep posterior half and a shallow anterior half, giving the involucrum a step-like dorsal profile

in medial view (e.g., ChM PV 5022; Figure 46). However, other specimens, like CCNHM 104 and 1077, have a far less extremely 'stepped' margin (Figure 46) than in *Albertocetus meffordorum*, *Cotylocara*, or *Echovenator*.

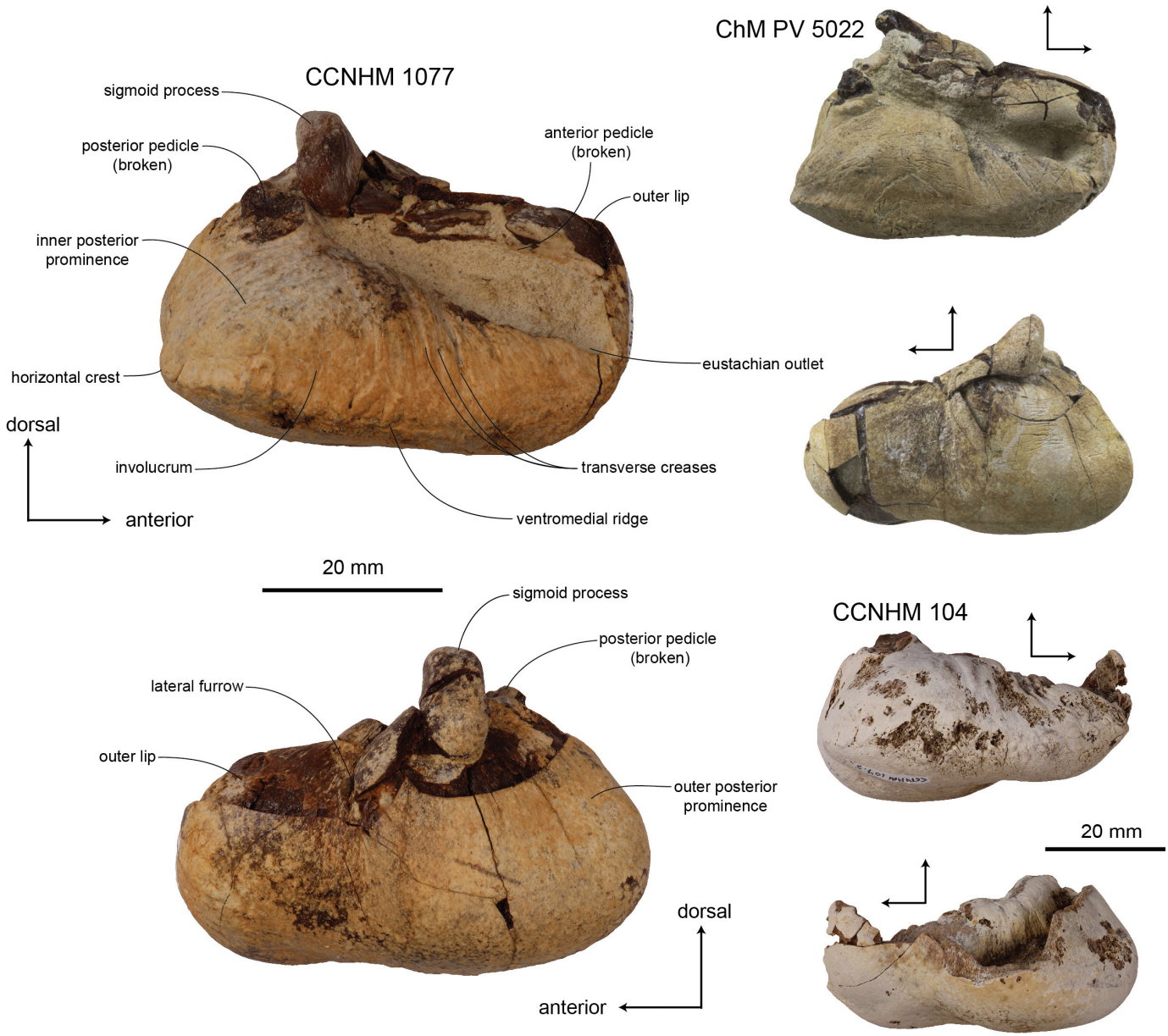


Figure 46. Tympanic bullae of referred specimens of *Xenorophus sloanii* in medial and lateral view.

In medial view, the involucrum is nearly bilobate, owing to the aforementioned transverse crease and a shallowly concave ventral margin of the involucrum (Figure 46); however, this condition is not nearly as extreme as in other xenorophids (*Albertocetus*, *Echovenator*, *Cotylocara*). In CCNHM 1077, the lateral margin is not nearly so excavated, giving the involucrum a less bilobate shape than other specimens.

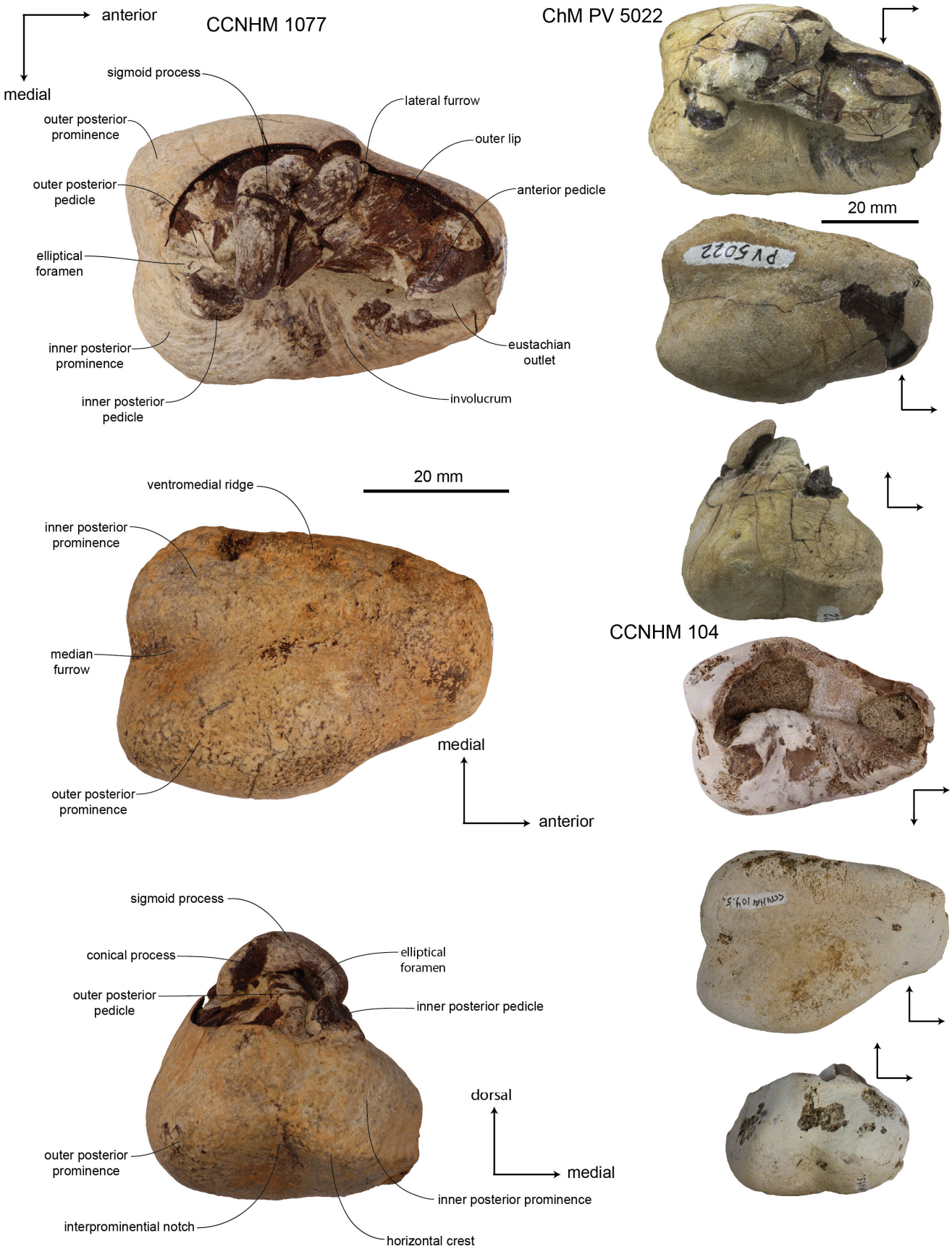


Figure 47. Tympanic bullae of referred specimens of *Xenorophus sloanii* in dorsal, ventral, and posterior view.

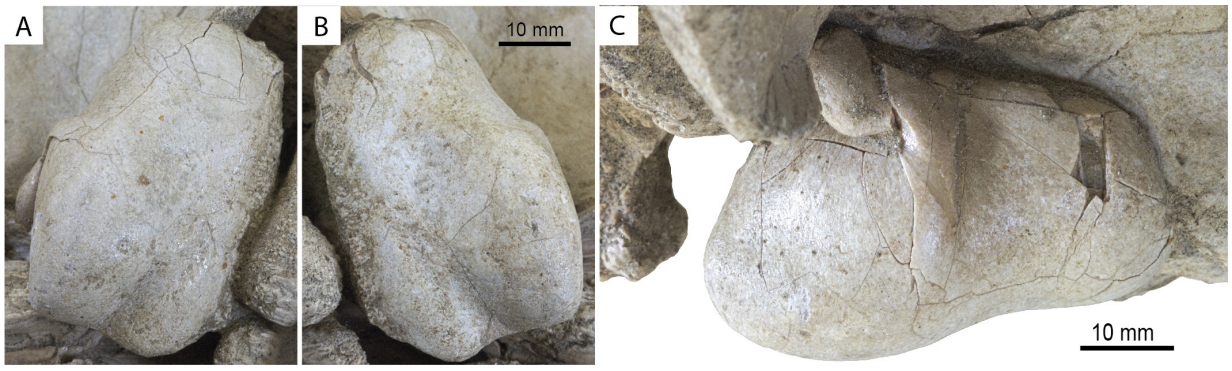


Figure 48. In situ tympanic bullae of referred specimen of *Xenorophus sloanii* (CCNHM 168) in ventral view (**A**,**B**) and lateral view (**C**).

Recent studies on protocetid earbones have recognized additional structures—tuberosities 1–5 (T1–5) on the involucrum—that help identify isolated bullae [95]. Subsequent studies of Basilosauridae and early Neoceti have, as of yet, not attempted to recognize or homologize these tuberosities. Owing to the archaic bullar morphology of *Xenorophus*, we attempted to evaluate which tuberosities may be present. An anterodorsal prominence just posterior to the transverse crease on the involucrum corresponds to T1; rather than being separate from T5, positioned medial to t1 in protocetids, these two tuberosities seem confluent. A similar condition is present in the mysticete *Coronodon havensteini* (CCNHM 108) and basilosaurid whales (e.g., CCNHM 167, cf. *Dorudon*, Tupelo Bay Formation), but some basilosaurids possess discrete T1 and T5 separated by a shallow fovea (e.g., CCNHM 4003, Basilosauridae indet.). A deeper fovea, and possibly T1, is present in some Eomysticetidae (e.g., CCNHM 207). The loss of these tuberosities broadly separates Pelagiceti from the protocetids and reflects the reduced contact of the pars cochlearis of the periotic with the tympanic bulla [95]. However, these observations suggest that some tuberosities persist into Pelagiceti and may prove fruitful for further studies of anatomical changes in the tympanoperiotic across the archaeocete–neocete transition.

A low, somewhat rugose ventral crest is present along the ventromedial edge of the involucrum (Figure 46); it is more strongly developed in ontogenetically older specimens, like CCNHM 1077 (relative to CCNHM 104). In CCNHM 1077, it is clear and slightly rugose along the posterior two-thirds of the bulla. This crest merges posteriorly with the well-developed horizontal crest on the posterior side of the medial lobe of the bulla. The interprominential notch is shallow and interrupted by the horizontal crest. A well-developed circular elliptical foramen is present dorsally; it is small, perhaps 4–5 mm in length. The inner posterior pedicle is swollen and subspherical; the outer posterior pedicle is much smaller and developed as a delicate (and broken) transverse crest terminating posteriorly into a low tubercle. In dorsal and ventral view, the bulla is "pear"-shaped and very wide (Figure 47); it widens slightly posteriorly and the greatest width is about 70% of its length. It narrows sharply just anterior to the shallow lateral furrow. The furrow is positioned within the anterior half of the bulla, making the posterior lobe slightly longer than the anterior lobe (Figure 47). The tympanic cavity is crescent-shaped and transversely narrow; it is divided into anterior and posterior compartments by a low transverse ridge that is positioned far anteriorly, about two-thirds of the distance from the posterior margin (Figure 47). The outer lip is preserved well in CCNHM 1077 and has a subrectangular outline in medial view. The sigmoid process is well preserved in this specimen and bears a ventral cleft; it nearly completely overlaps the low conical process, expressed as a slight thickening of the outer lip. The ventral surface is gently convex with an anteroposteriorly short and shallow median furrow on the posterior quarter of the bulla; a shallow median pit is present further anteriorly and separated from the furrow by a low ridge. The main ridge is low and evenly convex in cross-section. The involucral ridge (*sensu* [96]) is also low but includes the ventromedial crest.

Upper Dentition: The dental count of *Xenorophus sloanii* varies; most specimens (CCNHM 104, ChM 7677, USNM 11049) have 13 teeth (3Ix1Cx9PC), but one specimen (CCNHM 168) has 14 upper teeth (3Ix1Cx10PC), giving an upper dental formula of 3Ix1Cx9–10PC. The dental description is based chiefly on CCNHM 168 and 1077, owing to a lesser degree of tooth wear than in some specimens (e.g., CCNHM 104). CCNHM 1077 has an incomplete maxilla, and, for ease of description, is assumed to have the typical dental count and the posteriormost tooth is identified as PC9.

All specimens with well-preserved palates (holotype, CCNHM 104, 168) have asymmetry in tooth positions, generally with the right teeth shifted anteriorly by a few millimeters to nearly a centimeter relative to the teeth on the left (Figure 49). The posteriormost three–four cheek teeth positions (PC6–9, and PC7–10 in CCNHM 168) and the canines and incisors have the least asymmetry and deviations generally under 3 mm. The anterior cheek teeth (PC1–5) have the most extreme asymmetry, with some teeth shifted as much as 9 mm relative to the position of the opposite side (PC4, CCNHM 168). In CCNHM 104, the left PC4–5 are instead shifted 3–4.5 mm further anterior relative to the right PC4–5; PC6–9 however retain left teeth shifted anterior to those on the left by 0.7–3.6 mm. Anteroposterior dental shifts peak in magnitude around PC4–5, and decrease in magnitude anteriorly and posteriorly.

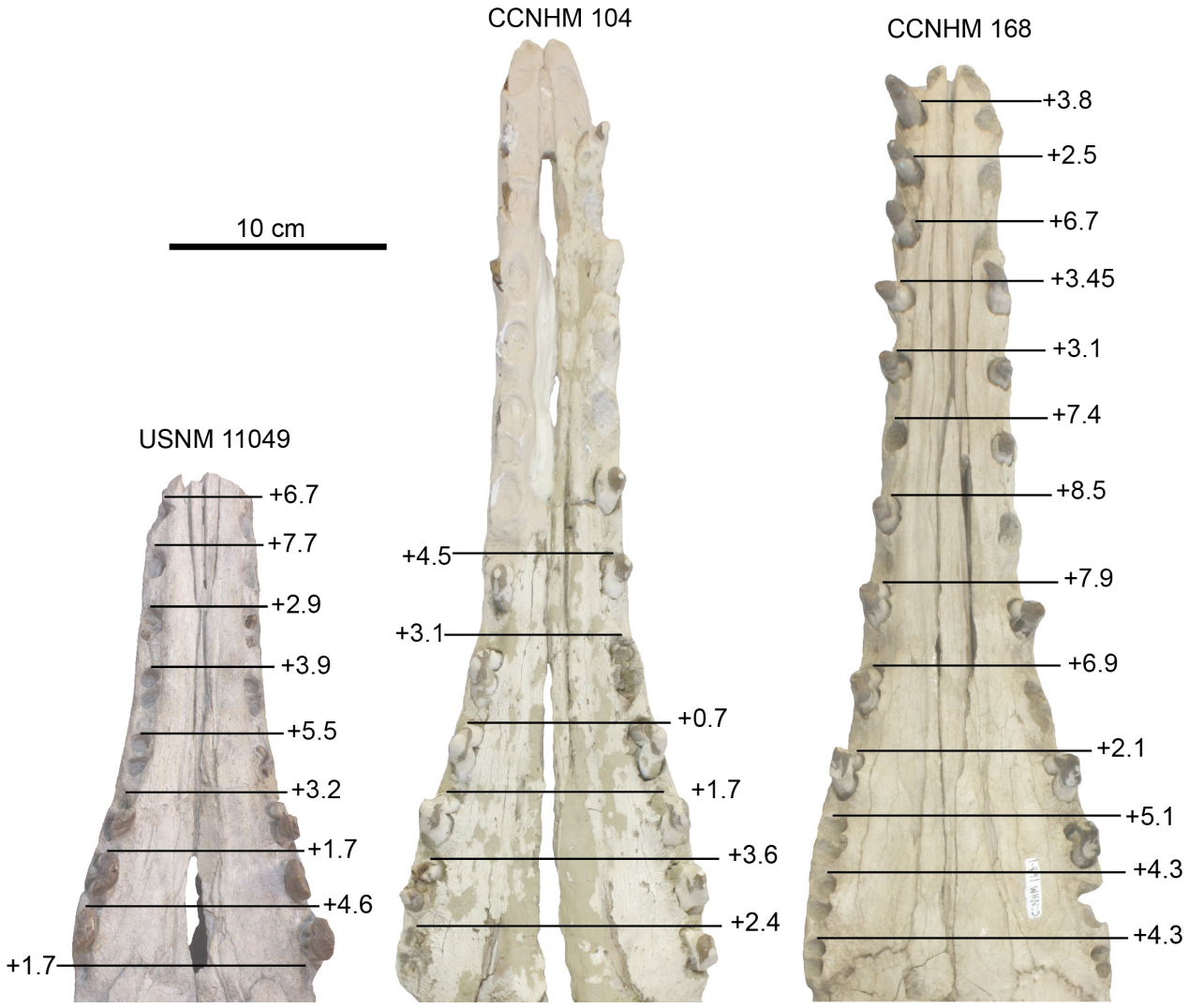


Figure 49. Asymmetry of the dentition in referred skulls of *Xenorophus sloanii* in ventral view. Values indicate how far anteriorly (in mm) bilateral structures are on the opposite side.

The upper incisor crowns (I2–3) are conical, distally curved, bear low carinae, and are nearly circular in cross section (Figures 50–53; Table 4). The labial enamel is smooth; lingually, there are discontinuous striae. The I1 is not preserved in any specimen. The canine is similar to I3 but has discontinuous lingual striae basally, which transition into continuous longitudinal fluting apically.

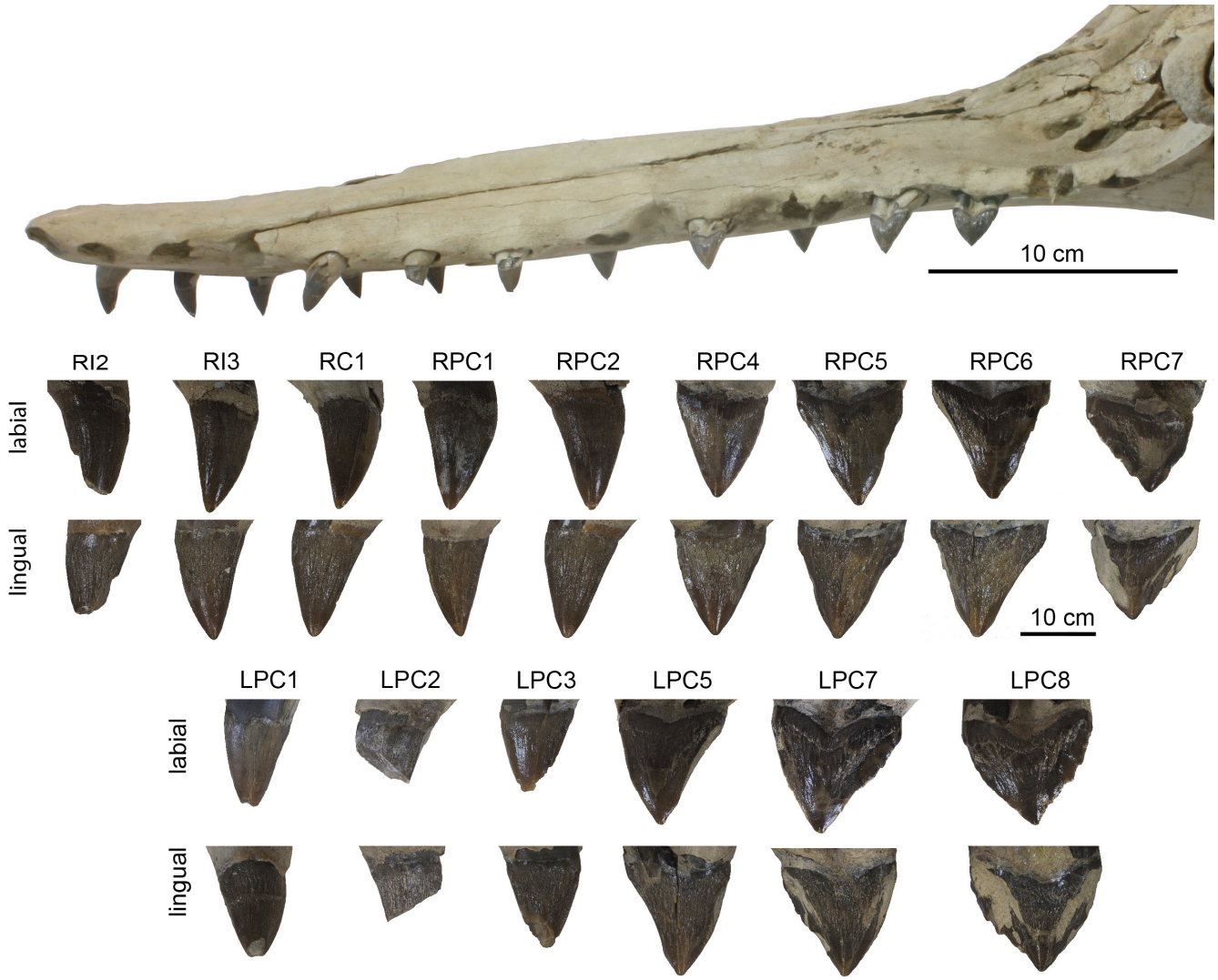


Figure 50. Upper dentition of *Xenorophus sloanii* (CCNHM 168).

PC1–2 are similar to the C1, but incipient labial striae are more evident (Figures 50–52; Table 4). PC1–3 are all single-rooted, though the roots of PC2–3 are more inflated. PC2–3 possess crowns that are less conical and, instead, are slightly triangular with a lenticular cross-section rather than round, with smooth and more sharply defined mesial and distal carina. PC4 has a single but bilobate root with labial and lingual sulci; it also bears a crown similar to PC2–3, but with an incipient lingual cingulum.

PC5–6 have triangular crowns with transversely narrower, lenticular cross-sections; they bear a posterolingual bulge and an incipient labial cingulum (Figures 50–52; Table 4). The roots are also bilobate and incompletely separated but are successively more widely divided than in PC4. PC7–8 have strong and dorsally arched lingual cingula and a well-developed nodular labial cingulum, and 3–4 min accessory cusps on the distal carina (Table 4). Mesial cusps are mostly worn away in CCNHM 168, but, in ChM PV 7677, two–three are present on PC5–9. In PC9 of CCNHM 104, at least one mesial accessory cusp was present. PC9 is absolutely smaller than PC8 (Table 4), and is single-rooted in

the holotype (USNM 11049) and double-rooted in others (CCNHM 104, 1077). Both PC7 and 8 are clearly double-rooted. The PC9 alveolus in CCNHM 168 seems to be larger than PC 10, perhaps suggesting that PC10 is the homologous tooth position of PC 9 in other specimens. The posterior postcanines are more completely preserved in CCNHM 1077, likely corresponding to PC6–9. In this specimen, all are strongly double-rooted with thick cementum (2–3.3 mm thick in upper postcanines; 2–3 mm thick in lower postcanines) and crowns that are triangular and roughly equidimensional. Deep embrasure pits are present within the diastemata between postcanine teeth along the middle of the toothrow. PC6–9 bear one–two mesial denticles and two–four distal denticles. The mesial carina is mostly obliterated by large wear facets on PC6, 8, and 9; the distal carina is unworn, and the apex of the crown is unworn in PC7–9; in PC6, the mesial wear facet extends all the way to the apex. The labial cingulum is irregular and bears a nodular crest; the basal two-thirds of the crown exhibits rugose enamel that becomes smoother apically. The labial surface is similar in being more rugose basally but, overall, is more smooth than the lingual surface. PC9 is double-rooted and the crown is similar to PC8 in CCNHM 104, while the alveolus of PC10 in CCNHM 168 is distinctly smaller than the preceding tooth (PC9); the PC10 alveolus is double-rooted in CCNHM 168.

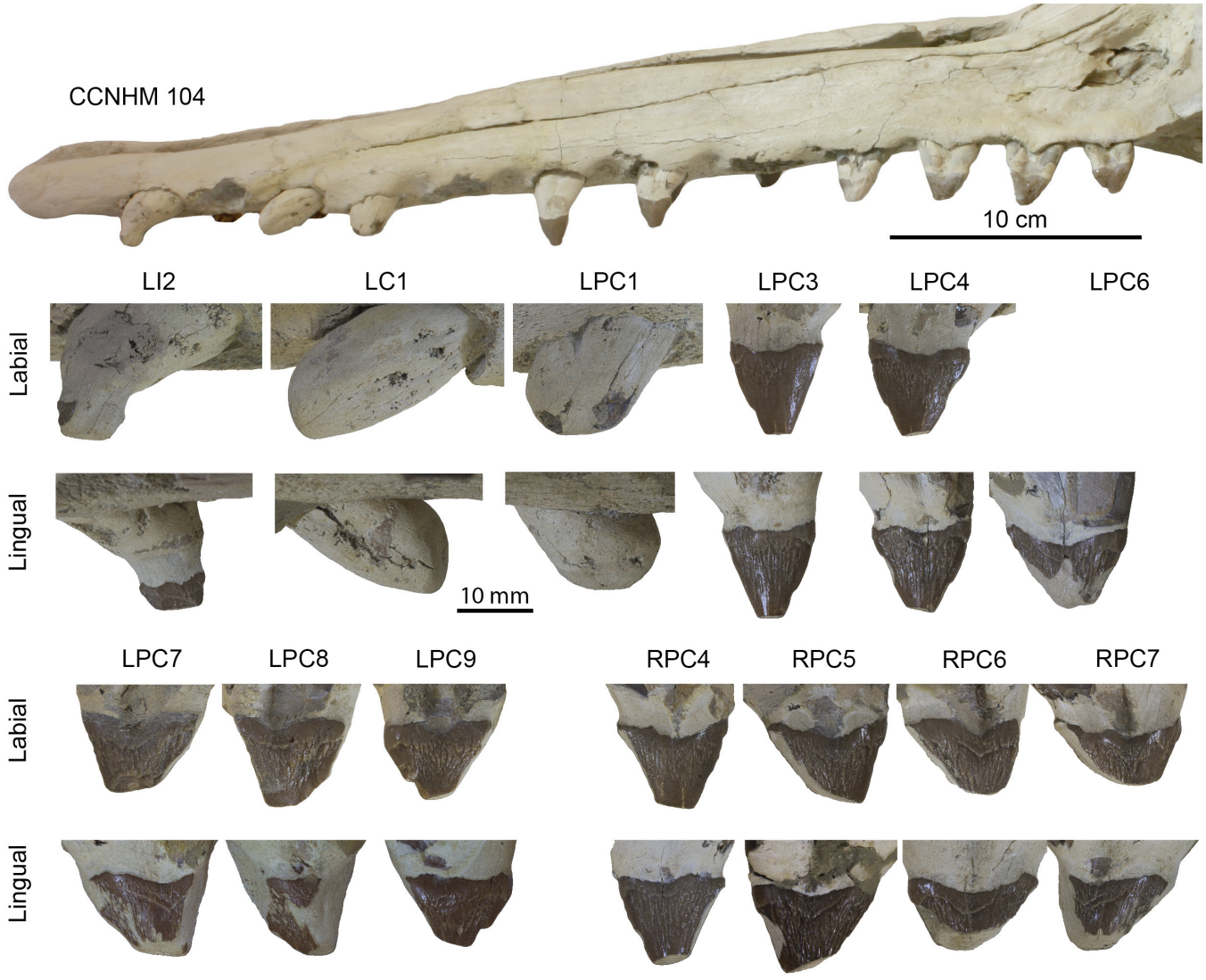


Figure 51. Upper dentition of *Xenorophus sloanii* (CCNHM 104).

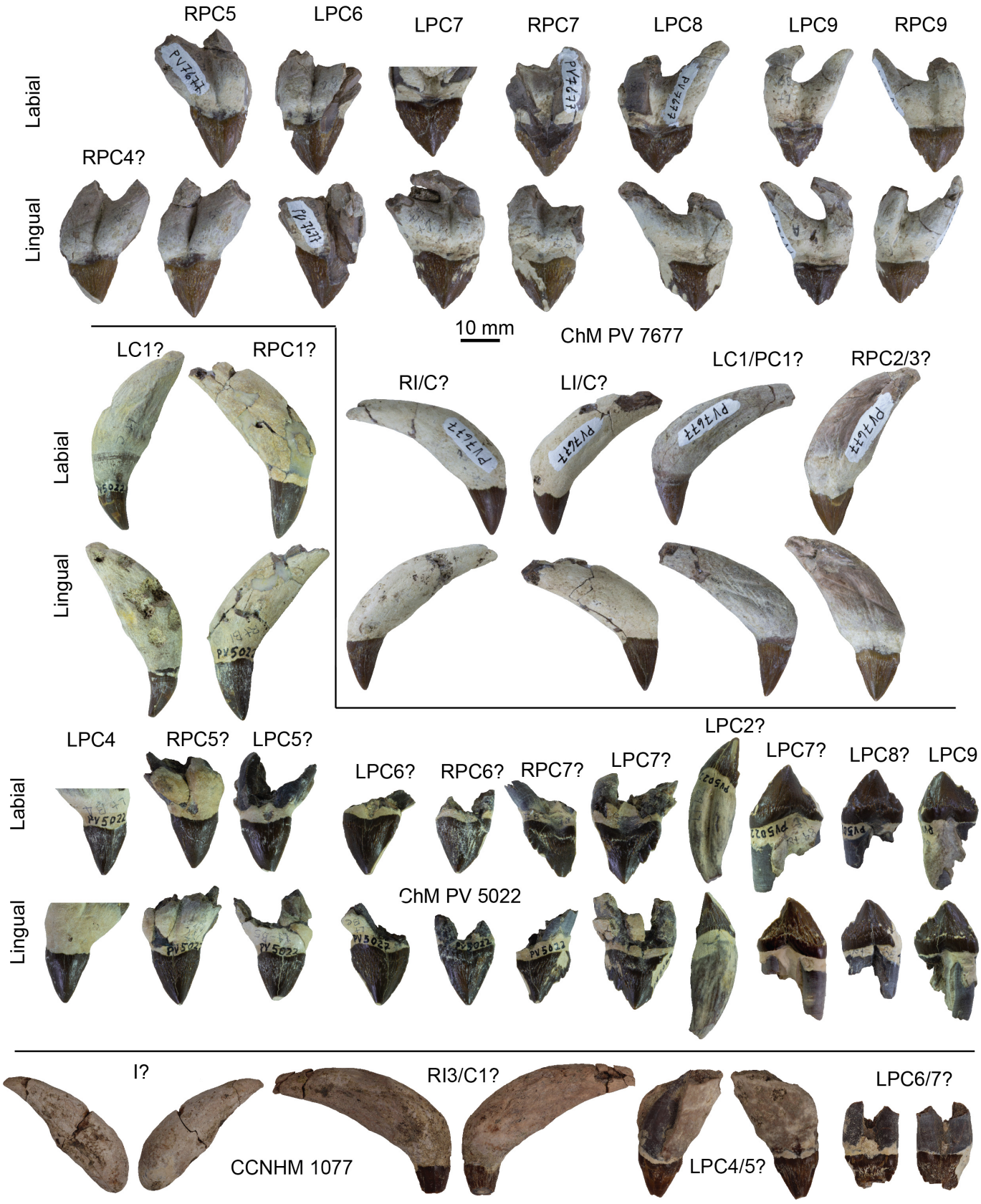


Figure 52. Upper and lower dentition of referred specimens of *Xenorophus sloanii*. Teeth with crowns pointing down are from the upper dentition and teeth with crowns pointing up are from the lower dentition. ? denotes uncertain tooth locus assignment.



Figure 53. Skull and mandible of *Xenorophus sloanii* (CCNHM 168) in anterolateral view.

Mandible: The mandible is long and the horizontal ramus is dorsoventrally shallow for most of its length; anteriorly, the mandible gradually shallows towards the anterior tip (Figures 53–57; Table 5). The horizontal ramus is twisted about its longitudinal axis so that the posterior half is facing slightly dorsolaterally rather than laterally. The symphysis is long (220 mm, ~30% of mandibular length); anteriorly, the symphyseal surface is faintly rugose with anteroposteriorly directed striations and transitions posteriorly into a ventrally placed longitudinal furrow (Figure 55). Within the symphyseal region, the alveoli are set about 10 mm from the medial edge and positioned dorsolaterally (Figure 56). Laterally positioned shallow embrasure pits are present between I1-PC1 and transition into much deeper pits aligned with the toothrow and between PC2–5, which are positioned along the dorsal edge of the mandible (Figures 54, 56 and 57). These transition into shallow embrasure pits positioned within the toothrow between PC6–7; pits are not developed between PC8–9 in CCNHM 168. However, in CCNHM 168 and 1077, deeply excavated embrasure pits are present between all of the postcanines, and, as preserved in articulation, the upper teeth were aligned with the lower tooth row and the upper postcanine crowns deep into the mandibular embrasure pits (Figures 58 and 59).

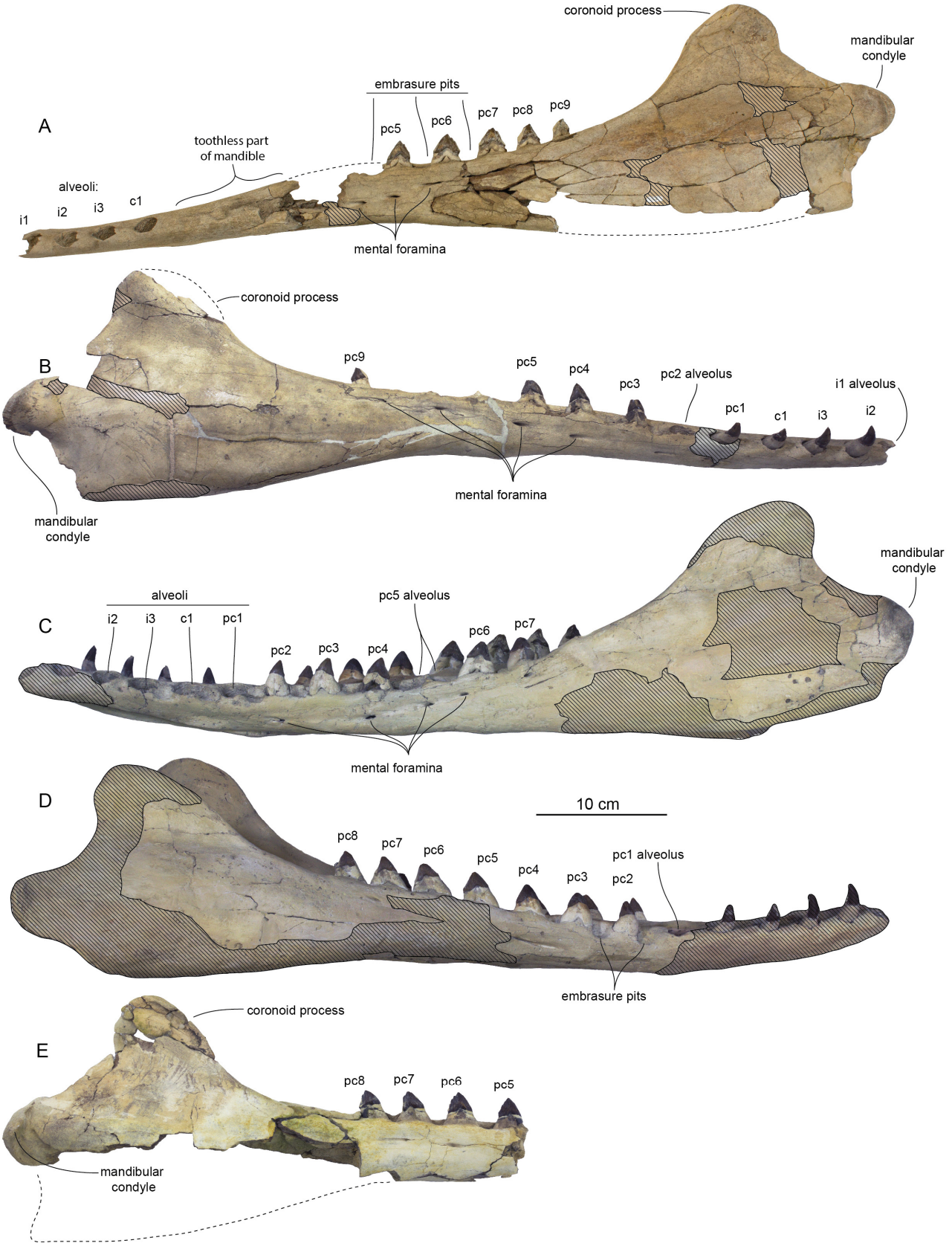


Figure 54. Mandibles of referred specimens of *Xenorophus sloanii* in lateral view. Left (**A**) and right (**B**) mandibles of CCNHM 168. Left (**C**) and right (**D**) mandibles of CCNHM 104. Right mandible of CCNHM 107 (**E**).

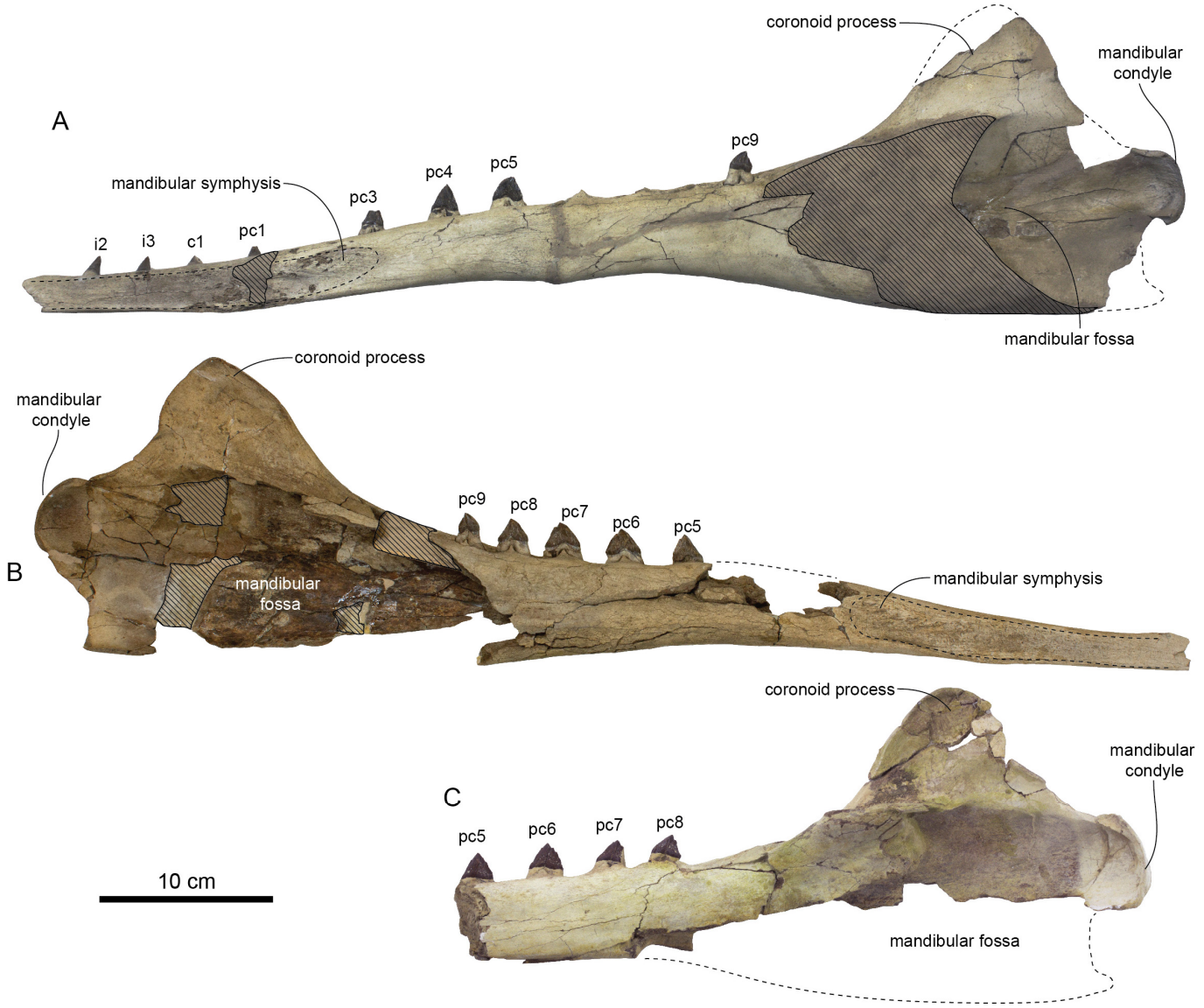


Figure 55. Mandibles of referred specimens of *Xenorophus sloanii* in medial view. Right (**A**) and left (**B**) mandibles of CCNHM 168. (**C**) Right mandible of CCNHM 107.

Most specimens of *Xenorophus sloanii* lack mandibles found in articulation, except for CCNHM 1077. Despite being incomplete, the mandible was found in articulation with the skull and informs the manner in which the teeth occlude (Figure 59). The upper and lower cheek teeth are vertically implanted and are anteroposteriorly aligned, unlike the situation in basilosaurids, where the lower cheek teeth fit lingually to the uppers. In CCNHM 1077, the upper teeth and lower teeth fit in between each other, the crown apices fitting into deep embrasure pits aligned with the toothrow, rather than the uppers being labially offset, as in basilosaurids. The teeth fit so deeply into these pits that, as fossilized, the base of the crown of the upper teeth actually lies a few mm ventral to the base of the enamel crown of the adjacent lower teeth. When occluded, the tooth crowns do not contact their antagonists but instead fit completely within the embrasure pit and, therefore, the crowns likely only contacted gingiva and possibly cementum of the antagonistic teeth.

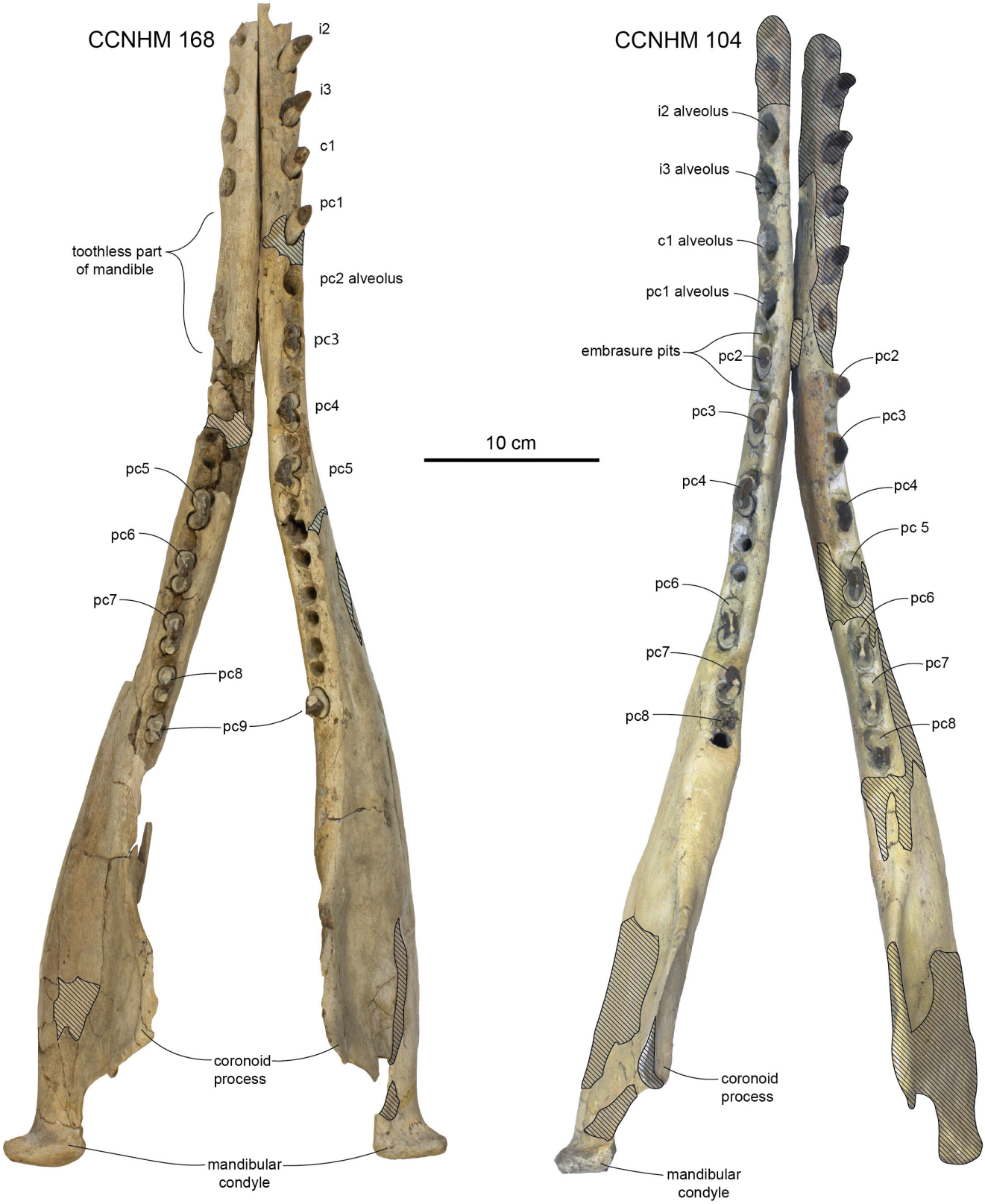


Figure 56. Mandibles of referred specimens of *Xenorophus sloanii* in dorsal view.

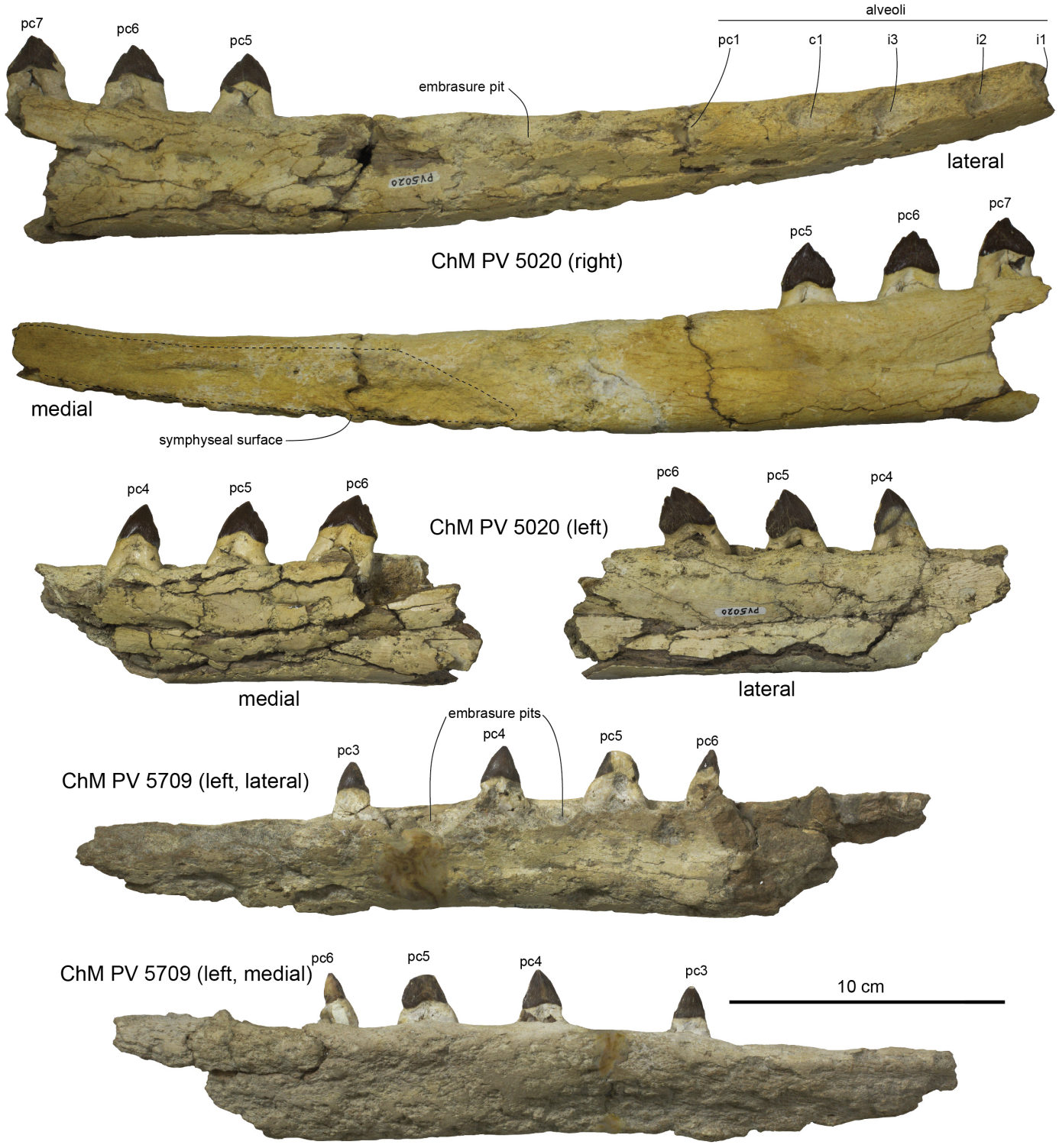


Figure 57. Isolated mandibles of *Xenorophus sloanii*.

Six mental foramina (2–3 mm wide) are present on the mandible; they have lanceolate outlines and transition into elongate sulci (15–20 mm long). The posteriormost mental foramina open posteriorly, and the remainder open anteriorly. Mental foramina are positioned below PC2, 4, 5, 6, 8, and 9; anteriorly, they are positioned on the dorsoventral middle of the mandible and become more dorsally elevated posteriorly. Some additional foramina are present near the ventral margin ventral to I1–2.

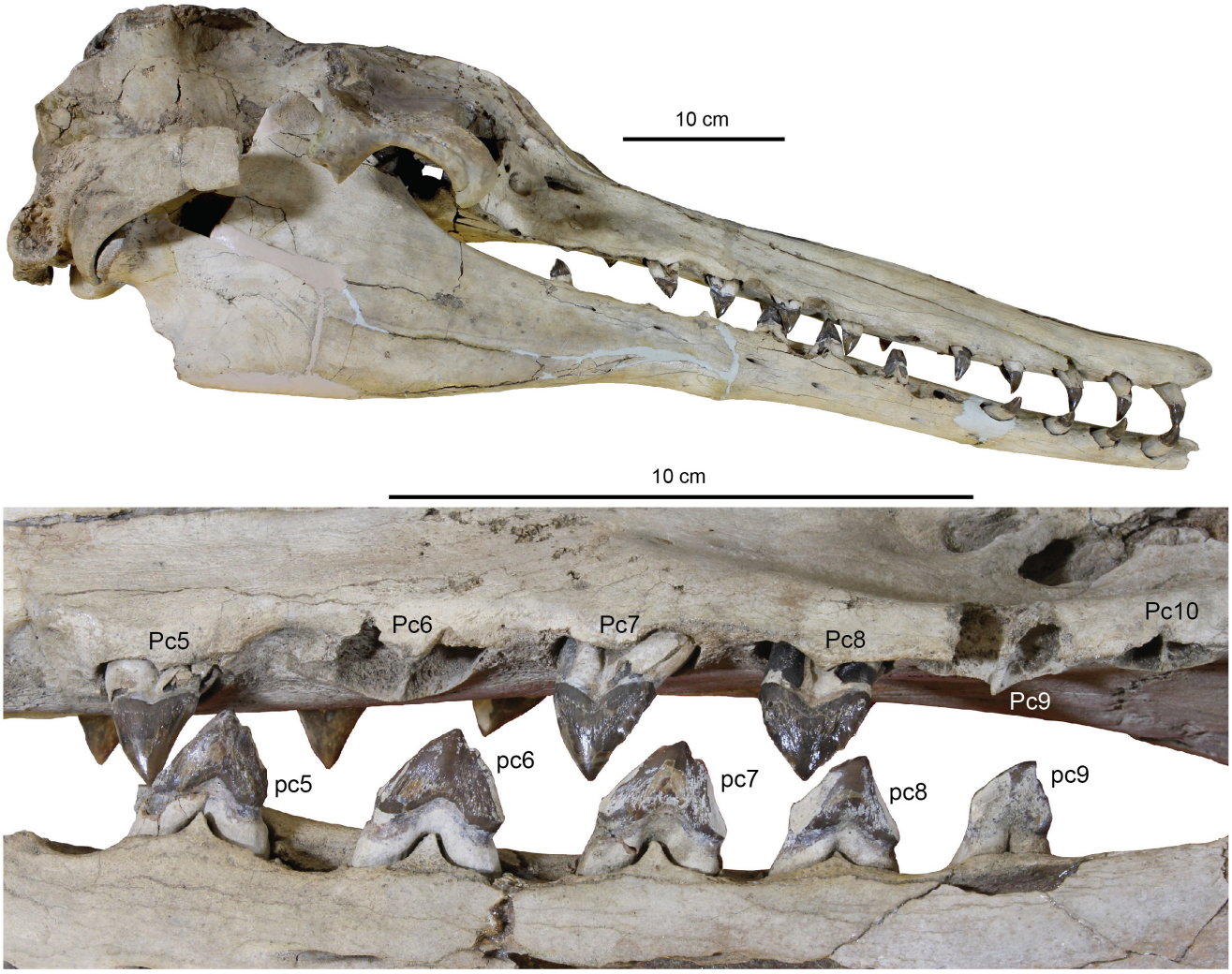


Figure 58. Referred skull and mandible of *Xenorophus* (CCNHM 168) in approximate occlusion; entire skull and right mandible in right lateral view (**top**) and close-up of postcanine teeth in skull and left mandible in left lateral view (**bottom**). Scale bar equals 10 cm.

Posterior to PC5–6, the mandible gradually deepens posteriorly and is expanded ventrally; the lateral surface is broadly convex. The ventral margin has a sinuous outline, and the dorsal margin is concave posteriorly where it leads to the coronoid (Figures 54 and 55). The coronoid process of CCNHM 168 is triangular with a low sloping anterior margin and a steep posterior margin. In CCNH 1077, the coronoid process is tongue-shaped rather than triangular (Figures 54 and 55). The anterior edge of the coronoid is transversely expanded with a narrow flange for insertion of the temporalis. The masseteric fossa is broadly concave but poorly delimited; it seems to have occupied the dorsal half of the mandible (Figure 54). Medially, there is a shallow anteroposterior trough on the coronoid, dorsal to the cavernous mandibular foramen. The margins are not preserved, but the mandibular foramen was likely about two-thirds of the dorsoventral depth of the mandible at the level of the coronoid. The 'pan bone' is well-developed, and the lateral wall of the mandible here is 2.9–3.5 mm thick.

The mandibular condyle is deeply excavated into a deep medial pit by the mandibular fossa (Figure 55). The articular surface of the condyle is gently convex and D-shaped in articular view with a straight medial margin. The toothrow is posteriorly slightly elevated above the level of the condyle (e.g., PC9 is entirely dorsal to the dorsal edge of the condyle; Figure 54).

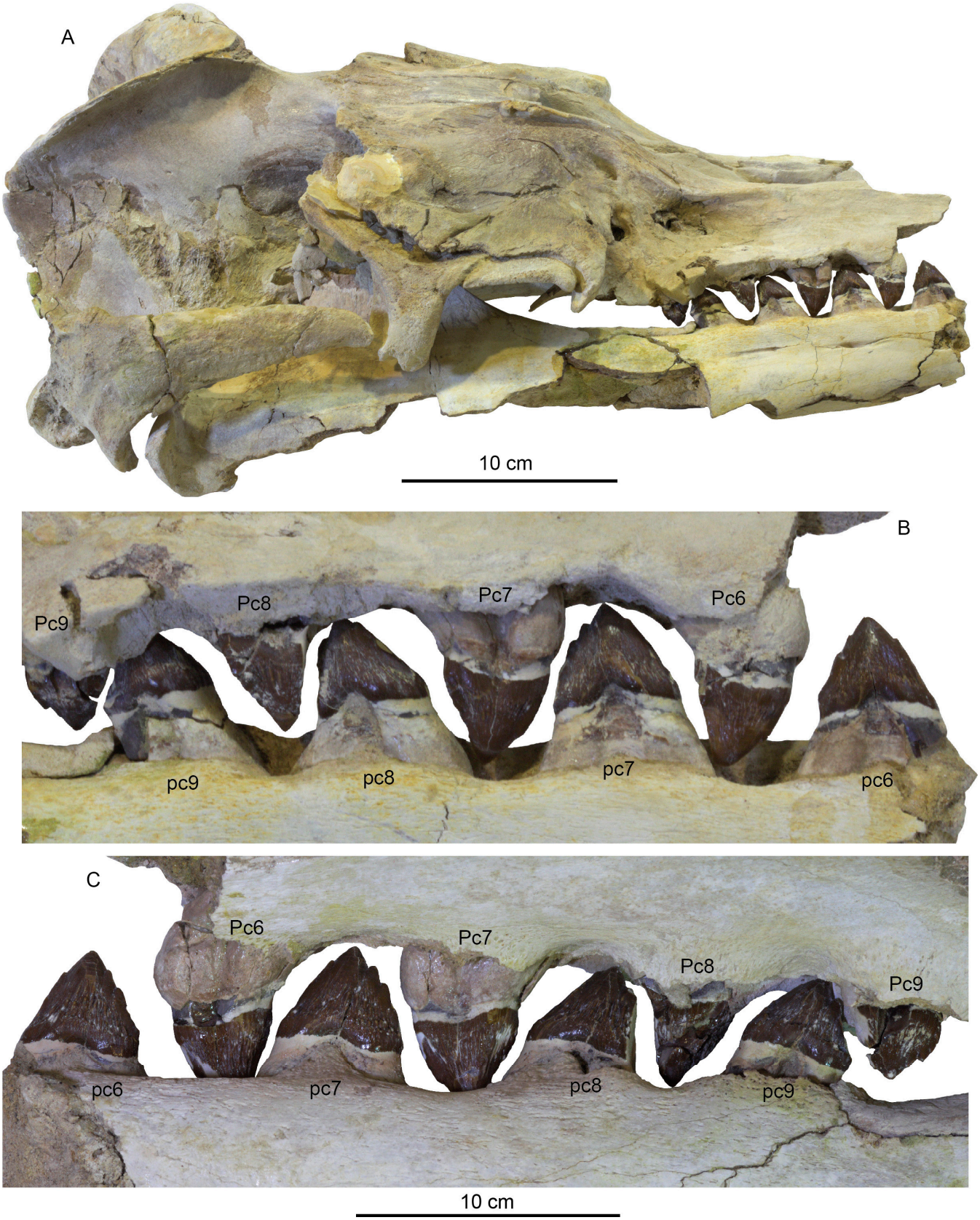


Figure 59. Referred skull and mandible of *Xenorophus* (CCNHM 1077) in occlusion as fossilized; whole skull and right mandible in dorsolateral view (**A**), teeth in labial view, (**B**) and lingual view (**C**).

Lower Dentition: The i1 is missing but i2–3 are similar in morphology to c1 and pc1: conical, slightly posteriorly recurved crowns with smooth (faintly striated) labial enamel and slightly stronger longitudinal striations lingually. Slight carinae are present on pc1 but not incisors or canine; i2–pc1 all lack lingual and labial cingulum. i1–pc1 roots are all anteriorly inclined (Figures 52, 54–56 and 60; Table 6).

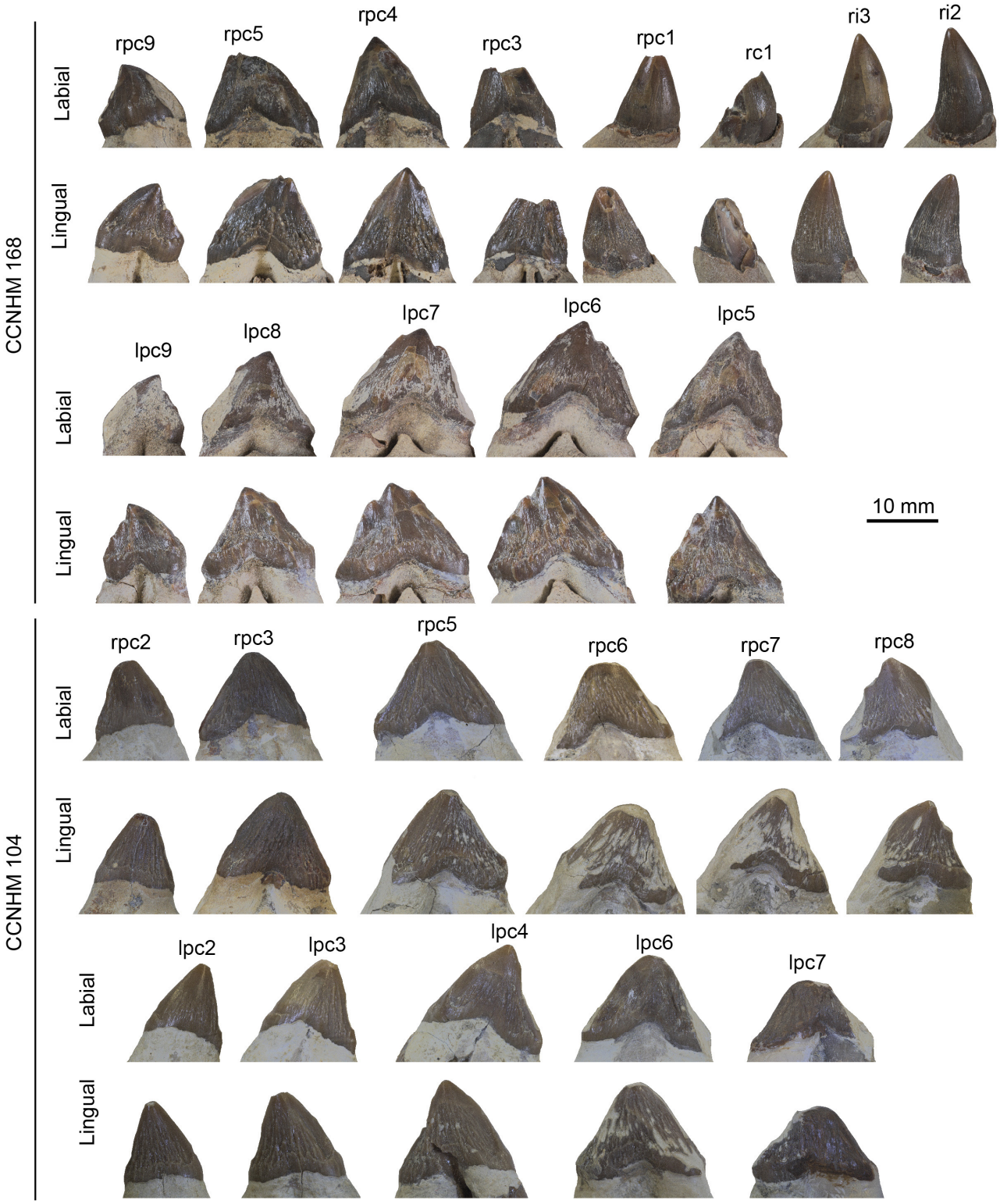


Figure 60. Lower dentition of referred specimens of *Xenorophus sloanii*.

The pc2 is missing but the alveolus accommodated a single oval root, slightly more anteroposterior elongate than pc1. All postcanines posterior to pc3 are double rooted; pc4–9 all bear a dorsally arched lingual margin of the crown (Figures 52 and 60; Table 6). The pc3 has a transversely narrow crown with weakly developed but rugose labial cingulum; it is triangular in lingual view and bears strongly developed mesial and distal carinae with some minute distal denticles. Anterior and mid postcanines (pc2–6) all share incipient, nodular lingual cingulum; in CCNHM 104, the cingulum is somewhat more ridge-like anteriorly in pc2. Lower pc4–5 are triangular like pc3 yet anteroposteriorly broader; they bear incipient labial cingula and strongly developed nodular lingual cingulum. The basal half of the lingual surface of the crown bears apicobasal ridges which are nodular and discontinuous, and become diffuse apically. The cingulum is 1.5–3 mm deep (apicobasally). Four distal accessory cusps are present; the mesial carina is smooth and lacks accessory cusps.

Lower pc6–7 are similar to pc4–5 but have rectangular rather than oval-shaped crowns in apical view (Figures 52 and 60; Table 6). In CCNHM 168 these teeth also have stronger lingual cingula with a nearly continuous crest (anteriorly more strong in CCNHM 104), and stronger labial cingula (Figure 60). The crowns are anteroposteriorly longer than pc4–5. PC7 has one–two mesial denticles and at least four distal denticles. PC6–7 have larger distal denticles than in pc4–5. PC8 is nearly identical to pc7 but is anteroposteriorly shorter with a more poorly developed labial cingulum; it bears two mesial denticles (Table 6). PC 9 is smaller yet and molariform with an equilateral crown, and is distally inclined; in occlusal view, the crown is subtriangular. It bears two distal denticles, lacks a labial cingulum, and bears smooth enamel on most of the crown. The mesial carina is convex. In CCNHM 1077, PC 6–9 are preserved (Figure 60; Table 6); all are double-rooted with triangular, equidimensional crowns similar to that of their upper counterparts. All possess thick cementum (2–3 mm thick), two–three minute mesial cusps, four distal cusps, and a weak labial cingulum consisting of rugose enamel fading apically into striated enamel. Lingually, the basal two-thirds of the enamel are strongly rugose with two–five nodules present on each apicobasal ridge. The lingual cingulum is strongly developed. Wear facets are present basally on the posterior three teeth, with a large facet removing 3–5 mm of the distal carina on PC8. In CCNHM 168, the posteriormost tooth, pc9, is triangular in occlusal view with a truncated/flattened anterior margin; it is anteroposteriorly shorter and stubbier than other teeth. The lingual cingulum is contiguous with the mesial carina and bears small cusps. A nearly identical (but isolated) tooth, presumed to represent the posteriormost lower postcanine, is preserved in ChM PV 7677. In CCNHM 104 and 1077, the posteriormost lower tooth (pc8) is, instead, nearly identical to the preceding tooth (pc7).

The termination of the toothrow is asymmetrical in CCNHM 168 (Figure 56). In the right mandible, PC9 is positioned approximately 11 mm further anterior than in the left mandible (measuring from the condyle to the anterior margin of PC9).

Tooth Wear and Dental Erosion: Juvenile and subadult specimens, such as the holotype (USNM 11049), CCNHM 5995, and ChM PV 7677, have no visible tooth wear (Figure 52; [5]: Figure 5). In adult specimen CCNHM 168, there is light tooth mesial and distal wear on the upper teeth (Figure 50). On the anterior teeth (I1–PC4), there is no apical, mesial, or distal wear. PC5 is the anteriormost tooth locus with wear facets; it bears lanceolate mesial facets along the middle third of the mesial carinae, and a long facet on the distal carina on the left PC5, removing three-quarters of the carina. The right PC5 has unworn distal carina. PC6 has some mesial wear basally and a long, narrow distal wear facet removing nearly the entire distal carina. Right PC6 also bears a minute apical wear facet. PC7 is missing nearly the entire mesial carina on both sides, though, on the left PC7, there is a narrow facet, but on the right, there is a large triangular facet that extends down onto the mesial root. In PC8, there is an irregular posterolingually placed wear facet with a tongue extending apically to the cingulum and tongues along the ridges leading to some (but not all) of the accessory cusps. PC8 has similar wear to PC7 but is more extremely worn, with longer tongues developed apical to the cingulum. In PC7–8, the mesial carina may be worn away, but the distal carina retains much of a functional cutting

edge as the wear facet is more lingually positioned. In the lower dentition, the i1–pc3 are unworn; the anteriormost wear facet is a small lanceolate facet on the distal carina of pc4. A mesial facet is not developed on left pc5, but the basal three-quarters of the distal carina is worn away by a lanceolate facet. In contrast, right pc5 has two-thirds of the mesial carina worn into a lanceolate wear facet and a small distal facet on the second and third distal accessory cusps. On pc6, there are paired apicobasal wear facets on the ridges leading to the mesial carina and a minute facet on the carina more apically; the distal carina is worn into a lanceolate wear facet along three-quarters of its length along with circular wear facets on the apicalmost two accessory cusps. Large mesial and distal wear facets removing three-quarters of the carinae are developed on pc7–8, but the apical 4–6 mm is intact, along with the principal cusp. A similar mesial oval-shaped mesial wear facet is present on pc9, though this facet is positioned entirely labial to the mesial carina, which is intact. Discontinuous oval-shaped facets are present along the distal edge of the distal accessory cusps in the right pc9; similar but much smaller facets are present in left pc9. Right pc9 also bears a small facet on the distal edge of the principal cusp. Tooth wear in the posterior postcanines (PC6–9, pc6–9) in CCNHM 1077 is less extreme than in CCNHM 168, consisting of only light posterolingual wear of rugose ridges, small mesial wear facets on some teeth (PC6), and large shear facets developed only on a few teeth (distally on pc8, mesially and distally on PC8, and mesially on PC9); apical wear is absent on these teeth (Figure 59).

In contrast, tooth wear in subadult specimen CCNHM 104 is substantially more extreme than in all other specimens (Figures 51 and 60). All preserved anterior teeth have extreme wear of the crowns. I2 preserves the lingual base of the crown only, and a large apico-labial wear facet is present. The crowns of left PC1–2 are completely missing, and these teeth are reduced to lozenge-shaped roots protruding from the alveolar margin with evenly rounded apices. PC3–4 are the least worn teeth in the dentition; they bear large apical wear facets with perhaps only 3–4 mm of the principal cusp missing, small apically positioned mesial wear facets along the carina, and small basal distal wear facets along the carina; the distal wear facet in right PC4 is much larger, occupying virtually the entire distal carina and nearly connecting with the apical wear facet. Right PC5 has a small mesial wear facet along the basal two-thirds of the mesial carina and a large apical wear facet that merges evenly with a continuous distal wear facet that has removed the entire distal carina. In right PC6–7 and left PC6 and PC8, the mesial, apical, and distal cusps are large and continuous, resulting in the loss of the principal and all accessory cusps and carinae. An exception is in left PC8, where a small remnant of carina is present between the base of the principal cusp and apicalmost distal accessory cusp. Left PC9 bears only minute apical wear facets on the two mesial accessory cusps, but a large and continuous wear facet apically and distally. In PC7–8, small facets are present where the enamel on rugose ridges has been removed from wear on the posterolingual surface. PC7–8 have large shear facets that cut basally into the root at least 8–10 mm basal to the crown base; these facets are continuous with the mesial wear facets. A similar, but less basally extensive distal wear facet is present on left PC8.

Evidence of dental erosion is also present in CCNHM 104 (Figures 51 and 60). Many teeth (left I2, PC3–4, PC6–9; right PC4–7; left pc2, pc6, right pc6–7) exhibit slight narrowing of the crown cervix (sensu [97]). This is most pronounced anteriorly, such as left I2 and left PC3–4, where the posterolingual portion of the crown cervix exhibits a transverse trough; in labial and lingual view the distal margin of the tooth is concave just basal to the crown, and the enamel appears slightly undercut in left PC3–4. In left I2, this trough nearly encircles the entire crown base. An isolated incisor tooth, either an upper right or lower left incisor, also has a narrowed crown cervix, albeit not as extreme as in left I2. This isolated tooth (along with left I2, and to a lesser extent, other teeth) bears an irregular base of the enamel crown with a clear ledge-like morphology at the edge of the enamel.

Stylohyal: One rod-like element in CCNHM 168 represents the ?left stylohyal (Figure 61). It is slightly curved ventrally and bears an oval cross-section with expanded distal and proximal ends; the large end articulates with the basihyal. The distal end has a lenticular pitted facet indicating a cartilaginous joint with the basihyal; the smaller (distal) end is also pitted but less extremely so. Scars are present as sharp ridges along the medial edge and proximally and distally on the lateral edge, identifying this as the left stylohyal. The medial crest on the proximal end is developed into two ridges separated by a crest—small tubercles of bone are developed along this crest.



Figure 61. ?Left stylohyal of *Xenorophus sloanii* (CCNHM 168) in ?dorsal (**A**), ?ventral (**B**), ?medial (**C**), and ?lateral (**D**) view.

Cervical Vertebrae: Complete cervical series are preserved in CCNHM 168, CCNHM 1077, and ChM PV 5022; CCNHM 104 preserves an Atlas and three mid-cervicals (C3–C5), and an isolated C3 or C4 is present in ChM PV 7677 (Figures 62–66; Tables 10–13). The atlas is similar to *Albertocetus meffordorum* but 135% larger (Figure 61). The atlas of CCNHM 168 (but not CCNHM 1077) is asymmetrical and slightly wedge-shaped in dorsal view (Figure 66A), being anteroposteriorly longer on the left (68 mm) than on the right (63 mm). The anterior articular surfaces have an oval outline, and are about 75% as tall as they are wide (Figure 62). In CCNHM 168, these surfaces are not separated but, in CCNHM 1077, a clearly incised sagittal furrow separates these facets. The ventral part of the body is dorsoventrally thick, almost as thick as the transverse width of the condylar fossa. The hypapophysis is prominent, knob-like, and posteroventrally projecting. A faint intercondylar notch is palpable ventrally on the anterior surface. The neural arch of the atlas is triangular in anterior view and bears a low, knob-like neural spine in CCNHM 104 and 168; it is somewhat more prominent in CCNHM 1077. The neural arch is pierced laterally by a nearly circular 10 mm wide lateral vertebral canal. The neural foramen is circular in anterior view (Figure 62). The transverse process is developed as a subtriangular, posterolaterally deflected, and anteroposteriorly flattened flange with a single lateral apex in CCNHM 168; a smaller secondary dorsal tubercle is positioned at the dorsal base of the process. In CCNHM 1077, the transverse process is more rectangular with equally sized dorsal and ventral processes. The transverse process is not perforated by a transverse foramen in any specimen. The posterior articular surface of the atlas is trilobate: a large, flat lateral facet and a transversely narrow but dorsoventrally deep median lobe that extends from the odontoid fossa to the posterior side of the hypapophysis; it is dorsoventrally constricted adjacent to the hypapophysis. In lateral view, the atlas is wedge-shaped and

widens dorsally. Pathologies on the atlas of CCNHM 168 include pitted, rugose, and unusually spongy bone on the neural spine and hypapophysis and lipping on the lateral and medial edges of the left condylar fossa. In CCNHM 1077, the hypapophysis is longer and more finger-like; a few linear scrape marks attributable to shark scavenging are present on the dorsal edge of the right transverse process of CCNHM 168.

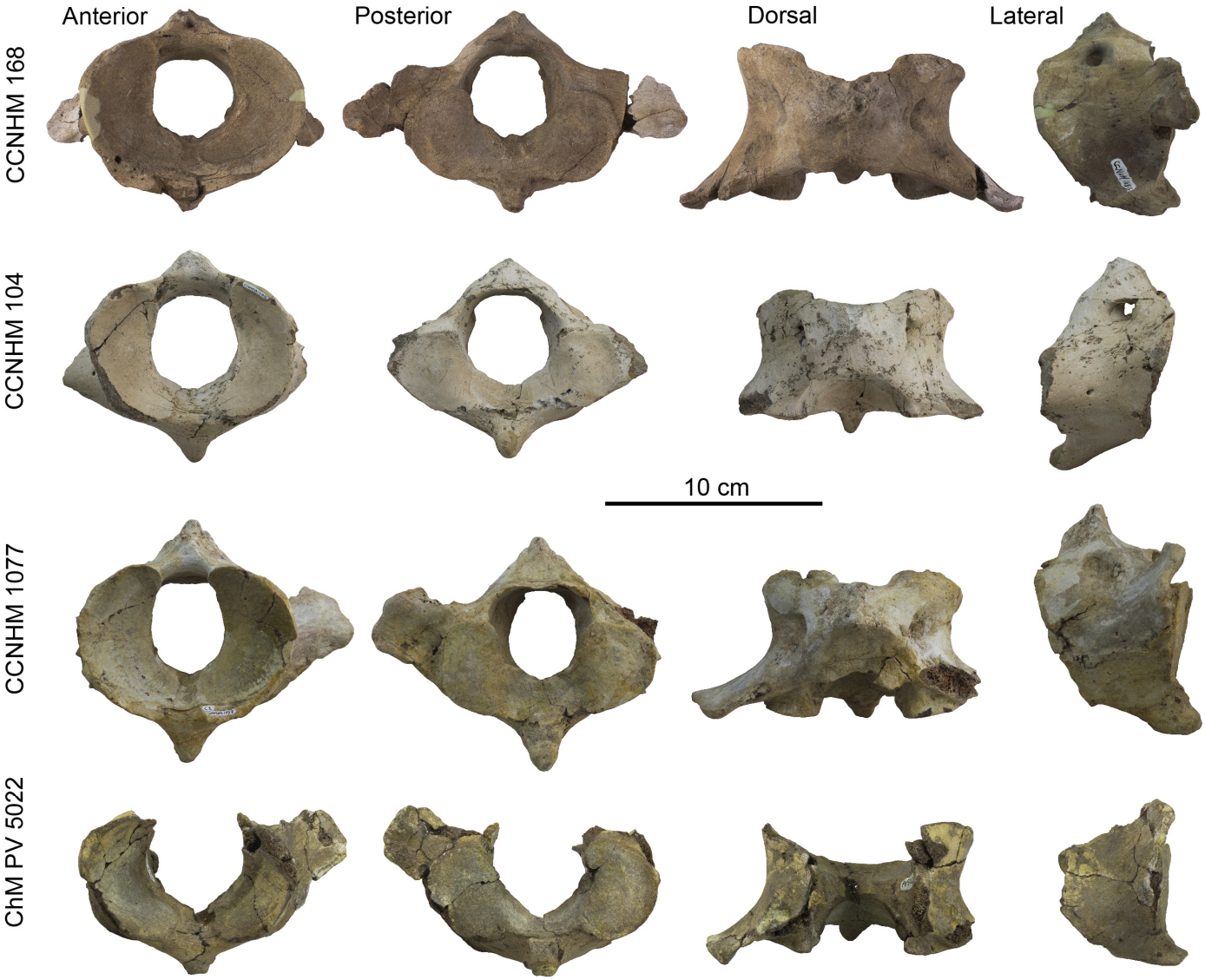


Figure 62. Atlas vertebrae of referred specimens of *Xenorophus sloanii*.

The axis (Figure 63) has a trilobate atlantal articulation with oval lateral facets and a median anteroventrally facing facet on the ventral half of the low, conical odontoid process; this facet articulates with the posterior face of the hypapophysis (Figure 63). The odontoid is somewhat more prominent in CCNHM 1077. The neural foramen is subtriangular with a dorsally convex ventral margin; it bears a median sagittal ridge on the centrum, extending from the posterior margin to the odontoid process. Ventrally, a low and indistinct hypapophysis is developed and a shallow fossa is present laterally on each side. The neural spine dorsally transitions into an anteroposteriorly flattened plate; all specimens (CCNHM 168, 1077) possess a neural spine with a bifurcated apex (resembling a heart in outline) like *Albertocetus* and *Echovenator*. The anterior tip of the neural spine is subtriangular in lateral view and extends anteroventrally, terminating in a flat facet that articulates tightly with a lunate facet on the posterior side of the atlas neural arch; this facet

is slightly wider in CCNHM 1077 than in CCNHM 168. In both CCNHM 168 and 1077, the neural spine is rotated 2° (CCNHM 168) and 9.7° (CCNHM 1077) to the right (Figure 66B). The postzygapophyses are visible in anterior view, as they project dorsolaterally above the lamina. The posterior epiphysis is nearly oval-shaped with a ventral apex for the hypapophysis, and is completely fused in CCNHM 168 yet bears a faint notochordal pit. The transverse processes are short, posterolaterally directed, and rectangular in anterior view, but taper in dorsal view; in CCNHM 168, the right transverse process is slightly larger and longer than the left. In CCNHM 1077, the transverse process extends further posterolaterally. A shallow fossa is present between the centrum and transverse process.

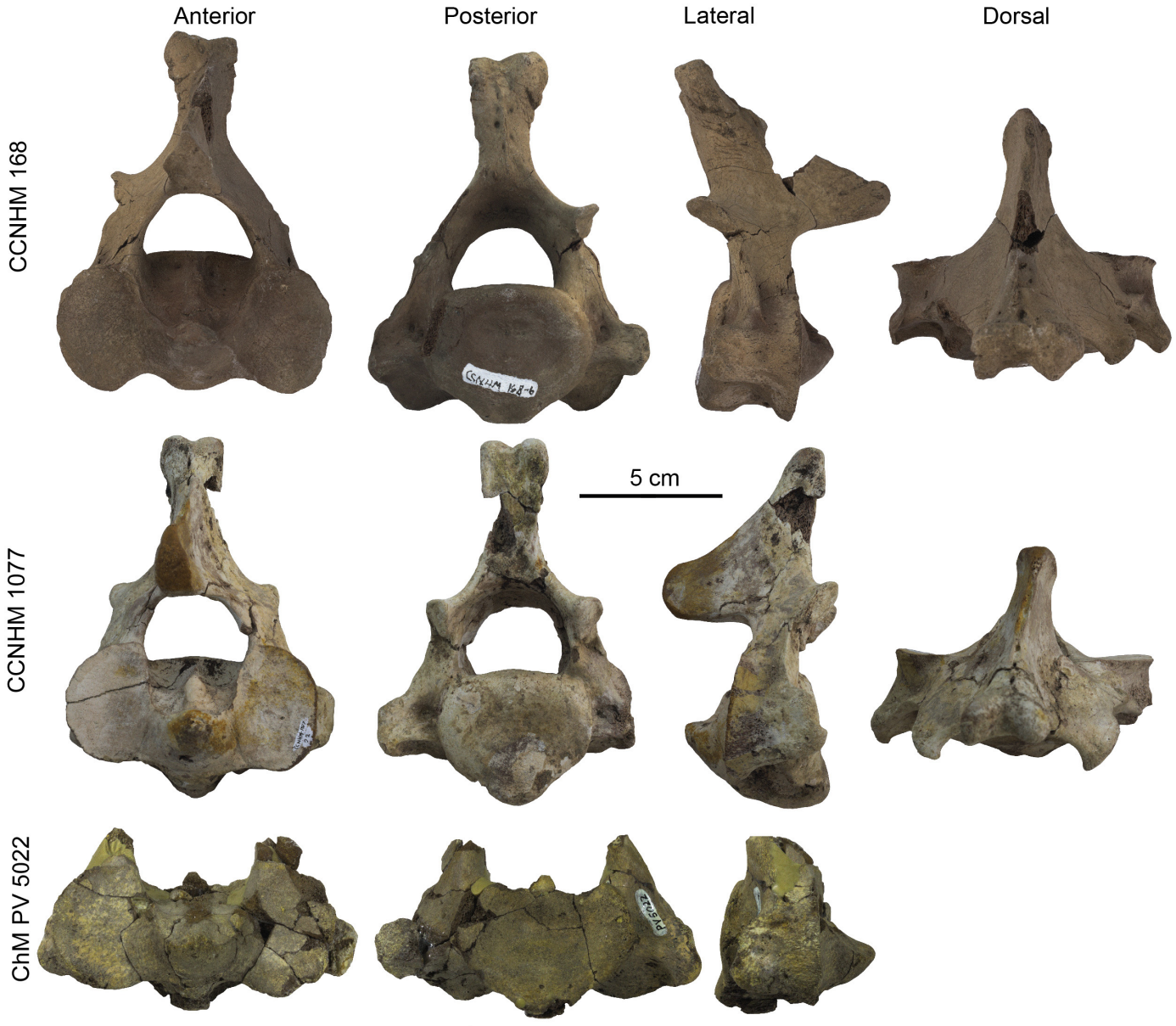


Figure 63. Axis vertebrae of referred specimens of *Xenorophus sloanii*.

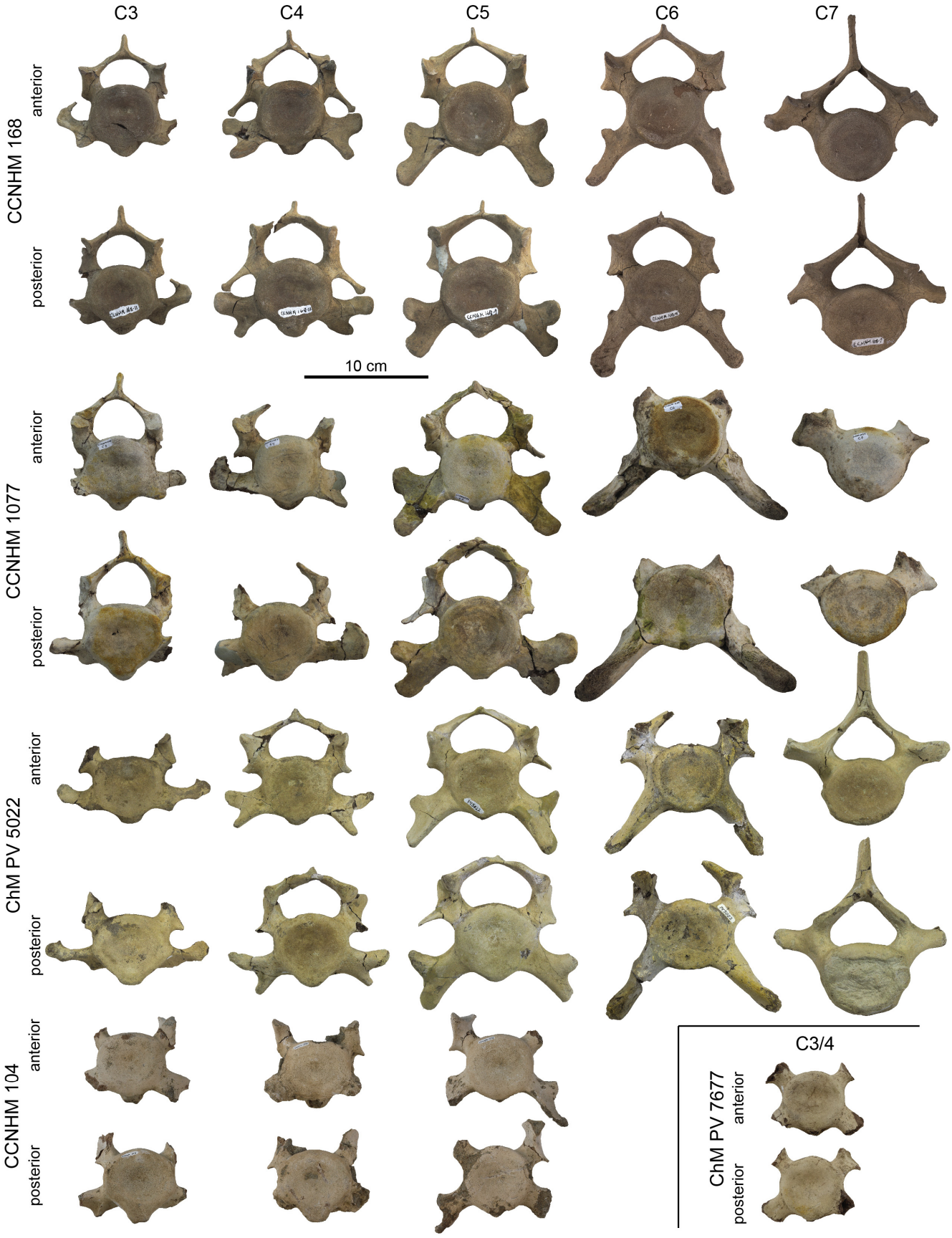


Figure 64. Cervical vertebrae (C3–C7) of referred specimens of *Xenorophus sloanii*.

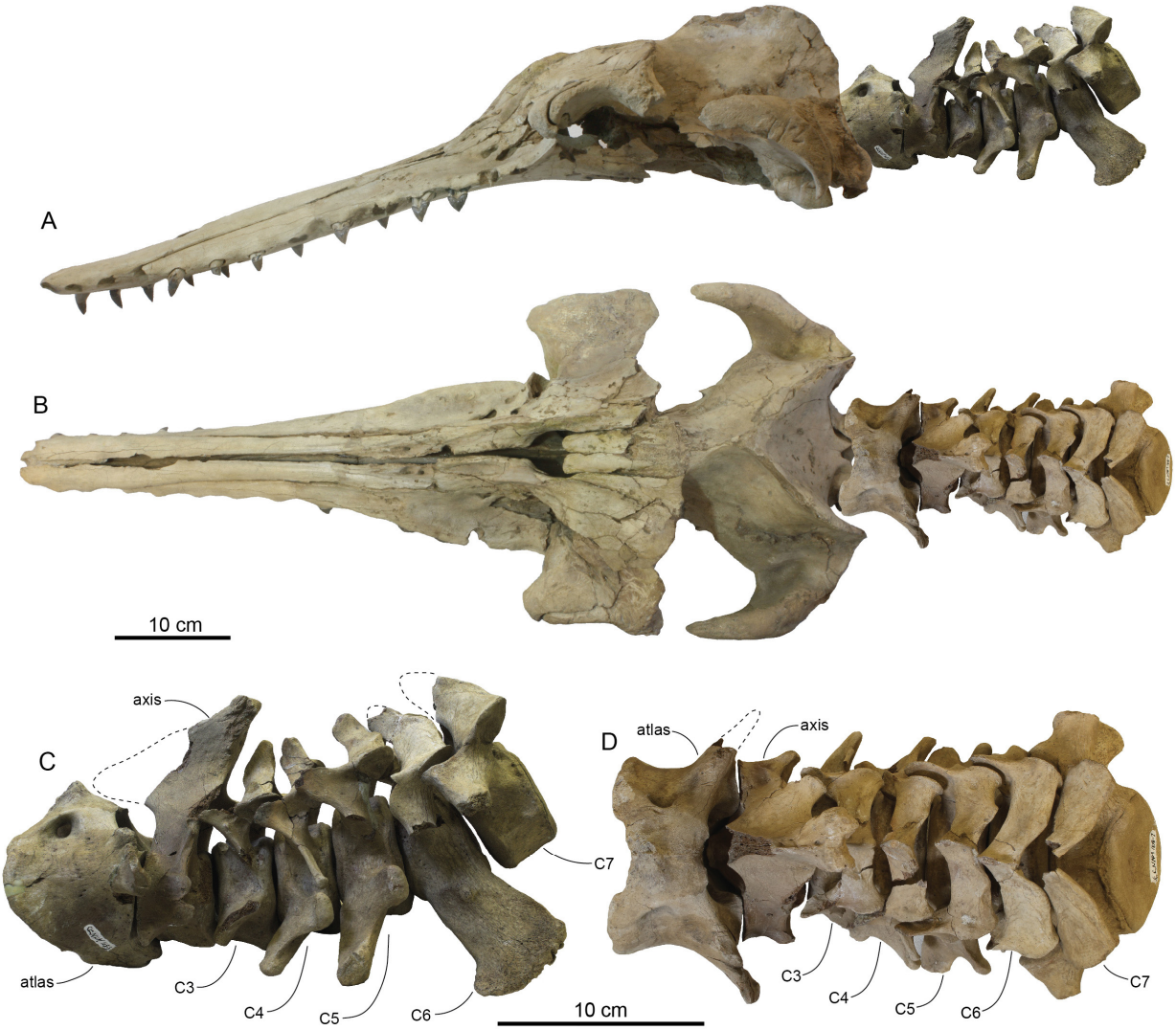


Figure 65. Articulated cervical vertebrae and skull of *Xenorophus sloanii* (CCNHM 168) in lateral (**A**) and dorsal view (**B**); Cervical vertebrae in lateral view (**C**) and dorsal view (**D**).

Table 10. Vertebral measurements (in mm) of *Xenorophus sloanii*, CCNHM 104. ? denotes missing measurements; e denotes an estimated measurement; + denotes a minimum measurement.

	Dorsoventral Depth of Centrum	Transverse Width Centrum	Anteroposterior Length of Centrum	Max d/v Depth	Max Width Across Transverse Processes	Neural Canal Transverse Width	Neural Canal Height
C1	64	93	57.3	99.4	?	38.7	43.4
C2	?	?	?	?	?	?	?
C3	?	?	?	?	?	?	?
C4	51.1	56.7	27.2	?	?	42	?
C5	49	57.6	28.4	?	?	39.7	?
C6	52	52.8	28.8	?	100e	45e	?
C7	?	?	?	?	?	?	?
TA	50e	63	51.7	145+	95e	31.6	27.5
TB	53.9	76.9	58.9	?	?	37.9	?
LA	56.3	67.8	66.2	?	?	?	?
LB	67.9	73e	75.9	150+	?	24.4	36.7

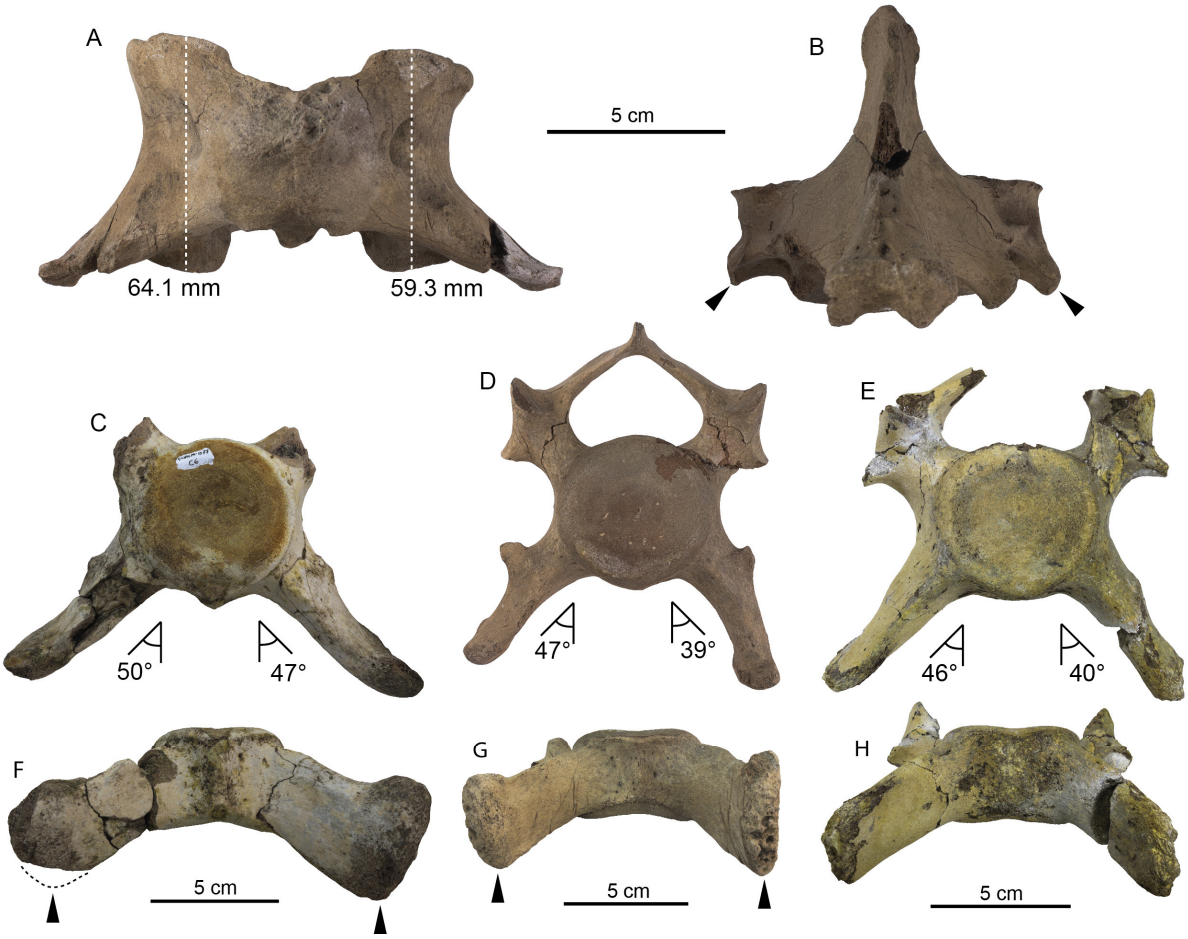


Figure 66. Asymmetry of the cervical vertebrae in *Xenorophus sloanii*. (**A**) Wedge-shape of the atlas in CCNHM 168. (**B**) Asymmetry of the transverse processes of the axis in CCNHM 168. (**C**–**H**) Asymmetry of the parapophyses of CCNHM 1077 (**C**,**F**), CCNHM 168 (**D**,**G**), and ChM PV 5022 (**E**,**H**); (**A**,**B**) In dorsal view, (**C**–**E**) in anterior view, (**F**–**H**) in ventral view.

Table 11. Vertebral measurements (in mm) of *Xenorophus sloanii*, CCNHM 168. ? denotes missing measurements; e denotes an estimated measurement; + denotes a minimum measurement.

	Dorsoventral Depth of Centrum	Transverse Width Centrum	Anteroposterior Length of Centrum	Max d/v Depth	Max Width Across Transverse Processes	Neural Canal Transverse Width	Neural Canal Depth
C1	68	99	64.1 L, 59.3 R	101	156e	40.1	39.6
C2	45.3	93.7	48.9	124.8	100	37.9	25
C3	52	60.3	32.5	107.9	114e	41.3	25.5
C4	53.4	55.2	29.7	114.3	121.2	46.2	27.3
C5	55.7	55.3	33.1	128	123.8	48.8	29.1
C6	57.1	58.2	37.1	145e	125.1	51.5	31.1
C7	57.8	60.7	34.5	110+	141.5	51.4	33e
T1	53.7	70	44.6	130+	138.4	49.5	33.1
TA	49.3	69.8	?	?	?	34e	?
TB	51.4	69	51e	?	?	38.1	?
LA	60.6	69.1	77e	225+	214	29.4	33.8
LB	64.9	70.4	78.6	250+	231.3	28.3	36.1
LC	67.3	72.3	80.5	?	?	26.4	

Table 12. Vertebral measurements (in mm) of *Xenorophus sloanii*, CCNHM 1077. ? denotes missing measurements, e denotes estimated measurements; + denotes a minimum measurement.

	Dorsoventral Depth of Centrum	Transverse Width Centrum	Anteroposterior Length of Centrum	Max d/v Depth	Max Width Across Transverse Processes	Neural Canal Transverse Width	Neural Canal Depth
C1							
C2	55	61	39	?	?	?	?
C3	55	58.5	30.5	115.1	115e	43	33
C4	56.5	56.5	31	?	136	51	?
C5	58.5	57	33	115+	135.5	52	34
C6	60	59	40.5	?	162	?	?
C7	59	61	38	?	126	?	?
T1	57.5	66	47	183	145	48	40
T2	56	70	48	?	?	?	?
T3	54	73.1	53.5	?	?	?	?
T4	50.5	73.9	53.4	?	?	?	?
T5	58	69.4	57.4	?	?	?	?
T6	58.5	70	60	?	?	?	?
T7	54.5	69	59.5	?	?	?	?
t8	52.5	76	65.5	?	?	?	?
T9	57	76.5	67	?	54.5	?	36
T10?	62	75	76	260	160	35.5	37
L1	67.5	70	82	?	?	30	43
L2	69	73.5	84	?	?	29	?
L3	73.5	76	87.5	?	?	?	?
L4	76.5	78	88.5	?	?	19.5	41.5
L9	81.5	86	92.3	?	?	17	48
L10	87.5	84	91.5	?	?	10e	45
Ca1	86.8	84.1	86.3	?	?	?	?
Ca-a	85.7	90.3	84.8	?	?	?	?
Ca-b	79.5	82.6	70	?	?	?	?
Ca-c	67.5	72.3	46.3	?	?	?	?
Ca-d	53.4	64	35.2	?	?	?	?

C3 and C4 are similar and possess a nearly circular centrum bearing a ventrally triangular apex formed by a well-developed hypapophysis, larger than that in the axis (Figure 64). The neural foramen is triangular with a convex ventral margin, giving it a lunate profile. The pedicle is stout and leads to a straight, dorsomedially sloping lamina topped by a low (15 mm high) neural spine. Large lateral vertebral canals are present and encircled by a narrow, splint-like diapophysis and a two-pronged parapophysis with a tongue-shaped dorsal part and shorter ventral part. The diapophysis and parapophysis are fused laterally in C3, completely encircling the canal; they are, however, separated by a 2 mm gap in C4. The entire parapophysis is posteroventrally sloping. In CCNHM 1077, the C3 is similar but bears a smaller ventral parapophysis that projects more anteriorly.

Table 13. Vertebral measurements (in mm) of *Xenorophus sloanii*, ChM PV 5022. ? denotes missing measurements; e denotes an estimated measurement; + denotes a minimum measurement.

	Dorsoventral Depth of Centrum	Transverse Width Centrum	Anteroposterior Length of Centrum	Max d/v Depth	Max Width across Transverse Processes	Neural Canal Transverse Width	Neural Canal Depth
C1	?	97.9	61.1	?	142e	45	?
C2	?	96	51.3	?	114e	45.2	?
C3	56.9	48.6	28.4	?	103e	44.5	?
C4	56.6	52.3	28.6	125	97.1	48.8	27.8
C5	56.4	55	31.5	123.3	93+	52.3	29.1
C6	56.6	51.9	35.9	129.7	?	52.3	?
C7	63.8	52.3	41	134.5	140+	51.3	35.1
T1	56.4	44.9	40e	122.8	?	31.9	?
T2	61.5	45	48e	53 × 2	?	32.2	30.5
T3	55.4	41e	46.6	?	?	25	?
T4?	28 × 2	41.5	47e	43.9 × 2	?	26.6	23.9
T8?	69.5	43.8	46.5	44.7 × 2	225	30.8	27.7
T9?	75.8	43.7	55.2	20.1 × 2	242.3	34.4	29.4e
T10?	37.5 × 2	42.4	54e	44.7 × 2	?	18.7	?
L1	70	47.2e	63.4	54.3 × 2	239.8	30.8	29e
L2	66.3	55.3	74.4	?	?	23.7	?
L3	67.4	58e	77.4	?	?	20.6	?
L4	67.6	63.4	74.7	117 × 2+	?	22.3	30e
L5	71.4	66.2	82.4	?	248	20	32e
L6	72.2	70.4	84.5	?	232+	16.2	36
L7	35.4 × 2	75.5E	87.1	?	222	17e	36e
L8	77.3	72.6	89.2	?	215+	16e	30e
L9	78	68.6	83.5	?	?	14e	<30
L10	45 × 2	85.0	86.4	114 × 2	?	12.7	33.8
CdA	82.8	81.5	85.5	?	?	15e	14e
CdB	87.8	79.7	81.9	108 × 2+	142+	17e	16e
CdC	88.6	79.4	79.5	65 × 2+	119.1	?	?

C5 is similar in morphology to C4 but has shorter diapophyses (Figure 65). C6 is distinguished by possessing elongate and robust parapophyses, that are rectangular in lateral view and distally become transversely swollen, and bears vascular pitting at its ventral apex. The left parapophysis is massive and anteroposteriorly longer than the right. The diapophysis is broken, but the lateral vertebral canal is not closed, as the dorsal parapophysis is developed as a low tubercle and does not appear to be broken. In CCNHM 1077, C5 also lacks a complete lateral bridge around the lateral vertebral canal but possesses longer dorsal and ventral parapophyses than CCNHM 168; these parapophyses also have enlarged tubercles at their apices. C6 lacks a hypapophysis. The centrum is anteroposteriorly thicker than C5. In CCNHM 1077, the C6 has a longer parapophysis that is anteroposteriorly broader distally and splayed more widely apart (60° in CCNHM 168, 90° in CCNHM 1077). In most specimens, the parapophyses are asymmetrical (Figure 66C–H), with the left parapophysis plunging more closely to vertical (e.g., 39° on left and 47° on right in CCNHM 168, and 40° on left and 49° on right in ChM PV 5022) and the distal end of the left parapophysis (51.9 mm) being 31.6% anteroposteriorly longer than the right (39.2 mm) in CCNHM 168 and approximately 30–24% in CCNHM 1077 (52.1 mm vs. ~40–

42 mm, accounting for breakage). In CCNHM 1077, the parapophyses are of asymmetrical size but nearly symmetrical in orientation (47° on left vs. 50° on right).

C7 has a centrum approximately as long as C6 but lacks a parapophysis; it is reduced to a low tubercle on the left side, and is completely absent on the right. The diapophysis (=transverse process) is larger and elevated to the level of the top of the centrum. The transverse process is subhorizontal, slightly ventrally inclined, and dorsoventrally thin. The pedicle is slightly longer than in C6 and the lamina is slightly shorter. The pre- and postzygapophyses are positioned further laterally. The centrum is more oval and dorsoventrally shallow than C6. The neural foramen of C7 is shallowly triangular. The arch bears dorsoventrally thin laminae and a 40 mm tall spine that is rectangular in lateral view. The apex of the spine is rotated 10° clockwise so that the left side faces slightly anterolaterally and the right faces slightly posterolaterally. The apex widens transversely relative to the spine and bears a rugose apical facet, presumably for the nuchal ligament. When placed in articulation, the cervical vertebrae of CCNHM 168 (Figure 65) indicate that the neutral posture of the neck was dorsally flexed.

Thoracic Vertebrae: T1 is preserved in CCNHM 168 and 1077, and differs from C7 in having knob-like distal ends of the transverse processes, and flat costal facets positioned low and anterolaterally on the centrum (Figure 67; Tables 10–13). T1 in CCNHM 1077 has a spine taller than C5–6, a triangular neural foramen, an oval-shaped centrum with a notochordal pit, shallow prezygapophyseal fossae, a knob-like transverse process with a flat lateral facet, and bears pits on the lateral side of the centrum. T2 and T3 are similar to T1 but possess minute capitular facets dorsolateral on the edge of the centrum; T4 also has more dorsally positioned transverse processes. An isolated anterior thoracic of uncertain position, but likely corresponding to T2–T4, preserves the only complete neural spine for the thoracic series. The arch delineates an oval neural foramen. The spine is tall (11 cm), is subrectangular in lateral view but narrows (in anteroposterior length) dorsally. The spine is slightly curved anteriorly; there is a tear-drop-shaped (posteriorly narrowing) rugose facet at the apex, presumably an attachment for the nuchal ligament.

T4–T6 of CCNHM 1077 are similar to the T2–3 and increase sequentially in centrum length posteriorly (Figure 67; Table 12). The anterior face becomes triangular and projects ventrally further than the posterior face. The anterior and posterior faces are at a 5° angle rather than parallel, giving the vertebra a slight wedge shape and widening ventrally. This indicates that the vertebral column was dorsally concave.

T7–T9 of CCNHM 1077 are similar and bear successively large capitular facets along the lateral edges of the centrum (Figure 67; Table 12). In T7, the posterior facet is larger than the anterior face, and, in T8, the posterior facet is only slightly larger. In T9, the anterior facet is large and there is no posterior facet; instead, there is a knob-like costal articular facet at the level of the dorsal margin of the centrum. T9 also bears a nearly circular neural foramen.

T10 of CCNHM 1077 and ChM PV 5022 resembles lumbar vertebrae but possesses short, ventrolaterally oriented transverse processes with flat capitular facets for the last rib (Figure 67; Table 12). Given that ChM PV 5022 and CCNHM 1077 only possess a single vertebra like this, perhaps *Xenorophus* only possessed a single "hanging" rib versus three in *Ankylorhiza*. Accordingly, the early toothed mysticete *Coronodon* appears to only have a single "hanging" rib [46].

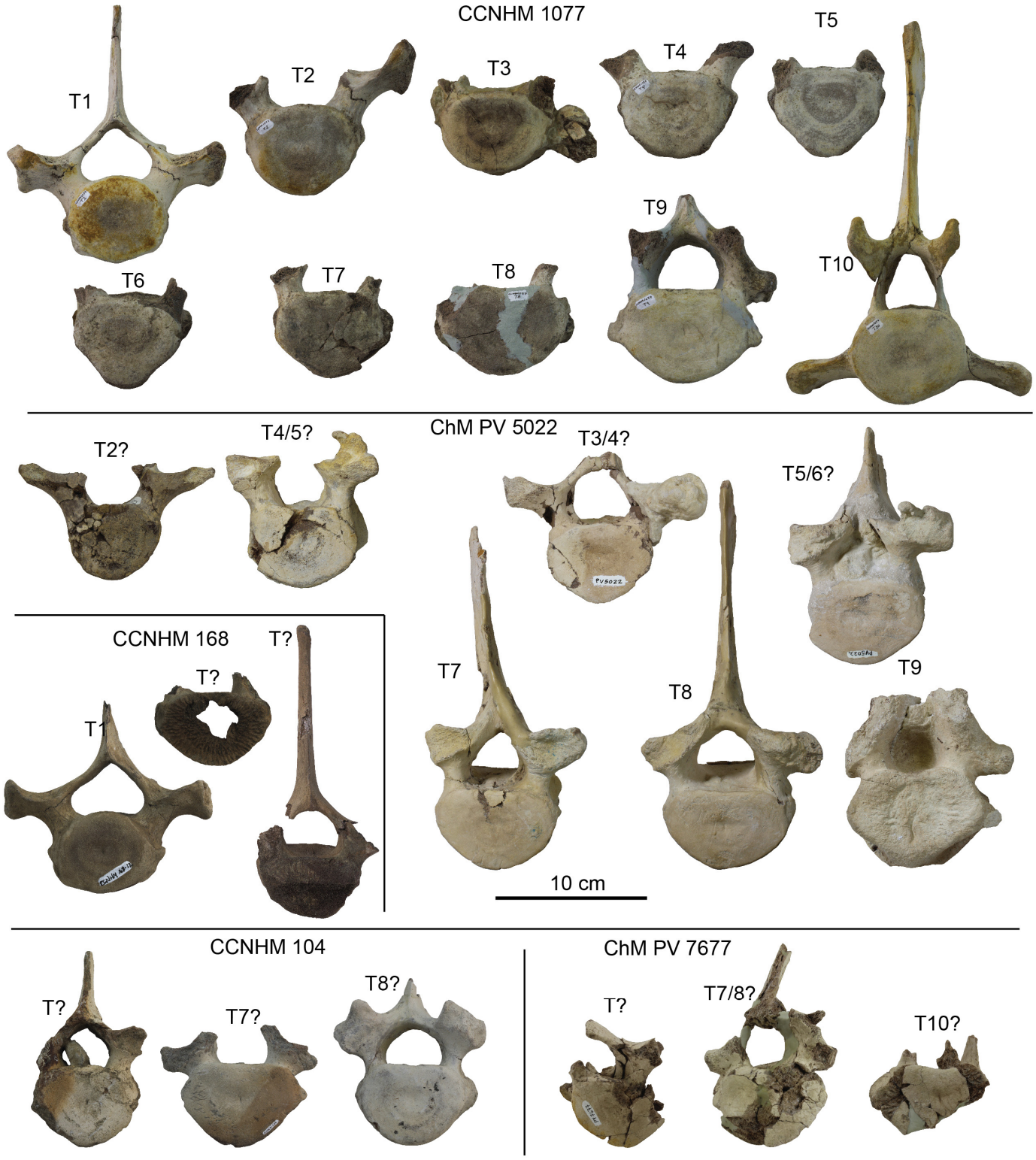


Figure 67. Thoracic vertebrae of referred specimens of *Xenorophus sloanii* in anterior view. ? denotes uncertain vertebral position.

Lumbar Vertebrae: In CCNHM 1077, six lumbars are preserved, corresponding to L1–4, L9, and L10 (Figure 68; Table 12); another nearly complete series is preserved in ChM PV 5022 (Table 13). The lumbars continuously increase in size posteriorly, continuing this gradual trend from the posterior thoracics. Lumbars are all quite similar in proportion and share a round centrum, small subtriangular neural foramen (decreasing in size posteriorly),

ventrolaterally projecting transverse processes, a ventral median ridge, and a high neural spine with rectangular outline in lateral view. A nearly complete series of lumbars (ten) are preserved and follow a similar trend. The anterior lumbars, chiefly L1–3, possess relatively smaller subcircular epiphyses with a truncated dorsal margin; L4 has a larger centrum with a slight dorsal truncation, and L5–L10 have large circular centra. L1–4 have prezygapophyses that are widely projecting, low, and set astride a triangular but equidimensional neural canal; L5–L10 have smaller, more medially positioned, and dorsally higher prezygapophyses adjacent to increasingly deeper and transversely narrower neural canals (Figure 68). The neural spines of L5 and L8 are curved slightly to the left side, as in all three lumbar vertebrae of CCNHM 168; the L1 of ChM PV 5022 and the T10 of CCNHM 1077 are similarly slightly, but less extremely, deflected to the left. In all lumbars with complete spines in CCNHM 158, 1077, and ChM PV 5022, the neural spines deviate to the left by 5.5–7.5°. The L10 of ChM PV 5022 bears low facets for the first chevron. Three lumbar vertebrae of uncertain position are preserved in CCNHM 104, including an anterior, mid, and posterior (L8/9) vertebra; all are consistent in morphology with ChM PV 5022 and CCNHM 1077 but are smaller in absolute size, similar to CCNHM 168 (Figure 68). All lumbar vertebrae in CCNHM 1077 have longitudinal ventral keels; the keel is broadly rounded and restricted to the center of the centrum in L1–L3; a sharp and anteroposteriorly longer keel is present in L4 and L9; a somewhat more rounded keel is present in L10. In the anteriormost lumbar vertebra of CCNHM 168 (lumbar A), there is no ventral keel.

Caudal Vertebrae: Six caudal vertebrae are preserved in CCNHM 1077, and three are preserved in ChM PV 5022; this description focuses on CCNHM 1077 (Figure 69; Tables 12 and 13). Caudal 1 is similar to L10 but bears hemal facets for the chevron posteroventrally, and transverse processes with a sinuous outline in anterior view. Caudal A is an anterior caudal with well-developed anterior and posterior hemal processes, and a narrower neural foramen than Ca1. Caudal B is a mid-caudal and lacks a transverse process, instead possessing anterior and posterior tubercles in the same location but separated by a prominent vertical sinusoidal sulcus for the vertebral canal. The neural arch is absent and consists of two anterior and two posterior tubercles, separated by a median longitudinal fossa (Figure 69). The hemal process consists of paired elongate anteroposterior ridges, which, on the left side, is separated by the lateral vertebral sulcus and, on the right, is perforated instead by an equidimensional foramen. Ca C and D are posterior caudals and increasingly anteroposteriorly flattened; both possess vertically perforating lateral vertebral canals and an anteroposterior sulcus at the homologous position to the transverse process (Figure 69). Ca E has bony tubercles extending beyond the centrum articulation (dorsolateral/ventrolateral) and is also rectangular, indicating this is an anterior fluke vertebra. Three caudals, two anterior and one mid caudal, are preserved in ChM PV 5022; these are similar to those of CCNHM 1077. The mid caudal preserves widely flaring prezygapophyses and a dorsoventrally low oval-shaped neural canal. A single posterior caudal is preserved in CCNHM 104, and has a round outline, indicating a position within the peduncle region rather than within the fluke.

Ribs: Several ribs are preserved in CCNHM 168, including left and right R1, and seven nearly complete ribs from other uncertain positions (Figure 70). R1 is the shortest and the most strongly bowed. Proximally, it bears a large triangular end with a deep notch between the capitulum and the tubercle, and a dorsally prominent tubercle. The entire rib is anteroposteriorly compressed. The distal end is transversely expanded.

Ra likely represents R2 or R3 and was probably longer than R1 but differs from it in having a lower tubercle that is not separated from the capitulum by a notch (Figure 70). Rb is missing both ends but has a similarly sized and proportioned shaft to Ra. Rc is several positions posterior to these and has a large capitulum and small tubercle; the shaft has an oval cross-section. Re and Rf are similar but possess smaller tubercles than Rc; Rc, Re, and Rf all have a low secondary tubercle positioned about 5–6 cm distal to the primary tubercle (Figure 70). Rf is about twice as long as R1 and bears a distal facet for the costal cartilage. Rd is similar in proportion to Rc-Rf, but the position is uncertain as it lacks both

ends. Rg is long and straighter and is missing the proximal end, but, unlike Rf, the distal end tapers and is transversely flat, indicating it is a posterior rib. Proximal fragments of at least eleven ribs are preserved in CCNHM 1077, including anterior ribs with clear capitula and tubercles and posterior ribs with large capitula and small or absent tubercles. Six mid-thoracic to posterior-thoracic ribs are preserved in ChM PV 5022; all have knob-like capitula. The mid-thoracic ribs have large tubercles positioned quite close to the capitulum and are more laterally bowed than the posterior ribs, which have low tubercles set far distally from the capitulum. One rib, perhaps the last rib, is nearly straight and entirely lacks a tubercle (Figure 70).

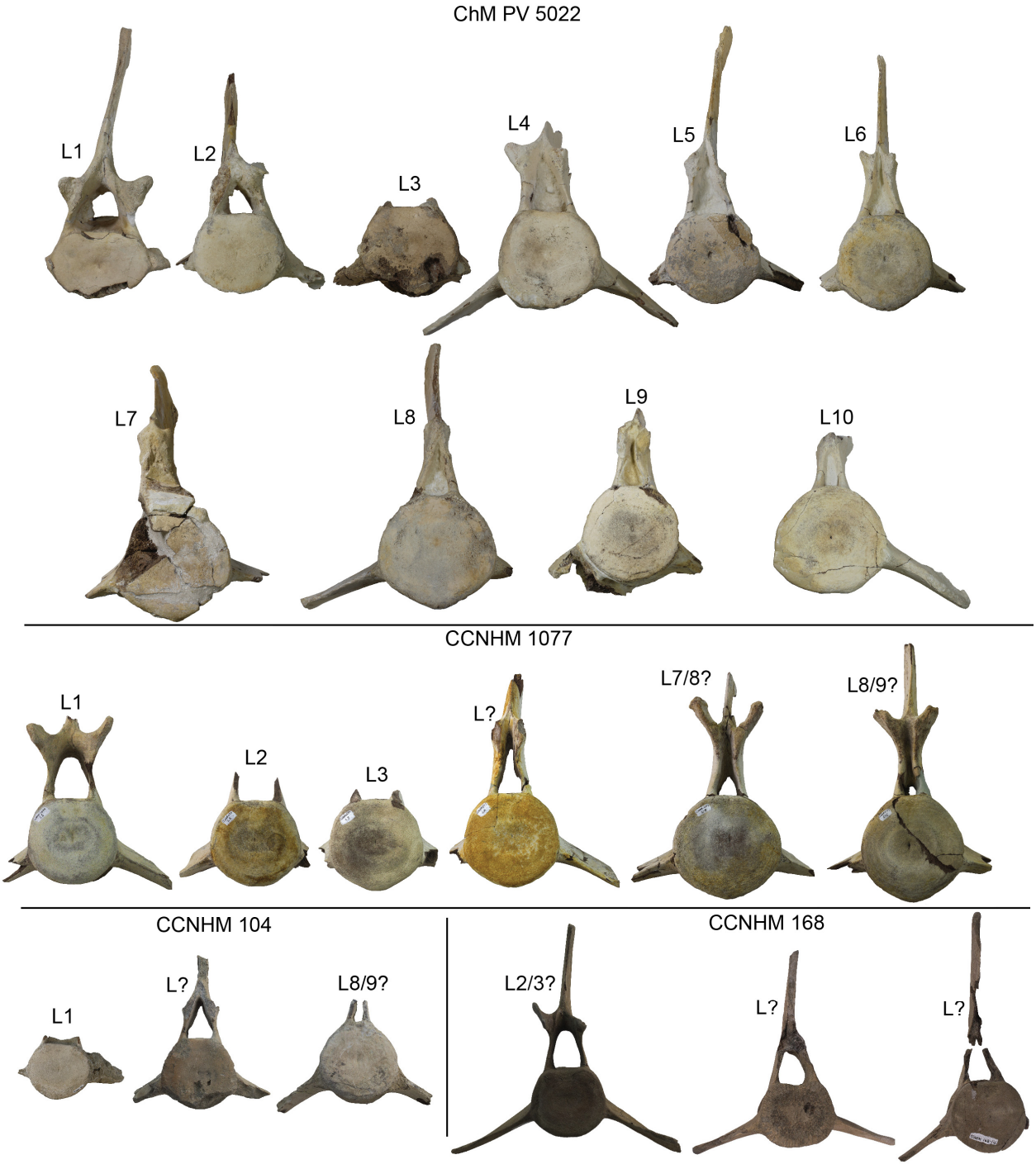


Figure 68. Lumbar vertebrae of referred specimens of *Xenorophus sloanii* in anterior view. ? denotes uncertain vertebral position.

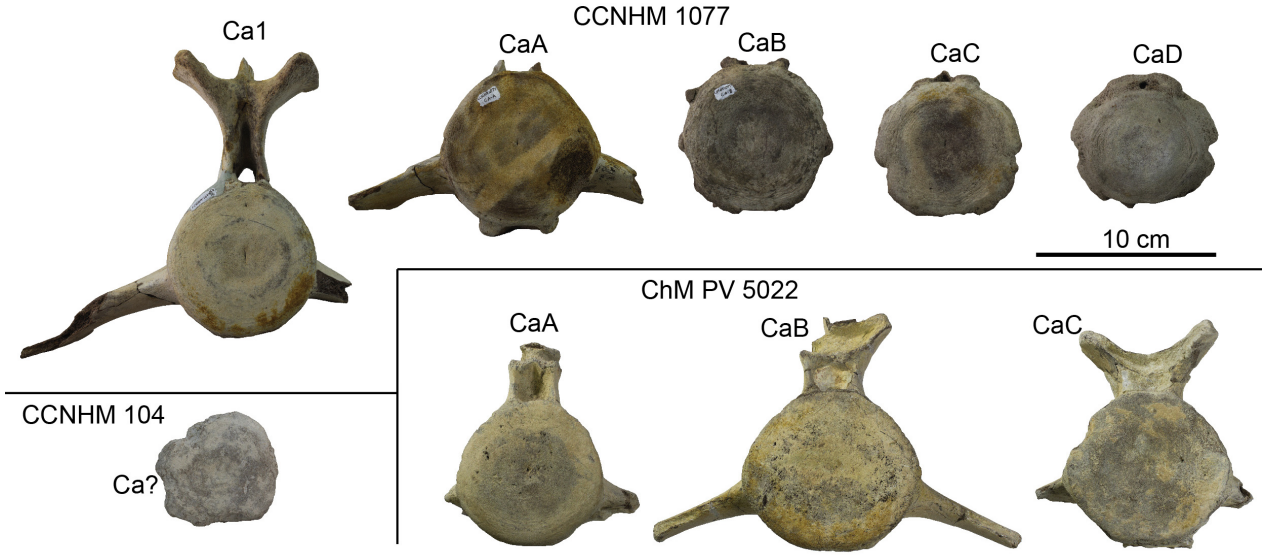


Figure 69. Caudal vertebrae of referred specimens of *Xenorophus sloanii* in anterior view. ? denotes uncertain vertebral position.



Figure 70. Ribs of referred specimen of *Xenorophus sloanii*, CCNHM 168, in anterior view.

5.2. Body Size Estimation

Estimation of body length using the bizygomatic width equation for stem odontocetes by Pyenson and Sponberg [98] resulted in an estimation of 2.68 m for subadult specimens like ChM PV 7677 and 2.92 m for the largest known specimen, CCNHM 1077. The partial

least squares equation of Pyenson and Sponberg [98] for a large specimen, CCNHM 168, resulted in a surprisingly small body length of 2.51 m. However, a length of 3 m is more likely when considering the length of the vertebral column (Tables 12 and 13). Prior studies have commented on the body length equations of Pyenson and Sponberg [98] underestimating the body length of early Neoceti [37,46].

5.3. Results of Phylogenetic Analysis

The phylogenetic analysis yielded a single most parsimonious tree, 289,736 steps in length (Figure 71). This tree resembles results obtained from earlier iterations of this dataset (e.g., [99]), including a monophyletic Neoceti, Mysticeti, and Odontoceti. Of particular relevance to the present study are basal odontocete relationships, including the relationships with Xenorophidae (sensu [5]). We found *Archaeodelphis* to be the sister-group of Xenorophidae, like nearly all previous studies ([9,10,25,37,100,101]; but see some analyses of [5]), and then *Ashleycetus* to be the sister-group to *Archaeodelphis* + Xenorophidae, unlike the analyses of Sanders and Geisler [5] and Boessenecker et al. [37]. A clade including *Ashleycetus*, *Archaeodelphis*, and Xenorophidae was also recovered by Vélez-Juarbe [25], but support for this grouping is very low (bootstrap: 7%) and is diagnosed by just two synapomorphies: elevated nasals (character 161:state 1) and rectus capitus anticus muscle fossa (238:1). The grouping of *Archaeodelphis* with Xenorophidae has much better support with a bootstrap of 60% and is supported by eight synapomorphies: narrow antorbital width of skull (11:2), frontal/maxilla suture is horizontal in lateral view (72:0), lacrimal abuts supraorbital process of frontal (76:1), premaxilla terminates over anterior half of orbit (107:2), premaxilla adjacent to nares form a steep slope in lateral view (124:2), posterior end of premaxilla faces anteriorly or anterodorsally (146:1), posterior end of nasal over posterior half of orbit (160:2), and posterior margin of paroccipital process at same level as edge of condyle (243:1). The *Ashleycetus*, *Archaeodelphis*, xenorophid clade is the second group to branch off of the odontocete stem, with *Mirocetus* being most basal. Previous studies have varied in the placement of *Mirocetus*, mainly because the skull is not that well preserved, but they typically place it in a more apical position, either as closer to Xenorophidae ([25]; some analyses of [5]) or slightly higher up the odontocete stem closer to *Olympicetus* and *Agorophius* ([84]; one analysis of [5]).

As in previous studies, Xenorophidae (sensu [5]) is well supported (Figure 71), with a bootstrap of 92% and nine supporting synapomorphies, including ventral exposure of lacrimal + jugal is intermediate in size (80:1), posterior border of supraorbital process extends posteromedially from lateral end (85:0), side of postorbital process faces laterally (89:1), premaxillae separated dorsally by a narrow gap (94:1), premaxilla expanded over supraorbital process of the frontal (106:1), premaxilla terminates over posterior half of orbit (107:3), anterior edges of nasal and orbit aligned (114:4), pachyostosis of premaxilla (125:1), and basioccipital crests from 45–68 degree angle (240:2). The fifth synapomorphy, which relates to the expansion of the premaxilla, is the feature that Sanders and Geisler (2015) used in their apomorphy-based definition of Xenorophidae. Consistent with previous studies (e.g., [3,4]), there is good support for the unnamed taxon ChM PV4746 being the most basal xenorophid, with the clade excluding it supported by a bootstrap value of 92% and six unambiguous synapomorphies, including lacrimal expanded dorsally over the supraorbital process of the frontal (76:2), bilateral antorbital basins present (92:1), posterior end of maxilla aligned with gap between frontal and zygomatic process (111:3), supraorbital process roofs over temporal fossa (173:0), ventral window in supraorbital process that exposes overlying maxilla and premaxilla (174: 1), and posterior end of premaxilla abruptly widens (390:3). Sanders and Geisler [5] listed three of these synapomorphies (i.e., 76, 92, 174) in their diagnosis for Xenorophidae, but it is important to realize that some of the features do not occur in ChM PV4746, and are actually diagnostic of this more exclusive clade.



Figure 71. Single most parsimonious tree of odontocete relationships with labels for *Xenorophus simplicidens*, *Xenorophus sloanii*, "*Albertocetus*", and *Echovenator*, each represented by multiple OTUs. Asterisks denote holotype OTUs within Xenorophidae.

Boessenecker et al. [2] placed the then newly described *Inermorostrum xenops* as the sister-group to *Cotylocara* + *Echovenator*, but here we find it to be the second most basal xenorophid (Figure 71). Boessenecker et al. [37] conducted two analyses, one with im-

plied weights and one with equal weights; the former supported a somewhat similar basal position for *Inermorostrum*, whereas the latter placed this taxon next to *Cotylocara* and *Echovenator*. The clade that excludes *Inermorostrum* has marginal bootstrap support (53%) and is diagnosed by eight synapomorphies. Three of these characters exhibit little homoplasy, including width across premaxillae at mid-rostrum is narrow (7:0), premaxilla at mid-length faces laterally (15:0), and embrasure pits on palate (24:0), whereas the remaining six putative synapomorphies display substantial homoplasy within Xenorophidae or adjacent clades and/or grades. Apical to the divergence of *Inermorostrum*, Xenorophidae splits into the genus *Xenorophus*, represented by two species, and a larger clade that includes *Albertocetus*, *Cotylocara*, *Echovenator*, and one or more taxa. The genus *Xenorophus* has good bootstrap support (72%) and is diagnosed by six synapomorphies: U-shaped anterior margin of nares (115:1), frontal between maxillae subequal to nares (165:1), anterior margin of supraoccipital level with zygomatic process (181:1), occiput lacks sagittal crest (200:0), shallow posterior pit in periotic fossa (233:1), and medium-sized skull (BZW 246–377 mm) (374:2). The second synapomorphy converges with the condition in PV4746; the third with two specimens of *Albertocetus*; the fourth with two specimens of *Albertocetus*, *Echovenator*, and *Cotylocara*; and the fourth and fifth with *Cotylocara*.

Within *Xenorophus*, there is strong support for our new species *X. simplicidens*, represented by ChM PV4823 and CCNHM 8720 (Figure 71). At first glance, this seems to be contradicted by a low bootstrap value of 49%, but this value rises to 82% if ChM PV4266 and PV4822 are excluded from the calculation of support. These two specimens, like ChM PV4823 and CCNHM 8720, were collected from the Chandler Bridge Formation, and are currently referred to this species. However, both consist of a neurocranium that lacks the rostrum, and thus does not preserve some key features that diagnose this new species. Specifically, *X. simplicidens* is supported by five synapomorphies, including ectocingulum absent (43:1), entocingulum absent (44:0), 36–18% toothrow is multicuspate (47:2), three distal denticles on molars (48:3), and median furrow of bulla (313:1). The remaining specimens in *Xenorophus* we refer to the paraphyletic species *X. sloanii*. There is substantial apparent phylogenetic structure within *X. sloanii*, but it should be noted that phylogenetic analyses will often find hierarchal relationships, even if none exists, and that most of these have very low bootstrap support ($\leq$20%). Slightly higher bootstrap support occurs for a grouping of ChM PV5022 with the holotype of *X. sloanii* and another grouping of CCNHM 107 and 104. With respect to PV5022 and the holotype, this grouping is supported by three putative synapomorphies: postorbital process is short (87:0), maximum width of nasals is subequal to nares (157:2), and frontal forming median wedge between nasals (159:1). When considering size and sutural closure, we are reasonably confident that the last feature is a consequence, in part, of ontogeny within *Xenorophus*, and this may also be the case with respect to the relative widths of the nasals and nares (see *6.1. Ontogeny and Taxonomic Unity of Ashley Formation* Xenorophus). The short postorbital process does not exhibit much homoplasy, and cannot be easily dismissed. If additional specimens of *Xenorophus* show this feature, and it correlates with the aforementioned features of the nasals and nares, then the referral of several specimens to *X. sloanii* should be revisited. The other potential clade with *Xenorophus* (CCNHM 1077 and 104) is supported by two features, including premaxilla slightly overhanging the maxilla (144:1) and a wide lateral exposure of the squamosal (189:2). Both features show substantial homoplasy within Xenorophidae, and at present, we interpret this "clade" as also representing variation within this species.

Our phylogenetic analysis represents the most comprehensive review of xenorophid relationships to date, and there are several other aspects worth commenting on. There is strong support (bootstrap = 71%) for a sister-group relationship between *Cotylocara macei* and the undescribed taxon represented by ChM PV2758 (Figure 71; [3,4]), although Boessenecker et al. (2020) found *Echovenator* to be closer to *Cotylocara* or for PV2758 to be more closely related to *Xenorophus*, depending on whether implied weighting was employed. In the present study, the clade of *Cotylocara* + PV2758 is supported by nine synapomorphies: anterior edge of nasal is thick (152:1), nasals elevated far above rostrum

(161:2), maxillae lateral to vertex face dorsally (162:2), frontals between maxillae narrower than nasals (165:2), exposure of squamosal lateral to exoccipital is wide (189:2), foramen spinosum absent (232:0), posterior pit in periotic fossa is shallow (233:1), medium-sized skull, BZW 246–377 mm (374:2), and posterior end of premaxilla nearly constant in width (390:1).

Roston et al. [92] referred six specimens to *Echovenator sandersi*, two of which were included here (i.e., CCNHM 217, 219) and all form a single clade, although with low bootstrap support (18%; Figure 71). The clade representing *E. sandersi* is supported by six features, including middle thirds of premaxillae have sporadic contact (14:2), middle of premaxilla faces dorsolaterally (15:1), five double rooted teeth (30:3), frontal higher than nasals (166:2), basioccipital crests form a 15–40 degree angle (241:1), and paranaris fossa (389:1). The last feature was noted in the original diagnosis of this taxon [3], but the other features constitute new diagnostic features. More detailed study is needed to confirm that all of these specimens indeed represent *E. sandersi*, instead of another species within this genus. We also find good support for the clade of *Echovenator*, ChM PV2758, and *Cotylocara* (i.e., bootstrap = 74%; Figure 71), in agreement with most previous studies ([3,4], implied weighting tree of [37]). This clade is diagnosed by eight synapomorphies: orbit well above rostrum edge (71:3), premaxilla terminates at level of zygomatic process (107:5), maxilla terminates at level of zygomatic process (111:4), nasals have median trough (156:2), postnarial fossa is shallow (167:1), occiput is semicircular (196:1), fenestra rotunda lacks fissure (269:0), and lateral side of IAM high wedge of bone (382:1). Characters 106 and 110 represent aspects of cranial telescoping, and contribute to the parallel development of telescoping observed and previously reported within Xenorophidae [3,4].

We included the holotype of *Albertocetus meffordorum* [9] and two specimens referred to this species [1]; however, these specimens do not form a clade in our most parsimonious trees (Figure 71). Instead, these specimens, and others that resemble *Albertocetus*, form a grade leading to the clade that includes *Cotylocara*, *Echovenator*, and ChM PV2758 (Figure 71). Bootstrap values for the nodes in this grade are typically low (<10%) and this is ascribed to character conflict, instead of missing data, because these values remain low even if the more poorly represented specimens are removed. Although preliminary, we are confident that there are at least two species represented among the specimens that resemble *Albertocetus*. The type and several specimens near the base of this grade (ChM PV4834, 5711, 8819) have all dorsal infraorbital foramina anterior to the orbit, whereas ChM PV9860 and CCNHM 6057 have a deep groove that course from the dorsal infraorbital foramina to the center of the supraorbital process. The same morphology is seen in *Cotylocara* and *Echovenator*, and we are confident that this morphology indicates that there are at least two species of *Albertocetus*; the holotype and one more closely related to *Echovenator* and *Cotylocara*. There could be more, and this is what our most parsimonious tree suggests, but additional changes should await a more detailed review of this genus, including an assessment of individual variation and the role of ontogeny.

5.4. Bone Modifications

Bone modifications attributable to feeding damage from sharks and/or fish and colonization by the bone-eating worm *Osedax* are present on several specimens (Figure 72). Tooth marks consisting of shallow grooves with a V-shaped cross-section are present on the postcrania of both CCNHM 168 and 1077, corresponding to the trace fossil *Linichus bromleyi* [102]; many of these are 1–1.5 mm in width and 1–3 cm long and straight or slightly curved (Figure 72H,I). One isolated neural spine from a lumbar or anterior caudal vertebra possesses a relatively deep and wide tooth mark with a V-shaped cross-section, slightly curved, 27 mm in length, and 2.5 mm in maximum width, and bearing a serrated margin (Figure 72J,K); this last feature identifies the trace as *Linichnus serratus* [103]. A similar and even more deeply cut trace, identifiable as *Linichnus serratus*, is present on a lumbar vertebra of CCNHM 168 (Figure 72G). The serrated margin in these traces is best interpreted as pressure flaking of the relatively soft bone as the tooth tip was drawn through it.

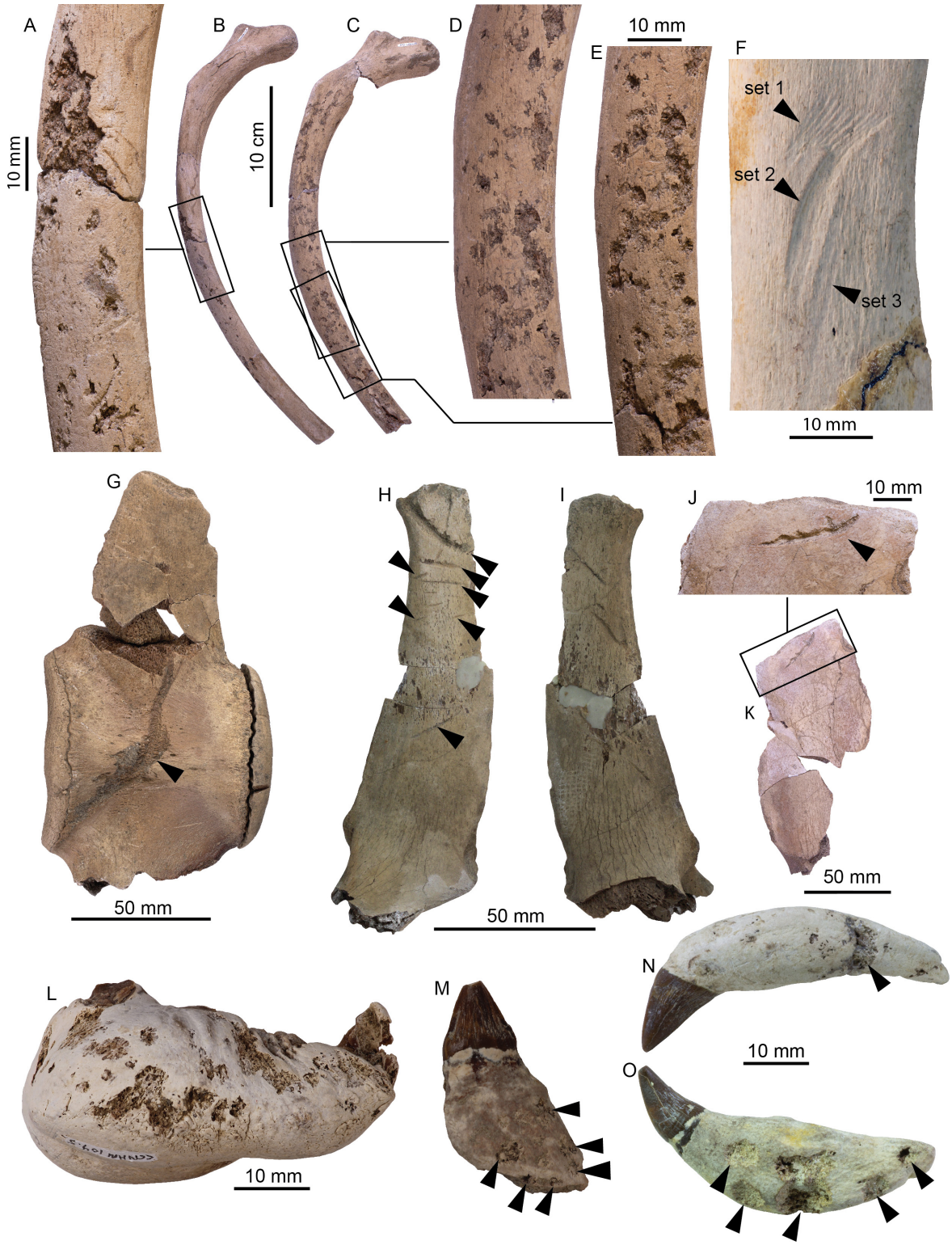


Figure 72. Bone modifications in *Xenorophus sloanii*. (**A**–**E**) *Osedax* biorerosion on ribs of CCNHM 168. (**F**) Traces (*Knethichnus parallelum*) attributed to serrated teeth of *Carcharocles angustidens* on rib of CCNHM 1077. (**G**) Deep trace (*Linichnus serratus*) attributed to *Carcharocles angustidens* on lumbar vertebra of CCNHM 168. (**H**,**I**) Traces (*Linichnus bromleyi*) attributed to shark and/or fish feeding on neural spine of CCNHM 168. (**J**,**K**) Deep trace (*Linichnus serratus*) attributed to *Carcharocles angustidens* on neural spine of CCNHM 168. (**L**) *Osedax* borings on tympanic bulla of CCNHM 104. (**M**) *Osedax* borings on tooth of CCNHM 1077. (**N**,**O**) *Osedax* borings on teeth of ChM PV 5022.

Another trace consists of three sets of semi-parallel grooves adjacent to one another on one of the ribs of CCNHM 1077 (Figure 72F). The first set consists of 0.6 mm wide semiparallel grooves 9 mm in length. The second set consists of less clearly defined and slightly curved grooves measuring 19 mm in length, overlapping or continuous with the first set. The third set consists of two shallowly incised grooves parallel with the second set. The semiparallel, slightly wavy grooves identify these traces as *Knethichnus parallelum* [103]. These traces are best interpreted as the serrated edge of a large tooth being drawn parallel to the bone surface rather than the tip incising into the bone surface as in *Linichnus*. The grooves in *Knethichnus parallelum* on CCNHM 1077, spacing of the grooves, and large size of certain *Linichnus* traces (specifically, the two *Linichnus serratus* traces on CCNHM 168) unequivocally identify the trace maker as *Carcharocles angustidens*, which is the only large shark with serrated teeth in the Oligocene of the western North Atlantic [59,76].

Scattered bone modifications consisting of 3–10 mm wide crater-like shallow holes with highly irregular floors and edges are common in marine tetrapod remains and even shark tooth roots from the Ashley and Chandler Bridge formations of South Carolina (e.g., [104]: 330). Within the sample of *Xenorophus*, the best examples of this form of bioerosion are present on two ribs of CCNHM 168 (Figure 72A–E). Each rib exhibits traces only on the posterior side. Craters are floored by irregular bone with semi-radial and branching circular channels 0.1–0.3 mm in diameter, and occasionally with a somewhat larger 0.5–0.7 mm central canal perpendicular to the exterior bone surface. These craters frequently coalesce into one another, forming pervasively bioeroded fields of highly irregular bone. In some areas, a network of small holes (~0.1–0.2 mm diameter) perforates the cortical bone surface in a circular or oval region 3–5 mm in diameter; the bone between these surficial traces is highly fractured. Craters with irregular floors are best interpreted as having porous, highly bioeroded bone and cortex at their center that was fractured away, perhaps during preparation or excavation, and likely originally resembled the circular to oval-shaped clusters of minute canals with a fractured cortex. These craters are best interpreted as galleries bioeroded by the bone-eating worm *Osedax* (e.g., [105,106]). Although not studied using microCT, the approximate dish-shape of these traces with a shallow central depression compare best with those formed by *Osedax* "nude palp" species C, and *Osedax japonicus*, and *Osedax mucofloris* reported by Higgs et al. [105,107]. Diagenetic damage to *Osedax* craters in an Oligocene eomysticetid whale from New Zealand was attributed to the thin cortex fracturing and 'sagging' into the emptied gallery below owing to burial pressure [104]. In the case of CCNHM 168, no such 'sagging' is evident, and it seems that these traces lacked a completely bioturbated void. In the two ribs of CCNHM 168 that are most intensely bioeroded, only one side is bioeroded. This could suggest colonization of an exposed bone surface; however, the lack of bonebed maps and orientation data for CCNHM 168, and most fossil marine mammals from the Oligocene of South Carolina, do not permit inferences of colonization. Further, some species of *Osedax* are infaunal rather than colonizing bone surfaces exposed above the sediment–water interface [105]. Light bioerosion is present on the skull of CCNHM 168, concentrated on the dorsal surface of the skull and principally around the nasals, nares, vertex, dorsal part of the supraoccipital, and left maxilla anterior to the antorbital fossa. The lack of obvious intense biorerosion on the remainder of this specimen is admittedly puzzling; if exposed bone surfaces were colonized, the skull ought to be more dramatically bioeroded rather than the ribs, as it would take much longer to bury, perhaps suggesting infaunal bioerosion of these ribs, and the dorsal surface of the skull (if deposited in a ventral-up position) rather than epifaunal, as the ribs are flat and the bioturbated side would have been in contact with the sediment immediately after skeletonization. Likewise, the skull of CCNHM 104 exhibits some *Osedax* traces on the palate.

In addition to the ribs of CCNHM 168, several teeth and earbones exhibit similar traces (Figure 72L–O). These teeth include the left C1 of ChM PV 5022, right I?/C1 and left I?/C1 of ChM PV 7677, and the left PC4/5 of CCNHM 1077. In each case, the traces consist of a similar network of even narrower canals shallowly incised into the cementum of these teeth, and in ChM PV 5022 and CCNHM 1077, only on one side of the root (Figure 72M,O). These canals are slightly radial in orientation. Similar traces are present on the tympanic bulla of CCNHM 104, and while some are crater-like, most are quite shallow and concentrated on the posterior, lateral, and medial surfaces and largely absent from the ventral surface. In ChM PV 5022, the exterior surficial 'roof' of the galleries has flaked away, revealing an irregular crater-like trace; several craters have laterally coalesced (Figure 72O). These are also best interpreted as *Osedax* traces; *Osedax* traces have previously been reported in cetacean teeth of Oligocene age from the Pysht Formation of Washington [108]. While it is possible that multiple species of *Osedax* may have colonized these skeletal remains (e.g., [105]), morphological differences in *Osedax* borings seem to correspond to differences in substrate, with shallower borings present in cementum and dense earbones and deeper borings in less dense bone in the ribs. Future attempted studies of *Osedax* boring disparity should control for physical properties of substrate, and comparative taphonomic approaches might be highly informative (e.g., [109]).

Oligocene strata are remarkable for preserving abundant evidence of *Osedax* borings in teeth and bones of bony fishes, sharks, sea birds, sea turtles, cetaceans, and sirenians ([104]: 330, and references therein) in shallow marine settings, despite extant *Osedax* largely colonizing marine vertebrate skeletons in deep marine settings and only colonizing skeletal material at shelf depths in a limited fashion or at high latitudes in the Southern Ocean [110, 111]. The intense bioerosion by *Osedax* in Oligocene marine vertebrate assemblages of South Carolina and New Zealand thus posits a paleoecological quandary demanding further study [104], perhaps through taphonomic surveys of material.

6. Discussion

6.1. Ontogeny and Taxonomic Unity of Ashley Formation Xenorophus

Prior to this study, it was the opinion of Albert Sanders, a former curator at The Charleston Museum, that newly discovered specimens collected in the Charleston area and deposited in that institution (namely ChM PV 4823 and other partial skulls from the Chandler Bridge Formation), were different enough from the *Xenorophus sloanii* holotype (USNM 11049) to warrant recognition as a new species [39]—a sentiment that was entered into the literature by Sanders and Geisler [5]. These latter authors also suggested that ChM PV 5022 from the Ashley Formation represented this same species ([5]: 1). While these authors did not explicitly state what morphological features prompted this, we will elaborate here. The holotype (USNM 11049) is unusual for possessing relatively small, anteroposteriorly short, and dorsally flat nasals with anterior edges completely posterior to the antorbital notch, transversely narrow antorbital processes, absolutely and relatively large posterior postcanine teeth with numerous accessory cusps (four–five mesial and six distal) and strongly developed labial cingulum (Figures 22–24). While we too were convinced by these differences at an earlier stage of this study, consideration of the entire hypodigm of Ashley Formation *Xenorophus* reveals considerable dental variation and ontogenetic variation in the nasals, and that the holotype specimen is a juvenile that falls within the range of variation of this sample. This sample further reveals nearly the entire morphology of the cranium of *Xenorophus sloanii* (Figure 73).

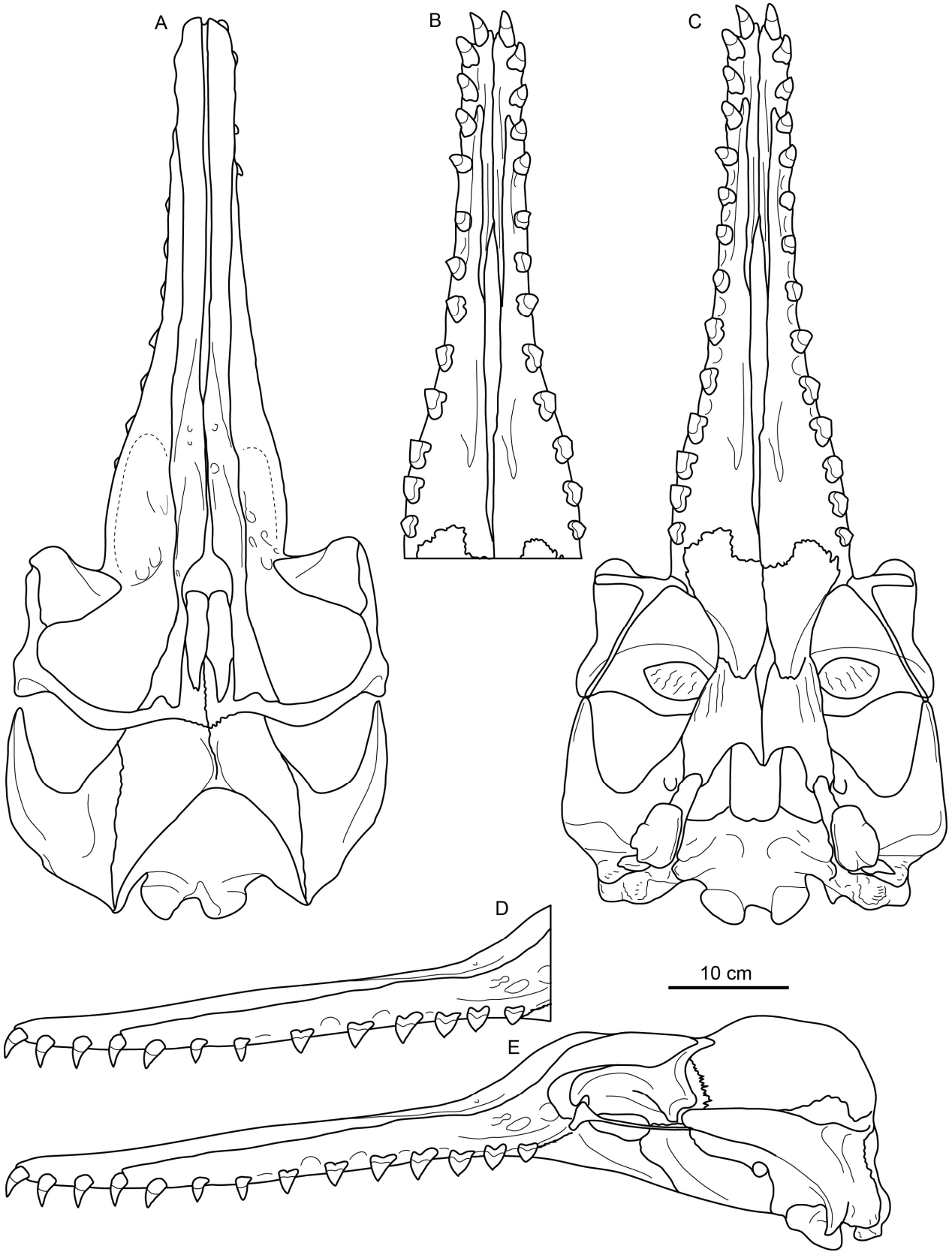


Figure 73. Line drawing of the skull of *Xenorophus sloanii*, chiefly based on CCNHM 168 in dorsal (**A**), ventral (**C**), and lateral view (**E**) with alternate versions of the rostrum with a more typical tooth count of nine maxillary teeth (**B**,**D**).

Within our sample, nasal length is directly correlated with bizygomatic width and other indicators of ontogenetic status (e.g., epiphyseal suture closure), and the nasals are absolutely longer in larger and ontogenetically more mature specimens (e.g., CCNHM 168, 1077; ChM PV 5022; Figures 30 and 31). In smaller specimens, the nasals are more similar to the holotype (USNM 11049), such as ChM PV 7677, which is slightly larger overall and has slightly longer nasals (Figure 22). The anterior margin of the nasal appears to shift anteriorly as it grows, as the nasal edge is far posterior to the antorbital notch in the holotype, slightly posterior in ChM PV 7677 and CCNHM 104, and nearly at the level of the notch in CCNHM 168, 1077, and ChM PV 5022, and furthest anterior in CCNHM 1077 (Figures 30 and 31). In CCNHM 168, 1077, and ChM PV 5022, the nasals also develop a shallow median furrow anteriorly—best interpreted as an ontogenetic change from the transversely flat condition in juveniles like the holotype (USNM 11049).

In dorsal view, the antorbital process is pointed in the holotype, though this is partially related to breakage of the lateral margin of the process. A similarly narrow process is developed in ChM PV 7677, a narrow but rounded process is present in CCNHM 104, and a broadly rounded or nearly rectangular process is developed in CCNHM 168, 1077, and ChM PV 5022. Transverse broadening of the process thus appears to be an ontogenetic change. Specimens of *Xenorophus sloanii* exhibit a degree of dental variation which the holotype specimen falls within (Figure 74). The largest preserved postcanine teeth of specimens like ChM PV 5022 and ChM PV 7677 are slightly smaller (17–18 mm) than the holotype (21.6 mm) (e.g., anteroposteriorly shorter crowns), but other specimens, such as CCNHM 104, 168, and 1077, are approximately the same size (20–20.4 mm; Figure 74). Some specimens have slightly smoother tooth enamel and more poorly developed cingula (e.g., CCNHM 168), but others have teeth that are just as rugose as the holotype (CCNHM 1077, ChM PV 5020, 5022). CCNHM 168 has one less mesial cusp than the holotype but the same number of distal cusps (five) on its posteriormost tooth (PC8), but PC7–8 in CCNHM 1077 has even fewer cusps (two–three mesial and three–four distal cusps). Though not confidently placed to locus, the cheek teeth of ChM PV 5022 and 7677 have up to five distal cusps like CCNHM 168 (Figure 74). Accessory cusps in Ashley Formation *Xenorophus* are basally small, and we observe that there is clearly a degree of variation within this sample, with the low count (three distal cusps) in ChM PV 5022 and CCNHM 1077 at one extreme, and the high count (five distal cusps) in the holotype at the other, and four to five distal cusps representing the norm for the hypodigm, as in CCNHM 168, ChM PV 5022, and 7677 (Figure 74). CCNHM 168 uniquely possesses ten rather than nine upper postcanines, but all other specimens that possess a complete enough rostrum have an identical count of nine maxillary teeth like the holotype, indicating that CCNHM 168 is the outlier.

Further evidence of young ontogenetic status in the holotype includes a very clear and minimally mortised nasofrontal suture (Figure 22), vertical paranaris crests that do not overhang laterally (Figure 22), minimal palatal exposure of the vomer (40–47% of rostral maxilla length vs. 72% in CCNHM 168; Figure 34), open maxillopalatine sutures (Figure 34), unworn teeth, and tooth crowding (diastemata are less than half the anteroposterior length of adjacent tooth crowns; Figures 23 and 24). Within this context, the *Xenorophus sloanii* holotype specimen (USNM 11049) is best considered to be a juvenile and several of its supposedly distinctive features are strongly influenced by ontogeny. Within the broader context of variation within the available sample of *Xenorophus sloanii* from the Ashley Formation, supposedly unique features of the holotype are interpreted here as a result of ontogenetic variation or dental variation within this species (Figure 74).

Some of these trends are paralleled in the smaller sample of *Xenorophus simplicidens*, though juvenile specimens are unknown. These include dorsal expansion of the nuchal crest and shortening of the midline exposure of the parietal owing to anterior thrusting of the occipital shield during postnatal ontogeny (Figures 2–8). Nasal length varies little within *Xenorophus simplicidens*, which is likely driven by the lack of juvenile (e.g., class III) specimens and the smaller adult size of this species (e.g., ChM PV 4266). Similarly, the antorbital process is pointed in all specimens regardless of ontogenetic class.

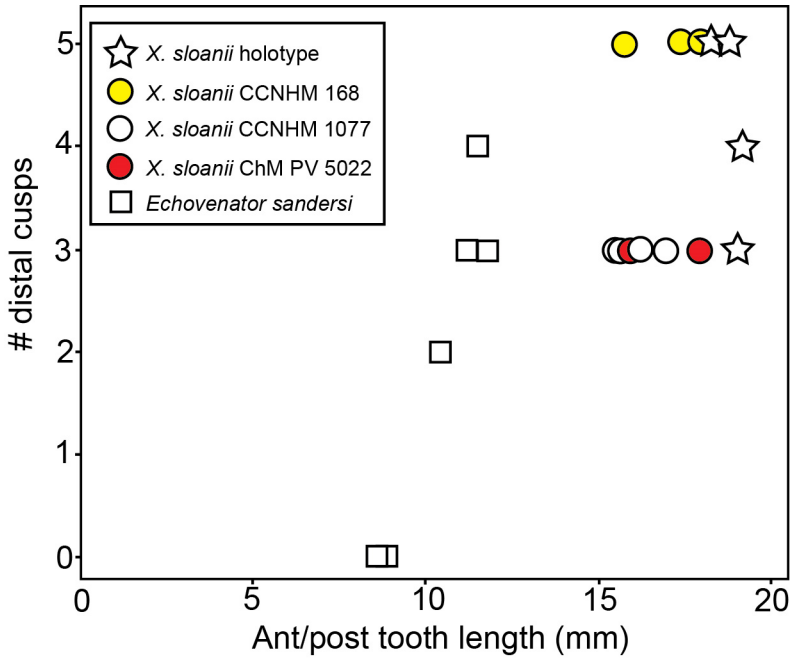


Figure 74. Dental variation in sample of *Xenorophus sloanii* and *Echovenator* holotype.

6.2. Ontogeny, Occlusion, and Tooth Wear in Xenorophus

Tooth wear corresponds to age in some odontocete species [97,112], but in some species, it varies considerably between adults of the same species. This may be due to differences in populations or even individual foraging differences [97,113,114]. Lateral wear (sensu [97]) in odontocetes is caused by tooth interlocking, which is not precise in extant odontocetes, unlike archaeocete whales where there is somewhat more precise occlusion with the upper teeth positioned labial to the lower teeth. The style of interlocking dentition found in modern Odontoceti is confirmed in *Xenorophus* by embrasure pits within the toothrow (rather than labiolingually staggered; Figures 53, 58 and 59). On the posterior part of the palate, embrasure pits are shallow to absent, and are instead quite deep on the mandible, indicating uneven accommodation with upper teeth extending more deeply into mandibular embrasure pits than lower teeth into maxillary embrasure pits. In ontogenetically younger specimens, the embrasure pits do not extend as far posteriorly as in CCNHM 1077. This suggests that the embrasure pits become deeper during postnatal ontogeny and more of the dentition becomes interlocking later in life. Occlusal wear, when present, occurs on the mesial and/or distal side of the tooth of odontocetes.

Juvenile specimens such as the holotype, CCNHM 5995, and subadult ChM PV 7677, possess shallow and ventrally positioned embrasure pits in the anterior and mid postcanines (p1–pc5), and differ from adult specimens CCNHM 168 and 104 in lacking deep, laterally positioned embrasure pits along the anterior half of the rostrum (anterior to PC4). In the holotype specimen (USNM 11049), embrasure pits are medial to a lateral margin of the maxilla that is straight and not 'scalloped' as in adult *Xenorophus sloanii* (e.g., CCNHM 168, 104). In ChM PV 7677, the left side of the rostrum is damaged, but shallow embrasure pits are present on the right side where upper teeth (C1–PC3) are pathologically absent. The presence of shallow embrasure pits between right C1–PC4 suggests that lower antagonists were likely still present in the mandible in ChM PV 7677 and that only the uppers were missing.

Most specimens (e.g., CCNHM 168, 1077, 8720, ChM PV 4823, 5022) have minimal apical wear, and most wear is focused on the mesial and distal cutting edges and, occasionally, quite low on the base of the crown. These mesial and distal wear facets are most extreme basally and the apical quarter of the crown and apical cusp seem to be intact in most teeth and in most specimens, except for some teeth in CCNHM 104. In the context

of tooth occlusion in older individuals with wide diastemata (CCNHM 1077), where the crowns fit entirely within embrasure pits, this tooth wear is most likely formed earlier during growth when the embrasure pits are shallower and the diastemata are narrower. In later growth, the larger embrasure pits and diastemata accommodated the entire tooth crown, limiting or stopping crown-to-crown contact during occlusion.

In *Xenorophus*, most specimens (e.g., CCNHM 168, 8720, ChM PV 4823) have light to moderate tooth wear, and one ontogenetically mature individual (CCNHM 1077) has very light tooth wear, whereas a subadult (CCNHM 104) has the most extreme wear of the sample (Figure 51). This suggests dietary variation in *Xenorophus sloanii*, since all specimens with varying wear are from the Ashley Formation and are the same age. Tooth wear varies in extant odontocetes, and different populations of *Orcinus orca* are known to have different patterns of tooth wear, with resident and transient *Orcinus* exhibiting limited tooth wear owing to a diet of fish and/or marine mammals and offshore *Orcinus* having extensive tooth wear owing to the abrasive denticulated skin of sharks they specialize on [113,114]. Extreme tooth wear (as well as a variety in the extent of tooth wear) similar to some specimens of *Xenorophus* exists amongst Basilosauridae [115,116]. Light to nonexistent apical wear in most specimens of *Xenorophus* suggests consumption of relatively soft-bodied prey such as fish and cephalopods. More extreme wear in CCNHM 104 could result from a more abrasive diet of sharks (e.g., [114]). An alternative explanation might be that the small body size and diastemata of CCNHM 104 are the result of stunted growth, with the teeth continually wearing without being accommodated by embrasure pits.

Two specimens of *Xenorophus sloanii* of different ontogenetic ages (CCNHM 104, subadult; CCNHM 1077, adult) possess one or more anterior caniniform teeth that are completely missing the crown (or nearly so), and the root of the tooth is worn down to the gumline (Figures 51 and 52). In CCNHM 104, these teeth include left C1 and PC1, and left I2 is nearly completely worn and retains only a sliver of enamel lingually. Because these teeth are adjacent in CCNHM 104, this suggests repeated feeding upon highly abrasive food. The absence of glossowear [117] argues against benthic feeding.

6.3. Ontogenetic Sequence for an Early Odontocete

The available sample of skulls of *Xenorophus sloanii* permit unparalleled examination of postnatal ontogenetic changes within a single species of stem odontocete. Such samples are rare even for more densely sampled Miocene strata, but exist for some small mysticetes (Piscobalaena, [118]), a ziphiid (*Messapicetus gregarius*, [119]), and some pontoporiids (*Brachydelphis*, [120]), all from the mid-upper Miocene of Peru and Chile. Most alpha taxonomic work on fossil odontocetes tends to report on "singletons" or small samples ([121]: 376; [122]: 6), and even postnatal changes within extant odontocetes are not widely studied aside from a few key taxa like *Stenella* [83,123], *Physeter* [124], *Pontoporia* [125]; *Sotalia* [126], and *Grampus* [127]. The existence of a large sample of an extinct odontocete permits reassessment of criteria used to distinguish between species in the odontocete fossil record, dominated by species known only from holotypes. Study of ontogenetic changes is key not only for establishing possible ontogenetic synonymies of dubiously diagnosed taxa, but is also critical for the assembly of hypodigms among other stem odontocete species as well as testing the polarity of phylogenetic characters.

Teeth do not change in size from juvenile to adult because odontocetes are monophyodont. As a result, the juvenile holotype (USNM 11049) has relatively large teeth with short diastemata between its teeth, and particularly between the PC7–9. Diastemata are more widely spaced in more mature specimens of *Xenorophus sloanii* (CCNHM 168, 1077). Similarly, the relative tooth size decreases during ontogeny (12.7% of BZW in holotype, 7.3% in CCNHM 104, 6.7% in CCNHM 168, 6.5% in CCNHM 1077) as the skull becomes larger.

Rostral proportion index (RPI) is remarkably consistent throughout postnatal ontogeny, with an RPI of 2.4–2.6 in all specimens complete enough to evaluate (CCNHM 104, 168; ChM PV 7677), including the juvenile holotype (USNM 11049). A proportionally shorter rostrum is expected at some stage in early ontogeny, perhaps to be discovered in

perinatal or neonatal specimens ontogenetically younger than the holotype. Similarly, the rostrum changes little during ontogeny in *Coronodon havensteini*, likely reflecting functional constraints of palate size and shape relating to the proposed filter feeding behavior [46,48].

The nasals in *Xenorophus* change shape dramatically from juvenile to adult (Figures 30 and 31), with anteroposteriorly short (30 mm) nasals with a lobate posterior margin and lacking a median frontal wedge in the juvenile holotype (USNM 11049), slightly longer nasals (46.7 mm) with a short median frontal wedge and short posterior splints in a subadult (ChM PV 7677), and the longer nasals and median frontal wedge with long posterior splints in young adults (61+ and 91 mm; CCNHM 104, 168) and a partly obliterated nasofrontal suture in old adults (71.1 and 74.0 mm; ChM PV 5022, CCNHM 1077). The nasals become proportionally longer relative to skull width during postnatal ontogeny. In addition to extending posteriorly, the nasals seem to grow anteriorly as well; in juveniles (USNM 11049), subadults, and young adults (CCNHM 104), the anterior edge of the nasals is 31–32 mm posterior to the antorbital notch (equivalent to 17 and 11% of postorbital width in USNM 11049 and CCNHM 104, respectively). However, within more mature adults (CCNHM 168) and old adults (CCNHM 1077), the anterior edge of the nasal is much closer to the posteriormost margin of the antorbital notch (19 and 10 mm, respectively), nearly overlapping it (equivalent to 5.9% and 3.5% of postorbital width, respectively). This condition is not present in ChM PV 5022 despite its maturity, though we interpret this as a result of the dorsal surface of the braincase being shifted posteriorly and to the left side by burial deformation. Lastly, the nasals have a dorsoventrally sharp and convex anterior margin as well as a flat dorsal surface in the juvenile holotype (USNM 11049). This condition is similar in subadult ChM PV 7677, though each nasal is now transversely convex and a shallow median trough is present. In adult specimens (CCNHM 104, 168, ChM PV 5022) there is a deep median trough and a shallow V-shaped median notch in the anterior margin of the nasals. Lastly, in adults, the frontonasal suture becomes mortised (CCNHM 168) and completely or partially obliterated in old adults (CCNHM 1077, ChM PV 5022). A similar condition was reported in the holotype of *Echovenator sandersi* [3]. Young adult CCNHM 104 appears to have a partially obliterated frontonasal suture, suggesting a degree of individual variation with the onset of suture closure and fusion within *Xenorophus sloanii*. Similarly, other specimens of *Echovenator* that are similar in size or larger than the *E. sandersi* holotype lack such an obliterated suture (CCNHM 217, 219; ChM PV 542, 2776, 9644), despite this feature being proposed as an autapomorphy of *E. sandersi* [3].

The occipital shield broadens during postnatal ontogeny (Figures 25 and 30), as juvenile (CCNHM 5995) and subadult (ChM PV 7677) specimens have shields that are triangular, whereas the lateral margin is slightly convex in adults (CCNHM 104, 168) and strongly convex in an old adult (CCNHM 1077; damaged in ChM PV 5022). The occipital shield also lengthens and becomes more anteriorly thrusted; in juveniles (CCNHM 5995), subadults (ChM PV 7677), and one small adult (CCNHM 104), the apex of the supraoccipital is posterior to the subtemporal crest, whereas in adult specimen CCNHM 168 and old adults CCNHM 1077 and ChM PV 5022, the apex is thrusted anterior to the posteriormost point of the temporal fossa. As a result, the sagittal crest shortens in length, being approximately 18–19% of bizygomatic width in subadult (ChM PV 7677) and young adult specimens (CCNHM 104), 14% in CCNHM 168, and 11% in old adults (CCNHM 1077, ChM PV 5022). Though difficult to measure, the nuchal crests heighten so that the occipital shield is transversely concave along most of its length in adults and old adults (CCNHM 104, 168, 1077; ChM PV 5022); in the subadult (ChM PV 7677), the anterior half is transversely flat, and in the juvenile (CCNHM 5995), nearly the entire supraoccipital is transversely flat. Lastly, the ventral part of the nuchal crest also lengthens so that in juveniles (CCNHM 5995) it is positioned entirely anterior to the occipital condyles, in line with the posterior edge of the condyles in subadults and young adults (ChM PV 7677, CCNHM 104, 168), and posterior to the condyles in an old adult (CCNHM 1077; difficult to assess in ChM PV 5022 owing to damage).

In addition to the anteroposterior shortening of the sagittal crest in *Xenorophus sloanii*, the crest becomes asymmetrical and rotates counterclockwise (Figures 30 and 31). The sagittal crest remains sagittally oriented in juveniles (CCNHM 5995), subadults (ChM PV 7677), and possibly young adults (possibly improperly reconstructed in CCNHM 104); in older adults, the sagittal crest deviates approximately 5–12° to the left (CCNHM 168, 1077, ChM PV 5022).

Xenorophus sloanii possesses occipital condyles set out on a short neck in subadults (ChM PV 7677) and adults (CCNHM 104, 168, 1077, ChM PV 5022). However, in juvenile specimen CCNHM 5995, the occipital condyles are nearly flush with the exoccipital and no neck is present (Figures 22, 23 and 25–30). The morphology of the paroccipital process also changes during postnatal ontogeny (Figure 25). In most specimens, the ventral margin of this structure is rounded in posterior view (CCNHM 104, 168; ChM PV 7677), but in old adults, the process develops a triangular ventromedial spur (ChM PV 5022, CCNHM 1077). The paroccipital processes of ChM PV 7677 and CCNHM 168 are well-preserved and the lack of a triangular process is not taphonomic in origin. A similar triangular paroccipital process has been documented in *Albertocetus* [1].

6.4. Dental Erosion in Xenorophus

In addition to tooth wear, at least one young adult specimen of *Xenorophus sloanii*, CCNHM 104, exhibits widespread evidence of dental erosion (Figures 51 and 60). Many of the teeth of this individual exhibit loss of dentine below the crown, chiefly on the distal margin of teeth. This erosion is distributed throughout the toothrow, being present in the most anteriorly preserved teeth with complete crowns (e.g., left I2, PC3–4 and left pc2–3) as well as buccal teeth further posteriorly. This wear was referred to as 'narrowing of the tooth cervix' or collaring by Loch et al. [97]. In addition, left PC1–2 are reduced to lozenge-shaped worn roots and have completely lost their crowns. Rather than resulting only from wear, it is possible that these teeth lost their crowns through extreme dental erosion (e.g., narrowing of the crown cervix) followed by catastrophic fracturing of the apical part of the tooth as the crown cervix was reduced further. More typical dental erosion such as enamel cupping was not identified in any specimen of *Xenorophus sloanii*. However, some criteria used to identify dental erosion in extant odontocetes include changes to the reflectivity and luster of tooth surfaces [97,128], which may not be reliable in fossils owing to diagenesis. Curiously, evidence of dental erosion seems to be concentrated on the distal margin of most teeth rather than the lingual side as reported in extant odontocetes [97,128]. Dental erosion in extant dolphins has a number of possible causes, including the expulsion of gastric acids, perhaps as a result of the retention of the forestomach from terrestrial artiodactyl ancestors [97]; the forestomach is apparently used to temporarily store water swallowed during suction feeding [129]. While it is possible that the rudimentary salivary glands of cetaceans may insufficiently buffer the oral environment, and the pH of the aquatic environment may further contribute to dental erosion, gastrointestinal disorders seem to be the most likely cause of dental collaring in odontocetes [97], owing to their lingual occurrence. Distolingual dental collaring in CCNHM 104 is consistent with this hypothesis. Because acid erosion can dissolve or soften enamel and dentine, it is further possible that the anomalous degree of tooth wear in CCNHM 104 may be related to dental erosion and softening of enamel and dentine. However, it is uncertain why narrowing of tooth cervices is concentrated on the anterior teeth.

6.5. Feeding Ecology of Xenorophus

Xenorophus sloanii has a number of adaptations consistent with raptorial pierce feeding on fish. *Xenorophus sloanii* is mesorostrine, with a Rostral Proportion Index (RPI; [2]) of 2.4–2.6, similar to modern delphinids like *Steno* (RPI = 2.63) and *Stenella* (2.89) but longer than *Tursiops* (RPI = 1.95), all of which are raptorial predators that feed on pelagic, demersal, and epibenthic fish, cephalopods, and other small invertebrates [130]. The dwarf xenorophid *Inermorostrum xenops* possesses two key adaptations for suction feeding: toothlessness and

a short rostrum (RPI = 1.19; [2]). *Xenorophus sloanii* possesses high RPI values and rod-like hyoid elements (stylohyal; Figure 61), like in Basilosauridae, and therefore does not possess specializations for suction feeding. However, clear suction feeding adaptations in *Inermorostrum* (low RPI, toothlessness) indicate that some degree of suction feeding was likely present amongst the xenorophids [2]; indeed, the capacity to suction feed likely evolved at the base of Neoceti [131]. It is therefore possible that *Xenorophus sloanii* had the ability to use both suction and pierce feeding, similar to many modern mesorostrine delphinoids [132] despite lacking obvious suction feeding specializations (e.g., [131]). The temporal fossae of *Xenorophus* are large amongst odontocetes (see *6.16 Evolution of Temporal Fossa Size in Odontoceti*), much larger than in extant odontocetes—suggesting a more powerful, but less rapid bite. Two different individuals of *Xenorophus sloanii* are pathologically missing four (or more) conical caniniform teeth (CCNHM 168: Lpc1–4; ChM PV 7677: RC1–PC3) used for prey capture, meaning that an entire quadrant of the anterior rostrum lacked antagonistic teeth in these two specimens. Yet, the alveoli are completely filled in with bone, indicating successful feeding after traumatic injury and likely for many months after the injury. Perhaps prey capture aided by suction permitted feeding in spite of pathological tooth loss. For example, the extreme suction feeding adaptations in extant *Physeter macrocephalus* permits individuals with grotesquely pathological mandibles to grow to adulthood ([133], and references therein).

The dentition of *Xenorophus* is heterodont and consists of five to six caniniform teeth, four to five triangular multicuspate molariform teeth, and three to four transitional triangular unicuspid anterior postcanines (Figures 50–60). These groupings are admittedly a gradient and approximate boundaries between these groupings occur in the anteriormost postcanines near PC2–3 (transition from conical to triangular unicuspid) and around PC5–6 (transition from triangular unicuspid to multicuspate molariform teeth). However, owing to the interdigitating occlusion (e.g., CCNHM 1077) and lack of apical wear on all postcanine teeth in most specimens and concentration of wear along the mesial and distal carinae (CCNHM 168, 1077; ChM PV 5022, 7677), the teeth are likely functionally homodont and used in pierce feeding. Most tooth wear seems to result from tooth-to-tooth contact at the crown base, with the apices of the crowns being protected from such wear by occluding within embrasure pits in postcanine diastemata when the mouth is closed (see above). This suggests feeding on relatively soft prey, such as cephalopods, fish, and perhaps batoids. Pervasive tooth wear in one specimen, CCNHM 104, suggests individual variation and specialization in diet, and tooth wear in this individual, in concert with subadult (rather than senescent) ontogenetic status, likely reflects an abrasive diet. Such prey could consist of sharks, the denticles of which wear the teeth of extant shark feeding offshore *Orcinus* down to the gumline [114]. Hard-shelled cephalopods such as the nautilids *Aturia* and *Eutrephoceras* were still abundant during the Paleogene [134] and could have also incurred such damage. Alternatively, extreme tooth wear in concert with the retention of large temporal fossae [135] could suggest the ability to prey on larger fish and small marine tetrapods (smaller odontocetes, sirenians, sea turtles, e.g., macrophagy), perhaps explaining the prevalence of oral pathologies in this taxon.

In sum, rostral proportions, tooth morphology, tooth wear, muscle attachments, and a long but unsutured mandibular symphysis indicate raptorial generalist feeding and likely a diet of fish. Intraspecific differences in tooth wear suggest some variability in diet and likely the consumption of more abrasive prey (e.g., sharks).

6.6. Mandibular Symphysis Morphology in Early Neoceti

The mandibular symphysis in *Xenorophus* is less rigid than in other odontocetes. In CCNHM 168, the articulation is restricted to the dorsal half of the mandible, and consists of relatively low longitudinal ridges and furrows, and ventrally, includes a somewhat deeper and continuous longitudinal furrow (Figures 55 and 56). The left mandible is somewhat more strongly rugose than the right. A ventral longitudinal furrow is present in juvenile specimens of the early diverging odontocete *Olympicetus* (e.g., CCNHM 8715, 8719, 8762),

and *Simocetus rayi* and other simocetid-grade odontocetes possess an unsutured mandibular symphysis [18,136], though a symphyseal groove is not present in *Simocetus rayi* [18]. The symphyseal articular surface in *Xenorophus* bears some gentle topography, differing from Basilosauridae, but also clearly differing from the barren symphyseal surface and pronounced symphyseal groove within Aetiocetidae and Chaeomysticeti (Kinetomenta). Curiously, a similar condition is also reported in the toothed mysticete *Coronodon* [46].

Unsutured mandibular symphyses are more widely distributed amongst mysticetes, especially the Aetiocetidae and Chaeomysticeti [78,137,138]; this clade was recently named the Kinetomenta after the distinctive loose mandibular connection [139]. Within mysticetes, this loose connection is clearly related to bulk filter feeding and is usually associated with some degree of mandibular kinesis [138–140]. A symphysis with an undulatory articular surface similar in morphology to *Xenorophus sloanii* is also documented in the early diverging toothed mysticete *Coronodon* [46,48]. A clearly firm articulation was present in *Mystacodon selenensis*; in other toothed mysticetes including *Llanocetus*, *Mammalodon*, and *Janjucetus*, the condition of the symphysis is unknown [47,141,142] but partial mammalodontid mandibles suggest a firm articulation in *Mammalodon* and *Janjucetus* [142,143].

Within the Kinetomenta, a groove usually appears within the ventral half of the mandible and in adults, extending a short ways posterior to the symphysis [139]. Though frequently interpreted as the site of attachment for the symphyseal ligament [78], this groove instead houses a mass of fibrocartilage in extant balaenopteroid whales [144], is recognized as a persistent remnant of the groove for the Meckel's cartilage [80,145] and in archaic mysticetes persists well into early postnatal growth [146]. We propose that this furrow is likely homologous to the symphyseal groove of mysticetes (albeit much shallower), and the condition of the symphysis in *Xenorophus*, *Olympicetus*, and other simocetid-grade odontocetes raises the possibility that a similar condition as present in Kinetomenta (albeit somewhat more firmly articulated) may be ancestral for Neoceti in general. Further study of the mandibular symphysis is needed, as well as further discoveries of early diverging odontocete mandibles, especially given the recent attention to this structure regarding the origin of baleen (e.g., [139]).

6.7. Evidence for Sound Production and Ultrasonic Hearing in Xenorophus

Xenorophid dolphins represent the earliest diverging odontocetes, and surprisingly already present anatomical evidence indicating the existence of specialized soft tissues relating to sound production and ultrasonic hearing [3,4,19]. *Cotylocara macei*, the most derived xenorophid, possesses large antorbital fossae on the rostrum and a deep postnarial fossa indicating the presence of facial sinuses (ventrolateral expansion of the premaxillary sinus fossa and a diverticulum of the inferior vestibule, respectively) likely related to sound production [4]. Another derived xenorophid, *Echovenator sandersi*, has antorbital fossae, a shallow postnarial fossa, and cochlear adaptations for ultrasonic hearing [3], suggesting that all xenorophids were capable of echolocation. The basal position of this clade within Odontoceti suggested a single origin of echolocation at the inception of the group [3], though the discovery of archaic odontocetes like *Olympicetus* with archaeocete-like cochleae suggest convergent development of echolocation in xenorophids and the Amblyoccipita [51].

The cochlear morphology of *Xenorophus* has not been studied using microCT (e.g., [3,51,147]), and it is not possible to confirm ultrasonic hearing in this taxon. Likewise, *X. sloanii* lacks the distinctive postnarial fossa present in *Echovenator* and *Cotylocara*. However, it does possess large antorbital fossae that are asymmetrical, and asymmetrical dorsal infraorbital foramina and premaxillary foramina—differing sharply from non-echolocating basilosaurids— and similar to other xenorophids in this regard. The antorbital fossae are hypothesized to house a ventrolateral expansion of the premaxillary air sinus [4], which in extant odontocetes is an acoustic reflector. Therefore, the presence of antorbital fossae strongly suggests that *Xenorophus sloanii*, like other xenorophids, was capable of echolocation (see *6.8. Asymmetry of Craniofacial Structures Associated with Sound Production in* Xenorophus). While the bony labyrinth of *Xenorophus* has not been

examined using microCT, the cochlear endocast of the broken periotic in ChM PV 5022 preserves a loosely coiled cochlea with approximately two turns (Figure 44), largely consistent with ultrasonic hearing (e.g., [3,19]). Testing this hypothesis will require micro-CT study of the periotics of *Xenorophus*. Of the presently existing material, we suggest that CCNHM 104, ChM PV 5022, or CCNHM 8720 will yield the best results for future micro-CT scanning, as these specimens have periotics freed from the skull with an intact, unbroken pars cochlearis. The fractured and reassembled pars cochlearis of ChM PV 7677 may also yield usable scans.

6.8. Asymmetry of Craniofacial Structures Associated with Sound Production in Xenorophus

Like other stem odontocetes [3–5,17,18], asymmetrical structures in the facial region of *Xenorophus* are likely associated with ultrasonic sound production in extant Odontoceti. As in other Xenorophidae, *Xenorophus* spp. Possess large and asymmetrical antorbital fossae [3–5] that happen to be asymmetrical with an anteroposteriorly longer left antorbital fossa in *X. sloanii* and a longer right antorbital fossa in *X. simplicidens*. In *Xenorophus sloanii*, the left fossa is consistently anteroposteriorly longer and more deeply excavated than the right fossa, and the lateral edge of the maxilla is dorsoventrally thinner lateral to the fossa. Though obscured by breakage in some cases, the dorsal infraorbital foramina on the left maxilla consistently are more coalesced into a single composite fenestra. A coalesced fenestra may also be present in *Echovenator sandersi* but absent in *Albertocetus meffordorum*, *Cotylocara macei*, and *Inermorostrum xenops*; if the condition in *Echovenator* is caused by damage, this would be unique to *Xenorophus*. In addition, the premaxillary foramina are asymmetrical in all specimens, with differing numbers of foramina and foramina shifted further anteriorly on the left side in some specimens (CCNHM 168, ChM PV 5022). In CCNHM 1077, the largest premaxillary foramina are offset with the left foramen shifted 10 mm posterior to its counterpart on the right. The premaxillary sac fossae are also asymmetrical, with the left premaxillary sac fossa being anteriorly shifted, and more deeply excavated and slightly transversely narrower (14 mm wide) relative to the more shallowly excavated and broader right premaxillary sac fossa (16 mm wide). Critically, all of these bony structures are associated with (or hypothesized to be associated with) soft tissue structures that are involved with sound production. The antorbital fossa is unique to xenorophids but convincingly shown to have housed air-filled facial sinuses, likely a ventrolateral expansion of the premaxillary sinus fossa [4]. The premaxillary foramen is unique to odontocetes, and is hypothesized to transmit the branch of the maxillary nerve that innervates the premaxillary air sac, melon, and connective tissue enclosing the melon [5]. The premaxillary sac fossae house the premaxillary sac sinuses, which likely reflect generated sounds anteriorly [11,148].

6.9. Directional Asymmetry of the Rostrum, Palate, Dentition, Mandibles, Neurocranium, and Vertebrae of Xenorophus

Several unusual cases of asymmetry are present in the crania, mandibles, teeth, and postcrania of *Xenorophus* (Figures 75 and 76), and they have no apparent relation to sound production, unlike the antorbital fossae and asymmetrical premaxillary sac fossae outlined above (see *6.8. Asymmetry of Craniofacial Structures Associated with Sound Production in* Xenorophus). The sum of this evidence indicates that *Xenorophus* possessed a rostrum that is deflected to the left of the midline, and possibly a neurocranium canted to the right of the midline, along with asymmetrical mandibles, dentition, and even postcrania. Evidence of asymmetry will be summarized briefly and followed with a functional interpretation and hypotheses for future evaluation.

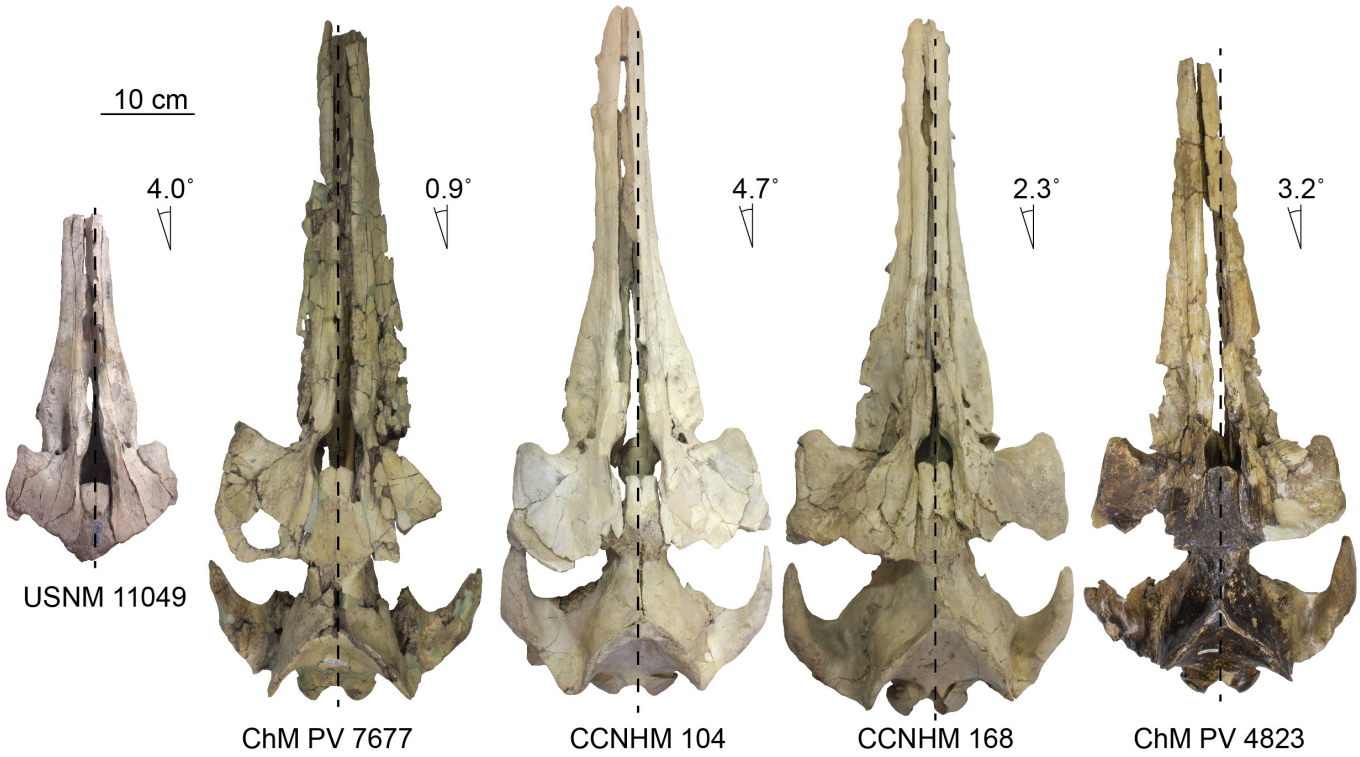


Figure 75. Sinistral rostral deviation in *Xenorophus sloanii* and *Xenorophus simplicidens*.

Rostral Torsion: *Xenorophus* possesses a longitudinally twisted rostrum (Figure 32). In anterior view, the rostrum is twisted clockwise 11° in *Xenorophus sloanii* (CCNHM 168) and 6.3° in *Xenorophus simplicidens* (ChM PV 4823). This rostral torsion is less extreme than that reported for basilosaurid archaeocetes [149]. Rostral torsion has also been convincingly documented in the Oligocene giant dolphin *Ankylorhiza* [37], the toothed mysticete *Coronodon* [48], and other xenorophid dolphins including *Cotylocara macei* and *Echovenator sandersi* [3,4], owing to the excellent 3D preservation of fossils from the Charleston Embayment.

Sinistral Rostral Deviation and Mandibular Asymmetry: Not previously reported within Neoceti is the deflection of the rostrum 2–4° to the left of the neurocranial midline in well-preserved skulls of *Xenorophus* (Figure 75), paralleling the deviated or curved rostra of basilosaurids and some protocetids [149]. This pattern is present in most specimens of *Xenorophus* that preserve both a rostrum and neurocranium, regardless of preservation (holotype USNM 11049, CCNHM 104, 168; ChM PV 7677, as well as *Xenorophus simplicidens*, ChM PV 4823). The distance between the posterior edge of the mandibular condyle and posteriormost tooth is asymmetrical in the mandibles of CCNHM 168, the left distance being approximately 10 mm less than on the right, reflecting the deviation of the rostrum and shortened distance between the jaw joint and the toothrow on the left.

Palatal Asymmetry: We observed, for the first time, asymmetrical palatines in some xenorophids (Figure 34). In *Xenorophus sloanii*, the right palatine is shifted further anteriorly than the left in all known specimens with a preserved palate. This same pattern is observed in all known specimens of *Albertocetus* (USNM 525001, ChM PV 4834, 8680, 9641). In other Xenorophidae, such as ChM PV 2758, *Cotylocara macei*, *Echovenator sandersi*, and *Inermorostrum xenops*, the palatines appear symmetrical. Accordingly, the rostrum of *Inermorostrum* is quite short and the rostra of *Cotylocara* and *Echovenator* are approximately symmetrical and do not deviate to the left, as in *Xenorophus*.

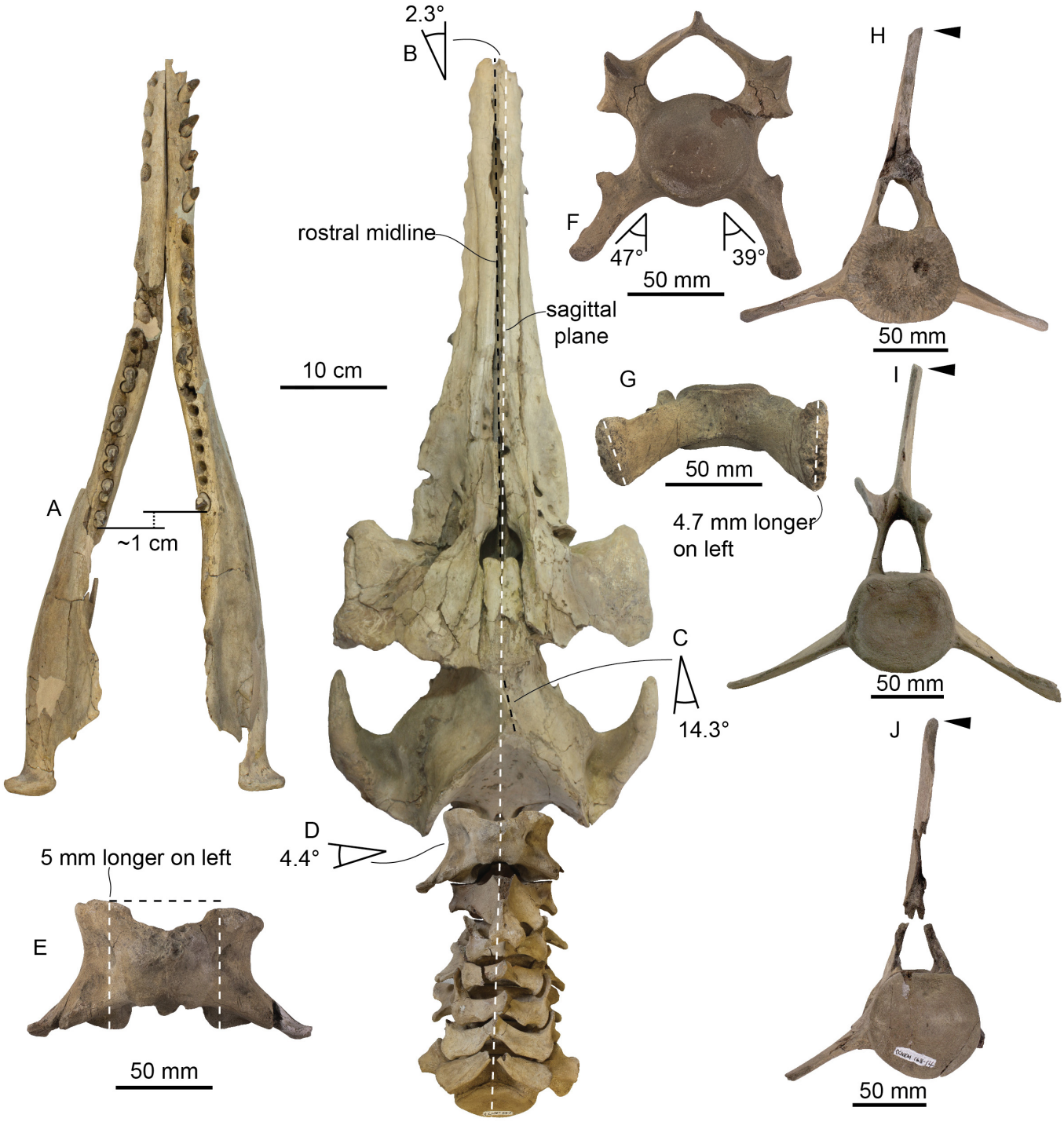


Figure 76. Summary of cranial, mandibular, and vertebral asymmetry in *Xenorophus sloanii* specimen CCNHM 168. (**A**) Anteroposterior offset in the last postcanine tooth. (**B**) Deviation of rostrum to left of midline. (**C**) Counterclockwise rotation of sagittal crest. (**D**–**E**) Wedge-shape of atlas vertebra. (**F**,**G**) Asymmetry of parapophyses of C6. (**H**–**J**) Deflection of neural spines of lumbar vertebrae to left.

The palatine–maxilla suture in *Xenorophus* is asymmetrical (Figure 34), unique amongst odontocetes. In *Xenorophus* and *Albertocetus* specimens, the right palatine is shifted further anteriorly than the left. In these specimens, the right antorbital fossa is anteroposteriorly shorter and less shallowly excavated than on the right. Few specimens preserve the posterior end of the palatine or the pterygoid. In ChM PV 9641, a specimen of the "robust" *Albertocetus* from the Ashley Formation that is 3D preserved and has the best preserved

palate of any xenorophid, the asymmetry appears to continue into the pterygoids; the pterygopalatine suture is shifted slightly posteriorly on the left hand side just like the maxillopalatine suture, and the left hamulus is positioned just slightly posterior to the right. This is also the case in the *Albertocetus* holotype, though only one hamulus is preserved. Furthermore, in the *Xenorophus sloanii* holotype (USNM 11049), referred skull CCNHM 1077, and *Albertocetus* specimen ChM PV 9641, the medial suture of the palatines and vomer are asymmetrical; they are shifted to the right and concave on the left side anterior to the pterygoids, and at the level of the pterygoids, the vomer is shifted instead to the left. In the holotype, when viewed posteroventrally, the vomer is rotated so that it is directed ventrolaterally to the left; rather than being parasagittal, it forms approximately an 80° angle with the horizontal plane on the left and an approximately 100° angle on the right, corresponding to a wider right internal choana and differing from all extant Odontoceti. In ChM PV 9641, the vomer is broken, but the base appears to point off to the left side at a similar angle, and regardless, the right choana appears wider than the left.

Dental Asymmetry: All specimens of *Xenorophus* (where both toothrows are preserved) share a surprising degree of dental asymmetry (Figure 49), with the right anterior postcanines (PC1–5 in USNM 11049, ChM PV 4823, and PC1–6 in CCNHM 168) shifted up to 8.7 mm (but more typically 2–4 mm) anterior relative to those on the left. In CCNHM 104, the right PC3–4 are shifted further anterior instead, but the rest of the posterior toothrow has the typical anterior shifted left teeth. Accordingly, tooth wear in all specimens with left and right teeth preserved is also asymmetrical (CCNHM 168, 8720). Dental asymmetry is not unique to *Xenorophus*, however, and similar degrees of asymmetry are also apparent in other xenorophids including *Cotylocara macei* and to a lesser degree in *Echovenator sandersi.* Some toothed mysticetes such as *Aetiocetus cotylalveus* and *Coronodon havensteini* also possess asymmetrical teeth, along with basilosaurids (*Basilosaurus isis*, MMMP VP 118204; *Dorudon atrox*, UMMP VP 101222; *Zygorhiza kochii*, USNM 11962). Extreme dental asymmetry is present in *Cynthiacetus peruvianus*, which may be a result of extreme rostral torsion and deflection to the left [29,149]. Dental asymmetry in *Xenorophus* is not simply related to the left-side deviation of the rostrum, as the locus of variation is most extreme in the anterior premolars (PC1–5). This region is the same region where an additional anterior postcanine tooth occurs in CCNHM 168 (see *6.17. Evolution of Polydonty in Neoceti*) and the presumed region of overlap between the Bmp4 and Fgf8 genes (e.g., [150]; see below) and therefore is possibly related to incipient homodonty. Dental asymmetry is not unique to Xenorophidae, but it does appear to be the most extreme within Neoceti.

Vertebral Asymmetry: The atlas of CCNHM 168 is wedge-shaped in dorsal view, being anteroposteriorly longer on the left than the right, leading to 5–7° of deviation of the neurocranial sagittal plane to the right side (Figures 66 and 75). In the axis (C2) of CCNHM 168 the right transverse process is larger than the left. In CCNHM 168 and 1077, the anterior tip of the neural spine is rotated to the right by approximately 2° (CCNHM 168) and 9.7° (CCNHM 1077; perhaps accentuated by compaction). The most profound directional asymmetry is found in the diapophyses of C6 in CCNHM 168, CCNHM 1077, and ChM PV 7677, where the left parapophysis is slightly longer and more vertically oriented than the right, and more rugose and anteroposteriorly widened (24–31% greater relative to right parapophysis) at its ventral apex. In addition to rampant asymmetry in the cervical series, lumbar vertebrae also exhibit asymmetry in all specimens where neural spines are preserved (CCNHM 168, 1077, and ChM PV 5022): the neural spine is consistently curved and deviated to the left side by 5.5–7.5°.

Functional Significance of Asymmetry and Hearing: *Xenorophus* possesses a rostrum and neurocranium that diverge from the midline—the neurocranium and rostrum meet at an angle of about 2–4° with the rostrum bent to the left (Figure 76). Owing to asymmetry of neck muscle insertions on the skull (e.g., sternomastoideus) and rampant asymmetry within the cervical vertebrae (especially C6), and asymmetry in length of the mandibles (post-dental mandibular length 10 mm shorter on the left; Figure 76A), it is clear that the neurocranium was canted slightly to the right and the rostrum likely did not deviate signif-

icantly from the anterior direction. The sagittal crest is asymmetrical in adult specimens (Figures 31 and 76), deviating 14° to the left of the neurocranial midline in CCNHM 168. The simplest explanation is a superficially different but functionally analogous style of mandibular asymmetry than that seen in Basilosauridae (e.g., *Cynthiacetus peruvianus*, [100]: Figure 25; *Basilosaurus isis*, UMMP VP 118204), with the left mandible facing somewhat more anterolaterally than the right. We hypothesize that lateral bowing of the midline of the skull results in slight clockwise rotation (in dorsal view) of the pan bones; by extension, the mandibular fat pads would have similarly exaggerated directional hearing in a fashion broadly analogous to owls. We predict that asymmetry in the thickness of the 'pan bone' will be encountered upon CT analysis of the mandibles of CCNHM 168 or possibly other xenorophids with left and right mandibles preserved.

Though rostral torsion and mandibular asymmetry was suggested to be related to directional hearing underwater [149], the exact mechanism remains unclear. In Basilosauridae, the left and right "pan bones" of the mandible are asymmetrical, with the thinnest part located further anterior on the left than on the right in *Basilosaurus isis*. The pan bone houses the mandibular fat pads which channel sounds into the acoustically isolated ears of cetaceans [148]. This asymmetry led Fahlke et al. [149] to propose that mandibular asymmetry reflects asymmetry of the mandibular fat pads in archaeocetes and was driven by directional hearing, with asymmetrical acoustic pathways exaggerating the left–right acoustic mismatch between left and right cochleae in a fashion broadly analogous to the directional hearing of owls.

Fahlke et al. [149] proposed that this asymmetry was lost in Mysticeti and subsequently elaborated upon in Odontoceti through the development of asymmetrical soft tissue facial structures used in echolocation and associated asymmetry in underlying skull morphology. However, we note that asymmetry of the auditory apparatus is unstudied in odontocetes and that asymmetry of the mandibles (e.g., analogous to that of archaeocetes) has not been demonstrated in any fossil or extant Odontoceti, aside from rostral torsion identified in other odontocetes from the Oligocene strata of Charleston, South Carolina (e.g., *Ankylorhiza*, *Cotylocara*, *Echovenator*; [3,4,37]), as well as the toothed mysticete *Coronodon* [48]. The precise function of rostral torsion in directional hearing was not explained by Fahlke et al. [149], except perhaps resulting as a consequence of mandibular asymmetry. Study of *Xenorophus* provides no insights into rostral torsion and further study is clearly warranted.

Hitherto unreported asymmetry of the dentition within early odontocetes like *Xenorophus* and basilosaurid archaeocetes similarly evades ready interpretation. Asymmetrical dentition seems maladaptive, but we outline two different hypotheses. Dental asymmetry may be adaptive given that early odontocetes only possess incipient polydonty, and within the middle of the toothrow where asymmetry is most extreme, the diastema are also the longest. Given that these teeth do not seem to occlude (and accordingly possess minimal wear in most specimens), unlike the molariform double-rooted posterior postcanine teeth, it is possible that staggering of the teeth may decrease functional gaps in the dentition and increase the likelihood of biting small prey that might otherwise escape. Another possibility, perhaps borne out by the rather extreme asymmetry of the dentition and extreme rostral deflection and torsion in *Cynthiacetus peruvianus* ([100]: Figures 7 and 25), is that dental asymmetry is simply a consequence of rostral deviation and/or torsion. We have identified dental asymmetry in basilosaurids, aetiocetids, *Coronodon*, and *Xenorophus*. It is likely that dental asymmetry is not unique to early Neoceti and Basilosauridae, and very well may be present in extant odontocetes and simply never looked for—and easily overlooked—given the small tooth size and high count of extant species. Further study, perhaps including the use of geometric morphometrics (e.g., [52]), is needed to better understand dental asymmetry.

Previous studies have identified possible origins of cranial asymmetry unrelated to sound production. MacLeod et al. [151] found a relationship between the diameter of the pyriform recess in the pharynx of odontocetes (and thus maximum food diameter) and the degree of facial asymmetry. MacLeod et al. [151] proposed that cranial facial symmetry

may not be related to the asymmetry of soft tissues associated with sound production and instead may be driven by the asymmetry of the pharynx. The larynx of odontocetes is unique in that it extends dorsally into the nasopharynx and thus divides the oropharynx into left and right piriform recesses that pass around it. To permit a larger bolus to pass, the right piriform recess is larger than the left [151,152]. Additionally, the larynx is shifted to the left, muscles attaching to the larynx and thyrohyal are asymmetrical and the entire hyoid apparatus is tilted so that the right thyrohyal is depressed ventrally and the left thyrohyal is elevated dorsally, and the entire hyoid apparatus is ventrally lowered on the right and elevated on the left [152]—though the hyoid bones themselves are symmetrical in morphology. Curiously, the premaxilla and the dorsal opening of the nares in many extant odontocetes are asymmetrical (right premaxilla wider than left, left naris wider than right), but ventrally the choanae are instead symmetrical throughout Odontoceti.

Limitations to the pharyngeal-driven cranial asymmetry hypothesis of MacLeod et al. [151] include the lack of bony asymmetry in the basicranium, palate, and hyoid apparatus of odontocetes [151,152]. MacLeod et al. ([151]: 541) argued that there is no internal choanae asymmetry because this would force asymmetry of the pterygoid, palatine, and maxilla, compromising function of the upper jaw, with the dorsal bony nares have no such selection pressure, but this is clearly an ad hoc hypothesis. A further problem is that in addition to simply possessing an enlarged right bony naris, the premaxillae, dorsal infraorbital foramina, muscle attachments, and frequently the vertex, antorbital notches and antorbital processes are also asymmetrical in Odontoceti [4,16–18,52,153].

However, for the first time, we have uncovered evidence of asymmetrical palatal bones in an early odontocete (Figure 34). At face value, this finding could support the hypothesis of MacLeod et al. [151] by demonstrating that the earliest odontocetes (Xenorophidae) underwent a phase with cranial asymmetry expressed both dorsally and ventrally. Simultaneously, these observations in *Xenorophus* conclusively disprove the assertion that odontocetes cannot exhibit palatal or basicranial asymmetry, and indicate that an evolutionary constraint against such asymmetry (outlined by [151]) does not exist. In the context of skull asymmetry, the asymmetrical palatines are likely structurally associated with the left-handed deviation of the rostrum, the asymmetrical excavation of the antorbital fossae, or both. Because the rostrum deviates approximately 2–4° to the left, perhaps the palatine is shifted further anteriorly on the right owing to clockwise (in ventral aspect) rotation of the antorbital/palatal region. Accordingly, the anteroposterior offset between the left and right palatine apices (17.4 mm) in CCNHM 168 parallels the difference in measurement from the mandibular condyle to the last tooth (10 mm) in the left and right mandible of CCNHM 168. Additionally, the antorbital fossa is more deeply excavated on the left than on the right maxilla, and this fossa directly overlies the maxillopalatine suture; perhaps asymmetrical fossae have driven the asymmetry of the sutures. We prefer the former hypothesis, given the preponderance of evidence indicating widespread asymmetry of the skull in *Xenorophus* and its relation to echolocation and directional hearing (see *6.8. Asymmetry of Craniofacial Structures Associated with Sound Production in* Xenorophus). However, we note that if the antorbital fossae have driven the asymmetry of the palatines, this would be associated with echolocation rather than feeding, because the antorbital fossae of Xenorophidae most likely accommodated air-filled expansions of the premaxillary air sinuses [4] associated with sound production.

The consistent 2–4° deviation of the rostrum to the left in multiple specimens (relative to the neurocranium; Figure 75), asymmetrical sternomastoid muscle fossae, maxillopalatine sutures, vomer, and muscle attachments and transverse process shape in the cervical vertebrae strongly argue against an unusual pathology and instead indicate that neutral orientation of the neurocranium was 2–4° to the right side, along with the rostrum deviated 2–4° to the left. Rather than the rostrum extending to the left side, which would have imparted asymmetrical hydrodynamic forces during swimming, neck muscle attachments and cervical vertebral asymmetry suggest that the anterior neurocranium and posterior rostrum (and palate) deviated from the sagittal plane of the axial skeleton. The sternomastoid fossae

of CCNHM 168 are asymmetrical with a slightly larger muscle attachment on the right, indicating that a greater muscle insertion cross-section was developed on the right side. The asymmetrical wedge-shape of the atlas would permit canting of the occiput by approximately 4–5° to the right (Figures 66 and 76). Asymmetrical parapophyses and diapophyses within the cervical vertebrae, as well as neural spines as far posteriorly as the lumbar vertebrae, suggest the development and attachment of asymmetrical axial musculature which could accommodate the unusual asymmetry of the skull and any possible uneven hydrodynamic forces imparted by the water column during locomotion. It is tempting to speculate that side-swimming, utilized by extant *Platanista gangetica*, could potentially explain cranial and postcranial asymmetry in *Xenorophus*. However, axial asymmetry has not yet been documented in *Platanista*.

Recognition of asymmetry of the neurocranium and mandibles in *Xenorophus* and the hypothesis that this is driven by asymmetrical hearing raises the possibility that cochlear morphology might be asymmetrical within Xenorophidae and even other odontocetes. Minute asymmetrical features are often present in the tympanoperiotics of fossil and extant odontocetes, but typically dismissed as simple variation. However, few studies have ever used microCT to examine the left and right bony labyrinth from the periotics of the same specimen. One exception to this is Racicot et al. [154], who found minor asymmetry in two different bony labyrinths of *Monodon monoceros*, with the left and right labyrinths plotting near each other on a PCA plot, but not identically so ([154]: Figure 10). These authors further found that the endocranial cast of *Delphinapterus* was asymmetrical. Thus far, the only specimen of *Xenorophus* with left and right periotics freed from the skull is ChM PV 7677 (Figures 40–43). MicroCT of other xenorophid specimens preserving freed left and right periotics may be fruitful, such as the *Echovenator sandersi* (GSM 1098). Other xenorophid specimens including ChM PV 4834 and 5711 (*Albertocetus*) have one freed and one in situ periotic (or two in situ periotics in the case of ChM PV 8680, *Albertocetus*, CCNHM 1077, *Xenorophus*), and perhaps future careful preparation could remove the in situ periotic. Minor cochlear asymmetry, paralleling *Monodon* [154] may be present in Xenorophidae.

6.10. Rostral Deflection in Xenorophus

Xenorophus sloanii and *Xenorophus simplicidens* possess rostra that are ventrally deflected (Figure 24) by about 18° from the basicranial stem in CCNHM 104, 15.5° in ChM PV 7677, and 26.5° in CCNHM 168; owing to incompleteness, adhering matrix, and/or deformation, it is difficult to measure this angle in CCNHM 1077, 8720, and ChM PV 5022, but the rostrum seems deflected in each by about 18–19°. Deflected rostra are present in other xenorophids like *Albertocetus meffordorum*, *Cotylocara macei*, *Inermorostrum xenops*, and *Echovenator sandersi* ([9]: Figure 9; [2–4]). The brevirostrine odontocete *Simocetus rayi* also possesses a deflected rostrum [18], initially interpreted to be related to epibenthic foraging by analogy with rostral deflection in sirenians [18,155]. A similar argument was made for *Inermorostrum* [2]. However, in *Cotylocara*, the deflected rostrum is hypothesized to be an adaptation for echolocation. The dense premaxillae—also present in *Xenorophus*—may function as acoustic reflectors that direct sounds anteriorly [4]. If a deflected rostrum is an acoustic adaptation amongst all xenorophids, it is possible that this condition was an exaptation for benthic feeding in the *Inermorostrum* lineage. The rostrum is deflected in many other early diverging odontocetes, including *Simocetus rayi*, *Olympicetus avitus*, *Ashleycetus planicapitis*, and possibly *Mirocetus riabinini*. The earliest diverging odontocetes with a horizontal rostrum are *Agorophius* and *Ankylorhiza*, which are later diverging than Xenorophidae and these simocetid-like odontocetes. This raises the possibility that a deflected rostrum may be the primitive condition within Odontoceti.

6.11. Oral Pathology in Xenorophus

Two specimens have lost several sequential teeth in vivo: maxillary teeth in ChM PV 7677 and mandibular teeth in CCNHM 168 (Figure 33). Maxillary alveoli for C1–PC3 are filled with woven bone in ChM 7677. In CCNHM 168, alveoli for lower left PC1–3 are absent and filled with woven bone. However, the upper left toothrow is not missing alveoli/teeth for any tooth position. Embrasure pits from the absent tooth positions are present between the antagonistic teeth in the left maxilla, indicating that they indeed formed and were emergent at some point earlier in ontogeny, though they are shallower than their counterparts on the right, suggesting partial remodeling. The existence of 'ghost' embrasure pits and the loss of several adjacent teeth indicate that these teeth were lost during life rather than not being formed at all during early development (agenesis). In addition, the left mandible of CCNHM 168 is swollen around the lower PC 4 and possesses a large pathologic fistula developed as a large fenestra on the lateral side of the mandible with a prominent anterior trough. The cause of this lesion and fistula is unclear, but in the case of this individual, likely dates to and was caused by the same injury that resulted in tooth loss. One possibility is periodontal injury resulting in osteomyelitis with a fistula forming as a response to drainage; a similar pathology has been reported in a kentriodontid dolphin mandible [156]. However, the presence of a callus on the right mandible and a lesion at the same location on the left mandible could also indicate a transverse fracture through both mandibles; CT examination will be needed for further investigation. Pathological tooth loss has been identified in extant odontocetes and attributed to trauma in some dolphins but a bone disease in other individuals with widespread bone resorption throughout the rest of the skeleton [157]. Such examples of missing teeth could potentially originate from intraspecific combat (though not considered in modern examples; [157]). Owing to the lack of widespread skeletal pathologies in the rest of the skeleton of CCNHM 168 and ChM PV 7677, these injuries are best interpreted as resulting from injuries sustained during feeding or perhaps agonistic behavior.

Healed mandibular fractures are common in extant *Globicephala*, but are concentrated around the posteroventral part of the pan bone and angular process [158] and are hypothesized to be the result of injuries from stranding events. Identical pathologies consisting of a section of missing teeth with resorbed alveoli have been reported within extant *Delphinus* (individuals of which were otherwise healthy) and likely resulted from some form of trauma [157]. Because two different individuals in the sample of *Xenorophus sloanii* ($n = 7$) are affected by tooth loss and subsequent alveolar resorption, and because these specimens lack further evidence of skeletal pathology, it is possible that this species engaged in risky feeding behavior that induced trauma, perhaps permitted by the relatively large size of this odontocete, second only to species of *Ankylorhiza* spp. In the case of CCNHM 168, the apparent presence of a healed mandibular fracture on the right mandible and a lesion on the left mandible may also suggest some sort of traumatic injury followed by infection that led to mandibular tooth loss. Such an injury could have been the result of stranding (or other impact with the seafloor), intraspecific fighting or other agonistic behavior [159], or failed predation by a larger predator (e.g., *Ankylorhiza*, *Carcharocles angustidens*). The complete resorption of alveoli in both CCNHM 168 and ChM PV 7677 indicates that each individual was able to feed regularly for at least a few months, and that missing several teeth did not affect survival. Some extant odontocetes may survive oral injuries by relying instead on suction feeding [157,159]. The extant sperm whale *Physeter macrocephalus* chiefly uses the dentition and mandible for social behavior and instead relies on gular suction for feeding upon cephalopods [160]; as a result, individuals of *Physeter* occasionally possess congenital deformities including bent, curved, or spiral-shaped mandibles that would otherwise negatively impact the survival of many other odontocete species [133,160–162].

6.12. Locomotion in Xenorophus

Like most other stem odontocetes, Xenorophidae are chiefly known from skulls [3,4,8,9]. Recent studies interpreting vertebral proportions using the methods outlined by Buchholtz [42] have reported partial or nearly complete vertebral columns of stem odontocetes from the Oligocene of South Carolina [163] including *Albertocetus meffordorum* [1] and *Ankylorhiza tiedemani* [37] have revealed the vertebral morphology, vertebral count, and some aspects of locomotor adaptations in early odontocetes. *Albertocetus meffordorum* was proposed to be a Pattern 1 swimmer (sensu [42]) like Basilosauridae and Mysticeti, and relatively wide anterior and mid-caudal vertebrae suggested that *Albertocetus* lacked a transversely narrow caudal peduncle. Because this feature is present in both extant odontocetes and mysticetes, this suggested independent derivation of this feature within each group. This finding was later confirmed by Boessenecker et al. [37], who similarly found transversely wide, circular anterior and mid caudal vertebrae in *Ankylorhiza*, which diverges later on the tree than Xenorophidae.

Vertebral proportions of the nearly complete vertebral column of *Xenorophus sloanii* specimen CCNHM 1077 compare well with *Ankylorhiza tiedemani*, and certain pattern 1 and pattern 2 swimmers in many respects (Figures 77 and 78). The column differs from Pattern 1 swimmers like *Balaenoptera* and *Zygorhiza* in possessing lumbar vertebrae that are anteroposteriorly longer and dorsoventrally deeper than wide (Figure 78); however, unlike some pattern 2 swimmers, like *Delphinapterus* and *Monodon*, *Xenorophus sloanii* possesses thoracic vertebrae that are wider than long; this difference between thoracic and lumbar proportions is similar to *Ankylorhiza* and *Aetiocetus* [37,42]. A slightly less similar condition is present in the toothed mysticete *Coronodon*, though the lumbar vertebrae in *Coronodon* are approximately as wide as they are long [37]; the peak in centrum width, length, and height is also lower in *Coronodon*, with less regionalization of the column than in *Xenorophus* (E. Buchholtz, pers. Comm., 2022). Although there are missing lumbar and caudal vertebrae, the posterior peak in vertebral length (e.g., lumbars, caudals) is more extreme than in *Ankylorhiza*, suggesting greater displacement of the caudal flukes than in *Ankylorhiza* (or *Coronodon*; E. Buchholtz, pers. Comm., 2022). However, *Xenorophus sloanii* differs from *Ankylorhiza* and other Pattern 2 swimmers in lacking foreshortening that extends from the caudal series into the posterior lumbars (Figure 78), indicating the lack of a stiffened caudal peduncle, though the L9-Ca1 appear to represent an anterior stabilized unit. We interpret *Xenorophus sloanii* as a Pattern 1 swimmer, and perhaps a somewhat faster swimmer than *Coronodon* spp. (E. Buchholtz, pers. Comm., 2022) but not *Ankylorhiza*.

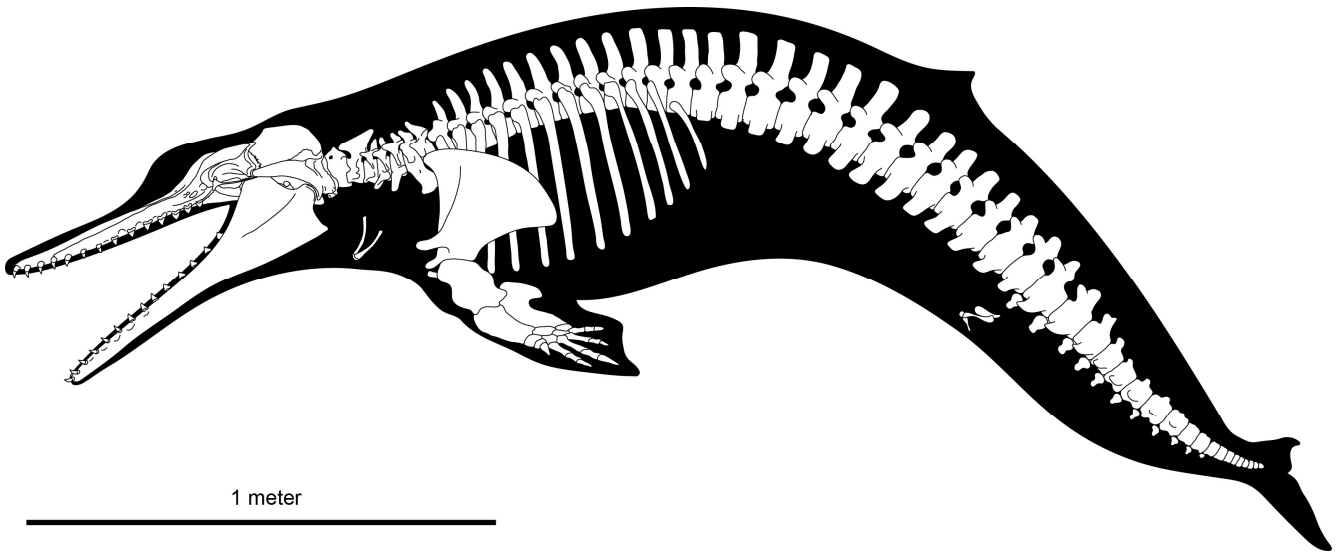


Figure 77. Skeletal reconstruction of *Xenorophus sloanii*, modified from *Albertocetus* skeletal reconstruction by Boessenecker et al. ([1]: Figure 1).

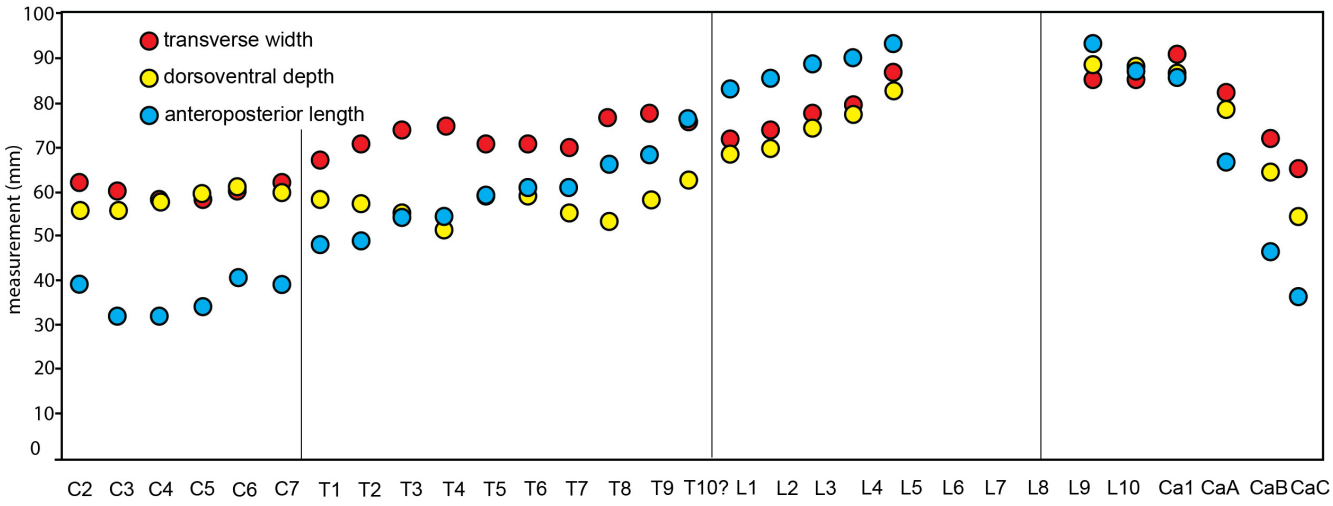


Figure 78. Vertebral proportions of *Xenorophus sloanii* (CCNHM 1077).

6.13. Evolution of Tooth Size in Neoceti

Modern odontocetes differ significantly from their terrestrial ancestors and archaeocete whales by possessing a homodont dentition. Early archaeocetes (e.g., pakicetids, remingtonocetids) retain incisors, canines, premolars, and molars; basilosaurids have canines that are approximately the same size and shape as the incisors and first premolar. However, the remainder of the postcanine dentition of basilosaurids is quite heterodont (e.g., large multicuspate premolars, small low crowned upper molars, small lower molars with distal accessory cusps only), permitting isolated teeth to be identified to position in many cases. This degree of heterodonty dissipated in the archaeocete–neocete transition, with many early Neoceti exhibiting gradational changes in tooth morphology in both toothed mysticetes (e.g., *Coronodon*, *Janjucetus*, *Llanocetus*; [46–48,141,143]) and Oligocene heterodont odontocetes (e.g., Xenorophidae, "waipatiids", "simocetids", "agorophiids", and "squalodontids"; [17,18,25,37]). Crown-clade odontocetes, with few exceptions (e.g., *Inia*, *Platanista*), generally have small teeth of uniform size along the toothrow.

We examined the evolution of tooth size as one aspect of the heterodonty–homodonty transition in Neoceti by recording maximum anteroposterior tooth diameter and plotting it against bizygomatic width (Figure 79). In most cases these were the posteriormost upper cheek teeth; in some cases, a slightly more anterior tooth was measured if the posteriormost teeth were missing, and therefore a slightly larger tooth diameter may be possible (albeit ultimately unknown).

Unsurprisingly, basilosaurid and protocetid archaeocetes possess the absolutely and proportionately largest tooth crowns (Figure 79). The largest tooth amongst all Cetacea is the 2–3 m long tusk boasted by the narwhal (*Monodon monoceros*) and amongst functional non-tusk teeth by the giant sperm whale *Livyatan*, though extreme wear makes the crown size difficult to assess. Archaeocetes show a narrow range of skull width (~30–45 cm) but a wide range in tooth sizes (30–80+ mm). Crown odontocetes on the other hand tend to have absolutely small teeth (3–17 mm) across a wide variety of body sizes (140–600+ mm bizygomatic width), and therefore have the proportionally smallest teeth (0.98–4.24% of BZW; these figures do not include the enlarged tusks of Ziphiidae, adapted for social interaction rather than feeding, and a few physeteroids owing to crown incompleteness). Toothed mysticetes occupy a zone on the scatterplot overlapping with archaeocetes and intermediate between them and crown odontocetes. Aside from a couple of outliers (e.g., *Llanocetus*), toothed mysticetes follow a similar trend as archaeocetes.

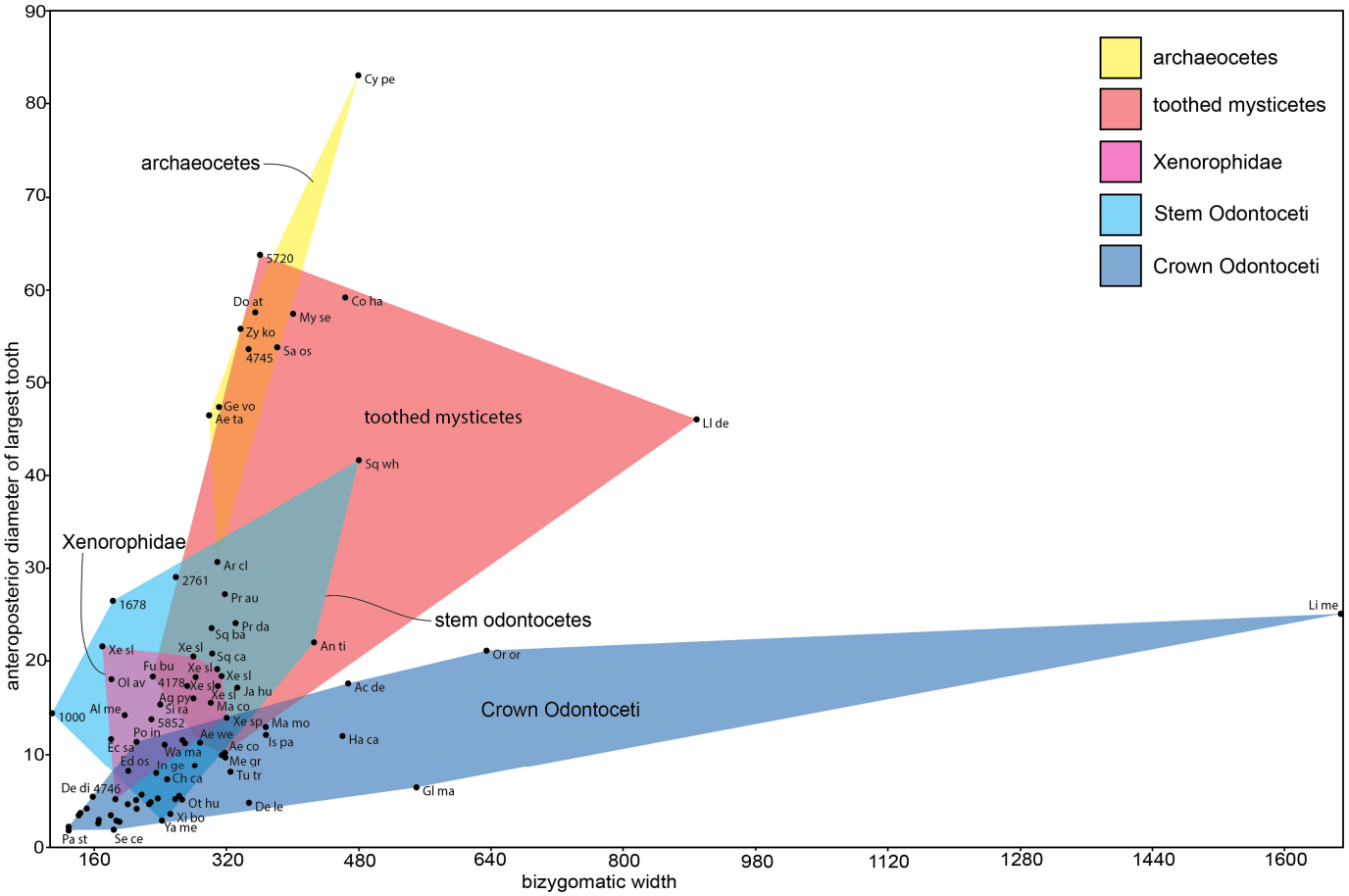


Figure 79. Scatterplot of anteroposterior diameter of largest tooth and bizygomatic width in Cetacea. Measurements are in mm. Taxon labels are first two letters of binomial names (after [93]), or specimen number; see Supplementary File S3.

Stem odontocetes, including xenorophids, barely overlap with archaeocetes (and only with *Artiocetus clavus*) but generally fill an intermediate zone of morphospace between archaeocetes and odontocetes, and slightly overlapping with some modern odontocetes (Figure 79). Stem odontocetes have a range of tooth sizes (5–28 mm) over a relatively narrow range of body sizes (150 to 430 mm bizygomatic width), though not as narrow as archaeocetes (298–600 mm). A somewhat different pattern emerges when tooth diameter is plotted against bizygomatic width. Crown odontocetes have a nearly horizontal zone in the scatterplot, possessing teeth between 1 and 6% of bizygomatic width. Archaeocetes occupy a narrow zone with teeth 10–17% of bizygomatic width. Xenorophids do not overlap with archaeocetes at all and occupy a much wider area of the scatterplot, with tooth sizes between 2 and 13% of bizygomatic width, and generally smaller body sizes than archaeocetes. Remaining stem odontocetes are slightly expanded from this xenorophid space, having a wider envelope of tooth sizes (1–15%) and body sizes (140–480 mm bizygomatic width). Stem odontocetes and xenorophids both overlap somewhat with crown odontocetes. Toothed mysticetes, on the other hand, are the only Neoceti to overlap with archaeocetes, and occupy a wide zone of variation (tooth size 3–18% of bizygomatic width, and BZW of ~20–90 cm), largely occupying a space between archaeocetes and crown odontocetes, and slightly overlapping with the latter. Aside from their initial large tooth size, toothed mysticetes seem to have evolved somewhat in parallel with stem odontocetes. The earliest diverging toothed mysticetes (*Coronodon*, *Mystacodon*) have relatively large teeth (12.7 and 14.3% BZW, respectively), similar in size and proportion to archaeocetes,

and later taxa like *Aetiocetus* spp. trended towards microdonty in the zone of overlap (3% of bizygomatic width) with crown odontocetes.

The evolution of tooth size in Cetacea was further investigated through time (Figure 80). Middle-late Eocene archaeocetes have proportionally large teeth, with basilosaurid whales in particular having teeth ranging from 14.1–17.3% of bizygomatic width; archaeocetes have an average of 15–16% during the Bartonian and Priabonian. Toothed mysticetes have a wider range of tooth sizes, ranging from 17.7% in the unnamed coronodonid ChM PV 5720 to as small as 3.1–3.8% in *Aetiocetus* spp. Toothed mysticetes have a smaller average tooth size during the Eocene–Oligocene than Eocene archaeocetes, ranging from 7.9–9.8%. This large variation in tooth size amongst toothed mysticetes reflects the highly disparate feeding morphology and behaviors of these taxa [4,46,47,138,141,142].

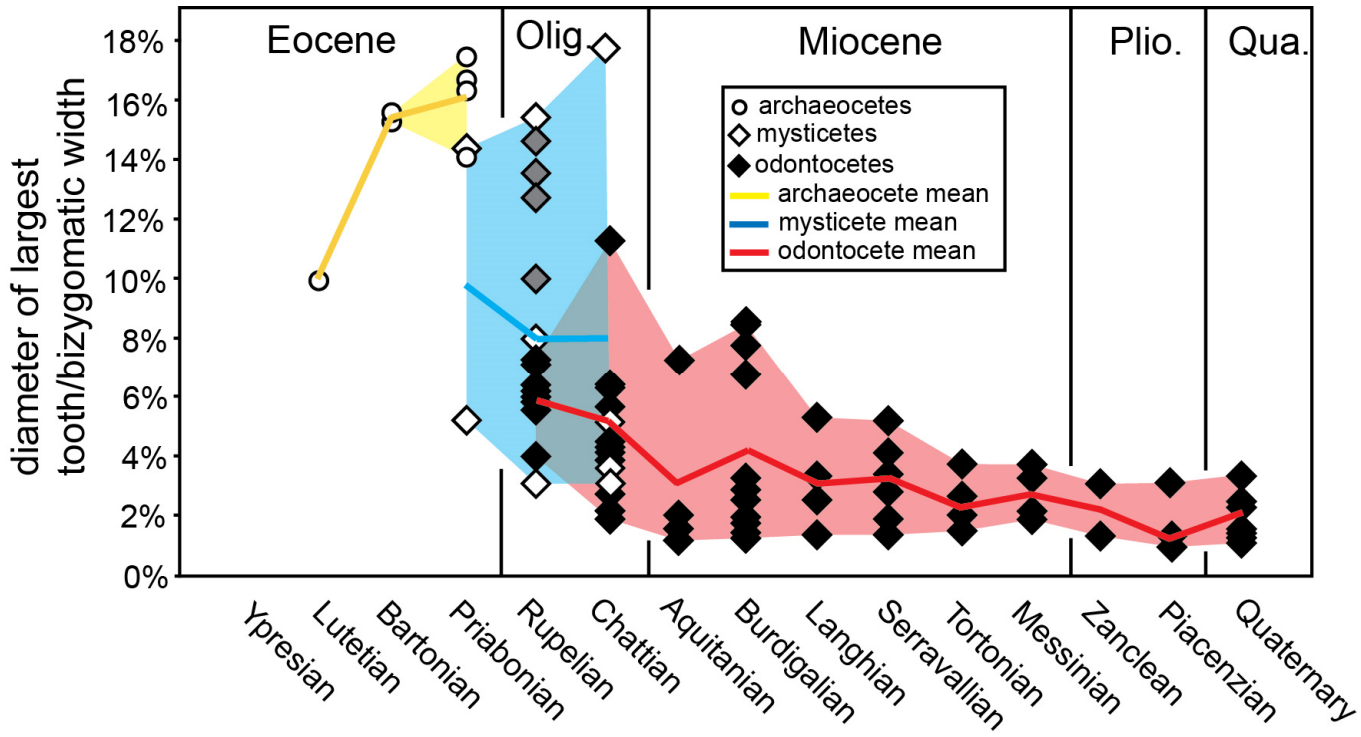


Figure 80. Plot of anteroposterior diameter of largest tooth as a proportion of bizygomatic width through time, measurements pooled by international marine stages.

Odontocetes, on the other hand, undergo a rapid and early decrease in tooth size relative to their archaeocete ancestors; Rupelian odontocetes range from 4% (*Ediscetus*) to 7.3% (*Xenorophus*), and a large gap is present between the archaeocete and odontocete envelopes of tooth size variation through time (Figure 80). A larger range is present in Chattian odontocetes, with a minimum tooth size of 1.8–1.9% (*Otekaikea* spp.) and a maximum of 11.2% in undescribed agorophiid-grade odontocete ChM PV 2761. We expect further study of Rupelian odontocetes to result in a similar range of tooth sizes. Tooth size continues to decrease in the Miocene, with maximum tooth size decreasing (maximum tooth size 7.3–8.5% in the Aquitanian and Burdigalian) by the middle Miocene (ranging from 2.4 to 5% in the Langhian) owing to the extinction of squalodontid-grade odontocetes. Modern ranges of tooth size, between 1.5 and 3% of bizygomatic width, become established in the middle to late Miocene. Average odontocete tooth size begins at 5.9% in the Rupelian and 5.2% in the Chattian, drops to 3–4% in the early and middle Miocene, and further drops to 2.7–1.1% in the late Miocene through the Holocene (Figure 80).

Tooth size seems to vary much more than maxilla length within Xenorophidae (tooth size 3–13% of BZW, RPI 2.4–4.0) and toothed mysticetes (tooth size 3–18% BZW, RPI 0.9–1.9) relative to other stem odontocetes (tooth size 1–9% BZW, RPI 0.9–4.8) or Crown Odontoceti (tooth size 1–4% BZW, RPI 0.8–7.0). This suggests that, as far as feeding morphology is concerned, tooth size does not follow a simple pattern of size decrease with increasing rostral length. This suggests that the retention of large teeth may have been functional in early Neoceti, and perhaps multicuspate teeth served the same function as multiple smaller unicuspid teeth. Selection towards multicuspate teeth, homogenization of the toothrow with teeth resembling premolars of basilosaurid ancestors, and incipient polydonty may explain the wide variation in tooth morphology amongst stem odontocetes.

6.14. Evolution of Rostral Proportions in Neoceti

Recent studies have linked the relative length of the rostrum in cetaceans with different feeding adaptations [2,132,164]. Relatively shorter rostra characterize many suction feeding specialists and small-bodied paedomorphic cetaceans, frequently co-occurring with toothlessness [2,132], whereas elongated rostra are typically thought to correspond to piscivory [2,164]. Mandibular Bluntness Index (MBI) was introduced by Werth [132], a metric approximating mouth shape in odontocetes by taking the width of the mandibles across the condyles and dividing it by mandibular length; higher scores have a blunter mouth and lower scores represent a longer mouth [132]. While this is useful for modern odontocete skeletal specimens with the mandibles in articulation, the delicate mandibles are rarely completely preserved, undistorted, and in association with skulls in the fossil record; when isolated, mandibles are often non-diagnostic and determining MBI may not be informative. For example, within the available sample of *Xenorophus*, only four out of eleven skulls preserve mandibles (CCNHM 104, 168, 1077, 8720). Of these, only one specimen (CCNHM 168) preserves complete left and right mandibles; however, these are still too distorted to accurately measure MBI.

The metric Rostral Proportion Index (RPI) was established by Boessenecker et al. [2] to easily quantify rostral proportions in the majority of cetacean specimens preserving nearly complete rostra by measuring the length of the maxilla from its terminus to the antorbital process and dividing it by antorbital width, with low scores (<1.5) indicating brevirostry, medium scores (1.5–3.0) indicating mesorostry, and high scores (>3.0) indicating longirostry. This method permits a much larger sample to be analyzed than the more recently proposed Rostral Index (RI; [164]), measured by dividing condylobasal length by braincase length; calculation of RI can only be attempted for rare, virtually complete skulls without any damage to the tip of the rostrum. This method, furthermore, does not distinguish between rostral shapes and is generally useful only for distinguishing between longirostrine and 'hyperlongirostrine' taxa, regardless of rostrum width.

Brevirostry and longirostry have evolved in parallel multiple times, but analyses of RPI indicate the influence of stabilizing selection and an optimal rostrum shape, with a rostrum approximately 2–2.5 times as long as it is wide, such as the condition in modern bottlenose dolphins, *Tursiops truncatus* [2]. Xenorophidae are noteworthy for their extreme disparity in RPI for a relatively small clade of short chronologic range, with extremely long rostrum present in an unnamed taxon ChM PV 4746 (RPI = 3.89), and the brevirostrine dwarf toothless xenorophid *Inermorostrum xenops* (RPI = 1.19). *Inermorostrum* was the geochronologically earliest odontocete to evolve suction feeding adaptations [2]. To investigate RPI in *Xenorophus sloanii* and the influence of body size, we plotted RPI against bizygomatic width for archaeocetes, xenorophids, other stem odontocetes, crown odontocetes, toothed mysticetes, and chaeomysticetes (Figure 81).

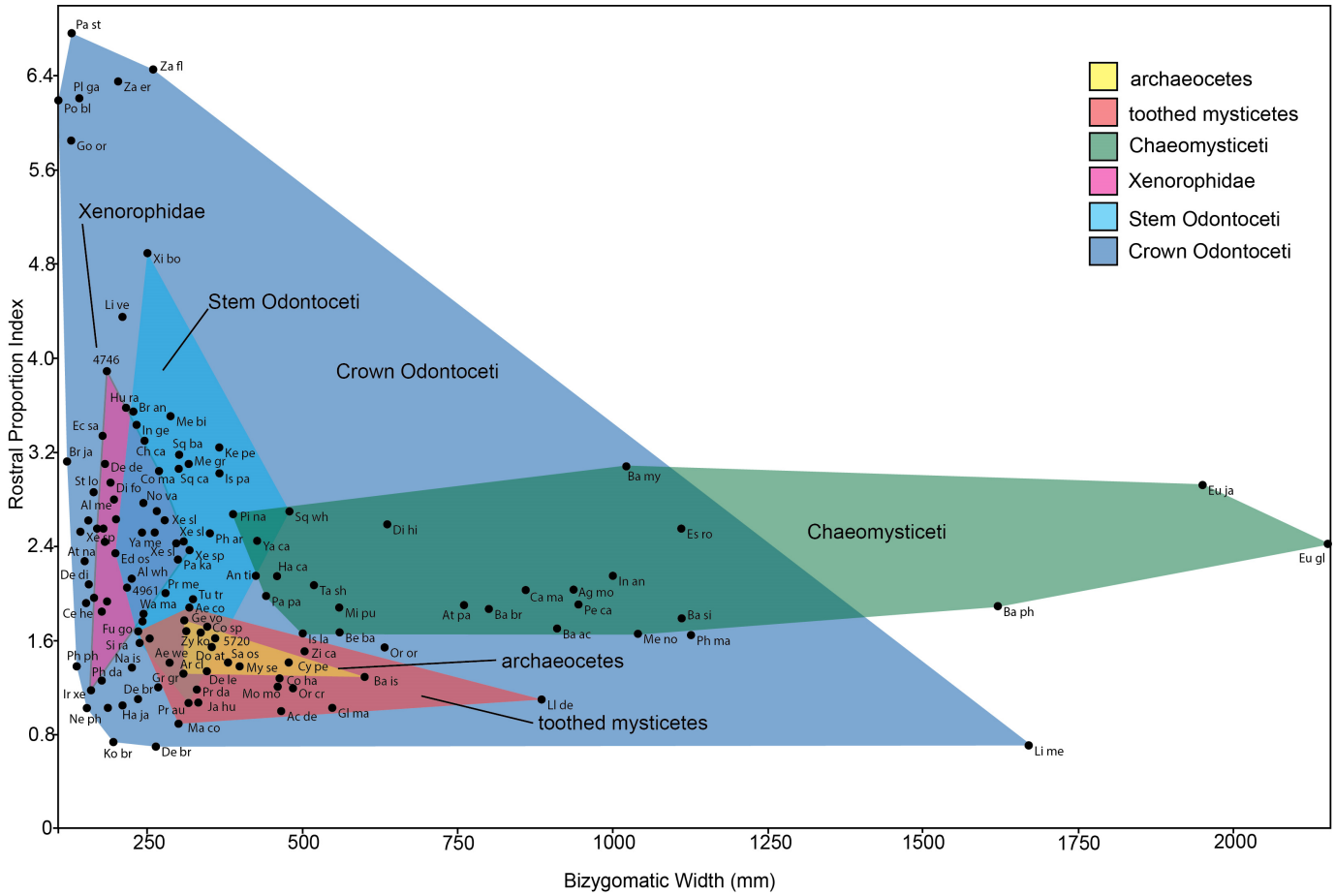


Figure 81. Scatterplot of rostral proportion index (RPI) and bizygomatic width in Cetacea. Measurements are in mm. Taxon labels are first two letters of binomial names (after Muizon et al., [93]), or specimen number; see Supplementary File S3.

Archaeocetes occupy a narrow band of this plot centered on an RPI of 1.6 and a range of BZW from about 300 to 600 mm; toothed mysticetes have a similarly narrow range of variation, completely enveloping the archaeocete zone within with RPI ranges from 1.8 to 0.9 and BZW ranges from 250 to 900 mm (Figure 81). Chaeomysticetes exhibit a wide range of body sizes (BZW ranging from 400 mm to 2200 mm) yet occupy a relatively narrow band of RPI, roughly 1.7–3.0. This suggests that the mysticete rostrum is constrained to a particular shape by the demands of filter feeding. In *Coronodon havensteini*, the rostrum of juveniles is nearly identical in proportion to that of adults, suggesting constraint on the shape throughout growth [46]. However, in eomysticetid whales, such as *Waharoa ruwhenua*, rostrum length increases considerably during postnatal ontogeny, interpreted as a peramorphic adaptation towards skim feeding [146].

Xenorophids do not overlap with toothed mysticetes (Figure 81), generally exhibiting higher RPI values (2.4–4.0), and overlapping in body size only with the smallest toothed mysticetes (e.g., Aetiocetidae, BZW = 230–318 mm). *Inermorostrum xenops* is an obvious exception, with RPI = 1.19, but, at approximately 145 mm BZW (extrapolated from postorbital width and the ratio of postorbital width to bizygomatic width in *Echovenator*), it is still far smaller than the smallest toothed mysticete, *Fucaia* (BZW = 230 mm). With an RPI of 2.37–2.62 and BZW of 279–318 mm, *Xenorophus sloanii* plots closest to other stem odontocetes like *Patriocetus kazakhstanicus*, *Phoberodon arctirostris*, and *Yaquinacetus meadi*. *Xenorophus sloanii* has a similar BZW to *Tursiops truncatus*, but with a longer RPI. Later diverging stem odontocetes have a larger minimum BZW of 200–250 mm, but indicate continued expansion of the RPI minimum and maximum along the odontocete stem, with

some brevirostrine 'squalodonts' (*Prosqualodon davidis*; RPI = 1.18) near mammalodontid toothed mysticetes (RPI= 0.89–1.08), some 'mesorostrine' (RPI = 2.2–2.5) large-bodied apex predators pushing the boundaries of body size upwards of 450 mm BZW (e.g., *Phoberodon arctirostris*, *Ankylorhiza tiedemani*, *Squalodon whitmorei*), many small-bodied species with generalist RPI proportions (e.g., *Waipatia*, RPI = 1.82), and at least one longirostrine dolphin (*Xiphiacetus bossi*, RPI = 4.89).

Crown odontocetes are clustered towards the small-bodied and brevirostrine–mesorostrine edge of the plot (Figure 81), including small-bodied piscivorous mesorostrine dolphins like delphinines (*Delphinus*, *Stenella*, *Lagenorhynchus*, *Tursiops*, *Steno*), some kentriodontids (*Atocetus*, *Delphinodon*, *Kentriodon* spp., *Wimahl*), and small to medium-sized brevirostrine piscivorous and/or teuthivorous crown odontocetes, like *Kogia*, *Orcaella*, *Denebola*, *Phocoena*, and *Neophocaena*; most of these taxa are between 200 and 400 mm BZW. Outliers of this cluster are either extant or extinct taxa with unique feeding morphologies (e.g., *Monodon*).

Two brevirostrine giants, *Orcinus* and *Livyatan*, also possess massive teeth and are either known or hypothesized macrophagous apex predators [130,165]. Curiously, both possess a more brevirostrine snout than other hypothesized macrophagous odontocetes (e.g., *Ankylorhiza*, *Squalodon*). If *Livyatan* and *Orcinus* evolved from ancestors with some suction feeding adaptations, brevirostry was perhaps an exaptation towards macrophagy. Many deep-diving teuthophagous odontocetes have evolved large body size and maintained mesorostry or even longirostry, such as *Physeter* (RPI = 1.65, BZW = 1126 mm) and *Berardius* (RPI = 1.67, BZW = 560 mm).

Few odontocetes exhibit an RPI between 5.7 and 4.0, with the exception of *Lipotes vexillifer* and *Xiphiacetus bossi*. The latter bears a highly elongate premaxilla, and, therefore, is actually hyperlongirostrine, as opposed to *Lipotes*. A cluster of small-bodied (200–300 mm BZW) odontocetes with hyperlongirostry (RPI 5.7–6.76; Figure 81) includes extinct and extant Platanistidae (*Platanista*, *Zarhachis*), an extant pontoporiid (*Pontoporia*), an extinct lipotid (*Parapontoporia*), and extinct Allodelphinidae (*Goedertius*, *Zarhinocetus*). This cluster may suggest the existence of a second adaptive peak in addition to the small-bodied mesorostrine morph typified by extant Delphininae. Few studies have evaluated the functional significance of hyperlongirostry and hypotheses include hyperlongirostry being a foraging specialization for small fish using rapid lateral snapping [2] or billfish-like clubbing of fish with the rostrum in some odontocetes and rapid lateral snapping in others [164]. The latter study found a loose correlation between longirostry and climate. However, the reduction in longirostry and lower mean RPI in late Neogene and extant odontocetes in this study and Boessenecker et al. [2] is likely driven by the decline of hyperlongirostrine clades (Allodelphinidae, Eurhinodelphinidae, Platanistidae; e.g., [166]) and simultaneous proliferation of delphinoids, which are typically brevirostrine or mesorostrine. Whether or not this represents a case of competitive exclusion, or response to environmental change (e.g., [166]), warrants further study. Delphinoids are some of the most adept echolocators [167], and perhaps longer rostra may instead be related to less precise biosonar in non-delphinoids. Likewise, most taxa with hyperlongirostry (*Zarhinocetus*, *Zarhachis*, *Inia*, *Lipotes*) included in morphometric analyses of cochlear morphology fall outside the narrow band high frequency envelope [167]. However, recent study of the longirostrine eurhinodelphinid *Xiphiacetus cristatus* found that its cochlear morphology places it near extant odontocetes with narrow band high frequency hearing capabilities such as *Phocoena*, *Phocoenoides*, and *Kogia* [168]. Future studies should examine a possible relationship between RPI, echolocation ability, environmental changes, and other factors.

6.15. Evolution of Orbit Size within Odontoceti

The size and orientation of the eyes frequently relates to hunting or foraging behavior [53,93] and may inform interpretations of the paleobiology and ecology of *Xenorophus*. We investigated orbit size and orientation in *Xenorophus* by expanding a dataset focused on archaeocetes and mysticetes first published by Muizon et al. [93] by including measurements from photographs derived using ImageJ for specimens of *Xenorophus* (n = 7) and 106

other extinct and extant odontocetes (Figure 82). To this dataset we also added additional Oligocene mysticetes (n = 3; *Eomysticetus*, *Micromysticetus*, *Fucaia* sp.). This prior study plotted orbital angle against the relative orbit size (orbit diameter divided by bizygomatic width) and found that toothed mysticetes generally possessed larger orbits (relative orbit size 23–34% of BZW) that were frequently angled anterolaterally (orbital angles as low as 53°). Archaeocetes (chiefly protocetids and basilosaurids) occupied a more restricted zone (relative orbit size 14–24% BZW, orbital angles 83–70°). Chaeomysticetes, on the other hand, generally had more laterally facing orbits (orbital angle 65–90°) that were smaller (relative orbit size 27–8% BZW).

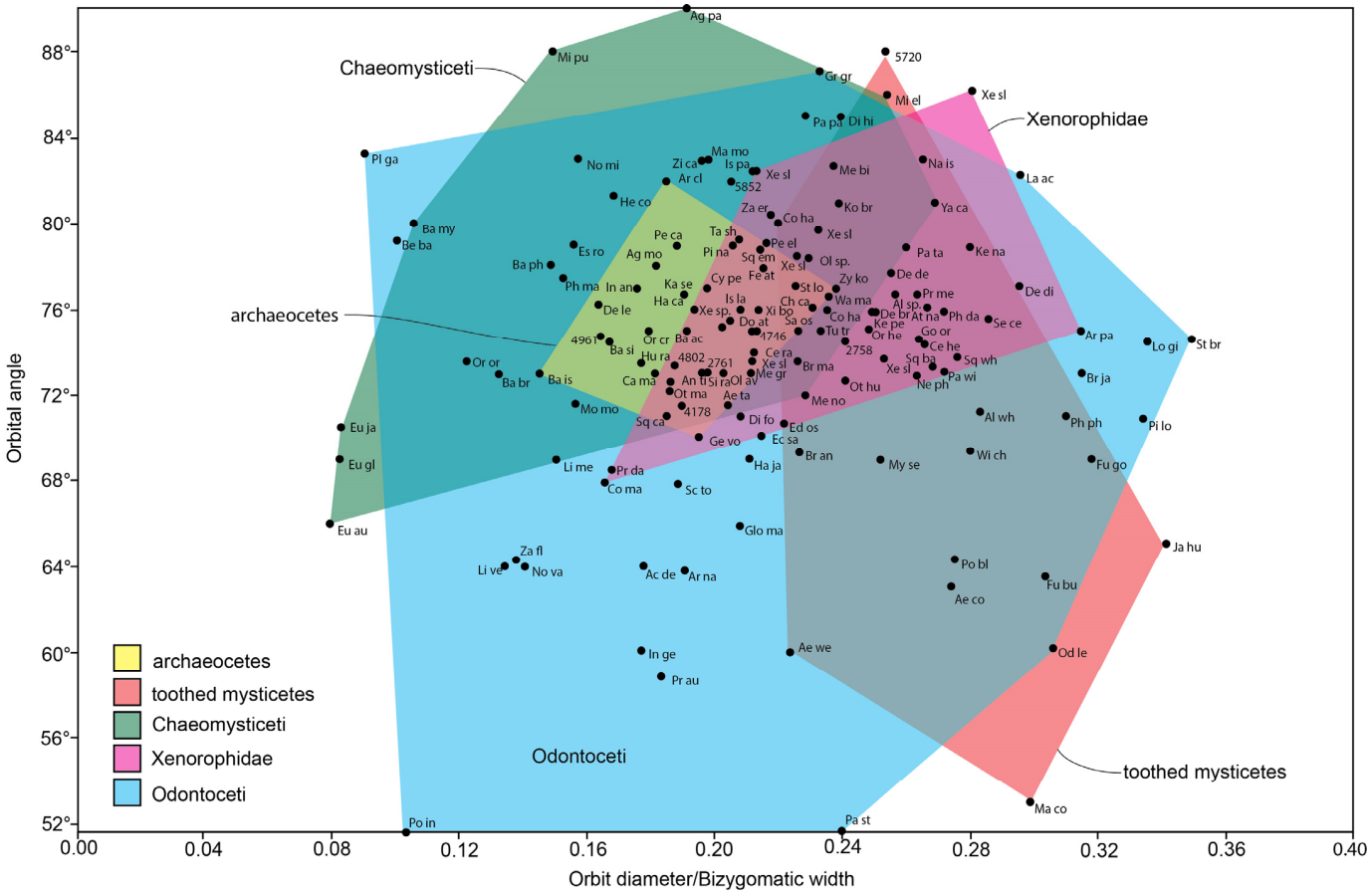


Figure 82. Scatterplot of orbital angle and orbit diameter as a proportion of bizygomatic width in Cetacea. Taxon labels are first two letters of binomial names (after [93]), or specimen number; see Supplementary File S3.

Xenorophidae occupied a zone shared by toothed mysticetes with laterally facing orbits, large-eyed archaeocetes, as well as the larger-eyed chaeomysticetes (relative orbit size 16–30%, orbital angles 70–85%; Figure 82). Odontoceti occupy a very wide zone across this morphospace, enveloping the zones of nearly every other group aside from right whales (Balaenidae) and Mammalodontidae. Though little signal is evident at this level of detail, the outliers warrant comment. *Platanista gangetica* is placed on one extreme, with proportionally tiny orbits (9% BZW) that face laterally. *Platanista* is sometimes referred to as the "blind river dolphin", has uniquely tiny eyes, and is thought to rely upon echolocation to navigate the perpetually murky waters of the Indus and Ganges River basins [53,169,170]. A close relative, *Pomatodelphis inaequalis*, bears similarly tiny eyes (10% BZW) but they face anterolaterally (52° orbital angle); *Pomatodelphis* has been recovered from nonmarine deposits of the Gulf Coastal Plain [171] and, similarly, may have inhabited low visibility rivers. Yet another "river" dolphin, *Parapontoporia*, from the late Neogene of the Pacific

Coast of North America, previously thought to be completely marine [172], has also been recovered from nonmarine deposits [173]. *Parapontoporia sternbergi* possesses relatively large orbits that also face anterolaterally, perhaps suggesting foraging for small fish in shallow but clear coastal waters. Some of the largest orbits among the Odontoceti are possessed by a variety of small-bodied delphinoids, including *Steno bredanensis*, *Piscolithax longirostris*, *Phocoena phocoena*, and *Brachydelphis jahuayensis*, the extant species of which are small-bodied active echolocating predators that consume pelagic to demersal fish, cephalopods, and crustaceans [130].

A recent and more elaborate study by Churchill and Baltz [53] investigated the interplay between orbit size evolution and the origin of echolocation within the Odontoceti. No change in orbit size was apparent at the base of Odontoceti, which is reinforced by the results here showing that Xenorophidae bear relatively similar orbit sizes and angles to archaeocetes and some toothed mysticetes. Large orbits in small cetaceans (e.g., Phocoenidae, *Cephalorhynchus*, and probably *Parapontoporia*) are likely driven by paedomorphosis [53]. These authors likewise found a similar link between small eyes and murky freshwater habitats, and also highlighted a slight increase in orbit size within the deep-diving Ziphiidae [53].

In sum, *Xenorophus sloanii* bears orbits that are laterally facing, like basilosaurid ancestors, and its modestly sized orbits are somewhat enlarged relative to basilosaurids and similar to many extant delphinoids. The retention of basilosaurid-like orbits might suggest that vision was no less important in the foraging ecology of *Xenorophus* than it was to basilosaurids.

6.16. Evolution of Temporal Fossa Size in Odontoceti

Xenorophus sloanii contrasts strongly with Crown Odontoceti in possessing a relatively large temporal fossa, similar to Eocene basilosaurid whales. The temporal fossa accommodates the jaw-closing muscles, chiefly the temporalis. The volume of jaw-closing muscles in mammals is strongly correlated with bite force [135]. Most crown Odontocetes possess a temporal fossa that is roofed over by the frontal; the temporal fossa is additionally anteroposteriorly shortened. In Crown Mysticeti, the temporal fossa becomes transversely wide and anteroposteriorly foreshortened as well. Reduction in size of the temporal fossa, and hence volume and length of the temporalis, is correlated with decreasing bite force and mastication in Cetacea [174].

The importance of jaw-closing muscles in *Xenorophus* and other Cetacea was estimated by evaluating the relative size of the temporal fossa by focusing on the greatest anteroposterior length of the fossa (posteriormost point on nuchal crest to anteriormost point of orbitotemporal crest or postorbital ridge) and plotting it against bizygomatic width (Figure 83). Two-dimenstional measurements were collected from photographs using ImageJ 1.50i.

Within archaeocetes, stem odontocetes, crown odontocetes, and toothed mysticetes, temporal fossa length is tightly correlated with bizygomatic width, though each group differs from the next (Figure 83). Archaeocetes occupy a steep zone with proportionally large temporal fossae (70–102% of BZW), whereas toothed mysticetes exhibit slightly smaller temporal fossae (50–91% of BZW). Most early diverging stem odontocetes (Xenorophidae, simocetid-grade dolphins, agorophiid-grade dolphins) exhibit a similar range with toothed mysticetes (50–70%). Crown odontocetes exhibit somewhat smaller temporal fossae, typically measuring 30–50% of BZW, with some outliers such as *Platanista* (65%), Inia (67%), *Brujadelphis* (60%), *Delphinodon* (60%), *Delphinapterus* (60%), and *Denebola* (65%). Size does not explain temporal fossa length within Crown Mysticeti, as there seems to be a ceiling (400 mm long temporal fossa) and floor (150 mm long temporal fossa) regardless of body size, with the envelope of these taxa occupying a horizontal zone on the plot.

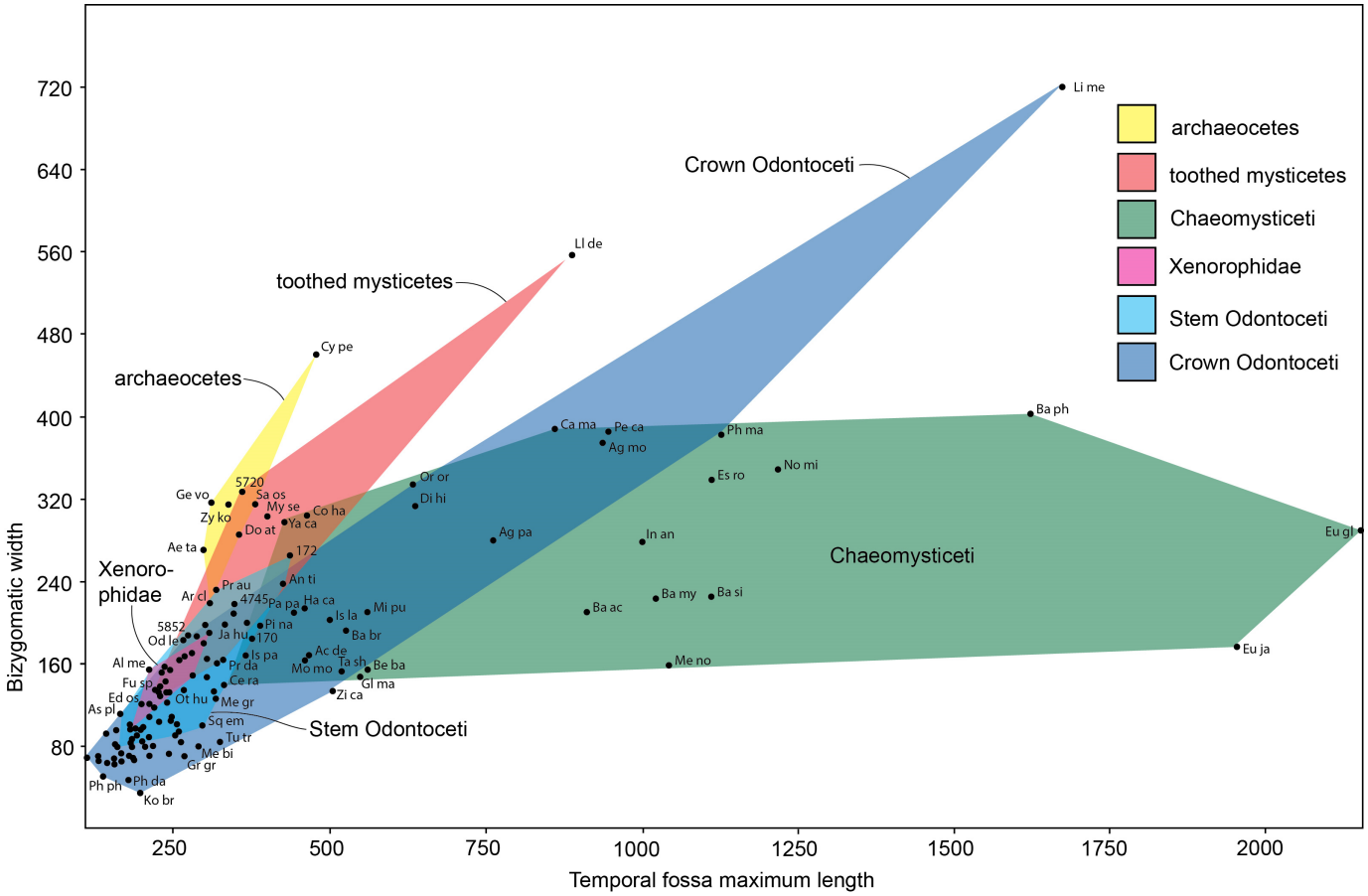


Figure 83. Scatterplot of temporal fossa length and bizygomatic width in Cetacea. Measurements in mm. Taxon labels are first two letters of binomial names (after [93]), or specimen number; see Supplementary File S3.

Xenorophus sloanii bears relatively large temporal fossae, measuring 53% of BZW in subadult specimens (CCNHM 104) and 60–61% in mature specimens (CCNHM 168, 1077; Figure 83). These values are somewhat smaller than in basilosaurids, yet represent the largest temporal fossae amongst Xenorophidae and some of the proportionally largest fossae of all Odontoceti, second only to some simocetid-grade taxa (*Ashleycetus planicapitis*, ChM PV 4178; 68% BZW) and *Prosqualodon australis* (73%). The proportional length of the temporal fossa in *Xenorophus* is similar to the large-bodied macrophagous dolphin *Ankylorhiza*. This evidence suggests that a powerful bite was still important in the feeding behavior of *Xenorophus*.

This simple analysis indicates that temporal fossa length became successively shorter, in parallel, within stem odontocetes and stem mysticetes, and smaller again in crown odontocetes (Figure 83). Within odontocetes, the reduction in temporal fossa length is likely explained by the change in shape of the fossa and expansion of the neurocranium. This suggests a lesser reliance on bite force through time, and may correspond to greater reliance on suction feeding within crown odontocetes [132], especially within the Ziphiidae, Physeteridae, and Delphinoidea. It is also possible that the evolution of biosonar permitted hunting behavior targeting smaller prey and less reliant upon powerful bite force. However, this analysis uses a single metric and makes no attempt to examine the shape or volume of the temporalis musculature. Such changes might not only affect absolute bite force, but potentially the speed of jaw closure. Future studies of temporal fossa morphology and bite force should explore these factors and their relation to other aspects of feeding morphology (e.g., rostral proportions, tooth size, tooth count).

6.17. Evolution of Polydonty in Neoceti

All specimens of *Xenorophus* with a complete maxilla (USNM 11049, CCNHM 104, 168, 8270, ChM PV 4823, 7677), preserve a minimum of nine postcanine teeth, two more than the primitive dental formula for mammals. In general, most xenorophids (except for the toothless *Inermorostrum*) show such incipient polydonty (*Albertocetus*: 9, based on ChM PV 4834; *Cotylocara*: $n = 11$; *Echovenator*, $n = 9$ or 10). Uniquely among these, however, is that the available sample of *Xenorophus sloanii* exhibit variation in tooth count. CCNHM 168 has ten, rather than nine postcanine teeth as in all other specimens. This is reflected in the mandible which possesses nine (rather than eight) lower postcanine teeth. Based on comparison with the holotype and CCNHM 104, CCNHM 168 has an identical number of double-rooted postcanines ($n = 6$), whereas it has four completely single-rooted anterior postcanine teeth versus only three in other specimens. We hypothesize that the PC2 or PC3 position was duplicated in CCNHM 168.

Several hypotheses have been advanced to explain how additional tooth positions were gained to achieve polydonty in the earliest odontocetes. Fordyce [175] suggested that the intercalation of deciduous and permanent teeth could have led to an increase in tooth count, based on the discovery of a squalodontid-grade dolphin mandible with supernumerary single-rooted teeth positioned between double-rooted postcanine teeth from the Oligocene of New Zealand. Studies of embryonic development in mammals indicate that different genes control tooth shape, with Bmp4 expressed in the incisor field and Fgf8 expressed in the postcanine field, and where these genes overlap, they produce a canine [150]. Expansion of this overlapping field results in the addition of caniniform, unicuspid teeth [150].

This pattern of tooth count variation within *Xenorophus sloanii* lends the first paleontological evidence to support the hypothesis of Armfield et al. [150] regarding the molecular underpinning of polydonty in Neoceti. In *Xenorophus*, the number of double-rooted molariform postcanines does not vary, but in specimens with a higher tooth count (CCNHM 168), it is achieved with teeth in the region of overlap between Bmp4 and Fgf8. Curiously, this region of the dentition in *Xenorophus* also exhibits the highest degree of tooth asymmetry (C1–PC6; see *6.9 Directional Asymmetry of the Rostrum, Palate, Dentition, Mandibles, Neurocranium, and Vertebrae of* Xenorophus).

Boessenecker et al. [46] investigated the evolution of polydonty in Neoceti using a dataset focused on mysticete phylogeny. Their taxonomic sample included 10 odontocetes, with *Xenorophus* and *Echovenator* sampled among xenorophids. They traced upper and lower tooth counts on two sets of trees, one derived from an analysis with equal weights and another using implied weighting; the trees from the former had a monophyletic Mysticeti, whereas the trees from the latter had Coronodonidae, *Mystacodon*, *Borealodon*, and *Metasqualodon* in a more basal position outside of Mysticeti and Neoceti. Those authors found evidence for separate origins of polydonty in the upper teeth of odontocetes and mysticetes, but a more complicated picture emerged for the mandibular teeth. Under their implied weights analysis, mandibular polydonty evolved once in the most recent common ancestor of Coronodonidae and all neocetes. By contrast, on their equal weights tree, mandibular polydonty originated twice, once in odontocetes and again in mysticetes (e.g., [46]). In the present study, we found support for separate origins of polydonty in the lower dentition of Mysticeti and Odontoceti (Figure 84); we could not test dual origins for maxillary polydonty because our sample did not include any mysticetes with nine or more postcanine teeth (i.e., *Aetiocetus polydentatus*). Our conclusions regarding separate origins for mandibular polydonty are not that surprising given that our single MPT has a monophyletic Mysticeti that includes *Mystacodon* and Coronodonidae, much like the equal weights trees of Boessenecker et al. [46].

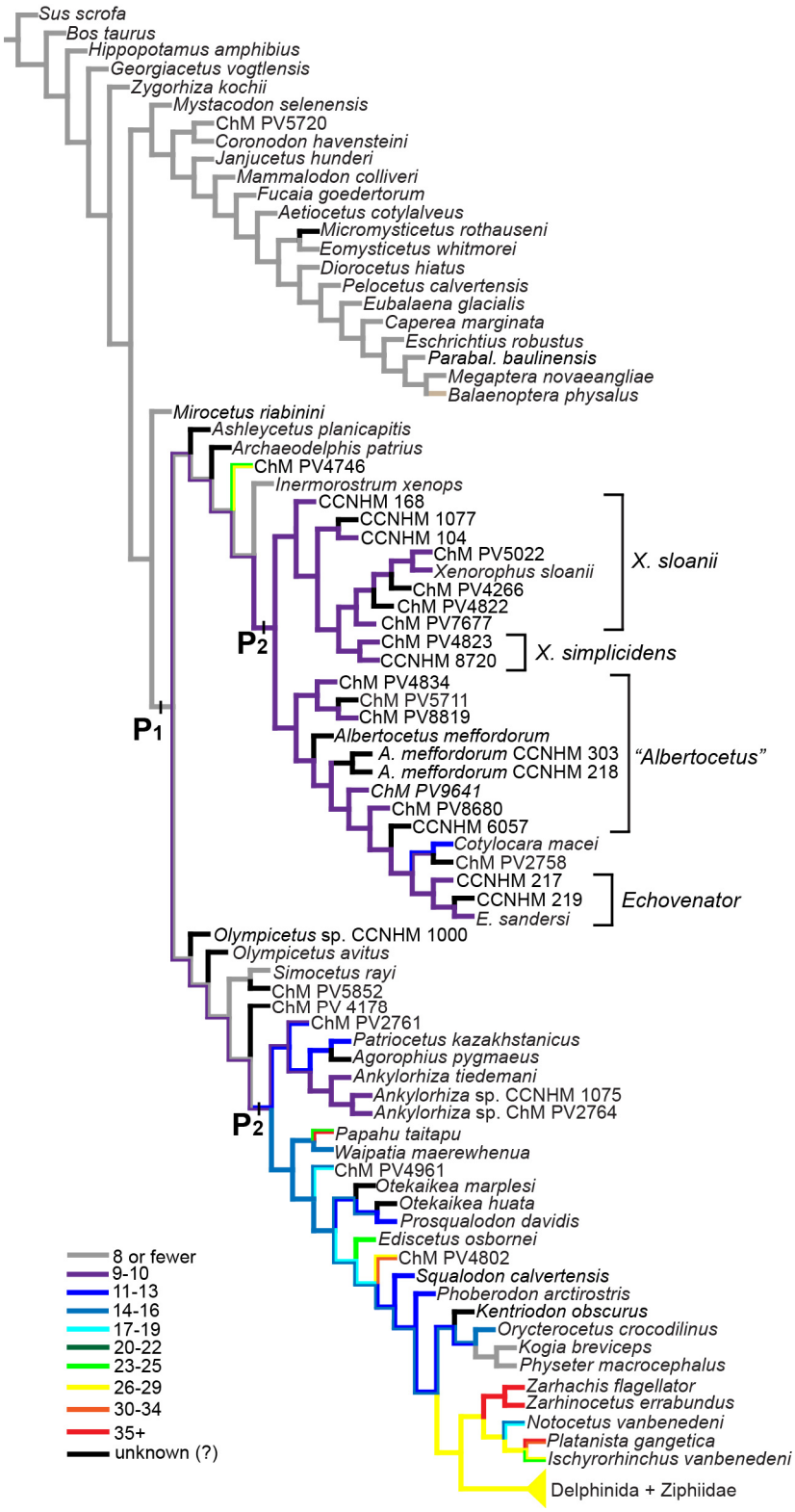


Figure 84. Parsimony-based ancestral character state reconstruction of polydonty within Cetacea, based on maxillary tooth count and 32, and reconstruction of polydonty marked with 'P1' using acctran optimization and 'P2' using deltran optimization.

More surprisingly, we found it equally parsimonious for polydonty in the upper and lower dentition to have evolved once (acctran) or twice (deltran) within Odontoceti, once in Xenorophidae and again on the stem leading to crown Odontoceti (Figure 84). Whereas the most recent common ancestor of the subclade within Xenorophidae including *Xenorophus*, *Albertocetus*, *Cotylocara*, and *Echovenator* is reconstructed as being polydont with 9–10 postcanine upper teeth and 12–13 total mandibular teeth, the number of teeth at the origin of Xenorophidae is unclear. This is largely a result of conflicting signals from the two most basal xenorophids: *Inermorostrum* has no maxillary teeth and the number of mandibular teeth is unknown, whereas the unnamed taxon represented by ChM PV4746 is clearly polydont (between 20 and 29 maxillary teeth). The ambiguous optimizations are also influenced by the non-polydont *Simocetus*, which has 7 maxillary teeth and 11 lower teeth, and is positioned fairly basal within Odontoceti. The most effective route to resolving whether polydonty evolved once or twice within Odontoceti is to determine the tooth count of *Olympicetus*, currently coded as "?". Given that it is more basal than *Simocetus*, its morphology could decisively resolve this uncertainty. Though not coded into our matrix, *Olympicetus thalassodon* was published while this study was under review [176]; crucially, this taxon presents a tooth count similar to *Simocetus* and Basilosauridae and lacks polydonty, further suggestive of multiple origins of polydonty within Odontoceti.

6.18. Evolution of the Articular Process of Odontocete Periotics

Most specimens of *Xenorophus sloanii*, and other xenorophids, possess a small to moderately sized articular process of the periotic. This process seems to fit into a small, approximately transverse fissure between the exoccipital and squamosal, just posterior to the periotic fossa. In one highly derived *Cotylocara*-like xenorophid, CCNHM 571, the articular process is long and hook-like. The articular process has been widely interpreted as a feature uniting the Platanistoidea (*sensu* [177]), as minute articular rims are present in the Waipatiidae and Squalodontidae, and larger articular processes are present in the Squalodelphinidae and Platanistidae [17,178,179]. However, an articular rim is also developed in the simocetid-grade odontocete cf. *Olympicetus* [51] as well as *Xenorophus* and other xenorophids (this study)—two of the earliest diverging odontocete lineages. The waipatiid-grade odontocete *Ediscetus osbornei* possesses a large and bluntly triangular articular rim, which suggested that the articular rim has evolved convergently [32], though this hypothesis awaited further analysis.

Ancestral character state reconstruction (Figure 85) suggests that rather than defining a platanistoid clade, this feature is plesiomorphic amongst the Odontoceti, widely distributed among stem odontocetes, and retained in the Platanistoidea sensu stricto (e.g., Squalodelphinidae + Platanistidae + Allodelphinidae). A small articular rim (character 286, state 1) is ancestral for Odontoceti, and a long and sigmoidal articular rim (state 2) occurs in several stem odontocetes including Xenorophidae (*Albertocetus*, ChM PV 4834, 5711, and CCNHM 303), the agorophiid-like unnamed odontocetes ChM PV 4178 and 2761, *Ediscetus osbornei*, in addition to the Platanistidae.

6.19. Evolution of Bulla Size in Cetacea

We initially hypothesized that xenorophid dolphins had proportionally smaller tympanic bullae than archaeocete whales, and collected measurements of bulla length and bizygomatic width for archaeocetes, odontocetes, and mysticetes in order to explore the evolution of relative bullar size in Cetacea. The length of the tympanic bulla across Cetacea correlates well with body size, but within each subgroup (Archaeocetes, Toothed Mysticetes, Stem Odontocetes, Crown Odontocetes), the trend of the convex hull for each group is quite similar, but with a slightly shallower slope for Mysticeti (e.g., proportionally smaller bullae at larger body sizes), broadly concordant with the findings of Groves et al. [180]. Further, large archaeocetes like *Basilosaurus* and physeteroids tend to have proportionally smaller bullae than close relatives with smaller body size. Within Neoceti, the smallest

taxa (e.g., *Echovenator*, Phocoenidae, Mammalodontidae, Aetiocetidae, Platanistidae) have proportionally larger bullae.

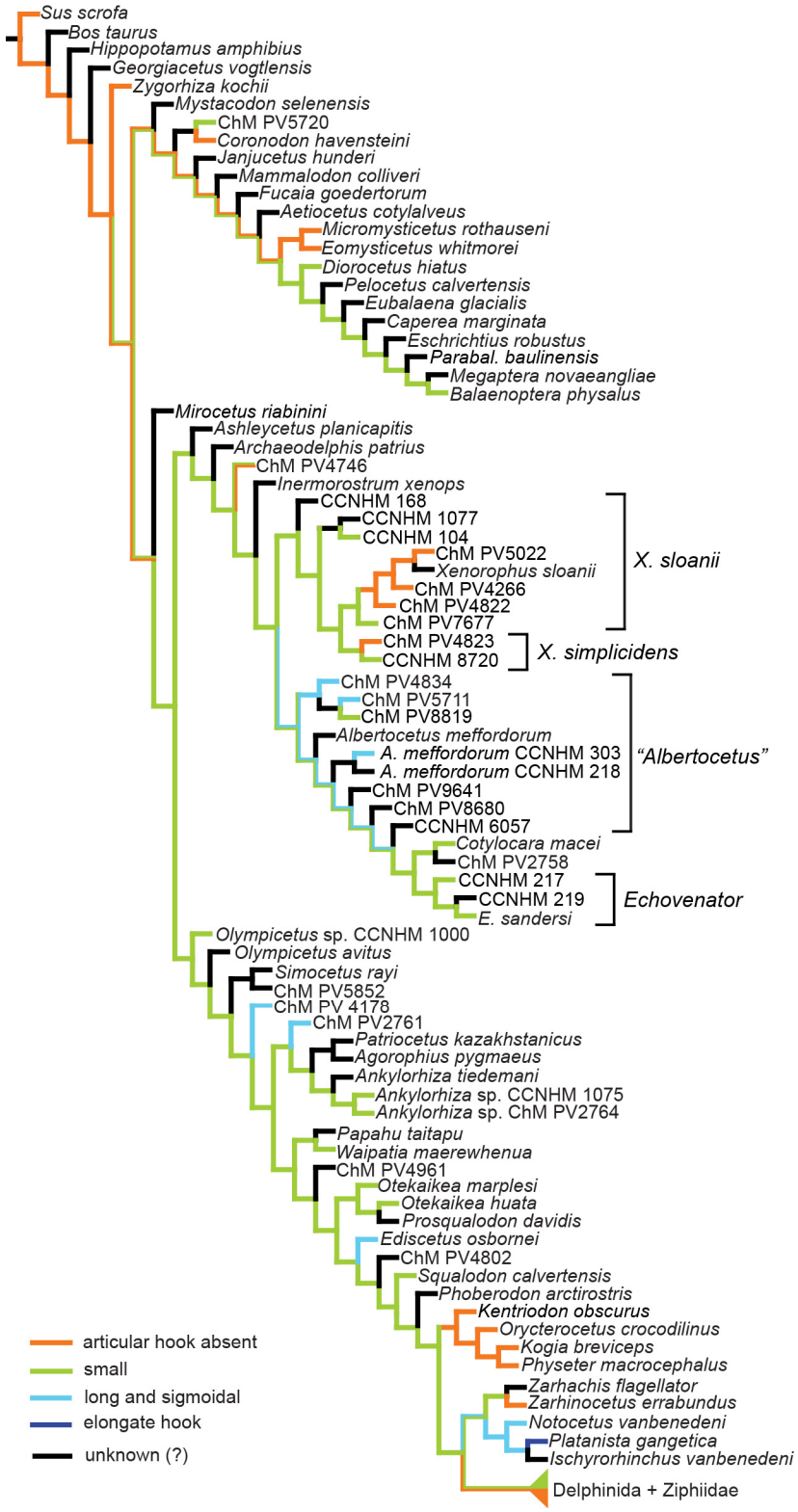


Figure 85. Parsimony-based ancestral character state reconstruction of articular process morphology within Cetacea.

6.20. Comparative Taphonomy: Periotic Disarticulation and Loss in Xenorophidae and Waipatiidae

Within Crown Odontoceti, periotics have reduced bony connections to the basicranium and are connected chiefly by soft tissues and surrounded by peribullary sinuses [15,80]. These adaptations towards directional and ultrasonic hearing result in the periotics typically separating from the rest of the skull after relatively minimal decomposition and skeletonization of the head [181], and the periotics are frequently not preserved in fossil specimens of Crown Odontoceti, especially within Delphinoidea. We hypothesize that within large samples, a greater degree of periotic association with skulls will correlate with a tighter bony connection of the periotic with the skull. Many xenorophid specimens preserve periotics, and in many, they remain in articulation with the skull and it takes some care to separate from the skull during preparation. Do xenorophid dolphins possess earbones that are more tightly connected to the skull, to the point that they are more frequently preserved in association with skulls than more derived stem odontocetes? To further investigate anatomical differences in the periotic–cranial articulation in *Xenorophus*, we surveyed xenorophid and waipatiid specimens including at least partial crania from the Oligocene Ashley and Chandler Bridge formations, and recorded the presence or absence of periotics.

Though many xenorophid skulls retain periotics in situ within the skull (e.g., CCNHM 168, 1077; ChM PV 5022), we focused on association because many specimens at both CCNHM and ChM had periotics but lacked preparation records (e.g., CCNHM 104; ChM PV 7677), and it is unclear whether some specimens were found with periotics in situ that were subsequently removed for study. Recording association of skulls and periotics, regardless of articulation status, sidesteps this problem. A periotic disarticulated from the skull but preserved in close association with it indicates that the periotic was either still in articulation with the skull at the time the carcass arrived at the seafloor, or disarticulated, but still connected by soft tissue (or, completely loose but contained by the "integumentary sack", e.g., [182]). This should be true for both the Xenorophidae and the Waipatiidae.

Waipatiids were chosen as a comparison because they represent a more derived clade or grade of odontocetes with a reduced bony connection of the periotic and skull [17,32], and in the Oligocene of South Carolina, few specimens preserve periotics in situ. Regardless, waipatiids possess an even more tightly articulated periotic–skull joint than most Crown Odontoceti [17]. Waipatiids are also similar in skull and body size to Xenorophidae, and have a sufficiently large sample to permit descriptive statistical comparisons with Xenorophidae. The general configuration of the periotic–squamosal articulation as described by Fordyce [17] does not differ appreciably within our sample of Waipatiidae from the Oligocene of South Carolina. Likewise, aside from some specimens of xenorophids like CCNHM 571, most xenorophids share a similar configuration of this region and can suitably be grouped together for the purpose of a comparative taphonomic analysis.

All xenorophid (n = 29) and waipatiid (n = 31) specimens from the Ashley Formation and Chandler Bridge Formation including at least a partial skull were surveyed, with the exception of specimens where braincase elements and earbones were missing. In these specimens, the periotic might have been articulated with the braincase still, and the braincase eroded away or destroyed prior to discovery; the *Xenorophus sloanii* type specimen is such an example where this may have been true. These specimens were not included within the survey. However, if a specimen was missing the braincase but preserved periotics anyway, this likely indicates that the periotic was disarticulated and the braincase elements were not recovered, or a disarticulated skull could have been partially disassociated prior to burial. These specimens are relatively rare (e.g., CCNHM 565).

Nearly all xenorophid specimens possess at least one associated periotic (90%; n = 26) and only a few were missing them (Figure 86). Out of the waipatiids, less than half (38%; n = 12) possessed associated periotics and most (62%; n = 20) lacked them entirely (Figure 86). These data clearly indicate that periotic preservation is more frequent within the Xenorophidae, likely reflected by a greater bony connection than in Waipatiidae. No actualistic data are known for comparison with Crown Odontoceti, but decomposition

experiments with extant odontocete carcasses could prove fruitful. Further, a similar survey of odontocetes from similarly densely sampled assemblages of crown odontocetes would make an interesting comparison with Oligocene stem odontocetes. Kentriodontid-grade delphinoids and the stem-delphinidan Eurhinodelphinidae are some of the most common odontocetes from the well-sampled Calvert Formation and are represented by many skulls in CMM and USNM collections; we predict that such future surveys will find even lower rates of periotic association than within Waipatiidae.

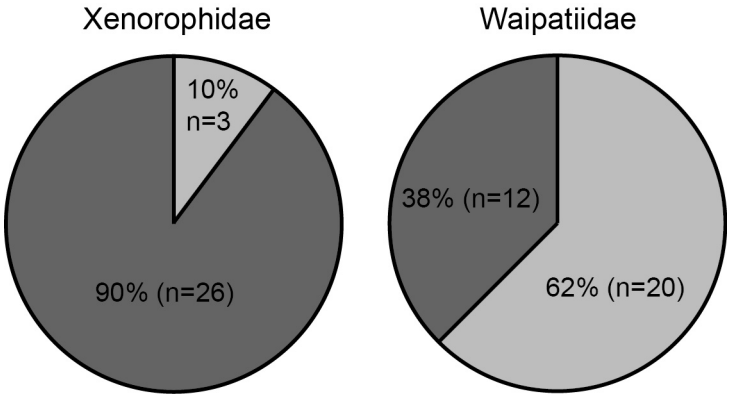


Figure 86. Comparative taphonomy of periotic association within Xenorophidae and Waipatiid-grade odontocetes from Oligocene rocks in the Charleston embayment; dark gray denotes specimens preserved with associated periotics and light gray indicates missing periotics.

Though articulation and association can be affected by changes in depositional environment [109], this sample is composed of specimens from the Ashley Formation and Chandler Bridge Formation. The former is a shallow marine open shelf sandy limestone and marl, and the latter is chiefly sandy silt of shallow marine or estuarine in origin [75]. Approximately half of all xenorophids and half of waipatiids originate from each unit. Little difference in association is evident between strata (65% association in Ashley vs. 60% association in Chandler Bridge formation, combined Xenorophidae and Waipatiidae samples). This further reinforces the contribution of anatomical differences to the disparate frequency of periotic preservation in stem odontocete groups.

6.21. Body Size Evolution in Early Neoceti

Xenorophus sloanii is one of the largest odontocetes from the Oligocene Ashley Formation of South Carolina (BZW = 307 mm in CCNHM 2077), surpassed only by the large macrophagous dolphin *Ankylorhiza* (BZW = 425–435 mm; [37]) and similar in size to *Agorophius* sp. (ChM PV 4256; BZW = 290 mm). *Xenorophus* is dramatically larger than all other xenorophids, including *Albertocetus* (BZW = 200–210 mm), *Cotylocara* (BZW = 269 mm), *Echovenator* (179 mm), and the diminutive *Inermorostrum* (estimated BZW = 143 mm). However, *Xenorophus* is still smaller than the smallest known basilosaurid whales from the late Eocene (e.g., *Zygorhiza kochii*). Previous studies of cetacean body size through time have used skull dimensions as a proxy for body size [165,183] or used equations that include skull measures [98,184,185] or skull and postcranial measures [186,187] to reconstruct evolutionary changes in body length through time [98,185]. Most studies have focused on body size trends within mysticetes [73,165,183,185,186], a few on the fitting of evolutionary models to the entire cetacean clade [184,187], and the few that have focused on body size evolution within Odontoceti have largely done so within the context of reconstructing brain size [1,98,165,188–190].

To put the body size of *Xenorophus* in a broader context, we first examined changes in body size throughout the Cenozoic for Cetacea by plotting bizygomatic skull width through time for archaeocetes, mysticetes, and odontocetes (Figure 87). This metric was chosen as it is a widely accepted proxy for body [98,165] and because many nominal cetaceans are based

off of isolated skulls lacking a complete vertebral series. Our sample was derived chiefly from the published literature, either based on published measurements or measurements collected electronically using ImageJ from published photographs. Taxa were assigned to time bins based on international geological stage; if the geologic range of a taxon spanned a boundary, the measurement was duplicated for each time bin. BZW for extant taxa is not exhaustive, but includes members of each extant family.

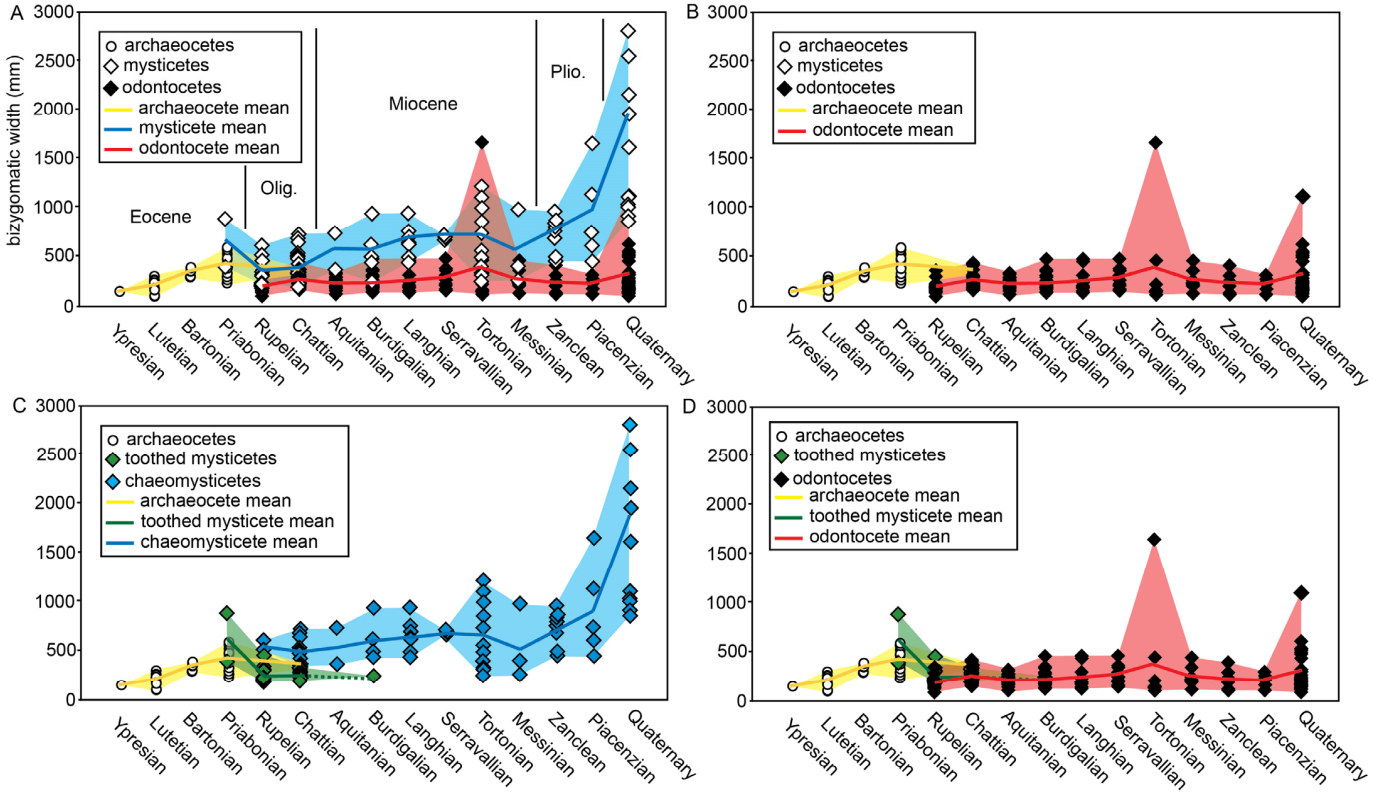


Figure 87. Body size evolution of Cetacea through time, with bizygomatic width measurements pooled by international marine stages. (**A**) scatterplot of bizygomatic widths of all cetaceans in analysis. (**B**) scatterplot of odontocetes and archaeocetes. (**C**) scatterplot of archaeocetes, toothed mysticetes, and chaeomysticetes. (**D**) scatterplot of archaeocetes, toothed mysticetes, and odontocetes.

Archaeocete BZW is relatively small (<250 mm) during the early Eocene but attains maximum sizes of 300–500 mm by the late middle Eocene, and archaeocete body size remains large through the late Eocene and Oligocene; average BZW remains 350–400 mm during the late Eocene (Figure 87). Mysticete BZW begins much larger than archaeocetes, with an average of 642 mm during the late Eocene, dominated by the gigantic *Llanocetus*. Average BZW drops to 345 and 373 during the Rupelian and Chattian (respectively), and steadily increases to 700 mm by the late Miocene, with a slight decrease during the Messinian. This is likely driven by the low sample size (n = 3) of sampled mysticetes from the Messinian, two-thirds of which are dwarf cetotheriids. Average BZW increases to 920 mm during the late Pliocene, and 1860 mm during the Quaternary. The envelope of mysticete BZW overlaps little with odontocetes, with three exceptions: (1) relatively small-bodied toothed mysticetes during the Oligocene and early Miocene, (2) dwarf cetotheriid whales during the late Miocene, and (3) the dramatic increase in maximum odontocete BZW driven by the gigantic sperm whale *Livyatan* in the Tortonian. Maximum mysticete BZW seems to parallel mysticete mean BZW, and sharply increases during the Pliocene–Quaternary interval. The mysticete BZW envelope becomes dramatically narrow during the Serravallian, which so far only records *Diorocetus*-grade mysticetes of similar skull size and shape.

When separated from toothless mysticetes, toothed mysticetes have an initial large mean BZW (642 mm in the Priabonian) but this rapidly decreases to a lower mean of 278 mm in the Rupelian and 285 mm in the Chattian (Figure 87); a single possible Burdigalian toothed mysticete has a similar BZW of 248 mm. There is a near-complete lack of overlap in BZW between toothed and toothless mysticetes. Curiously, toothed mysticetes almost completely overlap with the envelope of odontocete BZW, and similarly share nearly identical mean values during the Oligocene.

Mean odontocete BZW starts off small (200 mm) and remains relatively steady over the course of the Cenozoic (Figure 87), with a slight increase during the Tortonian (driven by the colossal size of *Livyatan melvillei*, an outlier) and the Quaternary (likewise driven by the enormous size of *Physeter macrocephalus*). Minimum odontocete BZW is occupied by a number of different small-bodied ecological specialists, including *Inermorostrum* (estimated BZW = 143 mm, Rupelian) and various taxa interpreted as "river dolphins" during the mid-late Neogene (e.g., *Brachydelphis*, *Pontoporia*, *Platanista*). Maximum odontocete BZW likewise is marked by *Ankylorhiza* spp. during the Oligocene (BZW = 425–435 mm), *Prosqualodon hamiltoni* (BZW = 340 mm) and *Squalodon whitmorei* (BZW = 480 mm) during the early Miocene, and chiefly by macroraptorial and teuthophagous sperm whales throughout the Miocene and Pliocene (BZW = 485–1670 mm). Ecological generalists tend to remain close to mean odontocete BZW, paralleling trends of RPI [2].

This geochronologic approach to body size evolution indicates that odontocetes became miniaturized relatively early on during their evolution, shortly after diverging from archaeocetes, from which they were reduced in size by half (e.g., Priabonian archaeocete mean BZW = 418 mm; Rupelian odontocete mean BZW = 205 mm). Curiously, toothed mysticetes parallel this trend during the Oligocene, with mean BZW of 278 mm in the Rupelian and 285 mm in the Chattian (Figure 87). Differences in body size suggest niche partitioning between toothed and toothless mysticetes, but toothed mysticetes and odontocetes are nearly completely overlapping. We also mapped the body size character from our phylogenetic analysis onto our MPT. This character is treated as discrete (five states), which is less precise than treating it as a continuous variable, but our taxon sample and phylogeny is unique, providing another opportunity to investigate cetacean body size evolution despite this limitation.

Based on our MPT, the internal branches leading up to Neoceti, which are comprised of archaeocetes, had a BZW of 246–347 mm (Figure 88). This is lower than our late Eocene average for basilosaurids, primarily because our average included all known taxa, whereas our phylogenetic analysis only included two, relatively small-sized archaeocetes as outgroups, *Zygorhiza kochii* and *Georgiacetus vogtlensis*. We have less confidence for the inferred skull size of the most recent common ancestor of Neoceti; it is optimized to be either the same size as ancestral archaeocetes or potentially even larger at 378–500 mm. This uncertainty is a result of conflicting information shortly after the initial diversification of Neoceti. Whereas some mysticetes suggest fairly large sizes, such as *Mystacodon* (399.6 mm) and coronodonids (359–463 mm), others suggest a much smaller skull size, including *Janjucetus* (332 mm) and *Fucaia goedertorum* (236 mm). On the odontocete side of this diversification, the most basal odontocete is a relatively large one; *Mirocetus* has a BZW of 400 mm. By contrast, the vast majority of other odontocetes are much smaller. Inferred skull size does drop between the origin of Odontoceti and the clade that includes all odontocetes but *Mirocetus*, but the amount is uncertain, resulting in a BZW < 245 mm and maybe even <185 mm. The smaller size estimates are influenced by the taxa at the base of Xenorophidae, including *Inermorostrum* and ChM PV4746 (BZW 185.3 mm), as well as *Olympicetus*, which is situated near the base of the stem that leads to extant odontocetes (Figure 88). Although the magnitude of the skull size decrease is uncertain, this observation is consistent with previous studies that have inferred a notable body size decrease near the origin of Odontoceti (i.e., [189,191]) but is at odds with the recent work of Waugh and Thewissen [190]. Waugh and Thewissen [190] calculated much greater body sizes for Oligocene odontocetes, including the xenorophids *Albertocetus* and *Xenorophus*,

with the result that the differences in encephalization quotients between basilosaurids and early odontocetes were statistically indistinguishable. On the one hand, we find the methodologies employed by Waugh and Thewissen [190] to be a convincing improvement, but we also have high confidence in our finding of a decrease in BZW width along the odontocete stem. We find it noteworthy that our phylogenetically informed reconstructed decrease in body size matches the change in average BZW that occurred between Rupelian and Chattian odontocetes (Figures 87 and 88), further evidence that this change is real. More detailed study is needed to resolve the discrepancies between our findings and those of Waugh and Thewissen [190], but we suspect that the solution might involve a decrease in body size near the origin of Odontoceti, but one that is of smaller magnitude than previously reconstructed.

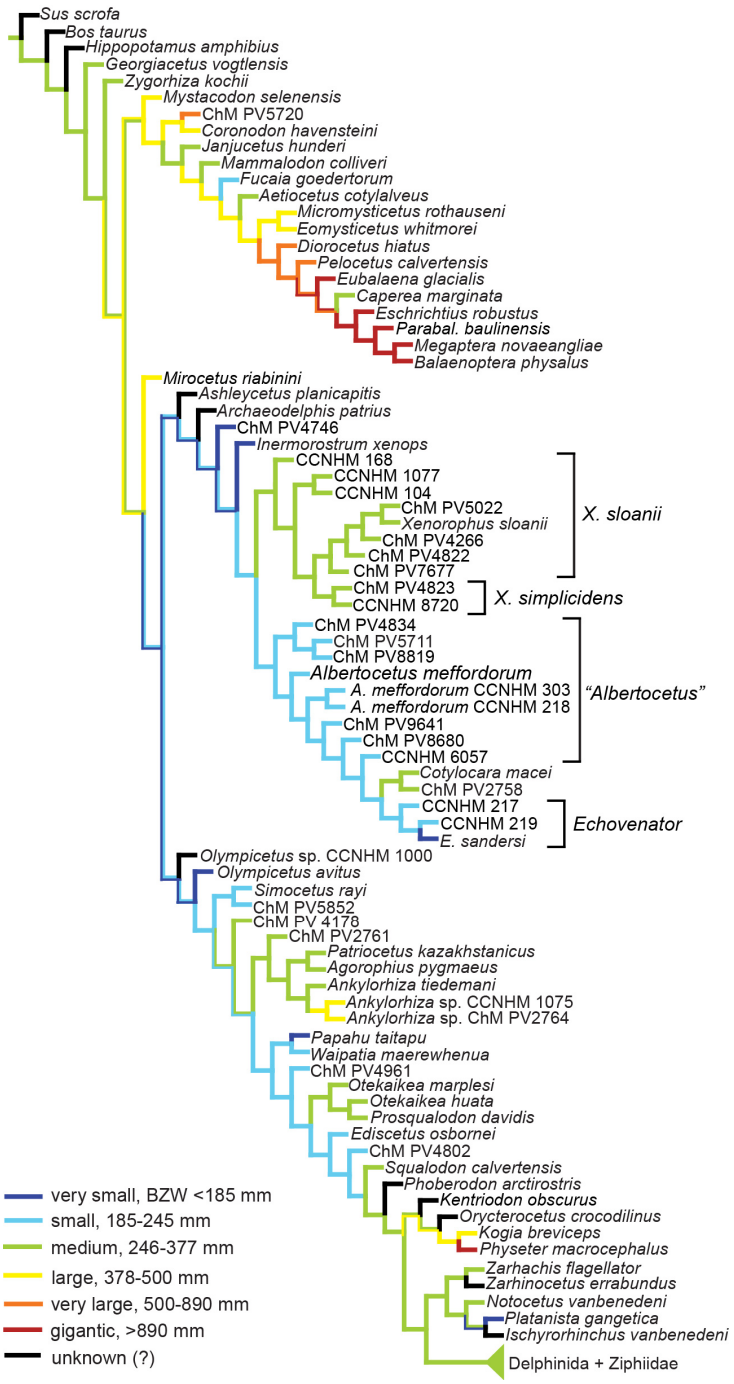


Figure 88. Parsimony-based ancestral character state reconstruction of body size within Cetacea.

6.22. *Anagenesis in* Xenorophus

Fossils of *Xenorophus* occur in two rock units in South Carolina: the Ashley Formation (late early Oligocene, 28–30 Ma), and the overlying Chandler Bridge Formation (late Oligocene, 23–25 Ma). At least some specimens from both units have been previously interpreted as a second, unnamed species of *Xenorophus* (e.g., ChM PV 5022 from the Ashley Formation and ChM PV 4823 from the Chandler Bridge Formation). All specimens from the Ashley Formation appear to represent *Xenorophus sloanii*—but what about specimens from the Chandler Bridge Formation? If these geochronologically younger specimens represent a single species, and none are referable to *X. sloanii*, then this younger species may share an ancestor–descendant relationship with *Xenorophus sloanii* and constitute an anagenetic lineage within Xenorophidae.

Anagenesis, or evolution between branching events (cladogenesis), likely explains most of evolution and the fossil record as cladogenesis is brief and temporally discrete. However, it can only be evaluated when large sample sizes are available, and is rarely considered among vertebrates (but see [192–194]). Anagenesis can be tested using measurements of densely sampled and stratigraphically separated specimens with tight stratigraphic control [193,194], probabilistic phylogenetic methods [195], or parsimony-based cladistics by comparing the ages of branch tips on a pectinate part of the cladogram [194,196]. A specimen-level phylogenetic analysis represents another method to evaluate hypotheses of anagenesis in fossil vertebrates [194]. We used our specimen-level phylogeny of Xenorophidae to test three hypotheses: (1) all specimens of the younger taxon will nest as a clade within the clade formed by the older taxon, which would support anagenetic evolution of the former from the latter; (2) the two taxa will form two separate clades sister to each other, which would indicate a ghost lineage for the younger taxon; or (3) the two taxa would be intermingled, and thus all specimens from both units would represent *Xenorophus sloanii* and indicate the existence of a ~7 my survival of this species.

Our phylogenetic analysis contradicted hypotheses 2 and 3, and failed to eliminate hypothesis 1 (Figure 71). Key specimens from the Chandler Bridge Formation including the holotype and paratype (CCNHM 8720, ChM PV 4823) form a clade nested within *Xenorophus sloanii* (constituted by OTUs ChM PV 5022, 7677, CCNHM 104, 168, 1077, and USNM 11049). This supports our hypothesis that *Xenorophus sloanii* and *Xenorophus simplicidens* from the Chandler Bridge Formation represent members of an anagenetic lineage, with *Xenorophus sloanii* being the ancestral population of the second species. Further testing of this hypothesis could consider the stratigraphic origin of *Xenorophus sloanii* specimens within the Ashley Formation, as specimens from the geochronologically older Runnymede Marl Member might be expected to be more plesiomophic, and therefore diverging earlier on a cladogram, than specimens from the Givhan's Ferry Member. Less completely preserved specimens ChM PV 4266 and 4822, which lack teeth and, therefore, most of the dental codings that might lend character support towards forming a clade with ChM 4823 and CCNHM 8720, are referred to *Xenorophus simplicidens*.

6.23. *Key Synapomorphies of Odontoceti*

The last comprehensive review of odontocete synapomorphies was that of Sanders and Geisler [5], and given the additional specimens of *Xenorophus* described here, as well as the addition of 83 characters to the matrix of those authors, this is an appropriate time to review previously suggested synapomorphies as well as document new ones. In our present study, we have found very strong character support for Odontoceti, including 7 unambiguous synapomorphies and 17 additional synapomorphies that may apply to this node. The seven unambiguous synapomorphies of Odontoceti are as follows: four distal denticles on main molars (character 49: state 4), lateral side of postorbital process also faces somewhat dorsally (89:0), longitudinally concave premaxillary sac fossae (99:0), maxilla covers most if not all of supraorbital process of frontal (110:1 or 2), maxilla terminates over posterior half of orbit (111:2), anterior edge of nasals and orbits roughly aligned (114:3), and 12 thoracic vertebrae (330:4). Four of these character states have been previously

suggested as odontocete synapomorphies, including premaxillary sac fossae [5,10,18], maxillary expansion over the frontals [5,17,30,31,153], maxilla terminating over posterior half of orbit [5,10], and anterior edge of nasals over anterior half of orbit [5]. These character states do display some degree of homoplasy; character 49 state 4 reverses along the stem to the odontocete crown group and again in the clade including *Cotylocara* and *Echovenator*; character 89 state 0 reverses in Xenorophidae and again in crown Odontoceti; character 99 state 0 reverses in Inioidea, Phocoenidae, and some Delphinidae; character 111 state 2 is convergent with *Eschrichtius*, character 114 state 3 also converges with some mysticetes; and character 330 state 4 converges with *Aetiocetus cotylalveus*.

The most basal odontocete in our most parsimonious tree is *Mirocetus*, which can only be coded for about 30% of the characters in the matrix. As a result, there are 17 character states that are optimized as either a synapomorphy of Odontoceti or the next clade up, which includes all odontocetes except for *Mirocetus*. These characters include, lacrimal and/or jugal forming posterior wall of antorbital notch (21:1), multicuspate teeth form an intermediate proportion of the total toothrow (47:1), loss of lacrimal foramen (77:1), thin jugal (81:1), three or more dorsal infraorbital foramina (91:2), premaxillary sac fossa is concave transversely (97:1), premaxillary foramen (100:1), intermediate slope for premaxilla in lateral view (124:1), premaxillary inflection anterior to orbit (142:2), posterior width of nasals subequal to nares width (158:1), frontal and nasals are same height (164:1), intertemporal region of intermediate thickness (180:1), lateral exposure of alisphenoid is narrow (184:1), wide hiatus epitympanicus (258:1), caudal tympanic process of periotic narrowly separated from crista parotica (273:1), lateral side of internal acoustic meatus is low (282:0), short posterior process (292:1), and two mesial denticles on mandibular molars (391:2). Overall homoplasy is low among most of these characters, but a few instances bear mentioning; character 21 state 1 reverses in some odontocetes, character 77 state 1 is convergent with Kinetomenta, character 91 state 2 is convergent with *Mammalodon* and *Diorocetus*, character 124 state 1 displays substantial homoplasy including convergence with *Mammalodon* and *Aetiocetus*, character 142 state 2 is convergent with some balaenopterids, character 158 state 1 is convergent with *Janjucetus* and *Zygorhiza*, character 164 state 1 is convergent with Chaeomysticeti, character 180 state 1 is convergent with *Diorocetus* and *Pelocetus*, character 184 state 1 reverses in the odontocete crown group, character 258 state 1 converges with *Coronodon*, character 273 state 1 converges with some mysticetes and also reverses along the stem to the odontocete crown group, and character 282 state 0 and character 292 state 1 are convergent with Eomysticetidae. Many of these characters have been previously suggested to be odontocete synapomorphies, including lacrimal and jugal forming the posterior wall of the antorbital notch [5,10], premaxillary foramen [153,197], intermediate slope for premaxilla [5], premaxillary inflection just anterior to orbit [5], frontals and nasals at same height [5,10], intertemporal region of intermediate thickness [5], wide hiatus epitympanicus [5], and short posterior process of periotic [5,94,198].

Our matrix does not support some previously suggested odontocete synapomorphies. Geisler and Sanders [10] suggested that having nasals elevated well above the rostrum was an odontocete synapomorphy. On our most parsimonious tree, this state is interpreted to have evolved once in the clade that includes Xenorophidae + *Archaeodelphis* + *Ashleycetus* and again in a clade that includes *Agorophius* and crown odontocetes. This optimization occurs because of *Olympicetus avitus* and CCNHM 1000, which are positioned between these clades and have lower nasals. If CCNHM 1000 and *Olympicetus avitus* form a clade, which is supported by a recent study of Simocetidae [176], then this character would likely once again be a synapomorphy of Odontoceti or the clade of all odontocetes, minus *Mirocetus*. Three putative odontocete synapomorphies suggested by Sanders and Geisler [5], are also not supported by the present study: maxilla of intermediate length, loss of cranial hiatus, and high tegmen tympani adjacent to IAM. There are of course other features that have been suggested as odontocete synapomorphies, but we refer readers to previous studies [5,10] for a more detailed review of why those characters are not synapomorphies or diagnose a more exclusive clade, such as the odontocete crown group.

6.24. The Antorbital Notch in Neoceti

The antorbital notch is typically formed as a groove, embayment, or trough medial to the antorbital process separating the orbital region from the rostrum, and is widely regarded as a synapomorphy of Neoceti [10,46,199]. The notch is not present in archaeocetes, and it has no homolog in protocetids or earlier diverging taxa; however, basilosaurids possess a longitudinal trough on the maxilla between the upper molars and the root of the jugal. This trough dissipates anterior to the orbit, and is horizontal in lateral view. This morphology is similar to that seen in *Mystacodon* and *Coronodon*, though an anterodorsally directed trough extends anterior to the antorbital process and defines a small zygomatic process of the maxilla [46]. In *Janjucetus*, the same condition is present, though the lateral edge of the maxilla sits further lateral than in *Zygorhiza* and the trough is deeper, providing sufficient relief to recognize the antorbital process. An anteroposterior trough-like antorbital "notch" is present in *Janjucetus* and *Zygorhiza*, and they differ chiefly in the orientation of the trough: ventral in *Zygorhiza* and other basilosaurids, and lateral in *Janjucetus*. In *Janjucetus*, the trough is somewhat anteromedially directed; the antorbital process is formed chiefly by the lacrimal and frontal. The condition in *Janjucetus* is similar to that of some early diverging odontocetes like *Olympicetus* (e.g., CCNHM 1000, 6059), though, in *Olympicetus*, the trough faces ventrally (like *Zygorhiza*) rather than ventrolaterally, as in *Janjucetus*.

A longer antorbital notch is developed in the Kinetomenta. In *Aetiocetus cotylalveus*, the trough is deep and anteroposteriorly short, directed strongly anteromedially, and situated ventral to a clear antorbital process formed by the maxilla and lacrimal. Few eomysticetids preserve the antorbital notch, except for *Yamatocetus* where the antorbital notch is developed as a long, anteromedially trending trough laterally adjacent to a ridge; this ridge is similarly developed in juvenile *Waharoa ruwhenua* ([146]: Figure 8). Unlike Aetiocetidae, the notch is positioned on the dorsal side of the rostrum rather than the lateral edge.

In many chaeomysticetes, the antorbital process of the maxilla becomes enlarged and plate-like, overlying the trough-like notch. In most chaeomysticetes, this trough is anteromedially directed (*Aglaocetus*; Balaenopteridae, Balaenidae, Neobalaenidae) in a manner broadly similar to Eomysticetidae, but is occasionally transversely oriented (e.g., *Diorocetus*). In the Cetotheriidae, the trough actually extends posteromedially (e.g., *Piscobalaena*, *Herpetocetus*).

In the Xenorophidae, the trough is broad, vertical, anteriorly facing, and forms a broad U-shaped embayment between the very strongly developed compound antorbital process and the rostrum (*Xenorophus*, *Albertocetus*; Figure 35). This differs quite strongly from the sharp, horizontal, laterally facing trough as seen in *Olympicetus*. However, this morphology is broadly concordant with the vertical, anteriorly facing antorbital notch in many extant odontocetes. The broad antorbital notch is superficially similar to extant *Platanista gangetica* and Squalodelphinidae (*Notocetus*, *Squalodelphis*).

Simocetus rayi is broadly similar to *Olympicetus* and shares an antorbital notch that is V-shaped in dorsal view; however, in *Simocetus*, the notch is vertically oriented and, in *Olympicetus* (CCNHM 6056), the notch is dorsomedially oriented with a sheet of maxilla underlying the frontal, which is particularly similar to the morphology in the toothed mysticete *Janjucetus*. A sheetlike plate of maxilla that underlies the frontal here is nearly identical to Mysticeti, in which this structure is called the zygomatic process of the maxilla and has been considered a synapomorphy of Mysticeti [10,141]. The somewhat more derived condition of the antorbital notch in *Simocetus* generally characterizes other early diverging stem odontocetes such as *Agorophius pygmaeus* (holotype, and referred specimen, ChM PV 4256), an unnamed dwarf agorophiid (ChM PV 5852), and *Ankylorhiza* (CCNHM 104, ChM PV 2764). Most waipatiid-grade and squalodontid-grade odontocetes have a shallow or deep V-shaped notch that is vertical (*Waipatia*, *Squalodon*), though in some waipatiid-grade taxa the notch forms a simple right-angle emargination with a straight transverse posterior margin (e.g., *Ediscetus*, *Otekaikea*, ChM PV 4961).

Crown odontocetes generally have a short, vertical, and deeply entrenched V or more broadly U-shaped notch (e.g., Delphinidae); in some, it forms a narrow longitudinal fissure that occasionally becomes occluded anteriorly (e.g., *Physeter*, *Kogia*, *Parapontoporia*). Such a condition is also present in some stem odontocetes like *Prosqualodon* spp. [200] and *Patriocetus kazakhstanicus* [201]. In modern and extinct Platanistoidea (sensu [177]), the antorbital notch is typically a wide embayment, as in Xenorophidae, though many species still possess a sharp notch rather than the broad embayment seen in *Xenorophus*. In Ziphiidae, the antorbital process is not anteriorly projecting, and the notch is typically shallow or a simple right angle, occasionally with an accessory notch. The notch is reduced in extant Phocoenidae (but not extinct Phocoenidae, many of which retain a V-shaped notch like delphinids).

In sum, crown odontocetes generally have a short notch that is vertical and on the anterior side of the orbit; it is long and trough-like in basilosaurids, mysticetes, and archaic odontocetes. In basilosaurids and early toothed mysticetes, it faces ventrally, whereas in some archaic odontocetes and some toothed mysticetes it faces laterally. Lastly, in eomysticetids, aetiocetids, and crown Mysticeti, it faces dorsally. Xenorophidae are unusual amongst stem odontocetes in possessing rather large, embayment-like antorbital notches that face anteriorly.

6.25. Maxillary Constriction in Odontoceti, Aetiocetidae, and Mammalodontidae

Studies of mysticete phylogeny have, on occasion, identified a clade including most toothed mysticetes, consisting of the Mammalodontidae and Aetiocetidae [49,202,203]. However, such a relationship is not recovered in other matrices with more character data [46,66,146] or successive versions of the same matrix [47]. Many synapomorphies for this proposed clade center around the orbital region, which is quite enlarged in the mammalodontids and aetiocetids [202]. One of the more convincing characters is a notch incised into the lateral margin of the maxilla in the vicinity of the antorbital notch (e.g., [49]). However, this condition is clearly present in *Xenorophus* and other Xenorophidae, which possess an enormous lacrimal that incises into the lateral margin of the maxilla at the level of the antorbital notch. A similar condition, albeit with a smaller lacrimal, is evident in many other stem odontocetes, such as *Olympicetus* sp. (CCNHM 1000; [51]), *Olympicetus thalassodon* [176] *Nihohae matakoi* ([204]: Figure 2A), *Simocetus rayi* ([18]: Figure 3), *Waipatia maerewhenua* ([17]: Figure 2A), and undescribed specimens from Charleston included within our phylogenetic analysis (aff. *Agorophius*, ChM PV 5852; *Ankylorhiza* sp., CCNHM 1075 and ChM PV 2764; aff. Agorophiidae, ChM PV 4178). Owing to the widespread distribution of this character within early Odontoceti, further study is clearly warranted and we speculate that it is homoplastic within early Neoceti.

6.26. New Odontocete Clades: Amblyoccipita and Stegoceti

Continued study of early odontocetes and a taxonomic proliferation of Stem Odontoceti, chiefly from the Oligocene, has resulted in a large stem group with numerous proposed family-level taxa or clades (Xenorophidae, Ashleycetidae, Mirocetidae, Simocetidae, Agorophiidae) and several others that are alternatively recovered as stem odontocetes or occasionally within the crown group (Waipatiidae, Squalodontidae, Inticetidae, Eurhinodelphinidae, Eoplatanistidae, Squaloziphiidae, "*Chilcacetus* clade"). We introduce two new clades (Figure 89), more inclusive than Crown Odontoceti and less inclusive than Odontoceti (or Pan-Odontoceti), in order to aid future discussion of stem odontocetes.

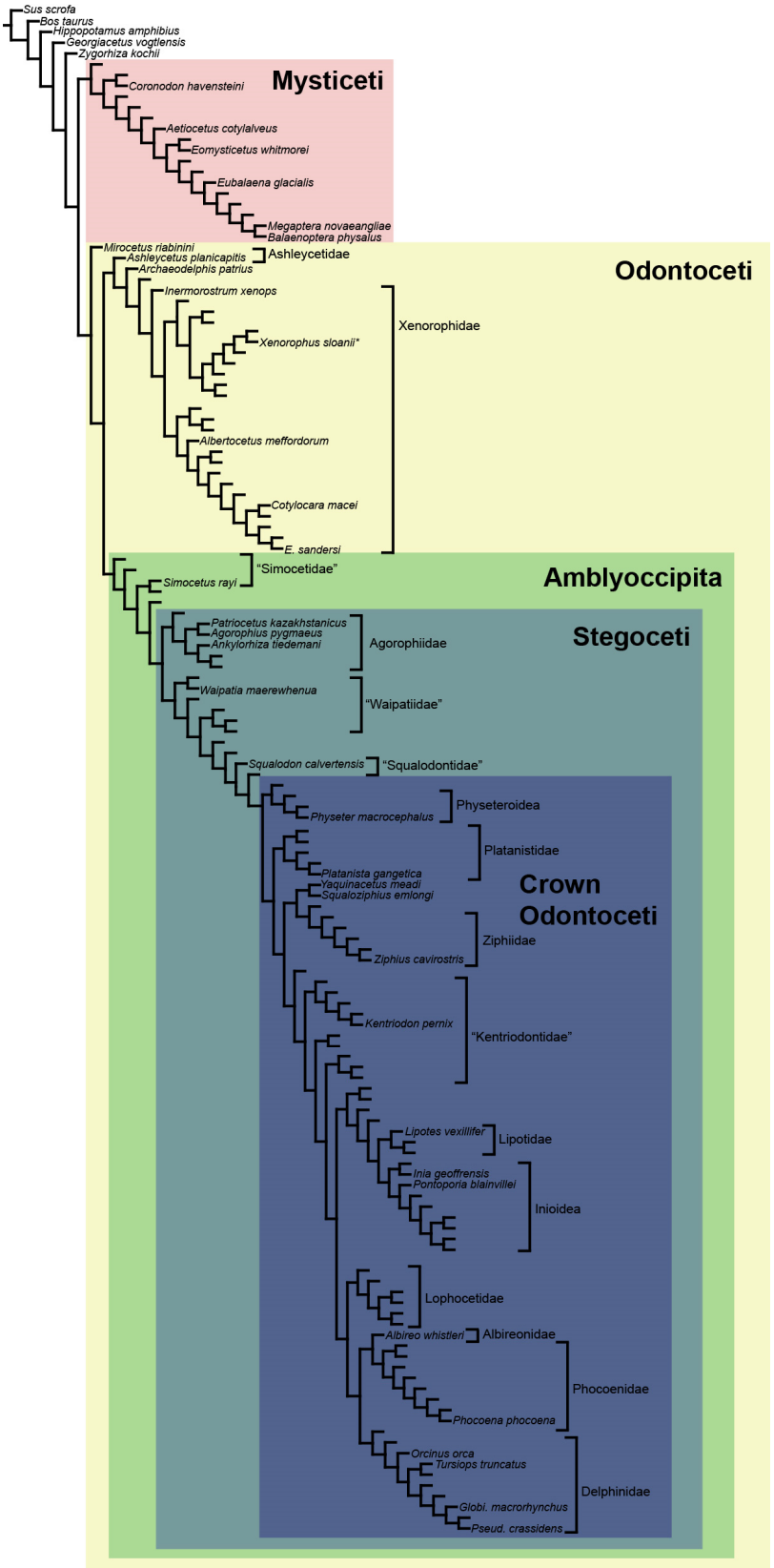


Figure 89. Simplified cladogram based on most parsimonious tree from this study, with new clades Amblyoccipita and Stegoceti highlighted.

6.26.1. Amblyoccipita, New Clade Name, Unranked

Definition 1. *Branch-based clade consisting of Globicephala melas and all odontocetes more closely related to Globicephala melas than to Xenorophus sloanii.*

Diagnosis: Odontocetes within Amblyoccipita are diagnosed by synapomorphies of the vertex and periotic, including semicircular apex of the occipital shield (character 196, state 1); loss of the capsuloparietal vein sulcus on the lateral side of the periotic (character 252, state 1); deep anterior bullar facet (character 255, state 3); and reduced superior process of the periotic at the posterodorsal angle (character 280, state 2).

Etymology: Derived from the classical Greek ambly, meaning blunt, and occiput, occipital bone, referring to the blunted (rather than triangular) apex of the occipital shield in these odontocetes.

Composition: Based on our phylogenetic analysis, Amblyoccipita (Figure 89) includes Crown Odontoceti and most family-level stem odontocete taxa/grades including "squalodontids", "waipatiids", "agorophiids", Simocetidae (sensu [176]), and other odontocetes variably placed in the stem group or within the crown group (*Inticetus*, *Prosqualodon*, Squaloziphiidae, "*Chilcacetus*-clade", Eurhinodelphinidae). Specifically excluded from this clade are the Xenorophidae. The phylogenetic position of *Ashleycetus* and *Mirocetus* varies between analyses, and these taxa occur occasionally as the earliest diverging odontocete outside the Xenorophidae + Amblyoccipita clade, at the base of Amblyoccipita, or as sister to Xenorophidae ([5,25,176]; this study). These taxa may belong to Amblyoccipita but require further study.

Remark 1. *Phylogenetic analyses of Odontoceti have repeatedly resulted in the placement of Xenorophidae as one of the earliest, if not the earliest, clade of odontocetes. Amblyoccipita is intended to provide a new name for all stem odontocete taxa along the main lineage leading to the crown group as well as Crown Odontoceti.*

6.26.2. Stegoceti: New Clade Name, Unranked

Definition 2. *Apomorphy-based clade consisting of all odontocetes with an expanded or greatly expanded intertemporal constriction (character 178, state 2 or 3).*

Diagnosis: Odontocetes included within the Stegoceti are diagnosed by several synapomorphic features of the premaxilla, intertemporal region, and periotic including premaxilla terminating within the posterior half of the orbit (character 107, state 4) or further posterior; inflection of premaxilla positioned within posterior half of orbit (character 142, state 4) or further posterior; parietals reduced to lateral triangular exposures (character 176, state 1); dorsally expanded or greatly expanded intertemporal constriction (character 178, state 2 or 3); tympanosquamosal fossa present and triangular (character 224, state 2); blunt apex of anterior process of periotic (character 247, state 1); anterior process of periotic circular in cross-section (character 254, state 2); aperture of cochlear aqueduct of periotic similar in size to aperture for vestibular aqueduct (character 274, state 1); superior process of periotic reduced to a low crest at posterodorsal angle (character 280, state 3); suprameatal fossa of periotic reduced to shallow but clearly defined longitudinal sulcus (character 378, state 2).

Etymology: Derived from the classical Greek "stegos", meaning roof, plus cetus, referring to the transverse expansion of the intertemporal region.

Composition: Based on our phylogenetic analysis, Stegoceti (Figure 89) includes all Crown Odontoceti and stem odontocetes within the "Squalodontidae", "Agorophiidae", "Waipatiidae", and several odontocete clades/grades variably placed in the stem group or crown group (*Inticetus*, *Prosqualodon*, Squaloziphiidae, "*Chilcacetus*-clade", Eurhinodelphinidae). Specifically excluded from this clade are odontocetes with a narrow intertemporal constriction with an ovoid cross-section, including Xenorophidae, *Ashleyce-*

tus, *Mirocetus*, Simocetidae (sensu [176]), and unnamed simocetid-like odontocete ChM PV 4178.

Remark 2. *The loss of the intertemporal constriction in Odontoceti is associated with cranial telescoping [24]. Many Xenorophidae, including* Xenorophus, *plesiomorphically retain a sagittal crest as in archaeocetes; a narrow intertemporal constriction or one with an ovoid cross-section and long anteroposterior dorsal expanse of the parietals (parietal length at midline 50–60% of intertemporal width) is present in Xenorophidae and Simocetidae. Within the Agorophiidae (here considered to include* Agorophius, Ankylorhiza, Patriocetus, *and unnamed taxon ChM PV 2761), the parietal exposure is considerably wider than its length (length at midline under 25% of intertemporal width) or the dorsal exposure of the parietal is limited to triangular exposures laterally [10]. All later diverging odontocetes have a dorsally widened intertemporal constriction that joins the supraorbital process of the frontal in roofing over the anterior part of the temporal fossa.*

7. Conclusions

1. *Xenorophus sloanii* is the type species of the Xenorophidae, a short-lived but surprisingly diverse and distinctive clade of early diverging odontocetes known only from Oligocene marine rocks of North and South Carolina as well as Virginia. *Xenorophus sloanii* is previously only known from a small skull with proportionally large teeth from the Ashley Formation of South Carolina.
2. The new species *Xenorophus simplicidens* is reported from multiple specimens from the overlying Chandler Bridge Formation of South Carolina, and is distinguished from *Xenorophus sloanii* in possessing shorter nasal bones and simpler teeth possessing striated rather than rugose enamel and fewer accessory cusps. Phylogenetic analysis of a specimen-based matrix of Xenorophidae and other odontocetes places the sample of *Xenorophus simplicidens* within *Xenorophus sloanii*, which in concert with its younger geochronologic age, indicates anagenetic evolution within the *Xenorophus* lineage, and identifies *Xenorophus sloanii* as a likely direct ancestral species to *Xenorophus simplicidens*.
3. A large new sample of *Xenorophus sloanii* reveals that this species is a large odontocete (70–74 cm CBL, 29–30 cm BZW) with a moderately long rostrum (RPI = 2.5) marked heterodonty, incipient polydonty and variable tooth count (13–14 teeth), prominent sagittal crest and intertemporal constriction. All specimens are from the Ashley Formation; this sample exhibits dental variation, within which the holotype is an outlier as other specimens have fewer cusps.
4. This new sample (n = 7 crania) reveals that the holotype specimen is a juvenile. Ontogenetic changes in *Xenorophus sloanii* include anterior lengthening of the nasal bones, fusion of the frontonasal, median frontal, and occipitoparietal sutures, shortening and counterclockwise rotation of the sagittal crest, and broadening of the occipital shield; RPI does not change during postnatal ontogeny.
5. Moderate RPI, mesiodistally interlocking teeth, flat palate, and delicate rod-like stylohyal indicate raptorial pierce feeding and lack of suction feeding specializations in *Xenorophus*. Tooth wear is minimized by large diastema and the growth of deep embrasure pits that reduce tooth–tooth contact during occlusion. The mandibular symphysis is long but lightly sutured and bears a shallow symphyseal furrow, unlikely but possibly homologous with the groove of mysticetes.
6. Variable tooth wear is attributed to variation in diet, with one specimen of *Xenorophus sloanii* possessing highly worn teeth, perhaps resulting from feeding on abrasive prey like sharks. Minor dental erosion is also evident in this individual. Two other specimens are pathologically missing three–four postcanine teeth in the mandible and rostrum, lost during postnatal ontogeny; in one, the mandible also exhibits a pathologic fistula with drainage channels at the location of the missing teeth, suggestive of traumatic tooth loss, perhaps caused by mechanically risky feeding behavior or intraspecific combat.

7. *Xenorophus* possesses asymmetrical cranial features supporting production of high frequency sounds with the nasofacial muscles as in modern Odontoceti, including asymmetrical antorbital fossae, premaxillary sac fossae, and premaxillary foramina.
8. Other modes of skeletal asymmetry in *Xenorophus sloanii* are best interpreted as relating to deviation of the rostrum to the left of the midline and possibly the neurocranium to the right, a first for odontocetes. These are confirmed in multiple specimens and include a 2–4° angle between the rostral and neurocranial midline, left palatine shifted anterior to right with median palatine suture shifted to the left, parallelogram-shaped palatal exposure of vomer, dental asymmetry with right toothrow shifted slightly further anterior, asymmetrical transverse processes and neural spines on cervical, thoracic, and lumbar vertebrae. Clockwise rotation of the posterior mandibles and neurocranium may improve directional hearing by exaggerating interaural time difference of incoming sounds used in echolocation.
9. Vertebral proportions from a nearly complete vertebral column for *Xenorophus sloanii* with moderate regionalization indicate Pattern 1 swimmers, with large, circular, and slightly long lumbocaudal vertebrae that would permit greater dorsoventral undulation of the caudal flukes relative to basilosaurids and mysticetes, with incipient narrowing of the caudal peduncle and lacking a stiffened caudal peduncle.
10. *Xenorophus* and Xenorophidae differ from archaeocetes in possessing small teeth, despite being some of the earliest odontocetes. Analysis of tooth size indicates early and rapid reduction in tooth size in Odontoceti with microdonty achieved across the clade by the late Miocene; toothed mysticetes have a broader range of tooth size but convergently evolve small teeth in Aetiocetidae.
11. Odontocetes exhibit a much wider range in rostral proportion index (RPI) than mysticetes, and Xenorophidae represent some of the higher RPI values in the Oligocene. Low RPI (brevirostry), associated with suction feeding, has evolved multiple times. High RPI (longirostry) has likewise evolved in several lineages in small-bodied odontocetes.
12. Xenorophidae possess laterally facing orbits like basilosaurids but are slightly enlarged like many extant delphinoids, perhaps suggesting that vision remained important for foraging. Variation in orbit size and orientation increases within remaining Stem Odontoceti (Stegoceti) and further within Crown Odontoceti.
13. *Xenorophus* retains a distinct but short intertemporal constriction and a long temporal fossa like archaeocete whales. Temporal fossa length independently decreased within odontocetes and mysticetes, suggesting reduced need for powerful bite force.
14. *Xenorophus* exhibits incipient polydonty (13–14 upper teeth). Ancestral character state reconstruction surprisingly found that it is equally parsimonious for maxillary and mandibular polydonty to have evolved once near the base of Odontoceti or twice, within Xenorophidae and again in Stegoceti.
15. Periotics of some specimens of *Xenorophus* possess a small articular process; in other Xenorophidae, a long or extremely long and hooklike articular process is developed. Though previously interpreted as an important synapomorphy for Platanistoidea, ancestral character state reconstruction indicates considerable homoplasy and that a small articular process is plesiomorphic for Odontoceti with longer articular processes evolving multiple times and being reduced in extant Odontoceti.
16. *Xenorophus* possesses moderately sized tympanic bullae (17–19% of BZW), slightly larger than extant delphinoid odontocetes (10–16%), considerably larger than in extant mysticetes (5–9%), and somewhat reduced compared to basilosaurids (16–24% BZW). Like previous studies, we found bullae to be proportionally larger in small-bodied cetaceans and proportionally smaller in larger taxa like mysticetes.
17. Specimens of *Xenorophus* possess linear scrape marks indicating feeding by sharks and/or fish, including tooth marks with serrations identifiable to the megatoothed shark *Carcharocles angustidens*. Bioeroded crater-like traces caused by the bone-eating

worm *Osedax* are identified on skulls, earbones, teeth, and postcrania, suggesting infaunal colonization, or possibly colonization of exposed bone.

18. Comparative taphonomic analysis of skull–periotic associations of Ashley and Chandler Bridge Formation odontocetes indicates that Xenorophidae more frequently preserve periotics (in situ or ex situ, 90%) than in waipatiid-grade odontocetes (38%), reflecting archaeocete-like tighter periotic/squamosal articulation in Xenorophidae versus the looser articulation in waipatiid-grade specimens.
19. *Xenorophus* spp. are relatively large for Oligocene odontocetes (BZW = 28–30 cm, estimated body length = 2.6–3 m). Early odontocetes like Xenorophidae demonstrate a decrease in body size near the base of Odontoceti, and a geochronologic approach to body size indicates an immediate and early decrease in body size among odontocetes relative to archaeocetes during the Oligocene along with minimal post-Oligocene overlap between mysticetes and odontocetes. We also found evidence for increasing maximum body size of odontocetes and increasing minimum and maximum body size of mysticetes in the Plio-Pleistocene.
20. There is strong evidence for monophyly of *Xenorophus*. *Albertocetus* is found to be paraphyletic, with some specimens forming successive sister taxa to the *Cotylocara-Echovenator* clade; *Inermorostrum* and *Xenorophus* are recovered as two of the earliest diverging clades within Xenorophidae. *Mirocetus* is recovered as the most basal odontocete, with *Ashleycetus* and *Archaeodelphis* as successive sister taxa to Xenorophidae.
21. Phylogenetic analysis permitted a review of proposed synapomorphies for Odontoceti. We found support for numerous characters (e.g., lacrimal/jugal forming antorbital notch, thin jugal, three or more dorsal infraorbital foramina, presence of premaxillary foramen, posterior nasals subequal to nares width, frontals and nasals at same height, narrow alisphenoid exposure, short posterior process of periotic) as supporting Odontoceti or the clade excluding *Mirocetus*. Several recently proposed synapomorphies of Odontoceti (e.g., intermediate length maxilla, loss of cranial hiatus, high tegmen tympani of periotic) were not supported.
22. *Xenorophus* possesses a large and broad antorbital notch. This structure is a proposed synapomorphy of Neoceti. We note some morphological disparity amongst Neoceti and further parallels within stem odontocetes and certain toothed mysticetes, and recommend further study of this region.
23. A constriction of the maxilla near the antorbital notch, with the lacrimal incising into the lateral margin of the maxilla, is a previously used character to diagnose a toothed mysticete clade including Aetiocetidae and Mammalodontidae. The presence of this feature in *Xenorophus*, other Xenorophidae, and many other stem odontocetes prompts reevaluation of this character.
24. The proliferation of new stem odontocetes, in concert with stabilizing phylogenetic relationships, permits the naming of two new odontocete clades: Amblyoccipita, a branch-based clade forming the inclusive sister taxon to Xenorophidae, and Stegoceti, an apomorphy-based clade defined on a dorsally expanded intertemporal region and including the common ancestor of *Agorophius* and all later diverging odontocetes, but excluding Xenorophidae, Simocetidae, *Mirocetus*, and *Ashleycetus*.

Supplementary Materials: The following supporting information can be downloaded at: https://www.mdpi.com/article/10.3390/d15111154/s1. File S1: cladistic matrix; File S2: list of cladistic characters; File S3: supplementary measurements of Odontoceti. References [4,5,8,10,12,15–18,23,24,30,37,78,80,84,91,94,100,131,141,152,153,172,177–179,198,205–231] are cited in the supplementary materials.

Author Contributions: Conceptualization, methodology, software, validation, formal analysis, investigation, resources, data curation, R.W.B. and J.H.G.; Writing—original draft preparation, R.W.B.; Review and editing, J.H.G.; Visualization, R.W.B. and J.H.G. All authors have read and agreed to the published version of the manuscript.

Funding: This research was funded by a research fellowship to RWB from M. Brown via the College of Charleston.

Institutional review Board Statement: Not applicable.

Data Availability Statement: All data used in the present paper are published in the paper.

Acknowledgments: We are indebted to our two mentors, the late A.E. Sanders, who began this work several decades ago, and the late R.E. Fordyce, who revolutionized the study and knowledge of early Neoceti. This study is dedicated to the memory of these two giants in paleocetology. We thank M. Brown for his financial support of this project. This study would not have been possible without the generous donations from collectors including B. Albright, P.S. Coleman, D. Cope, S. Faust, M. Havenstein, W. Hillenius, J. Malcolm, V. McCollum, the late S. Miller, B. Nemeth, A. Newton, C. Newton, A. Stokes, and B. Way. We thank K.M. Brown for acquiring several specimens of *Xenorophus sloanii*, and thank the late D. Aylor for donating the holotype specimen of *Xenorophus simplicidens*. Thanks to S.J. Boessenecker (CCNHM), M. Gibson and J. Peragine (ChM), and D.J. Bohaska (USNM) for their extensive curatorial assistance. We thank volunteer and student preparators at CCNHM, including Shelley Copeland, Samantha Czwalina, Megan Dia, Jane Kelly, and Ana Sillsbury for preparation of CCNHM *Xenorophus* material. This study benefited from discussions with B. Beatty, D.J. Bohaska, M. Brown, M. Churchill, and R. Racicot. Laborious reviews from two anonymous reviewers and efforts from the editors improved the quality of this manuscript. We thank M. Bisconti for inviting us to contribute to this volume.

Conflicts of Interest: The authors declare no conflict of interest.

References

1. Boessenecker, R.W.; Ahmed, E.; Geisler, J.H. New records of the dolphin *Albertocetus meffordorum* (Odontoceti: Xenorophidae) from the lower Oligocene of South Carolina: Encephalization, sensory anatomy, postcranial morphology, and ontogeny of early odontocetes. *PLoS ONE* **2017**, *12*, e0186476. [CrossRef]
2. Boessenecker, R.W.; Fraser, D.; Churchill, M.; Geisler, J.H. A toothless dwarf dolphin (Odontoceti: Xenorophidae) points to explosive feeding diversification of modern whales (Neoceti). *Proc. R. Soc. B* **2017**, *284*, 20170531. [CrossRef]
3. Churchill, M.; Martinez-Caceres, M.; Muizon, C.D.; Mnieckowski, J.; Geisler, J.H. The origin of high-frequency hearing in whales. *Curr. Biol.* **2016**, *26*, 2144–2149. [CrossRef]
4. Geisler, J.H.; Colbert, M.W.; Carew, J.L. A new fossil species supports an early origin for toothed whale echolocation. *Nature* **2014**, *508*, 383–386. [CrossRef] [PubMed]
5. Sanders, A.E.; Geisler, J.H. A new basal odontocete from the upper Rupelian of South Carolina, U.S.A., with contributions to the systematics of *Xenorophus* and *Mirocetus* (Mammalia, Cetacea). *J. Vertebr. Paleontol.* **2015**, *35*, e890107. [CrossRef]
6. Weems, R.E.; Boessenecker, R.W.; Sanders, A.E. Cetacean remains from the lower Oligocene Old Church Formation of Virginia. *Mosasaur* **2022**, *12*, 29–44.
7. Boessenecker, R.W. Oligocene-Miocene marine mammals from Belgrade Quarry, North Carolina. *Geobios* **2022**, *74*, 1–19. [CrossRef]
8. Kellogg, R. Description of an apparently new toothed cetacean from South Carolina. *Smithson. Misc. Collect.* **1923**, *76*, 1–7.
9. Uhen, M.D. A new *Xenorophus*-like odontocete cetacean from the Oligocene of North Carolina and a discussion of the basal odontocete radiation. *J. Syst. Palaeontol.* **2008**, *6*, 433–452. [CrossRef]
10. Geisler, J.H.; Sanders, A.E. Morphological evidence for the phylogeny of Cetacea. *J. Mamm. Evol.* **2003**, *10*, 23–129. [CrossRef]
11. Cranford, T.W. The sperm whale's nose: Sexual selection on a grand scale? *Mar. Mammal Sci.* **1999**, *15*, 1134–1158. [CrossRef]
12. Cranford, T.W.; Amundin, M.; Norris, K.S. Functional morphology and homology in the odontocete nasal complex: Implications for sound generation. *J. Morphol.* **1996**, *228*, 223–285. [CrossRef]
13. Au, W.W.L. *The Sonar of Dolphins*; Springer: New York, NY, USA, 1993.
14. Jones, G. Echolocation. *Curr. Biol.* **2005**, *15*, R484–R488. [CrossRef]
15. Fraser, F.C.; Purves, P.E. Hearing in cetaceans—Evolution of the accessory air sacs and the structure and function of the outer and middle ear in recent cetaceans. *Bull. Br. Mus. (Nat. Hist.) Zool.* **1960**, *7*, 1–140. [CrossRef]
16. Mead, J.G. Anatomy of the external nasal passages and facial complex in the Delphinidae (Mammalia: Cetacea). *Smithson. Contrib. Zool.* **1975**, *207*, 1–72. [CrossRef]
17. Fordyce, R.E. *Waipatia maerewhenua*, New Genus and New Species, Waipatiidae, New Family, an archaic late Oligocene dolphin (Cetacea: Odontoceti: Platanistoidea) from New Zealand. *Proc. San Diego Soc. Nat. Hist.* **1994**, *29*, 147–176. [CrossRef]
18. Fordyce, R.E. *Simocetus rayi* (Odontoceti, Simocetidae, new family); a bizarre new archaic Oligocene dolphin from the eastern North Pacific. *Smithson. Contrib. Paleobiol.* **2002**, *93*, 185–222.
19. Park, T.; Fitzgerald, E.M.G.; Evans, A.R. Ultrasonic hearing and echolocation in the earliest toothed whales. *Biol. Lett.* **2016**, *12*, 20160060. [CrossRef]

20. Leidy, J. The extinct mammalian fauna of Dakota and Nebraska, including an account of some allied forms from other localities, together with a synopsis of the mammalian remains of North America. *J. Acad. Nat. Sci. Phila. Second Ser.* **1869**, *7*, 8–472.
21. Fordyce, R.E. Systematics of the odontocete whale *Agorophius pygmaeus* and the family Agorophiidae (Mammalia: Cetacea). *J. Paleontol.* **1981**, *55*, 1028–1045.
22. Dooley, A.C. A review of the eastern North American Squalodontidae (Mammalia, Cetacea). *Jeffersoniana* **2003**, *11*, 1–26.
23. Allen, G.M. A new fossil cetacean. *Bull. Mus. Comp. Zool.* **1921**, *65*, 3–14.
24. Whitmore, F.C.; Sanders, A.E. A review of the Oligocene Cetacea. *Syst. Zool.* **1977**, *25*, 304–320. [CrossRef]
25. Vélez-Juarbe, J. A new stem odontocete from the late Oligocene Pysht Formation in Washington State, USA. *J. Vertebr. Paleontol.* **2017**, *37*, e1366916. [CrossRef]
26. Weems, R.E.; Bybell, L.M.; Edwards, L.E.; Lewis, W.C.; Self-Trail, J.M.; Albright, L.B., III; Cicimurri, D.J.; Harris, W.B.; Osborne, J.E.; Sanders, A.E. Stratigraphic revision of the Cooper Group and Chandler Bridge and Edisto Formations in the coastal plain of South Carolina. *South Carol. Geol.* **2016**, *49*, 1–24.
27. Uhen, M.D.; Fordyce, R.E.; Barnes, L.G. Odontoceti. In *Evolution of Tertiary Mammals of North America, Volume 2: Small Mammals, Xenarthrans, and Marine Mammals*; Janis, C.M., Gunnell, G.F., Uhen, M.D., Eds.; Cambridge University Press: Cambridge, UK, 2011; pp. 566–606.
28. Albright, L.B., III; Sanders, A.E.; Weems, R.E.; Cicimurri, D.J.; Knight, J.L. Cenozoic vertebrate biostratigraphy of South Carolina, U.S.A., and additions to the fauna. *Bull. Fla. Mus.* **2019**, *57*, 77–236.
29. Martinez-Caceres, M.; Lambert, O.; Muizon, C.D. The anatomy and phylogenetic affinities of *Cynthiacetus peruvianus*, a large *Dorudon*-like basilosaurid (Cetacea, Mammalia) from the late Eocene of Peru. *Geodiversitas* **2017**, *39*, 7–163. [CrossRef]
30. Miller, G.S. The telescoping of the cetacean skull. *Smithson. Misc. Collect.* **1923**, *75*, 1–55.
31. Kellogg, R. The history of whales—Their adaptation to life in water. *Q. Rev. Biol.* **1928**, *3*, 29–76, 174–208. [CrossRef]
32. Albright, L.B., III; Sanders, A.E.; Geisler, J.H. An unexpectedly derived odontocete from the Ashley Formation (upper Rupelian) of South Carolina, U.S.A. *J. Vertebr. Paleontol.* **2018**, *38*, 1–15. [CrossRef]
33. Boessenecker, R.W.; Boessenecker, S.J. Paleontology of the "Ashley Phosphate Beds" of Charleston: Insights from Northbridge Park, Charleston, South Carolina. *Geol. Soc. Am. Field Guide* **2019**, *53*, 1–8.
34. Sanders, A.E. Additions to the Pleistocene mammal faunas of South Carolina, North Carolina, and Georgia. *Trans. Am. Philos. Soc.* **2002**, *92*, 1–152. [CrossRef]
35. Sanders, A.E. Excavation of Oligocene marine fossil beds near Charleston, South Carolina. *Natl. Geogr. Res. Rep.* **1980**, *12*, 601–621.
36. Sanders, A.E.; Weems, R.E.; Lemon, E.M.J. Chandler Bridge Formation—A new Oligocene stratigraphic unit in the lower coastal plain of South Carolina. *US Geol. Surv. Bull.* **1982**, *1529-H*, H105–H124.
37. Boessenecker, R.W.; Churchill, M.; Buchholtz, E.A.; Beatty, B.L.; Geisler, J.H. Convergent evolution of swimming adaptations in modern whales revealed by a large macrophagous dolphin from the Oligocene of South Carolina. *Curr. Biol.* **2020**, *30*, 3267–3273. [CrossRef]
38. Godfrey, S.J.; Uhen, M.D.; Osborne, J.E.; Edwards, L.E. A new specimen of *Agorophius pygmaeus* (Agorophiidae, Odontoceti, Cetacea) from the early Oligocene Ashley Formation of South Carolina, USA. *J. Paleontol.* **2016**, *90*, 154–169. [CrossRef]
39. Sanders, A.E. The systematic position of the primitive odontocete *Xenorophus sloanii* (Mammalia, Cetacea) and two new taxa from the late Oligocene of South Carolina, U.S.A. *Paleontol. Soc. Spec. Publ.* **1996**, *8*, 338. [CrossRef]
40. Whitmore, F.C.; Kaltenbach, J.A. Neogene Cetacea of the Lee Creek Phosphate Mine, North Carolina. *Va. Mus. Nat. Hist. Spec. Publ.* **2008**, *14*, 181–269.
41. Boessenecker, R.W. Problematic archaic whale *Phococetus* (Cetacea: Odontoceti) from the Lee Creek Mine, North Carolina, USA, with comments on geochronology of the Pungo River Formation. *Pal Z* **2019**, *93*, 93–103. [CrossRef]
42. Buchholtz, E.A. Vertebral osteology and swimming style in living and fossil whales (Order: Cetacea). *J. Zool. Soc. Lond.* **2001**, *253*, 175–190. [CrossRef]
43. Lloyd, G.T.; Slater, G.J. A total-group phylogenetic metatree for Cetacea and the importance of fossil data in diversification analyses. *Syst. Biol.* **2021**, *70*, 922–939. [CrossRef]
44. McGowen, M.R.; Spaulding, M.; Gatesy, J. Divergence date estimation and a comprehensive molecular tree of extant cetaceans. *Mol. Phylogenet. Evol.* **2009**, *53*, 891–906. [CrossRef] [PubMed]
45. Steeman, M.E.; Hebsgaard, M.B.; Fordyce, R.E.; Ho, S.Y.W.; Rabosky, D.L.; Nielsen, R.; Rahbek, C.; Glenner, H.; Sørensen, M.V.; Willerslev, E. Radiation of extant cetaceans driven by restructuring of the oceans. *Syst. Biol.* **2009**, *58*, 573–585. [CrossRef] [PubMed]
46. Boessenecker, R.W.; Beatty, B.L.; Geisler, J.H. New specimens and species of the Oligocene toothed baleen whale *Coronodon* from South Carolina and the origin of Neoceti. *PeerJ* **2023**, *11*, e14975. [CrossRef]
47. Fordyce, R.E.; Marx, F.G. Gigantism precedes filter feeding in baleen whale evolution. *Curr. Biol.* **2018**, *28*, 1670–1676. [CrossRef]
48. Geisler, J.H.; Boessenecker, R.W.; Brown, K.M.; Beatty, B.L. The origin of filter feeding in whales. *Curr. Biol.* **2017**, *27*, 2036–2042. [CrossRef]
49. Marx, F.G.; Tsai, C.-H.; Fordyce, R.E. A new early Oligocene toothed 'baleen' whale (Mysticeti: Aetiocetidae) from western North America: One of the oldest and the smallest. *R. Soc. Open Sci.* **2015**, *2*, 150476. [CrossRef]

50. Churchill, M.; Geisler, J.H.; Beatty, B.L.; Goswami, A. Evolution of cranial telescoping in echolocating whales (Cetacea: Odontoceti). *Evolution* **2018**, *72*, 1092–1108. [CrossRef]
51. Racicot, R.; Boessenecker, R.W.; Darroch, S.A.F.; Geisler, J.H. Evidence for convergent evolution of ultrasonic hearing in toothed whales (Cetacea: Odontoceti). *Biol. Lett.* **2019**, *15*, 20190083. [CrossRef]
52. Coombs, E.J.; Clavel, J.; Park, T.; Churchill, M.C.; Goswami, A. Wonky whales: The evolution of cranial asymmetry in cetaceans. *BMC Biol.* **2020**, *18*, 86. [CrossRef] [PubMed]
53. Churchill, M.C.; Baltz, C. Evolution of orbit size in toothed whales (Artiodactyla: Odontoceti). *J. Anat.* **2021**, *239*, 1419–1437. [CrossRef]
54. Coombs, E.J.; Felice, R.N.; Clavel, J.; Park, T.; Bennion, R.F.; Churchill, M.; Geisler, J.H.; Beatty, B.L.; Goswami, A. The tempo of cetacean cranial evolution. *Curr. Biol.* **2022**, *32*, 2233–2247. [CrossRef]
55. Weems, R.E.; Sanders, A.E. Oligocene pancheloniid sea turtles from the vicinity of Charleston, South Carolina, USA. *J. Vertebr. Paleontol.* **2014**, *34*, 80–99. [CrossRef]
56. Cooke, C.W. Geology of the Coastal Plain of South Carolina. *U.S. Geol. Surv. Bull.* **1936**, *867*, 1–196.
57. Weems, R.E.; Lemon, E.M.J.; McCartran, L. Shallow subsurface geology of the North Charleston 7.5-minute quadrangle, South Carolina. *US Geol. Surv. Open File Rep.* **1985**, *85-274*, 1–62.
58. Zullo, V.A.; Katuna, M.P.; Herridge, K.C. Scalpellomorph and balanomorph barnacles (Cirripedia) from the upper Oligocene Ashley Formation, Charleston County, South Carolina. *South Carol. Geol.* **1991**, *34*, 57–67.
59. Miller, A.E.; Gibson, M.L.; Boessenecker, R.W. A megatoothed shark (*Carcharocles angustidens*) nursery in the Oligocene Charleston embayment, South Carolina, USA. *Palaeontol. Electron.* **2023**, *24*, a19. [CrossRef] [PubMed]
60. Fierstine, H.L.; Weems, R.E. Paleontology of the Oligocene Ashley and Chandler Bridge Formations of South Carolina, 4: Analysis and new records of billfishes (Perciformes: Ziphiodei). *Palaeo Ichthyol.* **2009**, *11*, 43–88.
61. Fallon, B.R.; Boessenecker, R.W. Multispecies leatherback turtle assemblage from the Oligocene Chandler Bridge and Ashley formations of South Carolina, USA. *Acta Palaeontol. Pol.* **2020**, *65*, 763–776. [CrossRef]
62. Hay, O.P. Characteristics of sundry fossil vertebrates; Part VII, New fossil turtle from Eocene marl of South Carolina. *Pan-Am. Geol.* **1923**, *39*, 119–120.
63. Weems, R.E.; Brown, K.M. More-complete remains of *Procolpochelys charlestonensis* (Oligocene, South Carolina) an occurrence of *Euclastes* (upper Eocene, South Carolina), and their bearing on Cenozoic pancheloniid sea turtle distribution and phylogeny. *J. Paleontol.* **2017**, *91*, 1228–1243. [CrossRef]
64. Müller, J. *Über die Fossilen Reste der Zeuglodonten von Nordamerica, mit Rücksicht auf die Europäischen Rste aus Dieser Familie*; Reimer, G.: Berlin, Germany, 1849; p. 38.
65. Allen, J.A. Note on squalodont remains from Charleston, S.C. *Bull. Am. Mus. Nat. Hist.* **1887**, *12*, 35–39.
66. Boessenecker, R.W.; Fordyce, R.E. A new eomysticetid from the Oligocene Kokoamu Greensand of New Zealand and a review of the Eomysticetidae (Mammalia, Cetacea). *J. Syst. Palaeontol.* **2017**, *15*, 429–469. [CrossRef]
67. Sanders, A.E.; Barnes, L.G. Paleontology of the Late Oligocene Ashley and Chandler Bridge Formations of South Carolina, 2: *Micromysticetus rothauseni*, a primitive cetotheriid mysticete (Mammalia: Cetacea). *Smithson. Contrib. Paleobiol.* **2002**, *93*, 271–293.
68. Domning, D.P. Fossil Sirenia of the West Atlantic and Caribbean Region. II. *Dioplotherium manigaulti* Cope, 1883. *J. Vertebr. Paleontol.* **1989**, *9*, 415–428. [CrossRef]
69. Domning, D.P. Fossil Sirenia of the West Atlantic and Caribbean Region. IV. *Crenatosiren olseni* (Reinhardt, 1976). *J. Vertebr. Paleontol.* **1997**, *17*, 397–412. [CrossRef]
70. Domning, D.P.; Beatty, B.L. Fossil sirenia of the west Atlantic and Caribbean region. XII. *Stegosiren macei*, gen. et sp. nov. *J. Vertebr. Paleontol.* **2019**, *39*, e1650369. [CrossRef]
71. Vélez-Juarbe, J.; Domning, D.P. Fossil sirenia of the West Atlantic and Caribbean region. X. *Priscosiren atlantica*, gen et sp. nov. *J. Vertebr. Paleontol.* **2014**, *34*, 951–964. [CrossRef]
72. Anthonissen, E.; Ogg, J.G. Cenozoic and Cretaceous biochronology of planktonic foraminifera and calcareous nannofossils. In *The Geologic Time Scale 2012*; Gradstein, F.M., Ogg, J.G., Schmitz, M., Ogg, G., Eds.; Elsevier: Amsterdam, The Netherlands, 2012; pp. 1083–1127.
73. Bisconti, M.; Pellegrino, L.; Carnevale, G. The chronology of mysticete diversification (Mammalia, Cetacea, Mysticeti): Body size, morphological evolution and global change. *Earth Sci. Rev.* **2023**, *239*, 104373. [CrossRef]
74. McCuen, W.N.; Ishimori, A.; Boessenecker, R.W. A new specimen of *Xiphiorhynchus* cf. *X. aegyptiacus* (Istiophoriformes, Xiphiodei, Xiphiidae) and billfish diversity in the Oligocene of South Carolina. *Vertebr. Anat. Morphol. Paleontol.* **2021**, *8*, 98–104. [CrossRef]
75. Katuna, M.P.; Geisler, J.H.; Colquhoun, D.J. Stratigraphic correlation of Oligocene marginal marine and fluvial deposits across the middle and lower coastal plain, South Carolina. *Sediment. Geol.* **1997**, *108*, 181–194. [CrossRef]
76. Cicimurri, D.J.; Knight, J.L. Late Oligocene sharks and rays from the Chandler Bridge Formation, Dorchester County, South Carolina, USA. *Acta Palaeontol. Pol.* **2009**, *54*, 627–647. [CrossRef]
77. Ksepka, D.T. Flight performance of the largest volant bird. *Proc. Natl. Acad. Sci. USA* **2014**, *111*, 10624–10629. [CrossRef] [PubMed]
78. Sanders, A.E.; Barnes, L.G. Paleontology of the Late Oligocene Ashley and Chandler Bridge Formations of South Carolina, 3: Eomysticetidae, a new family of primitive mysticetes (Mammalia: Cetacea). *Smithson. Contrib. Paleobiol.* **2002**, *93*, 313–356.

79. Vélez-Juarbe, J.; Domning, D.P. Fossil Sirenia of the West Atlantic and Caribbean Region. IX. *Metaxytherium albifontanum*, sp. nov. *J. Vertebr. Paleontol.* **2014**, *34*, 444–464. [CrossRef]
80. Mead, J.G.; Fordyce, R.E. The therian skull: A lexicon with emphasis on the odontocetes. *Smithson. Contrib. Zool.* **2009**, *627*, 1–248. [CrossRef]
81. Boessenecker, R.W.; Fordyce, R.E. A new eomysticetid (Mammalia: Cetacea) from the late Oligocene of New Zealand and a re-evaluation of '*Mauicetus*' *waitakiensis*. *Pap. Palaeontol.* **2015**, *1*, 107–140. [CrossRef]
82. Hammer, Ø.; Harper, D.A.T.; Ryan, P.D. Paleontological statistics software package for education and data analysis. *Palaeontol. Electron.* **2001**, *4*, 1–9.
83. Perrin, W.F. Variation of spotted and spinner porpoise (Genus *Stenella*) in the eastern Pacific and Hawaii. *Bull. Scripps Inst. Oceanogr.* **1975**, *21*, 1–206.
84. Bianucci, G.; Geisler, J.H.; Citron, S.; Collareta, A. The origins of the killer whale ecomorph. *Curr. Biol.* **2022**, *32*, 1843–1851. [CrossRef] [PubMed]
85. Maddison, W.P.; Maddison, D.R. Mesquite: A Modul$ar System for Evolutionary Analysis. 3.81. 2023. Available online: http://www.mesquiteproject.org (accessed on 1 October 2023).
86. Goloboff, P.A.; Catalano, S.A. TNT version 1.5, including a full implementation of phylogenetic morphometrics. *Cladistics* **2016**, *32*, 221–238. [CrossRef] [PubMed]
87. Goloboff, P.A.; Farris, J.S.; Nixon, K.C. TNT, a free program for phylogenetic analysis. *Cladistics* **2008**, *24*, 774–786. [CrossRef]
88. McGowen, M.R.; Tsagkogeorga, G.; Álvarez-Carretero, S.; Dos Reis, M.; Struebig, M.; Deaville, R.; Jepson, P.D.; Jarman, S.; Polanowski, A.; Morin, P.A.; et al. Phylogenomic resolution of the cetaecan tree of life using target sequence capture. *Syst. Biol.* **2020**, *69*, 479–501. [CrossRef] [PubMed]
89. Linnaeus, C. *Systema Naturae per Regna tria Naturae, Secundum Classis, Ordines, Genera, Species cum Characteribus, Differntiis, Synonymis, Oocis*; Laurentii Salvii: Stockholm, Sweden, 1758; p. 824.
90. Brisson, M.J. *Regnum Animale in Classes IX Distributum Sive Synopsis Methodica*; Batavorum, L., Haak, T., Eds.; chez Cl. Jean-Baptiste Bauche: Paris, France, 1762.
91. Flower, W.H. Description of the skeleton of *Inia geoffrensis* and the skull of *Pontoporia blainvillii*, with remarks on the systematic position of these animals in the Order Cetacea. *Trans. Zool. Soc. Lond.* **1867**, *6*, 87–116. [CrossRef]
92. Roston, R.A.; Boessenecker, R.W.; Geisler, J.H. Evolution and development of the cetacean skull roof: A case study in novelty and homology. *Philos. Trans. R. Soc. B* **2023**, *378*, 20220086. [CrossRef]
93. Muizon, C.D.; Bianucci, G.; Martinez-Caceres, M.; Lambert, O. *Mystacodon selenensis*, the earliest known toothed mysticete (Cetacea, Mammalia) from the late Eocene of Peru: Anatomy, phylogeny, and feeding adaptations. *Geodiversitas* **2019**, *41*, 401–499. [CrossRef]
94. Luo, Z.; Gingerich, P.D. Terrestrial Mesonychia to aquatic Cetacea: Transformation of the basicranium and evolution of hearing in whales. *Univ. Mich. Pap. Paleontol.* **1999**, *31*, 1–98.
95. Mourlam, M.J.; Orliac, M.J. Protocetid (Cetacea, Artiodactyla) bullae and petrosals from the middle Eocene locality of Kpogamé, Togo: New insights into the early history of cetacean hearing. *J. Syst. Palaeontol.* **2018**, *16*, 621–644. [CrossRef]
96. Oishi, M.; Hasegawa, Y. Diversity of Pliocene mysticetes from eastern Japan. *Isl. Arc* **1995**, *3*, 346–452. [CrossRef]
97. Loch, C.; Grando, L.J.; Schwass, D.R.; Kieser, J.A.; Fordyce, R.E.; Simões-Lopes, P.C. Dental erosion in South Atlantic dolphins (Cetacea: Delphinidae): A macro and microscopic approach. *Mar. Mammal Sci.* **2013**, *29*, 338–347. [CrossRef]
98. Pyenson, N.D.; Sponberg, S.N. Reconstructing body size in extinct crown Cetacea (Neoceti) using allometry, phylogenetic methods and tests from the fossil record. *J. Mamm. Evol.* **2011**, *18*, 269–288. [CrossRef]
99. Citron, S.; Geisler, J.H.; Collareta, A.; Biannucci, G. Systematics, phylogeny and feeding behavior of the oldest killer whale: A reappraisal of *Orcinus citoniensis* (Capellini, 1883) from the Pliocene of Tuscany (Italy). *Bolletino Della Soc. Paleontol. Ital.* **2022**, *61*, 167–186.
100. Lambert, O.; Bianucci, G.; Urbina, M.; Geisler, J.H. A new inioid (Cetacea, Odontoceti, Delphinida) from the Miocene of Peru and the origin of modern dolphin and porpoise families. *Zool. J. Linnaean Soc.* **2017**, *179*, 919–946.
101. Tanaka, Y.; Fordyce, R.E. Fossil dolphin *Otekaikea marplesi* (Latest Oligocene, New Zealand) expands the morphological and taxonomic diversity of Oligocene dolphins. *PLoS ONE* **2014**, *9*, e107972. [CrossRef] [PubMed]
102. Muñiz, F.; Beláustegui, Z.; Toscano, A.; Ramirez-Cruzado, S.; Gámez Vintaned, J.A. New ichnospecies of *Linichnus* Jacobsen & Bromley, 2009. *Ichnos* **2020**, *27*, 344–351.
103. Jacobsen, A.R.; Bromley, R.G. New ichnotaxa based on tooth impressions on dinosaur and whale bones. *Geol. Q.* **2009**, *53*, 373–382.
104. Boessenecker, R.W.; Fordyce, R.E. Trace fossil evidence of predation upon bone-eating worms on a baleen whale skeleton from the Oligocene of New Zealand. *Lethaia* **2015**, *48*, 326–331. [CrossRef]
105. Higgs, N.D.; Glover, A.G.; Dahlgren, T.G.; Smith, C.R.; Fujiwara, Y.; Pradhillon, F.; Johnson, S.B.; Vrijenhoek, R.C.; Little, C.T.S. The morphological diversity of *Osedax* worm borings (Annelida: Siboglinidae). *J. Mar. Biol. Assoc. United Kingd.* **2014**, *94*, 1429–1439. [CrossRef]
106. Kiel, S.; Goedert, J.L.; Kahl, W.; Rouse, G.W. Fossil traces of the bone-eating worm Osedax in early Oligocene whale bones. *Proc. Natl. Acad. Sci. USA* **2010**, *107*, 8656–8659. [CrossRef]
107. Higgs, N.D.; Glover, A.G.; Dahlgren, T.G.; Little, C.T.S. Bone-boring worms: Characterizing the morphology, rate, and method of bioerosion by *Osedax mucofloris* (Annelida, Siboglinidae). *Biol. Bull.* **2011**, *221*, 307–316. [CrossRef]

108. Kiel, S.; Kahl, W.; Goedert, J.L. Traces of the bone-eating annelid *Osedax* in Oligocene whale teeth and fish bones. *Paläontologische Z.* **2013**, *87*, 161–167. [CrossRef]
109. Boessenecker, R.W.; Perry, F.A.; Schmitt, J.G. Comparative taphonomy, taphofacies, and bonebeds of the Mio-Pliocene Purisima Formation, Central California: Strong physical control on marine vertebrate preservation in shallow marine settings. *PLoS ONE* **2014**, *9*, e91419. [CrossRef]
110. Glover, A.G.; Wiklund, H.; Taboada, S.; Avila, C.; Cristobo, J.; Smith, C.R.; Kemp, K.M.; Jamieson, A.J.; Dahlgren, T.G. Bone-eating worms from the Antarctic: The contrasting fate of whale and wood remains on the Southern Ocean seafloor. *Proc. R. Soc. B* **2013**, *280*, 20131390. [CrossRef] [PubMed]
111. Lundsten, L.; Schlining, K.L.; Frasier, K.; Johnson, S.B.; Kuhnz, L.A.; Harvey, J.B.J.; Clague, G.; Vrijenhoek, R.C. Time-series analysis of six whale-fall communities in Monterey Canyon, California, USA. *Deep-Sea Res. I* **2010**, *57*, 1573–1584. [CrossRef]
112. Ramos, R.M.A.; Di Beneditto, A.P.M.; Lima, N.R.W. Relationship between dental morphology, sex, body length and age in *Pontoporia blainvillei* and *Sotalia fluviatilis* (Cetacea) in northern Rio de Janeiro, Brazil. *Rev. Bras. Biol.* **2000**, *60*, 283–290. [CrossRef]
113. Foote, A.D.; Newton, J.; Ávila-Arcos, M.C.; Kampmann, M.-L.; Samaniego, J.A.; Post, K.; Rosing-Asvid, A.; Mikkel-Holger, S.; Gilbert, M.T.P. Tracking niche variation over millennial timescales in sympatric killer whale lineages. *Proc. R. Soc. B* **2013**, *280*, 20131481. [CrossRef]
114. Ford, J.K.B.; Ellis, G.M.; Matkin, C.O.; Wetklo, M.H.; Barrett-Lennard, L.G.; Withler, R.E. Shark predation and tooth wear in a population of northeastern Pacific killer whales. *Aquat. Biol.* **2011**, *11*, 213–224. [CrossRef]
115. Fahlke, J.M.; Bastl, K.A.; Semprebon, G.M.; Gingerich, P.D. Paleoecology of archaeocete whales throughout the Eocene: Dietary adaptations revealed by microwear analysis. *Palaeogeogr. Palaeoclimatol. Palaeoecol.* **2013**, *386*, 690–701. [CrossRef]
116. Gol'din, P.; Zvonok, E.; Rekovets, L.; Kovalchuk, A.; Krakhmalnaya, T. *Basilotritus* (Cetacea: Pelagiceti) from the Eocene of Nagornoye (Ukraine): New data on anatomy, ontogeny and feeding of early basilosaurids. *Comptes Rendus Palevol* **2014**, *13*, 267–278. [CrossRef]
117. Marx, F.G.; Hocking, D.P.; Park, T.; Pollock, T.I.; Parker, W.M.G.; Rule, J.P.; Fitzgerald, E.M.G.; Evans, A.R. Suction causes novel tooth wear in marine mammals, with implications for feeding evolution in baleen whales. *J. Mamm. Evol.* **2023**, *30*, 493–505. [CrossRef]
118. Bouetel, V.; Muizon, C.D. The anatomy and relationships of *Piscobalaena nana* (Cetacea, Mysticeti), a Cetotheriidae s.s. from the early Pliocene of Peru. *Geodiversitas* **2006**, *28*, 319–395.
119. Bianucci, G.; Lambert, O.; Post, K. High concentration of long-snouted beaked whales (genus *Messapicetus*) from the Miocene of Peru. *Palaeontology* **2010**, *53*, 1077–1098. [CrossRef]
120. Gutstein, C.S.; Cozzuol, M.A.; Vargas, A.O.; Suárez, M.E.; Schultz, C.L.; Rubilar-Rogers, D. Patterns of skull variation of *Brachydelphis* (Cetacea, Odontoceti) from the Neogene of the Southeastern Pacific. *J. Mammal.* **2009**, *90*, 504–519. [CrossRef]
121. Fordyce, R.E.; Barnes, L.G.; Miyazaki, N. General aspects of the evolutionary history of whales and dolphins. *Isl. Arc* **1995**, *3*, 373–391. [CrossRef]
122. Uhen, M.D.; Pyenson, N.D. Diversity estimates, biases, and historiographic effects: Resolving cetacean diversity in the Tertiary. *Palaeontol. Electron.* **2007**, *10*, 1–22.
123. Ito, H.; Miyazaki, N. Skeletal development of the striped dolphin (*Stenella coeruleoalba*) in Japanese waters. *J. Mammal. Soc. Jpn.* **1990**, *14*, 79–96.
124. Nakamura, G.; Zenitani, R.; Kato, H. Relative skull growth of the sperm whale, *Physeter macrocephalus*, with a note of sexual dimorphism. *Mammal Study* **2013**, *38*, 177–186. [CrossRef]
125. Castillo, D.L.D.; Flores, D.A.; Cappozzo, H.L. Ontogenetic development and sexual dimorphism of Franciscana dolphin skull: A 3D geometric morphometric approach. *J. Morphol.* **2014**, *275*, 1366–1375. [CrossRef]
126. Sydney, N.V.; Machado, F.A.; Hingst-Zaher, E. Timing of ontogenetic changes of two cranial regions in *Sotalia guianensis*. *Mamm. Biol.* **2012**, *77*, 397–403. [CrossRef]
127. Chen, I.; Chou, L.-S.; Chen, Y.-J.; Watson, A. The maturation of skulls in postnatal Risso's dolphins (*Grampus griseus*) from Taiwanese waters. *Taiwania* **2011**, *56*, 177–185.
128. Loch, C.; Grando, L.J.; Kieser, J.A.; Simões-Lopes, P.C. Dental pathology in dolphins (Cetacea: Delphinidae) from the southern coast of Brazil. *Dis. Aquat. Org.* **2011**, *94*, 225–234. [CrossRef] [PubMed]
129. Werth, A.J. A kinematic study of suction feeding and associated behavior in the long-finned pilot whale, *Globicephala melas* (Traill). *Mar. Mammal Sci.* **2000**, *16*, 299–314. [CrossRef]
130. Jefferson, T.A.; Webber, M.A.; Pitman, R.L. *Marine Mammals of the World: A Comprehensive Guide to Their Identification*; Academic Press: Cambridge, UK, 2007; p. 573.
131. Johnston, C.; Berta, A. Comparative anatomy and evolutionary history of suction feeding in cetaceans. *Mar. Mammal Sci.* **2011**, *27*, 493–513. [CrossRef]
132. Werth, A.J. Mandibular and dental variation and the evolution of suction feeding in Odontoceti. *J. Mammal.* **2006**, *87*, 579–588. [CrossRef]
133. Werth, A.J. Feeding in marine mammals. In *Feeding: Form, Function and Evolution in Tetrapod Vertebrates*; Schwenk, K., Ed.; Academic Press: San Diego, CA, USA, 2000; pp. 487–526.
134. Lindberg, D.R.; Pyenson, N.D. Things that go bump in the night: Evolutionary interactions between cephalopods and cetaceans in the tertiary. *Lethaia* **2007**, *40*, 335–343. [CrossRef]

135. Snively, E.; Fahlke, J.M.; Welsh, R.C. Bone-breaking bite force of *Basilosaurus isis* (Mammalia, Cetacea) from the Late Eocene of Egypt estimated by finite element analysis. *PLoS ONE* **2015**, *10*, 30118380. [CrossRef]
136. Barnes, L.G.; Goedert, J.L.; Furusawa, H. (Eds.) The Earliest Known Echolocating Toothed Whales (Mammalia; Odontoceti): Preliminary Observations of Fossils from Washington State. *Mesa Southwest Mus. Bull.* **2001**, *8*, 91–100.
137. Barnes, L.G.; Kimura, M.; Furusawa, H.; Sawamura, H. Classification and distribution of Oligocene Aetiocetidae (Mammalia; Cetacea; Mysticeti) from western North America and Japan. *Isl. Arc* **1995**, *3*, 392–431. [CrossRef]
138. Deméré, T.A.; McGowen, M.R.; Berta, A.; Gatesy, J. Morphological and molecular evidence for a stepwise evolutionary transition from teeth to baleen in mysticete whales. *Syst. Biol.* **2008**, *57*, 15–37. [CrossRef]
139. Gatesy, J.; Ekdale, E.G.; Deméré, T.A.; Lanzetti, A.; Randall, J.; Berta, A.; El Adli, J.J.; Springer, M.S.; McGowen, M.R. Anatomical, ontogenetic, and genomic homologies guide reconstructions of the teeth-to-baleen transition in mysticete whales. *J. Mamm. Evol.* **2022**, *29*, 891–930. [CrossRef]
140. Lambertsen, R.H.; Ulrich, N.; Straley, J. Frontomandibular stay of Balaenopteridae: A mechanism for momentum recapture during feeding. *J. Mammal.* **1995**, *76*, 877–899. [CrossRef]
141. Fitzgerald, E.M.G. A bizarre new toothed mysticete (Cetacea) from Australia and the early evolution of baleen whales. *Proc. R. Soc. B* **2006**, *273*, 2955–2963. [CrossRef] [PubMed]
142. Fitzgerald, E.M.G. The morphology and systematics of *Mammalodon colliveri* (Cetacea: Mysticeti), a toothed mysticete from the Oligocene of Australia. *Zool. J. Linnaean Soc.* **2010**, *158*, 367–476. [CrossRef]
143. Fitzgerald, E.M.G. Archaeocete-like jaws in a baleen whale. *Biol. Lett.* **2012**, *8*, 94–96. [CrossRef] [PubMed]
144. Johnston, C.; Deméré, T.A.; Berta, A.; Yonas, J.; St. Leger, J. Observations on the musculoskeletal anatomy of the head of a neonate gray whale (*Eschrichtius robustus*). *Mar. Mammal Sci.* **2010**, *26*, 186–194. [CrossRef]
145. Eales, N.B. The skull of foetal narwhal, *Monodon monoceros* L. *Philos. Trans. R. Soc. Lond.* **1950**, *B235*, 1–33.
146. Boessenecker, R.W.; Fordyce, R.E. Anatomy, feeding ecology, and ontogeny of a transitional baleen whale: A new genus and species of Eomysticetidae (Mammalia: Cetacea) from the Oligocene of New Zealand. *PeerJ* **2015**, *3*, e1129. [CrossRef]
147. Mourlam, M.J.; Orliac, M.J. Infrasonic and ultrasonic hearing evolved after the emergence of modern whales. *Curr. Biol.* **2017**, *27*, 1776–1781. [CrossRef]
148. Cranford, T.W.; Krysl, P.; Hildebrand, J.A. Acoustic pathways revealed: Simulated sound transmission and reception in Cuvier's beaked whale (*Ziphius cavirostris*). *Bioinspiration Biomim.* **2008**, *3*, 016001. [CrossRef]
149. Fahlke, J.M.; Gingerich, P.D.; Welsh, R.C.; Wood, A.R. Cranial asymmetry in Eocene archaeocete whales and the evolution of directional hearing in water. *Proc. Natl. Acad. Sci. USA* **2011**, *108*, 14545–14548. [CrossRef]
150. Armfield, B.A.; Zheng, Z.; Bajpai, S.; Vinyard, C.J.; Thewissen, J.G.M. Development and evolution of the unique cetacean dentition. *PeerJ* **2013**, *1*, e24. [CrossRef] [PubMed]
151. Macleod, C.D.; Reidenberg, J.S.; Weller, M.; Santos, M.B.; Herman, J.; Goold, J.; Pierce, G.J. Breaking symmetry: The marine environment, prey size, and the evolution of asymmetry in cetacean skulls. *Anat. Rec.* **2007**, *290*, 539–545. [CrossRef] [PubMed]
152. Reidenberg, J.S.; Laitman, J.T. Anatomy of the hyoid apparatus in Odontoceti (toothed whales): Specializations of their skeleton and musculature compared with those of terrestrial mammals. *Anat. Rec.* **1994**, *240*, 598–624. [CrossRef] [PubMed]
153. Barnes, L.G. The fossil record and evolutionary relationships of the genus *Tursiops*. In *The Bottlenose Dolphin*; Leatherwood, S., Reeves, R.R., Eds.; Academic Press: Cambridge, MA, USA, 1990; pp. 3–26.
154. Racicot, R.A.; Darroch, S.A.F.; Kohno, N. Neuroanatomy and inner ear labyrinths of the narwhal, *Monodon monoceros*, and beluga, *Delphinapterus leucas* (Cetacea: Monodontidae). *J. Anat.* **2018**, *233*, 421–439. [CrossRef]
155. Domning, D.P. Sirenian evolution in the North Pacific Ocean. *Univ. Calif. Publ. Geol. Sci.* **1978**, *18*, 1–176.
156. Dawson, M.R.; Gottfried, M.D. Paleopathology in a Miocene kentriodontid dolphin (Cetacea: Odontoceti). *Smithson. Contrib. Paleobiol.* **2002**, *93*, 263–270.
157. Robineau, D. Sur quelques cas d'edentation partielle chez *Delphinus delphis* et leur signification. *Aquat. Mamm.* **1981**, *8*, 33–39.
158. Oremland, M.S.; Allen, B.M.; Clapham, P.J.; Moore, P.J.; Potter, C.; Mead, J.G. Mandibular fractures in short-finned pilot whales, *Globicephala macrorhynchus*. *Mar. Mammal Sci.* **2010**, *26*, 1–16. [CrossRef]
159. Kompanje, E.J.O.; Post, K. Remarkable mandibular fracture healing in an early Holocene bottlenose dolphin (*Tursiops truncatus*). *Lutra* **2020**, *60*, 61–66.
160. Werth, A.J. Functional morphology of the sperm whale tongue, with reference to suction feeding. *Aquat. Mamm.* **2004**, *30*, 405–418. [CrossRef]
161. Murie, J. On deformity of the lower jaw in the cachalot (*Physeter macrocephalus*, Linn.). *Proc. Zool. Soc. Lond.* **1865**, *1865*, 390–396. [CrossRef]
162. Spaul, E.A. Deformity in the lower jaw of the sperm whale (*Physeter catodon*). *Proc. Zool. Soc. Lond.* **1964**, *142*, 391–395. [CrossRef]
163. Buchholtz, E.A.; Gee, J.K. Finding sacral: Developmental evolution of the axial skeleton of odontocetes (Cetacea). *Evol. Dev.* **2017**, *19*, 190–204. [CrossRef] [PubMed]
164. McCurry, M.R.; Pyenson, N.D. Hyper-longirostry and kinematic disparity in extinct toothed whales. *Paleobiology* **2018**, *45*, 21–29. [CrossRef]
165. Lambert, O.; Bianucci, G.; Post, K.; Muizon, C.D.; Salas-Gismondi, R.; Urbina, M.; Reumer, J. The giant bite of a new raptorial sperm whale from the Miocene epoch of Peru. *Nature* **2010**, *466*, 105–108. [CrossRef]

166. Lambert, O.; Goolaerts, S. Late Miocene survival of a hyper-longirostrine dolphin and the Neogene to recent evolution of rostrum proportions among odontocetes. *J. Mamm. Evol.* **2022**, *29*, 99–111. [CrossRef]
167. Galatius, A.; Olsen, M.T.; Steeman, M.E.; Racicot, R.A.; Bradshaw, C.D.; Kyhn, L.A.; Miller, L.A. Raising your voice: Evolution of narrow-band high-frequency signals in toothed whales (Odontoceti). *Biol. J. Linn. Soc.* **2019**, *125*, 213–224. [CrossRef]
168. Lambert, O.; Wanzenböck, G.; Pfaff, C.; Louwye, S.; Kriwet, J.; Marx, F.G. First eurhinodelphinid dolphin from the Paratethys reveals a new family of specialised echolocators. *Hist. Biol.* **2023**, *35*, 1074–1091. [CrossRef]
169. Pilleri, G. Side-swimming, vision, and sense of touch in *Platanista indi* (Cetacea, Platanistidae). *Investig. Cetacea* **1974**, *4*, 24–29.
170. Purves, P.E.; Pilleri, G. Observations on the ear, nose, throat and eye of *Platanista indi*. *Investig. Cetacea* **1975**, *5*, 13–58.
171. Hulbert, R.C.; Whitmore, F.C. Late Miocene mammals from the Mauvilla Local Fauna, Alabama. *Bull. Fla. Mus. Nat. Hist.* **2006**, *46*, 1–28.
172. Barnes, L.G. Fossil pontoporiid dolphins (Mammalia: Cetacea) from the Pacific coast of North America. *Contrib. Sci. Nat. Hist. Mus. Los Angeles Cty.* **1985**, *363*, 1–34. [CrossRef]
173. Boessenecker, R.W.; Poust, A.W. Freshwater occurrence of the extinct dolphin *Parapontoporia* (Cetacea: Lipotidae) from the upper Pliocene nonmarine Tulare Formation of California. *Palaeontology* **2015**, *58*, 489–496. [CrossRef]
174. Werth, A.J.; Beatty, B. Osteological correlates of evolutionary transitions in cetacean feeding and related oropharyngeal functions. *Front. Ecol. Evol.* **2023**, *11*, 1179804. [CrossRef]
175. Fordyce, R.E. Dental anomaly in a fossil squalodont dolphin from New Zealand, and the evolution of polydonty in whales. *N. Z. J. Geol. Geophys.* **1982**, *9*, 419–426. [CrossRef]
176. Vélez-Juarbe, J. New heterodont odontocetes from the Oligocene Pysht Formation in Washington State, U.S.A., and a reevaluation of Simocetidae (Cetacea, Odontoceti). *PeerJ* **2023**, *11*, e15576. [CrossRef]
177. Muizon, C.D. Are the squalodonts related to the platanistoids? *Proc. San Diego Soc. Nat. Hist.* **1994**, *29*, 135–146.
178. Muizon, C.D. The affinities of *Notocetus vanbenedeni*, an Early Miocene platanistoid (Cetacea, Mammalia) from Patagonia, southern Argentina. *Am. Mus. Novit.* **1987**, *2904*, 1–27.
179. Muizon, C.D. A new Ziphiidae (Cetacea) from the early Miocene of Washington State (USA) and phylogenetic analysis of the major groups of odontocetes. *Bull. Du Muséum Natl. D'histoire Nat. Paris* **1991**, *12*, 279–326.
180. Groves, S.L.; Peredo, C.M.; Pyenson, N.D. What are the limits on whale ear bone size? Non-isometric scaling of the cetacean bulla. *PeerJ* **2021**, *9*, e10882. [CrossRef]
181. Boessenecker, R.W. A new marine vertebrate assemblage from the Late Neogene Purisima Formation in Central California, Part II: Pinnipeds and cetaceans. *Geodiversitas* **2013**, *35*, 815–940. [CrossRef]
182. Schäfer, W. *Ecology and Paleoecology of Marine Environments*; University of Chicago Press: Chicago, IL, USA, 1972; p. 568.
183. Bianucci, G.; Marx, F.G.; Collareta, A.; Di Stefano, A.; Landini, W.; Morigi, C.; Varola, A. Rise of the titans: Baleen whales became giants earlier than thought. *Biol. Lett.* **2019**, *15*, 20190175. [CrossRef] [PubMed]
184. Sander, P.M.; Griebeler, E.M.; Klein, N.; Velez-Juarbe, J.; Wintrich, T.; Revell, L.J.; Schmitz, L. Early giant reveals faster evolution of large body size in ichthyosaurs than in cetaceans. *Science* **2021**, *374*, eabf5787. [CrossRef] [PubMed]
185. Slater, G.J.; Goldbogen, J.A.; Pyenson, N.D. Independent evolution of baleen whale gigantism linked to Plio-Pleistocene ocean dynamics. *Proc. R. Soc. B* **2017**, *284*, 20170546. [CrossRef]
186. Bisconti, M.; Pellegrino, L.; Carnevale, G. Evolution of gigantism in right and bowhead whales (Cetacea: Mysticeti: Balaenidae). *Biol. J. Linn. Soc.* **2021**, *134*, 498–524. [CrossRef]
187. Burin, G.; Park, T.; James, T.D.; Slater, G.J.; Cooper, N. The dynamic adaptive landscape of cetacean body size. *Curr. Biol.* **2023**, *33*, 1787–1794. [CrossRef] [PubMed]
188. Marino, L.; McShea, D.W.; Uhen, M.D. Origin and evolution of large brains in toothed whales. *Anat. Rec.* **2004**, *281*, 1247–1255. [CrossRef]
189. Montgomery, S.H.; Geisler, J.H.; McGowen, M.R.; Fox, C.; Marino, L.; Gatesy, J. The evolutionary history of cetacean brain and body size. *Evolution* **2013**, *67*, 3339–3353. [CrossRef] [PubMed]
190. Waugh, D.A.; Thewissen, J.G.M. The pattern of brain-size change in the early evolution of cetaceans. *PLoS ONE* **2021**, *16*, e0257803. [CrossRef]
191. Smaers, J.B.; Rothman, R.S.; Hudson, D.R.; Balanoff, A.M.; Beatty, B.; Dechmann, D.K.N.; De Vries, D.; Dunn, J.C.; Fleagle, J.G.; Gilbert, C.C.; et al. The evolution of mammalian brain size. *Sci. Adv.* **2021**, *7*, eabe2101. [CrossRef]
192. Boessenecker, R.W. New records of the fur seal *Callorhinus* (Carnivora: Otariidae) from the Plio-Pleistocene Rio Dell Formation of Northern California and comments on otariid dental evolution. *J. Vertebr. Paleontol.* **2011**, *31*, 454–467. [CrossRef]
193. Gingerich, P.D. Species in the fossil record: Concepts, trends, and transitions. *Paleobiology* **1985**, *11*, 27–41. [CrossRef]
194. Scannella, J.B.; Fowler, D.W.; Goodwin, M.B.; Horner, J.R. Evolutionary trends in *Triceratops* from the Hell Creek Formation, Montana. *Proc. Natl. Acad. Sci. USA* **2014**, *111*, 10245–10250. [CrossRef]
195. Parins-Fukuchi, C.; Greiner, E.; MacLatchy, L.M.; Fisher, D.C. Phylogeny, ancestors, and anagenesis in the hominin fossil record. *Paleobiology* **2019**, *45*, 378–393. [CrossRef]
196. Wagner, P.J.; Erwin, D.H. Phylogenetic patterns as tests of speciation models. In *New Approaches to Speciation in the Fossil Record*; Erwin, D.H., Anstey, R.L., Eds.; Columbia University Press: New York, NY, USA, 1995; pp. 87–122.
197. Heyning, J.E. Sperm whale phylogeny revisted: Analysis of the morphological evidence. *Mar. Mammal Sci.* **1997**, *13*, 596–613. [CrossRef]

198. Messenger, S.L.; McGuire, J.A. Morphology, molecules, and the phylogenetics of Cetaceans. *Syst. Biol.* **1998**, *47*, 90–124. [CrossRef] [PubMed]
199. Fordyce, R.E.; Muizon, C.D. Evolutionary history of cetaceans: A review. In *Secondary Adaptations of Tetrapods to Life in Water*; Mazin, J.M., Buffrenil, V.D., Eds.; Verlag Dr. Friedrich Pfeil: Munich, Germany, 2001; pp. 169–233.
200. Flynn, T.T. Description of *Prosqualodon davidi* Flynn, a fossil cetacean from Tasmania. *Trans. Zool. Soc. Lond.* **1948**, *25*, 153–197. [CrossRef]
201. Dubrovo, I.A.; Sanders, A.E. A new species of *Patriocetus* (Mammalia, Cetacea) from the late Oligocene of Kazakhstan. *J. Vertebr. Paleontol.* **2000**, *20*, 577–590. [CrossRef]
202. Marx, F.G. The more the merrier? A large cladistic analysis of mysticetes, and comments on the transition from teeth to baleen. *J. Mamm. Evol.* **2011**, *18*, 77–100. [CrossRef]
203. Marx, F.G.; Fordyce, R.E. Baleen boom and bust: A synthesis of mysticete phylogeny, diversity and disparity. *R. Soc. Open Sci.* **2015**, *2*, 140434. [CrossRef]
204. Coste, A.; Fordyce, R.E.; Loch, C. A new dolphin with tusk-like teeth from the late Oligocene of New Zealand indicates evolution of novel feeding strategies. *Proc. R. Soc. B* **2023**, *290*, 20230873. [CrossRef]
205. Aguirre-Fernandez, G.; Barnes, L.G.; Aranda-Manteca, F.J.; Fernandez-Rivera, J.R. *Protoglobicephala mexicana*, a new genus and species of Pliocene fossil dolphin (Cetacea; Odontoceti; Delphinidae) from the Gulf of California, Mexico. *Bol. Soc. Geol. Mex.* **2009**, *61*, 245–265. [CrossRef]
206. Barnes, L.G. Whales, dolphins and porpoises, origin and evolution of the Cetacea. In *Mammals. Notes for a Short Course. Studies in Geology 8 (1–4)*; Gingerich, P.D., Badgely, C.E., Broadhead, T.W., Eds.; University of Tennessee Department of Geological Sciences: Knoxville, TN, USA, 1984; Volume 8, pp. 139–154.
207. Bianucci, G. *Arimidelphis sorbinii* a new small killer whale-like dolphin from the Pliocene of Marecchia River (Central eastern Italy) and a phylogenetic analysis of the Orcininae (Cetacea: Odontoceti). *Riv. Ital. Paleontol. Stratigr.* **2005**, *111*, 329–344.
208. Buchholtz, E.A.; Schur, S.A. Vertebral osteology in Delphinidae (Cetacea). *Zool. J. Linnaean Soc.* **2004**, *140*, 383–401. [CrossRef]
209. Doran, A.H.G. Morphology of the mammalian ossicula auditûs. *Linn. Soc. Lond. Trans. 2nd Ser. Zool.* **1876**, *1*, 371–497. [CrossRef]
210. Flower, W.H. On the osteology of the cachalot of sperm-whale (*Physeter macrocephalus*). *Trans. Zool. Soc. Lond.* **1869**, *6*, 309–372. [CrossRef]
211. Flower, W.H. On the recent ziphioid whales, with a description of the skeleton of *Berardius arnouxi*. *Trans. Zool. Soc. Lond.* **1872**, *8*, 203–234. [CrossRef]
212. Galatius, A.; Kinze, C.C. Ankylosis patterns in the postcranial skeleton and hyoid bones of the harbour porpoise (*Phocoena phocoena*) in the Baltic and North Sea. *Can. J. Zool.* **2003**, *81*, 1851–1861. [CrossRef]
213. Geisler, J.H.; Godfrey, S.J.; Lambert, O. A new genus and species of late Miocene inioid (Cetacea, Odontoceti) from the Meherrin River, North Carolina, USA. *J. Vertebr. Paleontol.* **2012**, *32*, 198–211. [CrossRef]
214. Geisler, J.H.; Luo, Z. The petrosal and inner ear of *Herpetocetus* sp. (Mammalia: Cetacea) and their implications for the phylogeny and hearing of archaic mysticetes. *J. Paleontol.* **1996**, *70*, 1045–1066. [CrossRef]
215. Geisler, J.H.; Luo, Z. Relationships of Cetacea to terrestrial ungulates and the evolution of cranial vasculature in Cete. In *The Emergence of Whales*; Thewissen, J.G.M., Ed.; Plenum Press: New York, NY, USA, 1998; pp. 163–212.
216. Heyning, J.E. Comparative facial anatomy of beaked whales (Ziphiidae) and a systematic revision among the families of extant Odontoceti. *Nat. Hist. Mus. Los Angeles Cty. Contrib. Sci.* **1989**, *405*, 1–64. [CrossRef]
217. Heyning, J.E.; Mead, J.G. Evolution of the nasal anatomy of cetaceans. In *Sensory Abilities of Cetaceans*; Thomas, J., Kastelein, R., Eds.; Plenum Press: New York, NY, USA, 1990; pp. 67–79.
218. Kasuya, T. Systematic consideration of recent toothed whales based on the morphology of tympano-periotic bone. *Sci. Rep. Whales Res. Inst.* **1973**, *25*, 1–103.
219. Kellogg, R. Description of two squalodonts recently discovered in the Calvert Cliffs, Maryland; and notes on the shark-toothed dolphins. *Proc. United States Natl. Mus.* **1923**, *62*, 1–69. [CrossRef]
220. Luo, Z. Homology and transformation of cetacean ectotympanic structures. In *The Emergence of Whales*; Thewissen, J.G.M., Ed.; Plenum Press: New York, NY, USA, 1998; pp. 269–301.
221. McLeod, S.; Whitmore, F.C.; Barnes, L.G. Evolutionary relationships and classification. *Bowhead Whale. Soc. Mar. Mammal. Spec. Publ.* **1993**, *2*, 45–70.
222. Mead, J.G. Shepherd's beaked whale *Tasmacetus shepherdi* Oliver, 1937. In *Handbook of Marine Mammals, Volume 4*; Ridgway, S.H., Harrison, R., Eds.; Academic Press: San Diego, CA, USA, 1989; pp. 309–320.
223. Moore, J.C. Relationships among the living genera of beaked whales. *Fieldiana Zool.* **1968**, *53*, 209–298.
224. Muizon, C.D. Les vertébrés fossiles de la Formation Pisco (Pérou), Deuxieme partie: Les odontocètes (Cetacea, Mammalia) du Pliocène inférieur de Sud-Sacaco. *Trav. De L'institut Français D'études Andin.* **1984**, *50*, 1–188.
225. Muizon, C.D. Les relations phylogénétiques des Delphinida (Cetacea, Mammalia). *Ann. Paléontol.* **1988**, *74*, 159–227.
226. Murakami, M.; Shimada, C.; Hikida, Y.; Hirano, O. A new basal porpoise, *Pterophocaena nishinoi* (Cetacea, Odontoceti, Delphinoidea), from the upper Miocene of Japan and its phylogenetic relationships. *J. Vertebr. Paleontol.* **2012**, *34*, 491–511. [CrossRef]
227. Omura, H. A systematic study of the hyoid bones in the baleen whales. *Sci. Rep. Whales Res. Inst.* **1964**, *18*, 149–170.
228. Rice, D.W.; Wolman, A.W. The stomach of *Kogia breviceps*. *J. Mammal.* **1990**, *71*, 242–246. [CrossRef]
229. Schulte, H.V.W. The skull of *Kogia breviceps* Blainville. *Bull. Am. Mus. Nat. Hist.* **1917**, *37*, 304–320.

230. Yablokov, A.V. Convergence or parallelism in the evolution of cetaceans. *Int. Geol. Rev.* **1964**, *7*, 1461–1468. [CrossRef]
231. Zhou, K. Classification and phylogeny of the Superfamily Platanistoidea, with notes on evidence of the monophyly of the Cetacea. *Sci. Rep. Whales Res. Inst.* **1982**, *34*, 93–108.

Disclaimer/Publisher's Note: The statements, opinions and data contained in all publications are solely those of the individual author(s) and contributor(s) and not of MDPI and/or the editor(s). MDPI and/or the editor(s) disclaim responsibility for any injury to people or property resulting from any ideas, methods, instructions or products referred to in the content.